Mechanistic Investigations of Gold(I)-catalyzed Carbene Transfer and Hydrofunctionalization Reactions

by

Robert Gerard Carden, Jr.

Department of Chemistry
Duke University

Date:_____

Approved:

_____
Ross A. Widenhoefer, Supervisor

_____
Stephen L. Craig

_____
Richard A. MacPhail

_____
Steven J. Malcolmson

Dissertation submitted in partial fulfillment of
the requirements for the degree of Doctor of Philosophy
in the Department of
Chemistry in the Graduate School
of Duke University

2019

ABSTRACT

Mechanistic Investigations of Gold(I)-catalyzed Carbene Transfer and

Hydrofunctionalization Reactions

by

Robert Gerard Carden, Jr.

Department of Chemistry
Duke University

Date:_____

Approved:

_____
Ross A. Widenhoefer, Supervisor

_____
Stephen L. Craig

_____
Richard A. MacPhail

_____
Steven J. Malcolmson

An abstract of a dissertation submitted in partial
fulfillment of the requirements for the degree
of Doctor of Philosophy in the Department of
Chemistry in the Graduate School of
Duke University

2019

Abstract

Cationic gold(I) complexes have been recognized as efficient catalysts for a wide array of transformations, including carbene transfers to form cyclopropanes and hydrofunctionalization reactions. While there have been great strides made in the development of these reactions, far less is understood about the mechanisms by which these transformations occur. Here are reported kinetic and mechanistic analyses of gold(I)-catalyzed reactions as well as the interrogation of the properties of cationic gold(I) carbene complexes, which are commonly proposed intermediates in gold(I)-catalyzed transformations.

A series of gold(I) sulfonium benzylide complexes were synthesized by nucleophilic substitution of α-chloro gold(I) carbenoid complexes with sulfides. These complexes reacted efficiently with alkenes and dimethylsulfoxide to form cyclopropanes and benzaldehyde, respectively. Kinetic analysis of these reactions is consistent with the intermediacy of cationic gold(I) benzylidene complexes. Further mechanistic analysis revealed that alkene stereochemistry is preserved during cyclopropanation and a Hammett analysis of the reaction suggests a concerted mechanism for cyclopropanation.

To evaluate the electron donor ability of (L)Au fragments in cationic gold(I) carbene complexes, a series of cationic gold (β,β-disilyl)vinylidene complexes and cationic gold (fluorophenyl)methoxycarbene complexes were synthesized. ^{29}Si and ^{19}F

NMR analysis of these complexes compared to organic model compounds revealed that (L)Au fragments are significantly more inductively donating and comparably π-donating as *p*-substituted aryl groups. A comparison of various ligands showed that (P(*t*-Bu)$_2$-*o*-biphenyl)Au fragments are nominally stronger electron donors than (IPr)Au fragments, both of which are significantly more electron donating that (PPh$_3$)Au and [P(OMe)$_3$]Au fragments.

Kinetic and mechanistic analysis of the gold(I)-catalyzed hydrofunctionalization of 3-methyl-1,2-butadiene with alcohols and anilines was performed. Experimental data suggest a mechanism for the gold(I)-catalyzed hydroalkoxylation involving endergonic allene displacement of triflate from gold, followed by an outer-sphere attack of alcohol on gold(I)-π-allene complex, followed by rapid protodeauration. In contrast, for the gold(I)-catalyzed hydroamination, the active catalyst is the gold(I) bound nucleophile complex and a buildup of bis(gold) vinyl complex suggests a slow protodeauration.

A brief study evaluating student learning in the classroom is also presented. A series of team-based learning applications based on the spiropyran to merocyanine transformation were developed and assessed relative to a series of control application problems. There was no statistically significant difference in student outcomes based on the applications used in class, but student feedback suggests that the interconnected, and real-life examples were more engaging.

To my family and friends

Contents

List of Figures

List of Schemes

List of Tables

Acknowledgements

I would first like to thank my parents, Bob and Donna, for their unwavering support during my entire life, especially during this journey through graduate school. They have been there each step of the way. To my brother, Matthew, and to the rest of my family, your support and words of encouragement have not gone unnoticed.

I would be remiss if I did not extend a many thanks to my advisor and mentor, Ross. I would not be the scientist I am today without your guidance and support, for which I am extremely grateful. To my lab mates, Caroline, David, Liqi and Yichen, thank you for creating a strong, collaborative, and fun work environment that allows all of us to not only survive, but thrive in graduate school. Special thanks to Nana, you have been there since the beginning, and have been an amazing lab mate, and more importantly, a great friend. Thanks also to my former undergraduate students, Nathan, Nick and Scott, for teaching me patience and how to be a good mentor as well as previous members of the Widenhoefer lab, especially Brad, Jacob and Robert.

I have had the luxury of some other great mentors during this journey. To Justin, I would not have gotten to where I am without you, your frank advice and support have helped me achieve my goals. To Claire, thank you for helping to shape who I am as a teacher and for helping me to work through challenging learning experiences. To Dori, thank you for taking some chances on me and helping me to come into my own as a teacher.

To members of my committee, Steve C., Steve M. and Dick, thank you for being a constant support through this process and challenging me during this journey. I was fortunate to work next door to some great scientists during graduate school, members of the Malcolmson and Roizen labs, thank you for being great colleagues always willing to share an idea, help with a problem, or lend a reagent. I also had some amazing classmates to share graduate school with, Allison, Anastasia, Hyunji, Lizzie, Meghan, and all the rest, we have accomplished so much already, I cannot wait to see what comes next.

This graduate school journey did not begin five years ago here at Duke, but what now seems like ages ago in Mrs. Ansley's high school chemistry class, thank you for inspiring me to pursue chemistry. To my undergraduate research mentor, Dr. Graham, thank you for taking a chance on me, introducing me to scientific research and pushing me to strive for more. Also, thanks to Dr. Forman and Dr. Zurbach, for helping give me the nudge to pursue graduate school.

Beyond Duke, special thanks to Elizabeth, Erin, Greg, Lisa, Marcus, Nick, Nicole, Sheri, and many others, you provided support from both near and far to help me on this journey. You all kept me sane and helped me to enjoy my time in graduate school beyond working in the lab.

1. Introduction

1.1 Recent interest in gold(I)-catalyzed reactions

Gold(I) catalysis has been a growing field in the past two decades since the gold(I)-catalyzed hydroalkoxylation of alkynes with alcohols was first reported.[1] Since then, cationic gold(I) complexes have been shown to facilitate a wide array of transformations, including cyclopropanation[2-11] and the hydrofunctionalization of C–C multiple bonds.[12-14] This ability of gold(I) catalysts to perform seemingly disparate transformations is often attributed to its unique properties compared to other transition metals. Due to a relativistic contraction of the *6s* orbitals on gold,[15] gold has a relatively high electronegativity for a transition metal (2.4 on the Puling scale) and can act as a soft Lewis acid, forming complexes with soft Lewis bases, like C–C multiple bonds.[13,14] Gold(I) also has a low oxophilicity and is generally resistant to oxidation,[13,16] unless a strong oxidant is present, which make gold(I) catalysts particularly robust to a wide range of reaction conditions.[14,17,18]

This versatility of gold(I) catalysts to perform a wide variety of transformations allows for the formation of complex molecular architectures from simple starting materials with high efficiency. Such reactions exemplifies the potential great utility of gold(I) catalysis in organic synthesis. But, there are still challenges that must be overcome to enhance the application of gold(I) catalysis to organic synthesis as a whole.

As new reactivities for gold(I) catalysts have been uncovered, recent research efforts have now begun to turn toward understanding how these transformations are achieved by these catalysts.

Efforts to probe the mechanisms of gold(I)-catalyzed reactions have focused on computational analysis and the synthesis of reactive intermediates, such as cationic gold π-complexes and cationic gold(I) carbenes.[19-29] Current efforts to better understand the mechanism of gold(I)-catalyzed processes are presented as part of this dissertation, including the kinetic analysis of gold(I)-catalyzed transformations and studies on ligand donor ability in gold(I) carbenes, a commonly proposed intermediate in gold(I)-catalyzed reactions.

1.2 Gold(I) carbenes as intermediates

One of the most commonly proposed intermediates in gold(I)-catalyzed transformations are cationic gold(I) carbenes, particularly in gold(I)-catalyzed enyne cycloisomerizations and gold(I)-catalyzed cyclopropanation reactions.[22,30-35] These cationic gold(I) carbene intermediates are generated from a variety of different sources, including cyclopropene ring opening, reactions with diazo compounds and rearrangements of enyne cycloisomerization intermediates (Figure 1).[2,12,32,35]

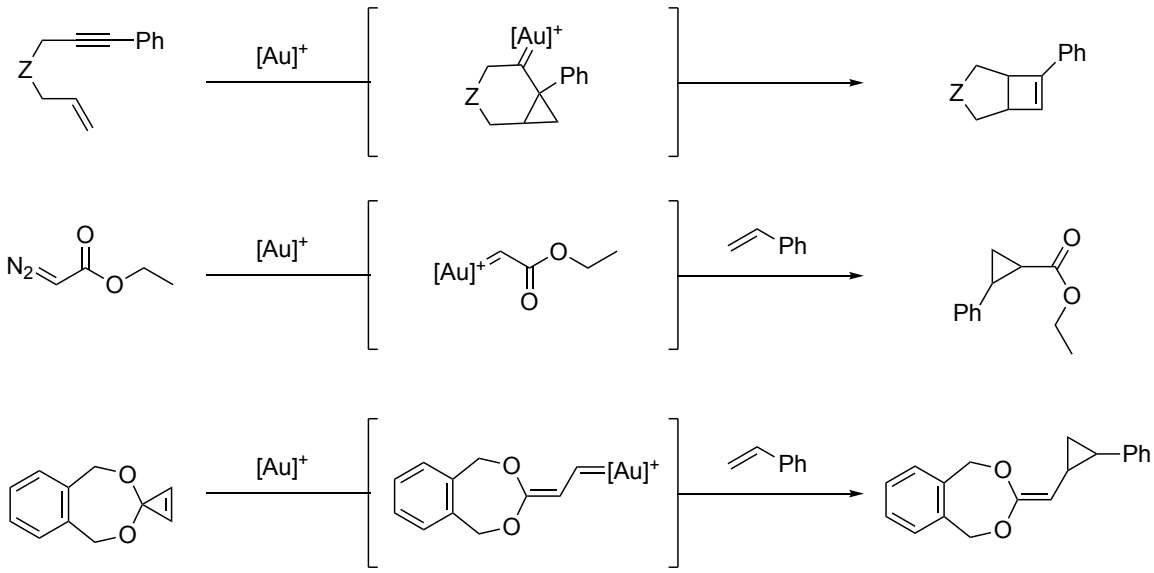

Figure 1. Common methods for generation of cationic gold(I) carbene intermediates in gold(I)-catalyzed reactions.

While these cationic gold(I) carbenes have been well accepted as intermediates in gold(I)-catalyzed transformations, there are still some inconsistencies in the terminology used to describe these complexes, specifically the use of the terms carbene and carbenoid to describe cationic gold(I) carbene complexes. For the purposes of this dissertation, carbene will be used to describe divalent gold(I) complexes with a formal positive charge on the gold atom and a double bond between gold and the adjacent α-carbon and carbenoid will refer to complexes with a single bond between gold and the adjacent α-carbon and a leaving group bound to the α-carbon (Figure 1.2).[36]

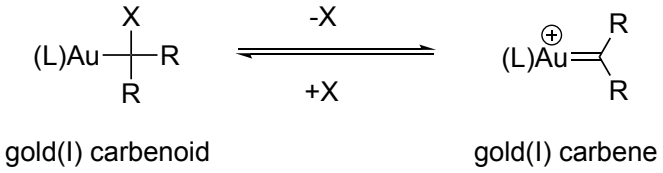

Figure 2. Examples of gold(I) carbenoid and gold(I) carbene terminology

Once generated in gold(I)-catalyzed reactions by means explained above, these cationic gold(I) carbenes most commonly undergo carbene transfer reactions with alkenes to form cyclopropane products. Though common in many gold(I)-catalyzed processes, the mechanism by which carbene transfer occurs is less understood. Two commonly proposed mechanisms are (1) a concerted process forming both new C–C bonds of the cyclopropane in one step or (2) a stepwise pathway via carbocation intermediates, with the initial formation of one C–C bond followed by ring closure to

reform to form the second C–C bond. Much of our current understanding of this gold(I) carbene transfer mechanism has been gleaned from indirect experimental evidence, such as product ratios from catalytic reactions, and computational analysis. These studies are summarized below, providing context for some of the studies presented in this dissertation.

1.3 Recent studies on the mechanism of gold(I)-catalyzed carbene transfer

1.3.1 Studies of catalytic gold(I)-catalyzed cyclopropanation reactions

In 2005, Toste reported a ligand effect on the diastereoselectivity of the gold(I)-catalyzed cyclopropanation of propargylic ester **1.1** with *p*-methoxystyrene (Scheme 1.1).[3] When $[(Ph_3P)Au]^+ SbF_6^-$ was used as the active catalyst a 1:1 mixture of *cis:trans* isomers of cyclopropane **1.2** was overserved, but when $[(t\text{-}Bu)_3PAu]^+ SbF_6^-$ was used, the *cis:trans* ratio increased to 5:1. Changing to propargylic ester **1.3** led to the exclusive formation of *cis* cyclopropane **1.4** (Scheme 1).

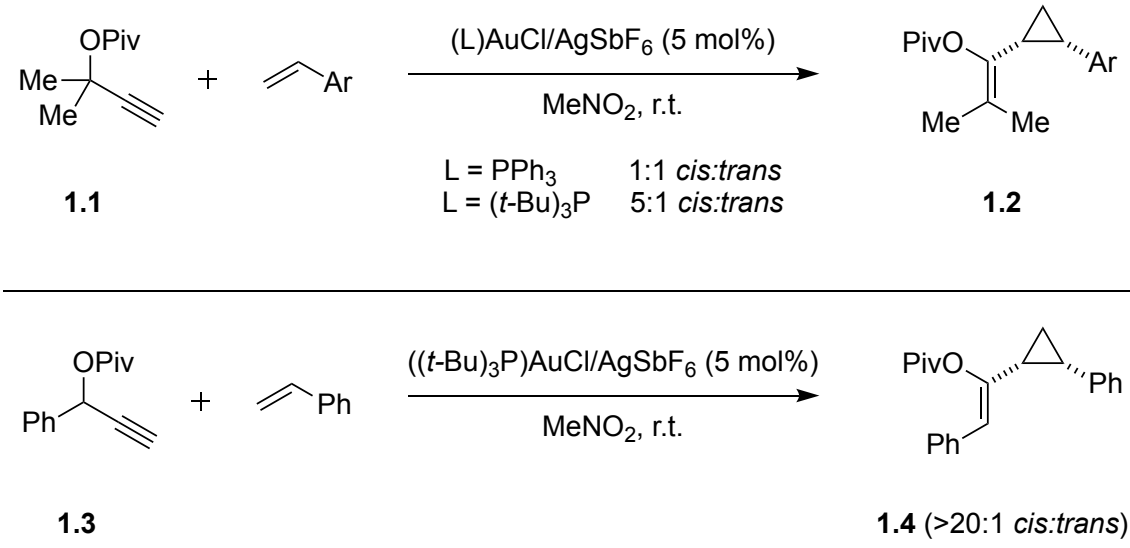

Scheme 1. Gold(I)-catalyzed cyclopropanation of propargylic esters with styrenes (Ar = *p*-methoxyphenyl).

From these observations, a stereochemical model accounting for the stereoselectivity of the reaction was developed, featuring the concerted addition of styrene to gold(I) carbene intermediate **I** from the less sterically encumbered transition state (**II-*cis***) due to the steric interaction between the phenyl group and bulky $(t\text{-Bu})_3P$ ligand on gold (**II-*trans***) (Figure 3). Reactions of *cis*- and *trans*-β-methylstryene with propargyl pivolate **1.3** proceeded with high stereospecificity, providing further support for the mechanistic hypothesis of a concerted addition of styrene to gold(I) carbene intermediate **I** (Scheme 2).

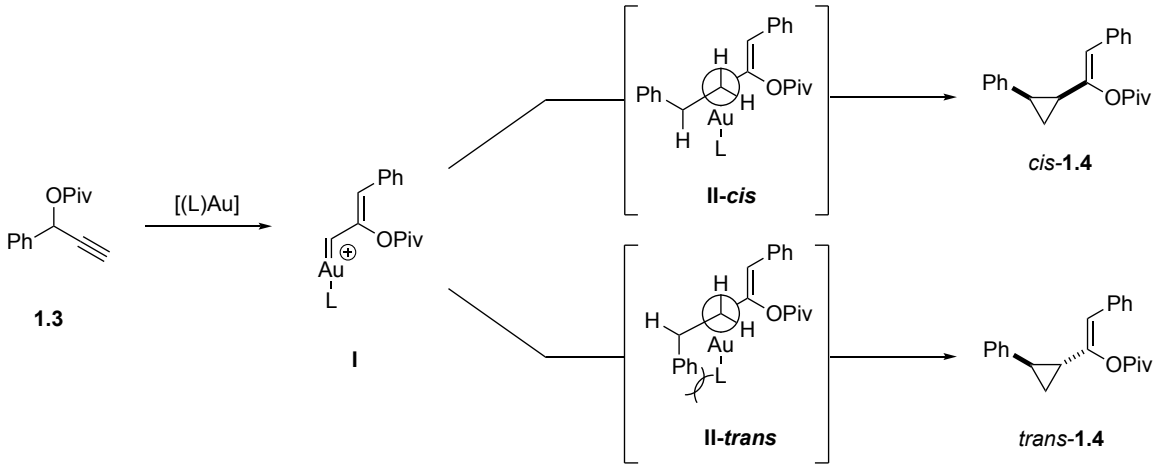

Figure 3. Model for stereoselectivity of gold(I)-catalyzed cyclopropanation of propargylic ester **1.3** with styrene.

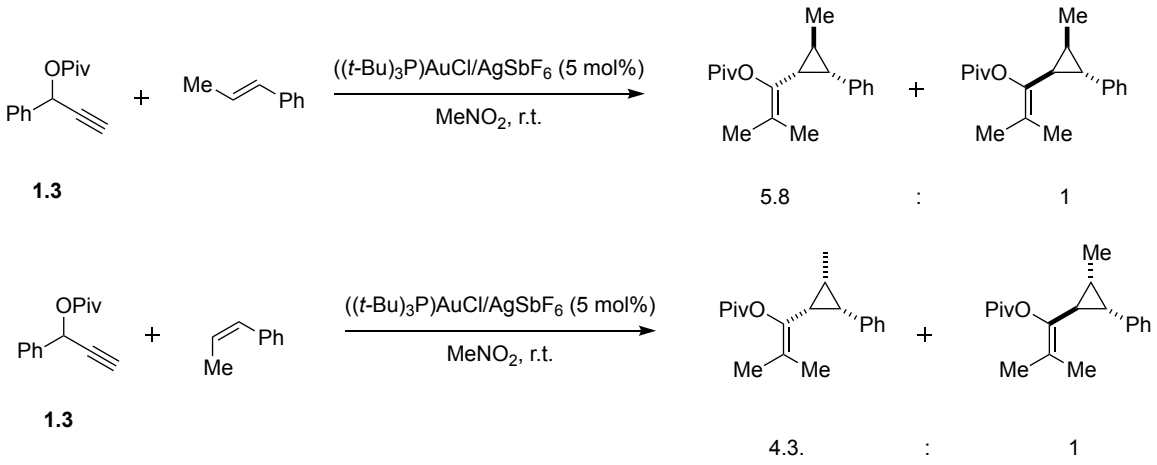

Scheme 2. Stereoretention in gold(I)-catalyzed cyclopropanation reaction

While the retention of alkene stereochemistry in isolated products provides evidence for a concerted pathway for gold(I)-catalyzed carbene transfer, there are potential pathways for gold(I)-catalyzed carbene transfer that could likewise lead to net retention of alkene stereochemistry that are not concerted. To gain additional experimental insight into the mechanisms of carbene transfer from cationic gold(I) carbenes, Echavarren recently reported a combined experimental/computation study on the intermolecular cyclopropanation of cationic gold(I) carbenes generated during 1,6-eneyne cycloisomerization reactions.[37] In the presence gold(I) catalyst, enyne **1.5** cyclizes to form proposed cationic gold(I) carbene intermediate **III**, which then underwent intermolecular cyclopropanation with styrene to give cyclopropane **1.6** (Scheme 3).

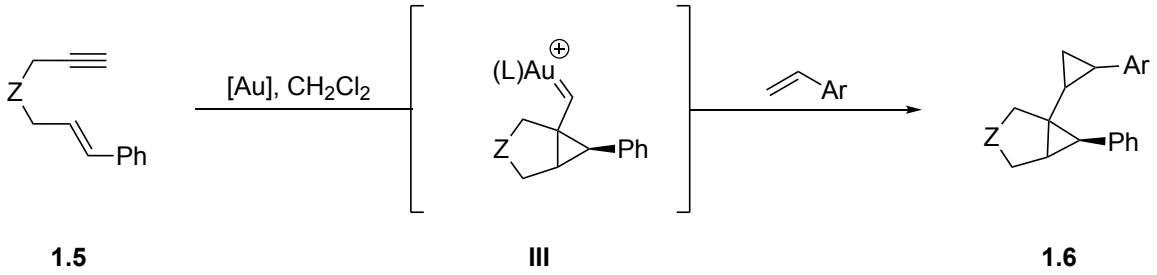

1.5 **III** **1.6**

Scheme 3. Tandem gold(I)-catalyzed enyne cycloisomerization/cyclopropanation reaction.

A Hammett analysis of the rate of tandem cyloisomerization/cycloisomerization with a series of *p*-substitued styrene derivatives showed a good correlation with Hammet σ parameters with ρ = –1.3 and –1.93 for two gold(I) catalysts with NHC and phosphine ligands, respectively. The negative rho values suggest the buildup of positive charge in the transition state of the rate-determining step for gold(I)-catalyzed cyclopropanation. The sign and magnitude of the rho values were in accord with other electrophilic cyclopropanation reactions (Table 1).

Table 1. Known rho values of electrophilic cyclopropanation reactions

Conditions	ρ
$Zn(Cu)/CH_2I_2$[38]	–2.4
$ZnEt_2/ CH_2I_2$[39]	–1.6
$TpCuI/N_2CO_2Et$[40,41]	–0.9 to –1.2
$(L)Au^+$/enyne[37]	–1.3 to 1.9

In experiments similar to those performed by Toste, reactions of enyne **1.5** with gold(I) catalyst and *cis*- and *trans*-β-methylstryene, respectively, led to cyclopropanation, forming a mixture of diastereomers. Analysis of the ^{1}H NMR spectrum of the products revealed that in each diastereomer, the stereochemistry of the original styrene was preserved, consistent with previous observations regarding the stereo-retention of alkene geometry in gold(I)-catalyzed cyclopropanation reaction. While the experimental observations alone did not provide a strong picture for a different mechanistic perspective than that described by Toste,[3] to evaluate the mechanism further, Echavarren turned to computational analysis to aid in determining the mechanism of gold(I)-catalyzed carbene transfer reactions.

Computational analysis of gold(I)-carbene transfer was performed for the gold(I) carbene transfer of simplified gold(I) carbenes to both aliphatic alkenes and styrene Computational analysis of the reaction of gold(I) carbene **1.7** with propene predicted the experimentally observed diastereomer, with the lowest energy pathway occurring being a concerted pathway with an activation energy ranging from 7.5–8.4 kcal/mol for NHC, phosphine and phosphite ligands (Scheme 1.4). A similar analysis of carbene transfer of gold(I) carbene **1.8** to styrene revealed that cyclopropanation occurs in a stepwise fashion via open intermediate **IV**, followed by rapid ring closure to form cyclopropane (Figure 4).

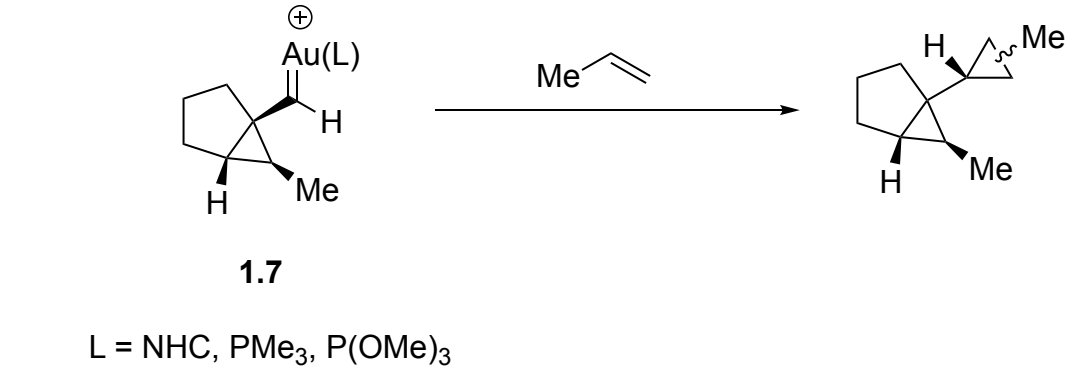

1.7

L = NHC, PMe_3, $P(OMe)_3$

Scheme 4. Cyclopropanation of cationic gold(I) carbene complex **1.7** with simple aliphatic alkene.

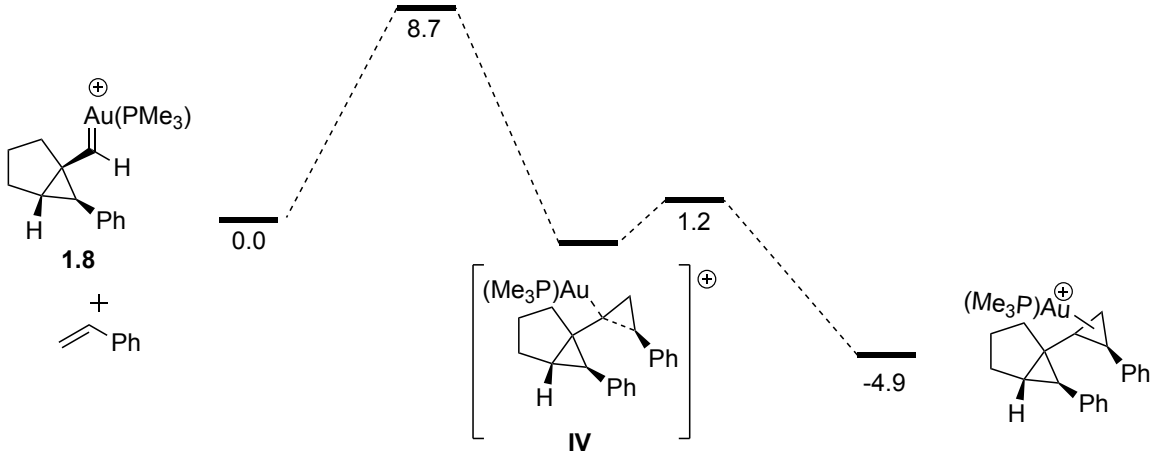

Figure 4. DFT analysis of Cyclopropanation of cationic gold(I) carbene complex **1.8** with stryene

Given the formation of open intermediate, the lack of erosion of alkene stereochemistry in the final cyclopropane is unexpected. However, computational analysis revealed the barrier to C–C bond rotation around the H_2C–CHPh bond was

higher (7.3 kcal/mol) relative to ring closure (1.2 kcal/mol), maintaining the original stereochemistry of the C=C bond in the alkene, which was consistent with experimental observations. This computational analysis is consistent with the reported experimental evidence for gold(I)-catalyzed carbene transfer from gold(I) carbenes generated via enyne cycloisomerization, where polarized alkene, like styrene, undergo cyclopropanation via a stepwise process and aliphatic alkenes undergo cyclopropanation via a concerted process, both occurring with stereo-retention of the geometry of the starting alkene. Still missing from the conversation regarding the mechanism of gold(I) carbene transfer is experimental evidence for a cationic gold(I) carbene complex.

1.3.2 Gas-phase gold(I) carbene transfer

Efforts to fill this gap have, to date, largely come from the generation and study of the reactivity of cationic gold(I) carbene complexes formed in the gas-phase. In 2008, Chen reported the first experimental observation of a gold(I) benzylidene complex in the gas-phase.[42] Electrospray ionization of a solution of gold(I) carbenoid complex **1.9** led to the dissociation of bound triphenylphosphine leading to the formation of cationic gold(I) carbene complex **1.10** as the sole product, based on the observed mass-to-charge ratio (m/z = 591) (Scheme 5).

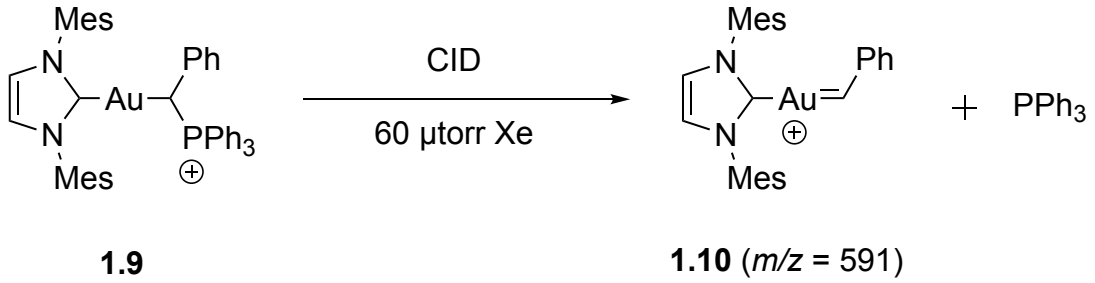

1.9 **1.10** (*m/z* = 591)

Scheme 5. Gas-phase generation of cationic gold(I) benzylidene **1.10** by collision-induced dissociation from gold(I) carbenoid **1.9**

The structure of the signal with *m*/*z* = 591 was confirmed on the basis of the gas-phase reactivity with alkenes. Ionization of gold(I) carbenoid complex **1.9** in the presence of *cis*-3-hexene led to the formation of cationic gold(I) carbene complex **1.10** and two new molecular ions with *m*/*z* = 675 (major) and 501 (minor), which were assigned as gold metallocyclobutane complex **1.11** and $(L)Au^+$, respectively (Scheme 6). The formation of a gold metallocyclobutane complex is consistent with the carbene reactivity of other transition metals and monocoordinated gold(I) is consistent with benzylidene transfer to the C=C bond of *cis*-3-hexene, that has been observed in the solution phase. This report represented the first observation of cationic gold(I) carbenes in the gas phase, and provided a platform with which to further evaluate their intermediacy in gold(I)-catalyzed cyclopropanation reactions.

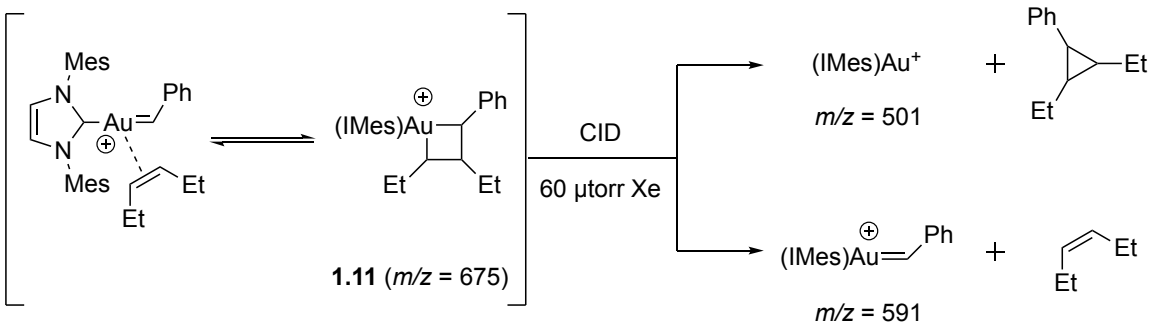

Scheme 6. Gas-phase cyclopropanation of *cis*-3-hexene with gold(I) benzylidene complex **1.10**

Following their initial report, Chen utilized gold(I) carbenoid complex **1.9** as a precursor for the formation of other cationic gold(I) carbene complexes formed from cyclopropane ring opening.[43] Ionization of gold(I) carbenoid complex **1.9** in the presence of 1-ethoxy-2-methoxy-cyclopropane (mixture of *cis*/*trans* isomers) led to the formation of gold(I) cyclopropane adduct **1.12**. When subjected to collision-induced-dissociation, gold(I) cyclopropane adduct **1.12** formed daughter ions with *m*/*z* = 545 and 559, assigned as methoxy- and ethoxymethylidene gold(I) carbene complexes (**1.13**), respectively (Scheme 7). Based on the principle of microscopic reversibility, which says that the mechanism of a forward process is the same in reverse, this work provided insight into the mechanism of gold(I) carbene transfer to form cyclopropanes. The observed formation of cationic gold(I) carbene complexes **1.13**, alone does not constitute enough

evidence to propose a mechanism, and to help better understand how the mechanisms by which ring opening occurred, computational analysis was utilized.

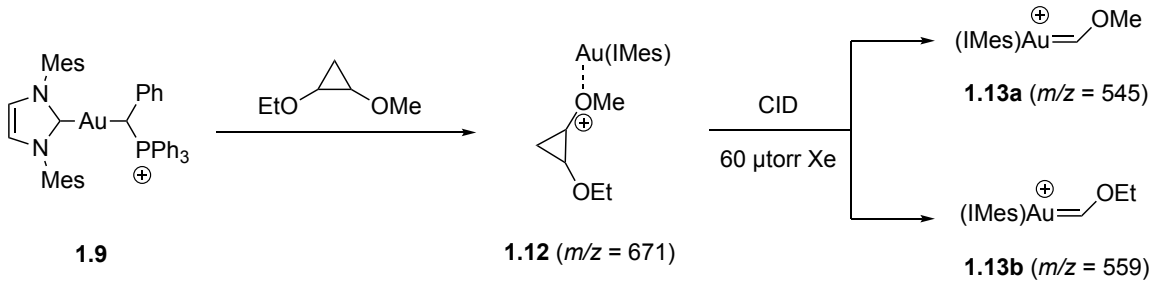

1.9 **1.12** (*m/z* = 671) **1.13a** (*m/z* = 545) **1.13b** (*m/z* = 559)

Scheme 7. Gold(I) cyclopropane adduct formation followed by ring opening to form gold(I) carbene complexes.

Density functional theory (DFT) analysis of the conversion gold(I) cyclopropane adduct **1.14** to cationic gold(I) carbene complex **1.13a** were performed, revealing Au–O bounded complex **1.14** as an energy minimum. In the transformation of complex **1.14** to cationic gold(I) carbene complex **1.13a**, computational analysis revealed local energy minima corresponding to resonance stabilized carbocations **1.15** and **1.16**. The barrier for cation **1.16** to form gold(I) adduct **1.17** is low, which releases cationic gold(I) carbene complex **1.13a** upon alkene dissociation (Figure 5). These calculations are in accord with the proposed stepwise mechanism for cyclopropane formation from electron-rich alkenes and cationic gold(I) carbene complexes.

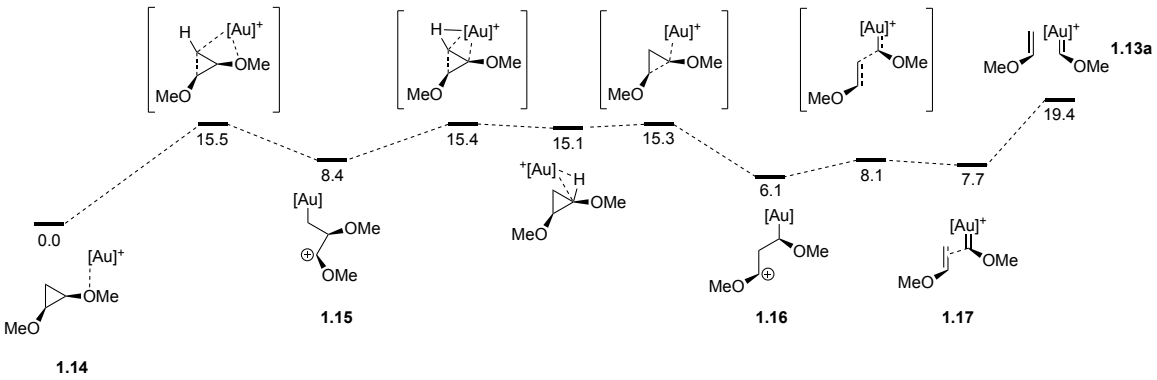

Figure 5. Energy diagram for gold(I) mediated cyclopropane ring open to form cationic gold(I) carbene complex **1.13a.**

To probe this mechanism experimentally, Gronert has employed a similar methodology to that reported by Chen. Ionization of gold(I) carbenoid complex **1.18** in the gas phase led to the formation of gold(I) benzylidene **1.19**, which readily reacted with a variety of electron-rich and electron-neutral alkenes, but did not form cyclopropane products with electron deficient alkenes (Scheme 8).[44] To gain further insight into the mechanism, a linear free energy relationship was established for the reaction of cationic gold(I) benzylidene complex **1.19** with a variety of *p*-substituted styrene derivatives. A Hammett analysis showed a good correlation between the rate of reaction and Hammett σ parameters, with the slope giving ρ = –0.9, suggesting little positive charge build on the alkene during cyclopropanation. However, the low magnitude of the rho value makes it challenging to make definitive claims regarding charge build up in gold(I) carbene transfer.

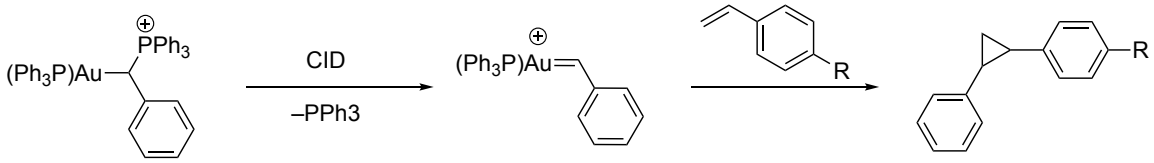

1.18 **1.19**

Scheme 8. Gas-phase cyclopropanation of gold(I) benzylidene complex **1.19** with *p*-substituted styrene derivates.

These gas-phase studies have allowed for the direct observation of cationic gold(I) complexes that undergo carbene transfer. The ease of generation and relative simplicity of the cationic gold(I) carbene complexes discussed above have allowed for some mechanistic studies of gold(I) carbene transfer, with the caveat being that these reactions are performed in the gas-phase, which is likely distinct from solution-phase gold(I) carbene transfer. To develop a more complete picture of the mechanism of gold(I) carbene transfer, methods must be developed to perform kinetic and mechanistic analysis of gold(I) carbene transfer in a condensed phase.

1.3.3. Solution-phase gold(I) carbene transfer

Challenges to performing such analysis in the solution phase lie in the generation of cationic gold(I) carbene complexes that (1) undergo carbene transfer reactions and (2) are generated under conditions that facilitate mechanistic analysis. Recently, a number of cationic gold(I) carbene complexes have been synthesized that undergo carbene transfer to alkenes to form cyclopropanes, but many are highly stabilized gold(I) carbenes with multiple electron donating groups, or are generated under cryogenic conditions by Lewis acid abstraction of a leaving group (Figure 6).[45-47] Ideal candidates for mechanistic studies are complexes that are isolable, that can therefore be well characterized, and that generate cationic gold(I) carbene complexes under mild conditions, making analysis of carbene transfer reactions more straightforward.

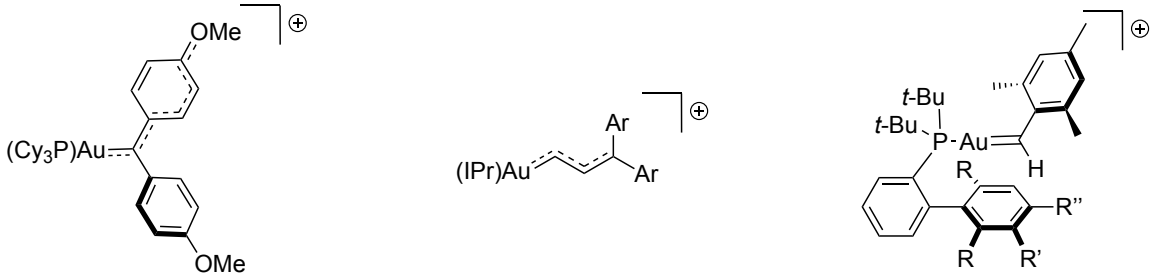

1.20 **1.21** **1.23**

Figure 6. Cationic gold(I) carbene complexes known to undergo carbene transfer with alkenes.

Towards this goal, in 2013, Chen reported the design and synthesis of isolable gold(I) carbenoid complex **1.24a** (Figure 7). Electrospray ionization of gold(I) carbenoid **1.24a** revealed a molecular ion with *m*/*z* 706 which corresponds to mass of cationic gold(I) carbene complex **1.25a** (Scheme 9). In contrast to previous gold(I) carbenoid precursors synthesized by Chen, when gold(I) carbenoid complex **1.24a** was heated in the presence of excess *p*-methoxystyrene at 120 °C, 1,2-bis(*p*-methoxyphenyl)cyclopropane was formed in 99% yield, confirming the formation of cationic gold(I) carbene complex **1.25a** from the decomposition of gold(I) carbenoid complex **1.24a**, likely driven by the irreversible loss of SO_2 gas (Scheme 9). This gold(I) carbenoid complex represented one of the first examples of the gold(I) carbenoid complex that could form a cationic gold(I) carbene complex without Lewis acid activation.

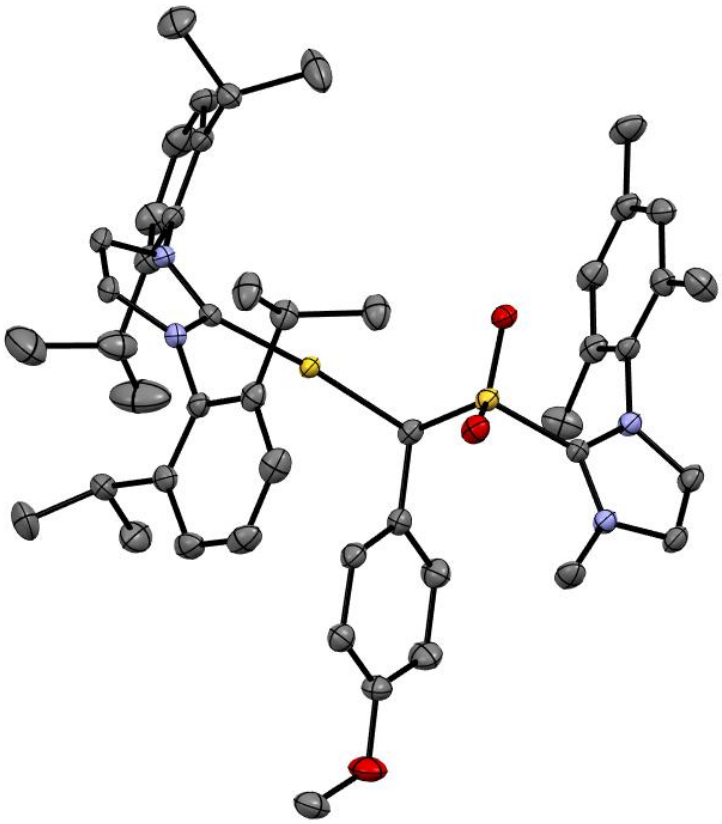

Figure 7. ORTEP diagram of gold(I) carbenoid complex **1.24a** with thermal ellipsoids shown at 50% probability level with counterion and hydrogen atoms omitted.

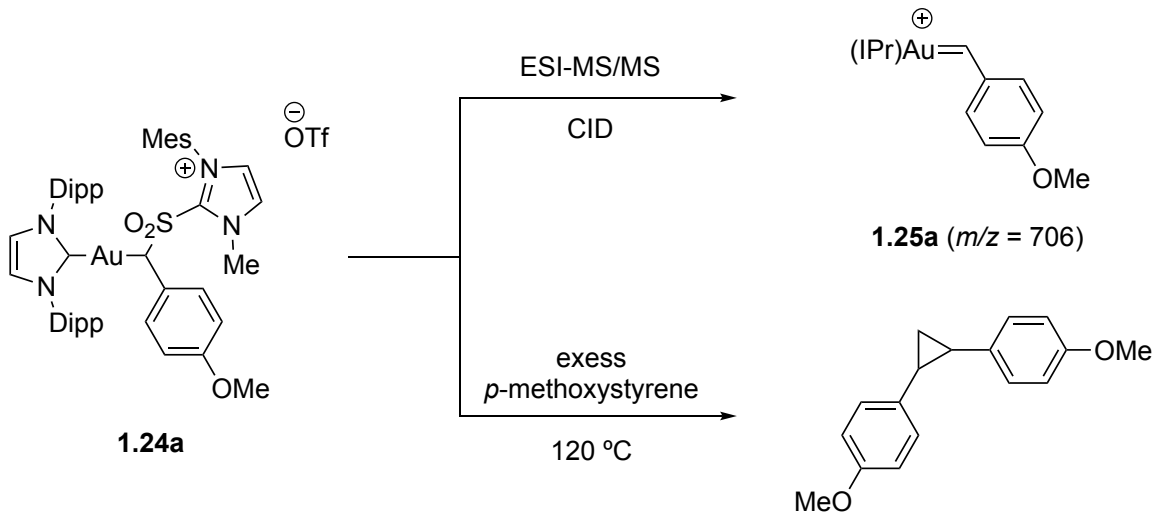

Scheme 9. Generation of cationic gold(I) carbene complex **1.25a** from ionization of gold(I) carbenoid complex **1.24a** and subsequent cyclopropanation.

In a follow-up study based on their initial proof of concept, Chen reported the synthesis of a series of gold(I) carbenoid complexes **1.24** with varied ligand on gold and C1 aryl group.[48] In accord with their previous findings, upon ionization in the gas-phase each of the gold(I) carbenoid complexes **1.24** showed the formation of gold(I) benzylidene complexes **1.25** (Scheme 10). DFT analysis of the ionization showed a range of E_0 values (46.6 kcal/mol for **1.24a**, 49.6 kcal/mol for **1.24b,** 48.9 kcal/mol for **1.24c**) for gold(I) benzylidene complexes **1.25** formation from gold(I) carbenoid precursors **1.24**.

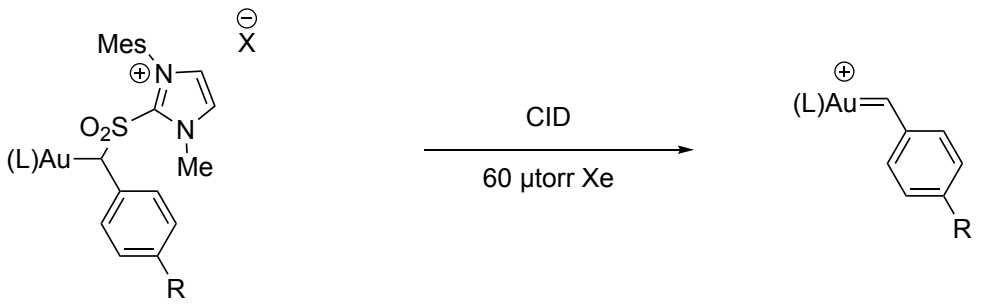

1.24a (L = IPr, R = OMe, X = OTf)
1.24b (L = IPr, R = H, X = OTf)
1.24c (L = JohnPhos, R = OMe, X = SbF_6)

1.25a (L = IPr, R = OMe)
1.25b (L = IPr, R = H)
1.25c (L = JohnPhos, R = OMe)

Scheme 10. Generation of cationic gold(I) carbene complexes **1.25** by ionization of gold(I) carbenoid complex **1.24**

Gold(I) carbenoid complex **1.24a** had been previously reported to undergo cyclopropanation in the solution phase, forming 1,2-bis(*p*-methoxyphenyl)cyclopropane in excellent yield in the presence of excess *p*-methoxystyrene at 120 °C. Treatment of gold(I) carbenoid complexes **1.24b-c** under the same conditions, led to the formation of cyclopropane products in 5 and 80% yield, respectively. Kinetic analysis of the reaction of gold(I) carbenoid **1.24a** in the presence of excess *p*-methoxystrene revealed a first-order dependence in cationic gold(I) carbenoid **1.24a** ($t_{1/2}$ = 5.5–7 min) and a pseudo-first-order dependence for the formation of cyclopropane (k_{obs} = 0.19 – 1.99 $\times 10^{-3}$ s^{-1}). Upon heating gold(I) carbenoid complex **1.24b** for 97 h at 120 °C, small amounts of starting material were observed as well as substantial amounts of benzyl imidazolium sulfone salt. Under similar conditions, gold(I) carbenoid complex **1.24c** completely decomposed

after only 3 h. These results suggest that gold(I) carbene formation from **1.24b-c** occurs, but due to high activation barriers, other decomposition pathways become active, explaining the lower yields for cyclopropanation reactions with gold(I) carbene complexes **1.25b-c** compared to complex **1.25a**.

These results presented by Chen are consistent with the intermediacy of gold(I) benzylidene complexes, but require forcing conditions as well as stabilization of the gold(I) benzylidene by a *p*-methoxy group, as evidenced by the low yield for the cyclopropanation reactions involving **1.24b**, likely due to the high activation energy to form appreciable concentrations of gold(I) benzylidene complex **1.25b** in solution. This represents an experimental challenge to performing key kinetic and mechanistic experiments required to obtain a more complete picture of the mechanism of gold(I) carbene transfer. These challenges can be overcome by utilizing gold(I) carbene complexes that are either (1) isolable or (2) can be generated *in situ* in solution under mild conditions.

In 2014, Fürstner reported the synthesis and isolation of cationic gold(I) carbene complex **1.20**. Analysis of the structure of cationic gold(I) carbene complex **1.20** revealed similarities with *p*-methoxylphenyl substituted trityl cations, suggesting that cationic gold(I) carbene complex **1.20** may be better defined as a gold(I)-stabilized carbocation (Figure 8). To examine the reactivity of cationic gold(I) carbene complex **1.20**, a solution

of complex **1.20** was treated with *p*-methoxystyrene at –78 °C. Upon warming to –20 °C, cationic gold(I) carbene complex **1.20** started to react and upon reaching 25 °C, GC analysis revealed the formation of 1,1,2-tris(*p*-methoxyphenyl)cyclopropane in 95% yield, confirming the ability of complex **1.20** to undergo gold(I) carbene transfer.

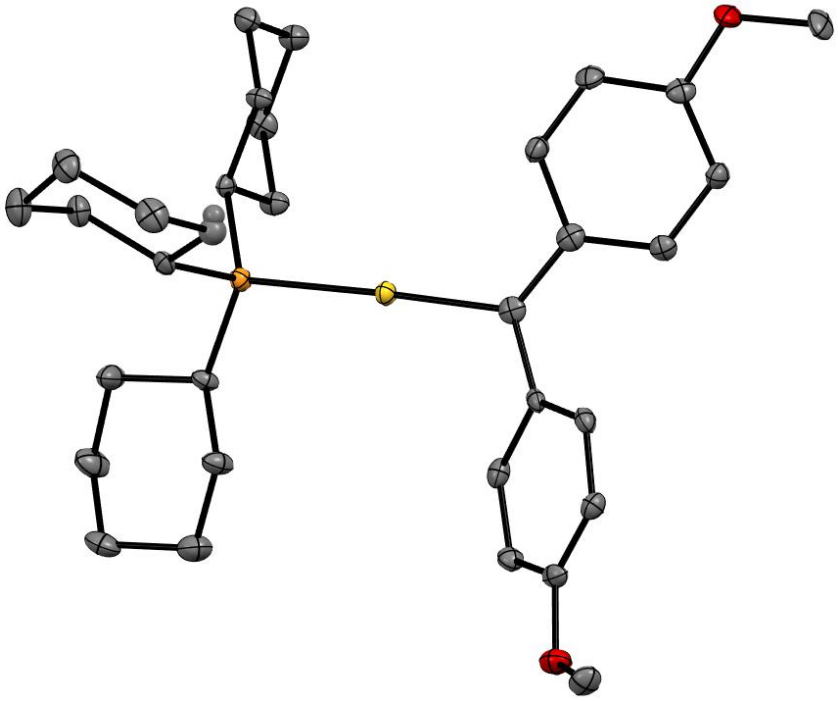

Figure 8. ORTEP diagram of gold(I) carbenoid complex **1.20** with thermal ellipsoids shown at 50% probability level with counterion and hydrogen atoms omitted.

While a promising example of stoichiometric gold(I) carbene transfer, cationic gold(I) carbene complex **1.20** exhibits extensive positive charge stabilization from the *p*-methoxyphenyl groups, which fails to mimic the structure of proposed gold(I) carbene intermediates in gold(I)-catalyzed reactions, many of which contain simple alkyl and phenyl substitution. A currently unmet challenge is the generation of simple, well-defined gold(I) benzylidene complexes that undergo gold(I) carbene transfer.

To address this challenge, we have recently reported the synthesis of α-sulfonium gold(I) benzylide complexes that generate a gold(I) benzylidene in solution that undergoes gold(I) carbene transfer with alkenes and DMSO to form cyclopropanes and aldehydes, respectively (Scheme 11). Complete details on our findings can be found in the following chapter, but key kinetic and mechanistic experiments of the gold(I) benzylidene transfer suggest that gold(I) carbene transfer occurs in a concerted manner, with retention of the original stereochemistry of the alkene. This work represents the first experimental study on kinetics of simple gold(I) benzylidenes in the solution phase and provides a platform with which further mechanistic information can be gleaned, including the effect of supporting ligand and the electronic demands of the gold(I) carbene transfer.

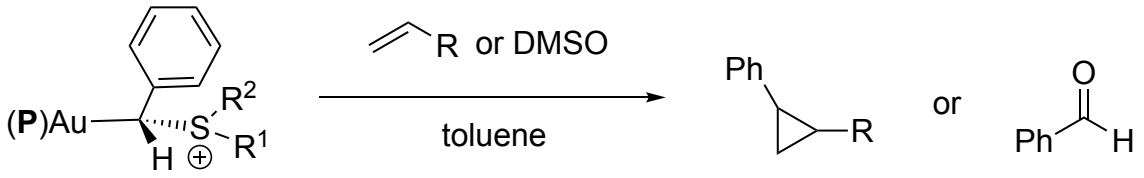

1.26

Scheme 11. Gold(I) benzylide complexes undergo carbene transfer under mild conditions.

1.4 Summary and Outlook

Since their discovery as active catalysts, cationic gold(I) complexes have been shown to facilitate a wide array of transformations. While these new reactivities have been discovered, a more complete understanding of the mechanisms of these transformations has not yet been realized. Initial attempts to understand the mechanisms by which cationic gold(I) complexes achieve such a wide array of reactivities have focused on information gained from product ratios and reaction stereoselectivity. More recently, efforts have been put forth to gain information from thorough kinetic and mechanistic analysis as well as the interrogation of both structural and chemical properties of reactive intermediate analogues.

Even with the increased interest in a mechanistic analysis of gold(I)-catalyzed reactions, few of the proposed model systems allow for the direct analysis of gold(I) carbene transfer in the solution phase. There have been a number of studies on gold(I) carbene transfer in the gas phase, but it is unclear whether the findings from these studies translate to the solution-phase reactivity of cationic gold(I) carbene complexes. Herein is presented a new model system for the kinetic and mechanistic analysis of gold(I) carbene transfer that addresses challenges presented by current systems including (1) the ease of gold(I) carbene complex generation and (2) the range of reactivities of generation gold(I) carbene complex.

Since initial reports of the synthesis of cationic gold(I) carbene complexes, there has been a recent push for the synthesis of cationic gold(I) carbene complexes lacking heteroatom stabilization. Such complexes more accurately mimic the structure and reactivities of proposed intermediates in gold(I)-catalyzed reactions, and therefore will provide further insight into the structure of such proposed intermediates. Herein are presented the results of such a study examining the effect of ligand donor ability in cationic gold(I) vinylidene complexes.

Beyond gold(I) carbene transfer, one of the most common reactions of gold(I) catalysts are gold(I)-catalyzed hydrofunctionalizaiton reactions. Few rigorous mechanistic studies of these reactions have been reported. Herein is reported a kinetic and mechanistic analysis of both the gold(I)-catalyzed hydroalkoxylation and gold(I)-catalyzed hydroamination of allenes.

2. Synthesis and Reactivity of Gold(I) Sulfonium Benzylide Complexes

Portions of this chapter have been submitted of publication to *Chem. Eur. J.*

2.1 Background

Of the various reactions attributed to cationic gold carbene intermediates,[11,34-36,49-62] perhaps none is more prevalent than alkene cyclopropanation and related carbene transfer processes.[11] Although carbene transfer reactions are certainly not unique to gold,[54-58,60,61,63-68] the particular properties of gold including high *d*-electron count and electronegativity,[69,70] poor d $\rightarrow$ π back bonding,[21] and the formation of stable π-complexes[71-73] likely render the mechanisms of gold to alkene carbene transfer distinct from other transition metals.[54-58,60,61,63-66,68] However, our understanding of the mechanisms of gold(I) to alkene carbene transfer is largely restricted to information gleaned from indirect experimental observations, such as the product ratios and stereoselectivity of catalytic reactions,[37,74] from gas-phase reactions,[42-44,48,75,76] and from computational analyses.[37,43,48,74-76] As such, many gaps remain in our understanding of the mechanisms of the carbene transfer processes of gold including control of stereoselectivity, the nature of C–C bond formation, and the involvement of carbocationic and/or metallacyclobutane intermediates.[11,37,43,74-76]

Largely absent from the discussion of the mechanisms of gold to alkene carbene transfer are the potential insights gained from analysis of carbene transfer processes

from well-defined carbene complexes in the condensed phase.[11,62] Recent efforts in this area have led to identification of a small number of well-defined gold carbene complexes that undergo carbene transfer to alkenes (Figure 9).[45,46,77,78] However, extracting detailed mechanistic information relevant to catalysis from these stoichiometric carbene transfer processes is complicated by the (1) excessive stabilization of the carbene complex, (2) *in situ* generation of the carbene complex with strong Lewis acids under cryogenic conditions, and/or (3) the extreme facility of carbene transfer.[45-47,77]

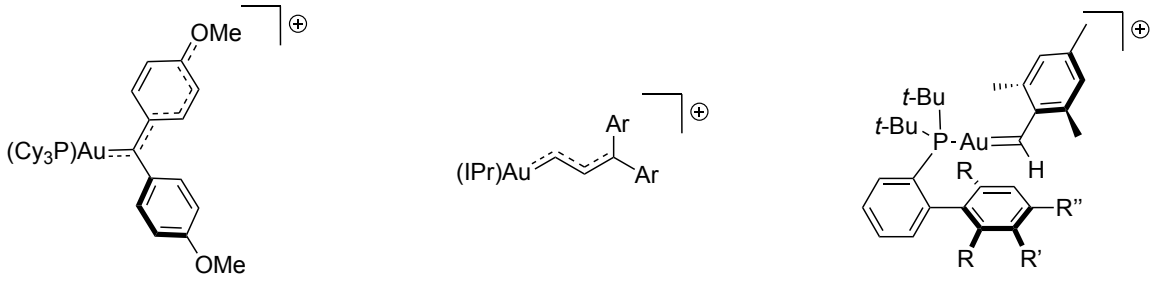

2.1 **2.2** **2.3**

Figure 9. Known gold(I) carbenes that undergo carbene transfer to alkenes (Ar = *p*-(MeO)C_6H_5)

As an alternative to free gold carbene complexes, we sought to identify gold carbenoid complexes that would spontaneously and reversibly generate reactive gold carbene complexes in solution under mild conditions,[36] thereby allowing kinetic and mechanistic analysis of carbene transfer processes from otherwise inaccessible gold

carbene complexes. Although a small number of gold(I) carbenoid complexes that undergo carbene transfer to alkenes have been identified (Figure 10),[42-44,79] only imidazolium sulfonyl complex **2.6** does so in solution without Lewis acid activation.[48,67,76,80-92] However carbene transfer from **2.6** requires forcing conditions and a stabilizing C1 anisyl group for spontaneous activation and undergoes irreversible carbene formation, all of which would complicate kinetic and mechanistic analysis of carbene transfer.

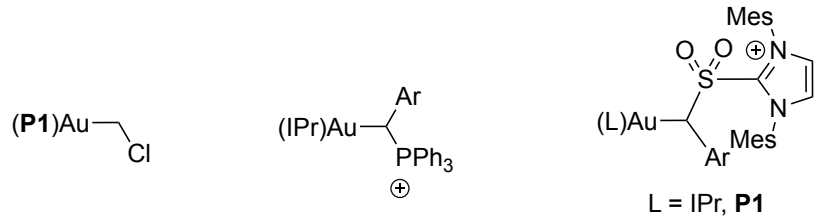

2.4 **2.5** **2.6**

Figure 10. Known gold(I) carbenoid complexes that undergo transfer to alkenes after activation.

Here we report the synthesis of thermally stable gold sulfonium benzylide complexes that undergo benzylidene transfer to alkenes under mild conditions without activation via the intermediacy of an unstabilized gold benzylidene complex.

2.2 Synthesis of gold(I) sulfonium benzylide complexes

Inspired by the facile alkylidene transfer reactions of iron sulfonium ylide complexes,[93-97] and the generation of well-defined Rh, Os, and Ru benzylidene complexes from sulfonium benzylides,[98] we targeted gold sulfonium benzylide complexes of the form $[(L)AuCHPh(SR^1R^2)]^+$ as potential carbene transfer reagents.[78,99-106] Initial efforts to synthesize gold sulfonium benzylide complexes via S-alkylation of gold α-thiobenzyl complexes[91,93-97] or through ligand displacement with sulfonium benzylides[98] proved unsuccessful. However, a third approach involving nucleophilic substitution of a gold α-chlorobenzyl carbenoid complex with sulfide, which was modelled after similar transformations reported by Steinborn[91] and Echavarren,[79] proved effective. In an optimized procedure, treatment of (**P1**)AuCHClPh[24] [**P1** = P(*t*-Bu)$_2$-*o*-biphenyl] with sodium tetrakis[3,5-bis(trifluoromethyl)phenyl]borate ($NaBAr^F{}_4$; 1.1 equiv) and excess tetrahydrothiophene (THT; 10 equiv) in toluene at room temperature led to isolation of the gold (tetramethylene)sulfonium benzylide complex $[(\mathbf{P1})AuCHPh(THT)]^+ BAr^F{}_4{}^-$ (**2.7a**) in 68% yield after crystallization (Scheme 12). The ethylphenylsulfonium benzylide complex **2.7b** and diphenylsulfonium benzylide complex **2.7c** were isolated employing similar procedures. Complexes **2.7** were stable indefinitely in the solid state at room temperature and complexes **2.7a** and **2.7b**

displayed no detectable decomposition in solution after 24 h at room temperature, whereas **2.7c** decomposed slowly ($t_{1/2}$ = ~7 h) under these conditions.

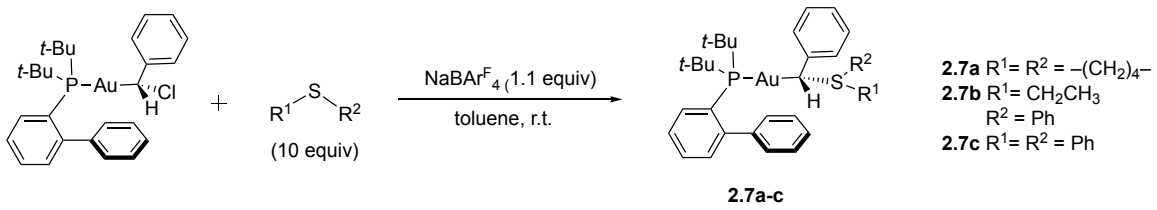

Scheme 12. Synthesis of gold benzylide complexes **2.7**

Gold sulfonium benzylide complexes **2.7** were characterized by NMR spectroscopy and X-ray crystallography (Figures 11–13, Table 2). Complexes **2.7** displayed diagnostic phosphorous-coupled doublets in both the ^{1}H (δ 2.28 - δ 3.75, $J_{PH} \approx$ 6 Hz) and ^{13}C (δ 62.7 - δ 66.6, $J_{PC} \approx$ 85 Hz) NMR spectra assigned to the benzylic proton and carbon atom, respectively. In the solid state, complexes **2.7** adopt slightly distorted linear conformations with P–Au–C angles ranging from 171 - 175° (Figures 11–13, Table 2). The benzylic carbon atom adopts a distorted sp^3 geometry with a larger Au–C1–C2 angle (113-117°) and a smaller Au–C1–S angle (101-106°).

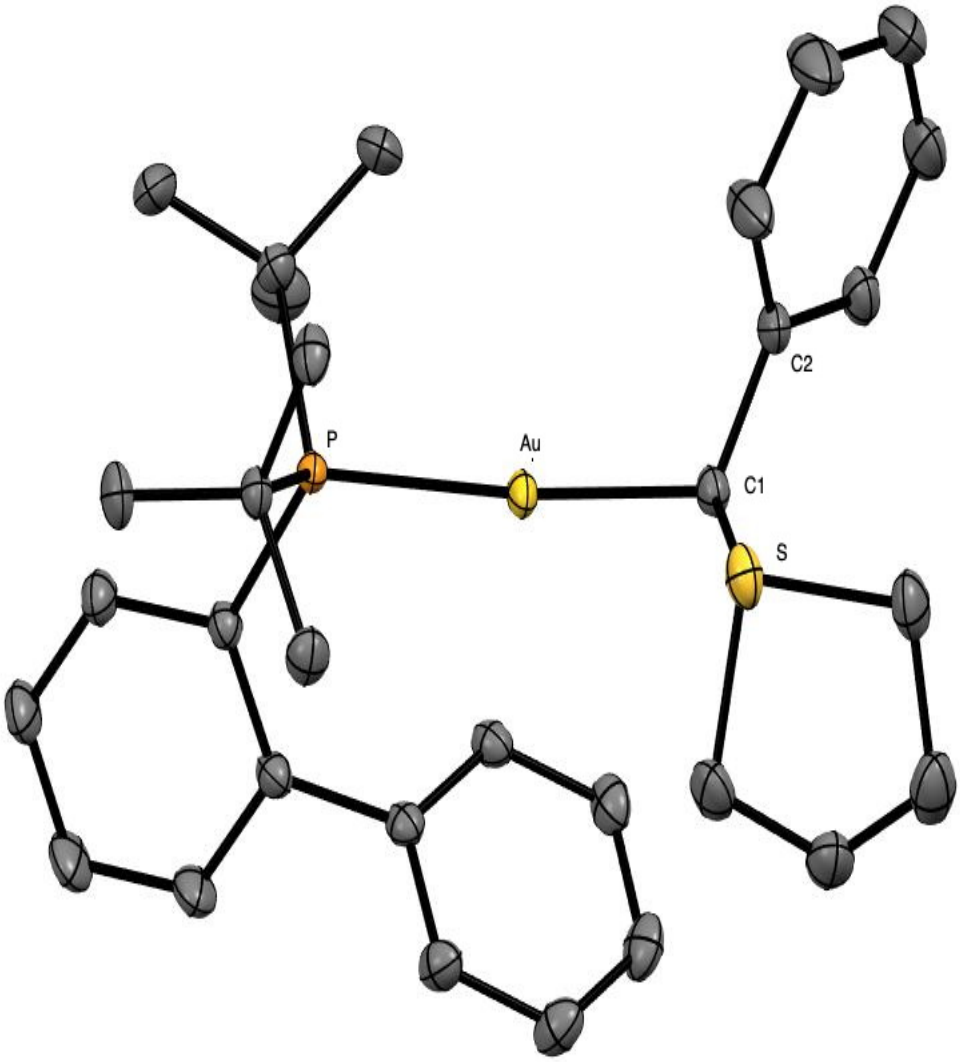

Figure 11. ORTEP diagram of gold benzylide complex **2.7a** with ellipsoids shown at 50% probability level and with counterion, solvent and hydrogen atoms omitted.

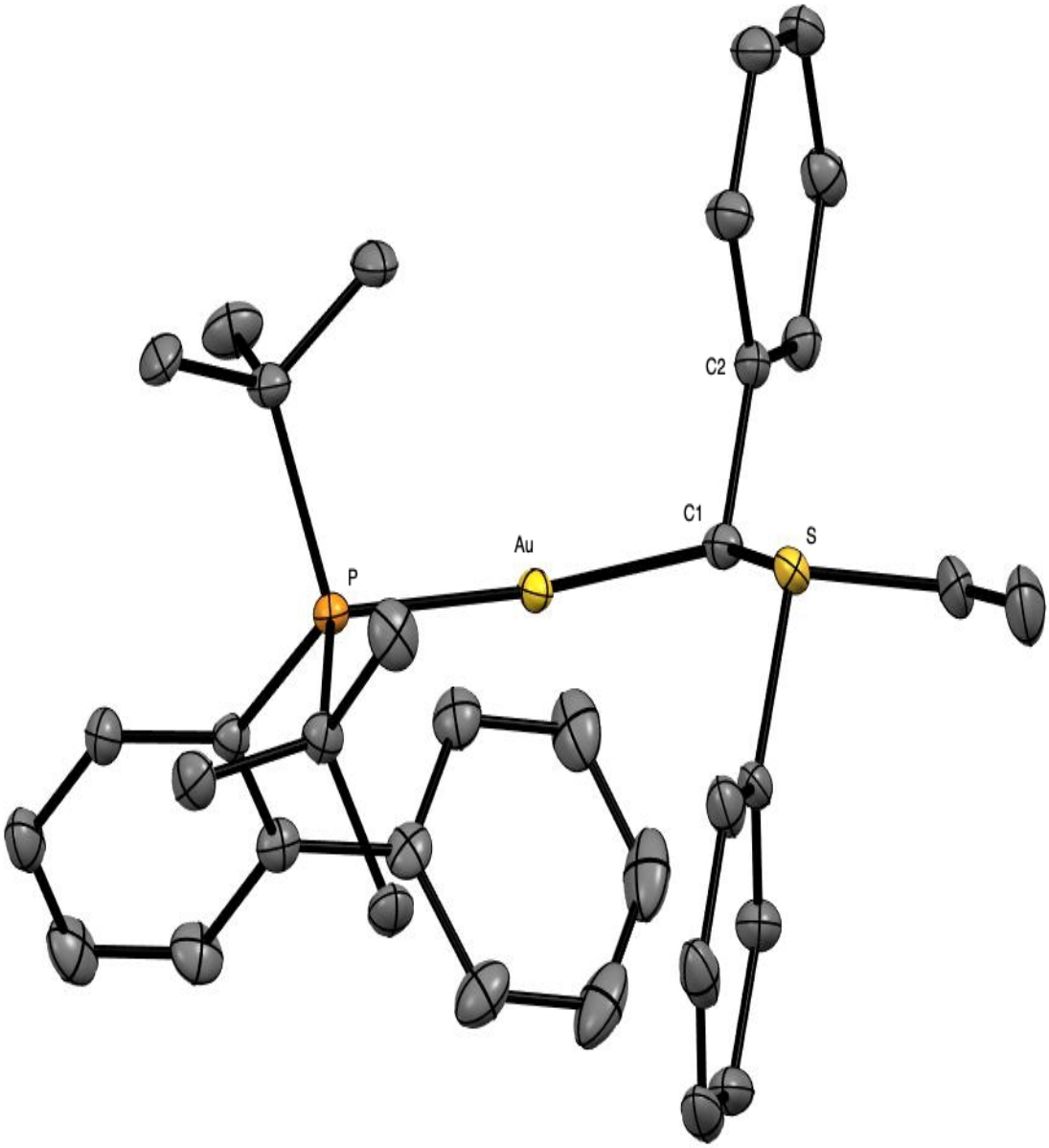

Figure 12. ORTEP diagram of gold benzylide complex (S*,R*)-**2.7b** with ellipsoids shown at 50% probability level and with counterion, solvent and hydrogen atoms omitted.

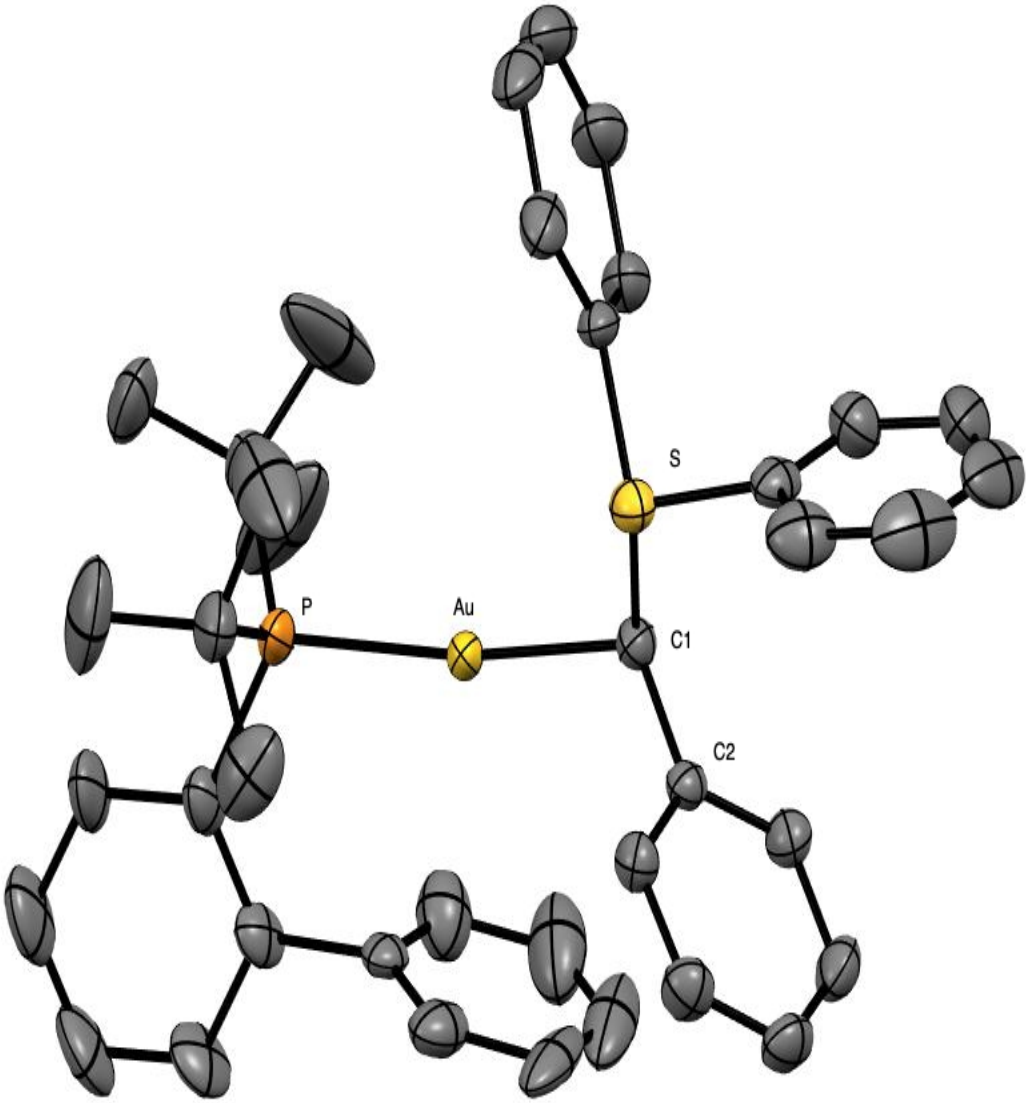

Figure 13. ORTEP diagram of gold benzylide complex **2.7c** with ellipsoids shown at 50% probability level and with counterion, solvent and hydrogen atoms omitted.

Table 2. Selected bond lengths (Å) and angles (deg) for **2.7a**, (S*,R*)-**2.7b**, and **2.7c**

	2.7a	(*S*,R**)-**2.7b**	**2.7c**
P–Au	2.2920(6)	2.294(1)	2.298(1)
Au–C1	2.096(2)	2.095(4)	2.125(2)
C1–S	1.796(2)	1.787(4)	1.813(3)
C1–C2	1.507(3)	1.513(4)	1.513(3)
P–Au–C1	174.63(6)	171.9(1)	171.37(8)
Au–C1–S	105.3(1)	106.3(2)	101.5(1)
Au–C1–C2	116.6(1)	113.3(2)	116.5(2)
S–C1–C2	114.6(2)	108.0(2)	104.1(2)

2.3 Reactivity of gold(I) sulfonium benzylide complexes

2.3.1 Sulfide Exchange

With complexes **2.7** in hand, we then turned our interest to determining their reactivity with different nucleophiles, including sulfides, oxygen atom donors, and alkenes. Complex **2.7b**, which contains a stereogenic sulfur atom, crystallized exclusively as the *S*,R** diastereomer [(*S*,R**)-**2.7b**] (Figure 12), but isomerized in toluene-d_8 at 25 °C ($t_{1/2}$ = 25 min) to form an equilibrium 2.5:1 mixture of (*S*,R**)-**2.7b** and (*S*,S**)-**2.7b** (Scheme 13). Kinetic analysis of the conversion of (*S*,R**)-**2.7b** to (*S*,S**)-**2.7b** established first-order approach to equilibrium with forward and reverse rate constants $k_f = 1.33 \pm 0.15 \times 10^{-4}$ s^{-1} and $k_r = 3.3 \pm 0.4 \times 10^{-4}$ s^{-1}.

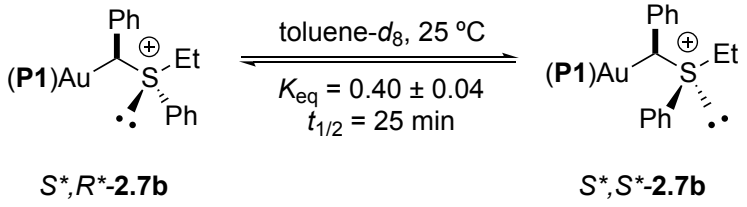

Scheme 13. Isomerization of **2.7b** in toluene-d_8 at 25 °C.

Periodic analysis of an equimolar solution of (*S*,R**)-**2.7b** and THT (13 mM) revealed that isomerization of (*S*,R**)-**2.7b** was not significantly inhibited by THT (k_f = $1.4 \pm 0.20 \times 10^{-4}$ s^{-1}) and was ~5 times faster than was conversion of **2.7b** to **2.7a** (k_{obs} = 2.8

$\pm 0.5 \times 10^{-5}$ s^{-1}). These observations argue against isomerization of (*S*,R**)-**2.7b** via a dissociation/reassociation pathway and instead point to isomerization via inversion at sulfur.[107-114]

Treatment of **2.7c** (15 mM) with THT (15 mM) led to the formation of **2.7a**, but kinetic analysis showed the reaction was second order, suggesting a direct nucleophilic displacement via an S_N2 pathway, rather than through a carbene intermediate. We surmised that reaction with a less nucleophilic sulfide would lead to sulfide exchange through a carbene intermediate. Indeed, a reaction of **2.7c** (13 mM) with S(*p*-tol)$_2$ (15 mM) led to the formation of a mixture of **2.7c** and **2.7d** with K_{eq} = 18.29 and $t_{1/2}$ = 10 min (Scheme 14). Kinetic analysis of the reaction established a first-order approach to equilibrium with forward and reverse rate constants of $k_f = 1.11 \times 10^{-2}$ s^{-1} and $k_r = 6.11 \times 10^{-4}$ s^{-1}.

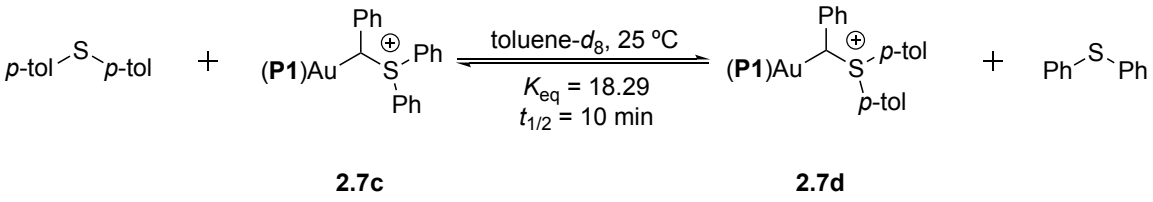

Scheme 14. Equilibrium for the conversion of **2.7c** to **2.7d**

2.3.1 Benzylidene Transfer Reactions

Treatment of sulfonium benzylide complex **2.7a** (32 mM) with excess *p*-methoxystyrene (**2.8**; 10 equiv) at 75 °C led to first-order decay ($t_{1/2}$ = 51 min) to form 1-phenyl-2-anisylcyclopropane in 95% yield (^{1}H NMR) as a 6:1 mixture of *cis*/*trans* diastereomers and the gold THT complex [(**P1**)Au(THT)]$^+$ in quantitative yield (Table 3, entry 1). In a similar manner, treatment of **2.7a** with excess DMSO at 75 °C led to first-order decay ($t_{1/2}$ = 95 min) to form benzaldehyde in 75% yield and a mixture of gold THT and dimethylsulfide complexes (Table 3, entry 4). The reactivity of gold sulfonium benzylide complexes **2.7** toward both **2.8** and DMSO increased significantly in the order **2.7a** < **2.7b** < **2.7c** (Table 3, entries 2, 3, 5, and 6),[115][34] such that the reactions of **2.7c** with **2.8** and DMSO were complete within ~2 min at 25 °C (Table 3, entries 3 and 6). Owing to the high reactivity of **2.7c** toward **2.8**, we considered that **2.7c** might likewise undergo benzylidene transfer to less reactive alkenes. Indeed, **2.7c** reacted efficiently with styrene, norbornene, cyclohexene, and 1-hexene at room temperature within 5 min to form the corresponding cyclopropanes in good yield (Table 3, entries 7-10).

Table 3. Reactions of gold carbenoid sulfonium benzylide complexes **2.7** (12 -32 mM) with alkenes and DMSO (10 equiv) in toluene-d_8

Entry	Complex	Nucleophile	Product[a]	Temp (°C)/ $t_{1/2}$ (min)	Yield (%)/ d.r.
1[b]	**2.7a**	**2.8**		75/51[c]	96/6:1[d]
2[e]	**2.7b**	**2.8**		40/29[c]	95/6:1[d]
3[f]	**2.7c**	**2.8**		25/0.7[c]	87/6:1[d]
4[b]	**2.7a**	DMSO	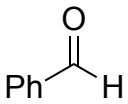	75/95[c]	78/–[d]
5[e]	**2.7b**	DMSO		40/29[c]	65/–[d]
6[f]	**2.7c**	DMSO		25/≤2[h]	65/–[d]
7[f]	**2.7c**	styrene		25/0.7[c]	82/≥20:1[d]
8[g]	**2.7c**	norbornene	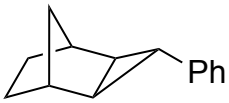	25/≤2[h]	67/2:1[d]
9[f]	**2.7c**	Cyclohexene	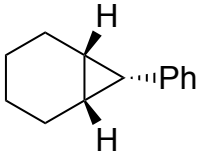	25/≤2[h]	79/4:1[i]
10[f]	**2.7c**	1-hexene	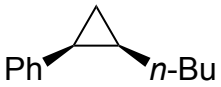	25/≤2[h]	76/3:1[i]

[a] Major diastereomer depicted. [b] [Nuc] = 0.32 M. [c] Reaction displayed pseudo first-order kinetics to ≥3 half-lives. [d] Yield and d.r. determined by ^{1}H NMR versus internal standard. [e] [Nuc] = 0.22 M. [f] [Nuc] = 0.15 M. [g] [Nuc] = 0.20 M. [h] Estimated half-life. [i] Yield and d.r. determined by GC analysis versus internal standard.

2.4 Mechanistic Analysis of Gold(I) Benzylidene Transfer

2.4.1 Potential Mechanisms

Reactions of sulfonium benzylide complexes **2.7** with alkenes could occur by two potential mechanisms, (1) a concerted, direct attack of the alkene nucleophile on complex **2.7** (Figure 14A) or (2) attack on a carbene intermediate **I** arising from reversible sulfide loss from **2.7** (Figure 14B).

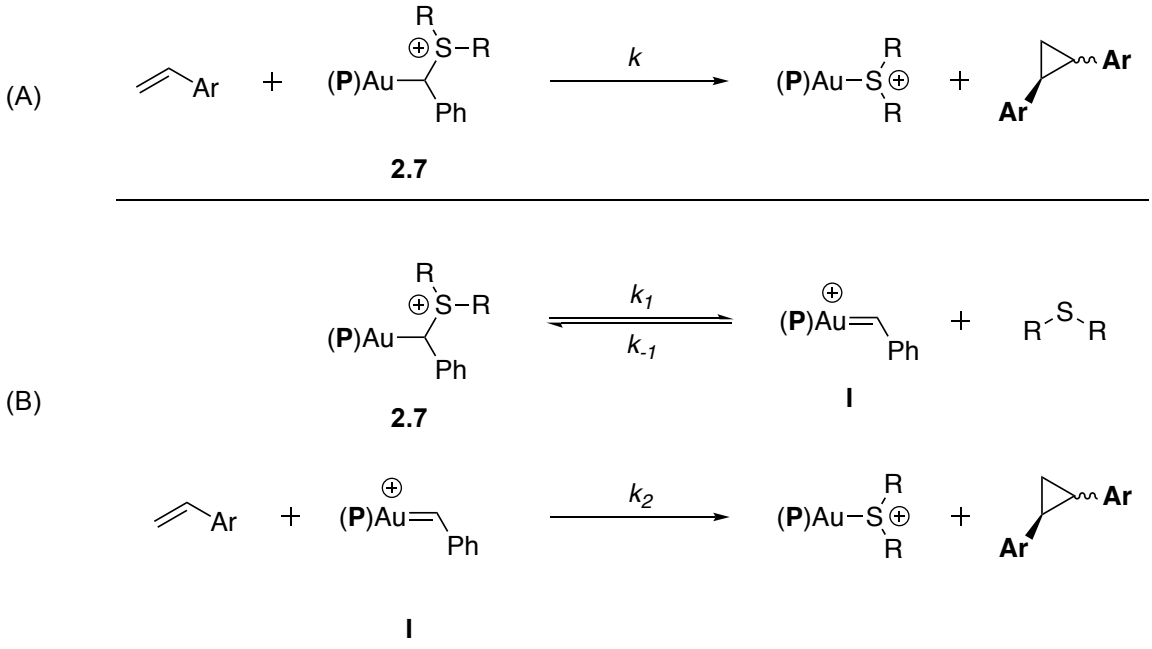

Figure 14. Potential mechanism for carbene transfer of **2.7** to alkenes

2.4.2 Kinetic Experiments

To probe the mechanism of benzylidene transfer from sulfonium benzylide complexes **2.7**, we studied the kinetics of the reaction of **2.7c** with styrene in toluene-d_8 at 25 °C employing ^{1}H NMR spectroscopy. To this end, pseudo-first-order rate constants for the reaction of **2.7c** (16 mM) with styrene were determined as a function of [styrene] (0 - 1.53 M) at constant [Ph_2S] (150 mM) and as a function of [Ph_2S] (0 - 610 mM) at constant [styrene] (150 mM). A plot of k_{obs} versus [styrene] at constant [Ph_2S] established the positive, non-integer dependence of the rate on [styrene], while a plot of k_{obs} versus [Ph_2S] at constant, excess [styrene] established the negative, non-integer dependence of the rate on [Ph_2S] (Figure 15).

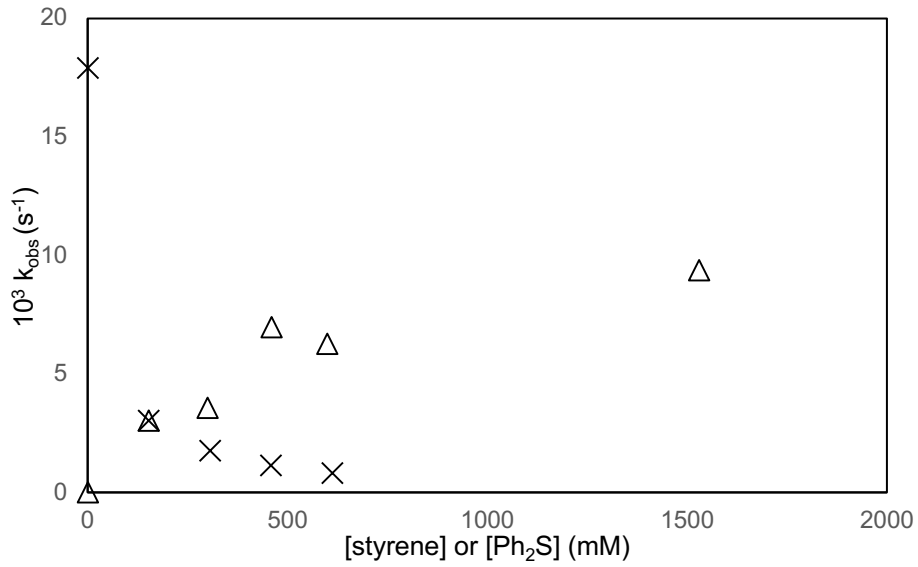

Figure 15. First order rate constants (k_{obs}) versus [styrene] (Δ) and [Ph_2S] (×).

Inhibition of the rate of reaction of **2.7c** with styrene by Ph_2S rules out mechanisms for benzylidene transfer involving either direct attack of styrene on **2.7c** or irreversible loss of Ph_2S from **2.7c**, both of which would display zero-order rate dependence on [Ph_2S]. Rather, our kinetic data are consistent with a mechanism involving reversible generation of gold benzylidene complex **I** followed by irreversible carbene transfer to styrene (Figure 14B). Steady state treatment of intermediate **I** produces rate equation 1, which is of the same form as the experimentally determined rate law. Under conditions of constant [Ph_2S] and [styrene], rate equation 2 can be expressed as: rate = k_{obs}[**2.7c**] with k_{obs} defined by eq 2 and $1/k_{obs}$ defined by eq 3. In accord with this latter relationship, a plot of $1/k_{obs}$ versus [Ph_2S]/[styrene] was linear, which provided the values $k_1 = 1.3 \pm 0.4 \times 10^{-2}$ s^{-1} ($\Delta G^{\ddagger} = 20.0 \pm 0.2$ kcal/mol) and $k_{-1}/k_2 = 3.5 \pm 1.1$ (Figure 16). The former value corresponds to the first-order rate constant for dissociation of Ph_2S from **2.7c** while the latter value corresponds to the relative kinetic affinities of Ph_2S and styrene toward benzylidene intermediate **I**.

$$\text{rate} = \frac{k_1 k_2[\mathbf{2.7c}][\text{styrene}]}{k_{-1}[Ph_2S] + k_2[\text{styrene}]} \qquad \text{(eq 1)}$$

$$\text{rate} = k_{obs}[\mathbf{2.7c}], \text{ where } k_{obs} = \frac{k_1 k_2[\text{styrene}]}{k_{-1}[Ph_2S] + k_2[\text{styrene}]} \qquad \text{(eq 2)}$$

$$\frac{1}{k_{obs}} = \frac{k_{-1}[Ph_2S]}{k_1 k_2[\text{styrene}]} + \frac{1}{k_1} \qquad \text{(eq 3)}$$

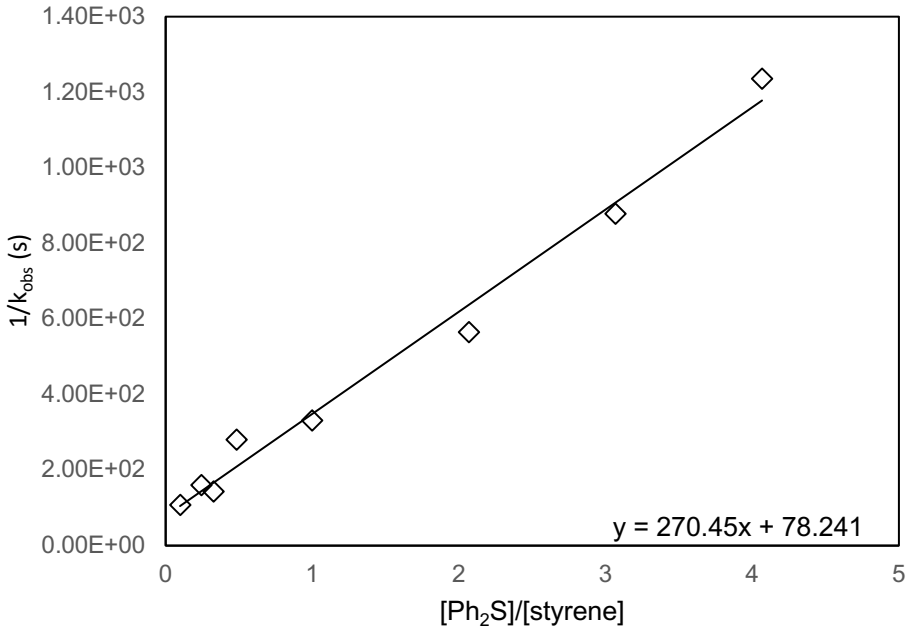

Figure 16. Plot of $1/k_{obs}$ versus [Ph_2S]/[styrene] for the reaction of **2.7c** with styrene in toluene-d_8 at 25 °C

2.4.3 Stereochemistry of Gold(I) Benzylidene Transfer

To assess the stereochemistry of gold(I) benzylidene transfer, we examined the gold(I) benzylidene transfer of **2.7c** with *Z*-β-deuteriostyrene (**2.9**). This system was chosen due to (1) the high selectivity for the formation of *cis*-1,2-diphenylcyclopropane observed for the gold(I) benzylidene transfer from **2.7c** to styrene and (2) the distinct *cis* and *trans* coupling constants in the ^{1}H NMR spectrum of *cis*-1,2-diphenylcyclopropane (Figure 17).

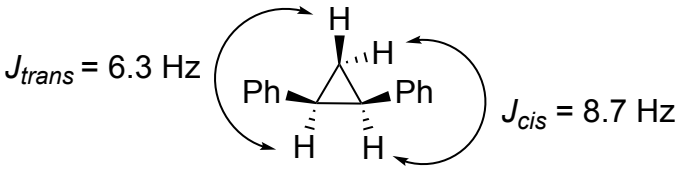

Figure 17. Three-bond coupling constants (*J*) in *cis*-1,2-diphenylcyclopropane

Treatment of the solution of **2.7c** in toluene-d_8 with an excess of **2.9a** at 25 °C led to the formation of cyclopropane **2.10a** (Scheme 15). Analysis of the ^{1}H NMR spectrum revealed a single doublet at δ 2.18 with a coupling constant of 8.6 Hz. This coupling constant allowed us to assign the stereochemistry for cyclopropane **2.10a** in Scheme 15, with the *cis* relationship between the phenyl group and deuterium in **2.9a** preserved. In a similar experiment with **2.9b**, analysis of the cyclopropane product revealed three triplets at δ 2.19, 2.15, and 1.14 with coupling constants of 8.8 Hz, consistent with retention of the stereochemistry of **2.9b**. This retention of stereochemistry is consistent with both a concerted mechanism[3] or a stepwise mechanism with rapid ring closure described by Echavarren.[37]

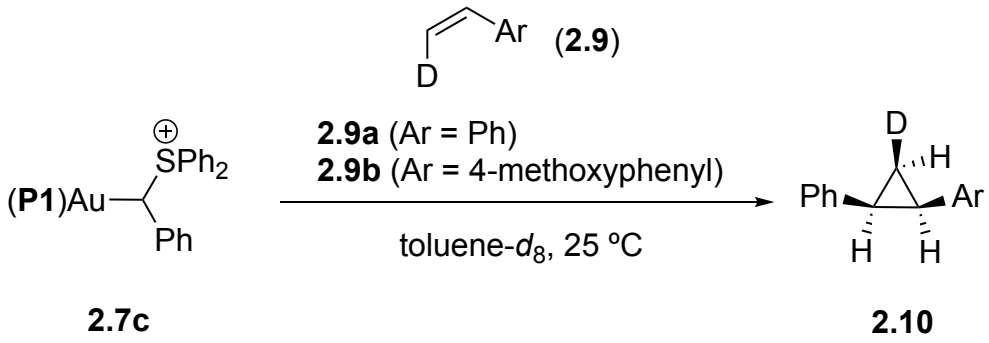

Scheme 15. Gold(I) benzylidene transfer from **2.7c** to **2.9**

2.4.4 Hammett Analysis of Gold(I) Benzylidene Transfer

Given the observed retention of alkene stereochemistry in the gold(I) benzylidene transfer from **2.7c** to **2.9**, we sought to gain some experimental evidence for the mechanism of the carbene transfer process. To this end, we performed a Hammett analysis on rate of the gold(I) benzylidene transfer of **2.7c** with an array of *p*-substituted vinyl arenes with a range of electronic properties. In order to probe the electronic dependence of gold(I) benzylidene transfer, we required a straightforward way to access values for k_2 which represents the rate of carbene transfer, following sulfide dissociation. To achieve this, we utilized our kinetic model to ascertain values of k_2 from the slope of line for a plot of $1/k_{obs}$ versus [SPh_2]/[vinyl arene]. Based on rate equation 2, the slope of the of a plot of $1/k_{obs}$ versus [SPh_2]/[vinyl arene] is equal to k_{-1}/k_1k_2. The values of k_1 and k_{-1} should be invariant of the identity of the vinyl arene, therefore, a comparison of the slopes of plots of $1/k_{obs}$ versus [SPh_2]/[vinyl arene] for a variety of vinyl arenes, will allow

for the direct comparison of k_2 values for the gold(I) benzylidene transfer for a range of vinyl arenes.

To assess the rate dependence on the vinyl arene, we treated gold(I) benzylide complex **2.7c** with a variety of *p*-substituted vinyl arenes to obtain values for k_2. To assess the dependence of the rate on the electronics of the *p*-substituted vinyl arene, we compared the k_2 values for the gold(I) benzylidene transfer with both Hammett σ_p and Hammett-Brown σ^+ parameters. A plot of $\log(k_{2,X}/k_{2,H})$ versus Hammett σ_p parameters for the *p*-substituted vinyl arenes was linear with a rho value of $\rho = -1.7$ (Figure 18, $R^2 = 0.99$) while a plot of $\log(k_{2,X}/k_{2,H})$ versus Hammett σ^+ parameters for the *p*-substituted vinyl arenes showed a poor correlation (Figure 19, $R^2 = 0.87$). The poor correlation between k_2 and Hammett σ^+ parameters as well as the relatively low rho-value,[116,117] point to a concerted mechanism for gold(I) benzylidene transfer, with little positive charge buildup at the benzylic position during cyclopropanation.

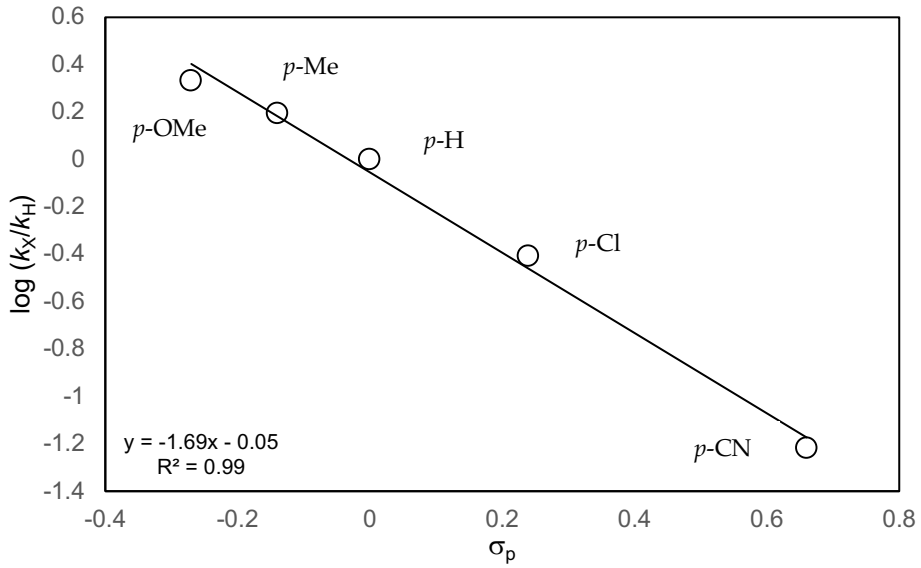

Figure 18. Plot of log($k_{2,X}/k_{2,H}$) versus Hammett σ_p parameters for the *p*-substituted vinyl arenes

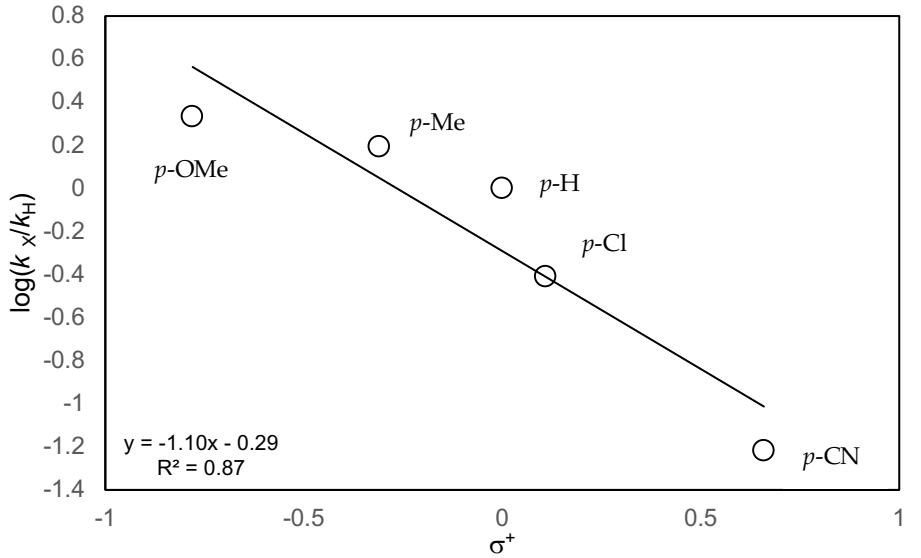

Figure 19. Plot of log($k_{2,X}/k_{2,H}$) versus Hammett σ^+ parameters for the *p*-substituted vinyl arenes.

2.5 Summary

In summary, we have synthesized gold sulfonium benzylide complexes **2.7** that undergo benzylidene transfer to alkenes and DMSO under mild conditions without external activation. The reactivity of complexes **2.7** increased significantly in the order **2.7a** < **2.7b** < **2.7c** such that the diphenylsulfonium benzylide complex **2.7c** underwent benzylidene transfer to vinyl arenes, aliphatic alkenes, and DMSO within minutes at room temperature. Kinetic analysis of the reaction of **2.7c** with styrene established a mechanism involving reversible formation of the free gold benzylidene complex **2.7** followed by irreversible benzylidene transfer to the alkene. Deuterium-labeling studies of vinyl arenes revealed that alkene stereochemistry is preserved during gold(I) benzylidene transfer. A Hammett analysis of gold(I) benzylidene transfer with an array of vinyl arenes with electronic properties suggests a concerted mechanism for gold(I) benzylidene transfer, which explains the high selectivity for some gold(I)-catalyzed cyclopropanation reactions. Ongoing studies in our laboratory are directed toward kinetic analysis of carbene transfer from gold sulfonium benzylide complexes as a function of supporting ligand and C1-aryl group.

2.6 Experimental Details

2.6.1 General Methods

Reactions were performed under a nitrogen atmosphere employing standard Schlenk and glovebox techniques unless specified otherwise. NMR Spectra were obtained on a Varian spectrometer operating at 500 MHz for ^{1}H NMR, 125 MHz for ^{13}C NMR, and 101 MHz for ^{31}P NMR in CD_2Cl_2 at 25 °C unless noted otherwise. ^{1}H and ^{13}C were referenced to residual solvent signal, ^{31}P was referenced to an external phosphoric acid (neat) standard ($\delta = 0.0$). NMR Probe temperatures were determined employing an ethylene glycol thermometer.[118] Toluene-d_8 was dried over Na/benzophenone, distilled and stored over 3 Å molecular sieves in a glove box prior to use. Toluene was purified by passage through columns of activated alumina under nitrogen. All other reagents were obtained through major chemical suppliers and used as received. Error limits for rate constants refer to the standard deviation of the slope and/or intercept of the linear regression plot.

2.6.2 Gold(I) sulfonium benzylide complexes

[(P1)AuCHPh(THT)]$^{+}$ [BAr$^{F}_{4}$]$^{-}$ (2.7a). A solution of (**P1**)AuCHClPh[79] (102 mg, 0.16 mmol) and tetrahydrothiophene (142 μL, 1.61 mmol) in toluene (2 mL) was added to $Na^{+}\{B[3,5\text{-}(CF_3)_2C_6H_3]_4\}^{-}$ ($NaBAr^{F}_{4}$; 157 mg, 0.177 mmol) and the resulting solution was stirred at room temperature for 30 min. The resulting suspension was allowed to

settle and the solution was decanted and added to cold pentane (4 °C). The resulting white suspension was cooled overnight at –20 °C to give a crystalline solid that was dissolved in minimal CH_2Cl_2, layered with hexanes, and cooled at 4 °C overnight to give **2.7a** (167 mg, 68%) as colorless crystals. ^{1}H NMR: δ 7.87 (m, 1H), 7.73 (br m, 8H, $BAr^{F}{}_4$), 7.57 (br s, 4H, $BAr^{F}{}_4$), 7.53 (m, 2H), 7.45 (t, J = 8 Hz, 1H), 7.40 (m, 1H), 7.35 (t, J = 8 Hz, 2H), 7.23 (m, 4H), 7.13 (d, J = 8 Hz, 2H), 7.04 (m, 2H), 3.28 (m, 1H), 2.94 (m, 3H), 2.82 (d, J = 6 Hz, 1H), 2.08 (m, 2H), 1.04 (m, 2H), 1.39 (d, J = 15.2 Hz, 9H), 1.38 (d, J = 15.3 Hz, 9H). ^{13}C{^{1}H} NMR: δ 162.3 (dd, J = 99.6, 50.1 Hz), 149.6 (d, J = 14.8 Hz), 144.5 (d, J = 5.9 Hz), 138.1 (d, J = 3.7 Hz) ,135.4 (br s, $BAr^{F}{}_4$) 135.01, 133.6 (d, J = 7.6 Hz), 1=31.5 (d, J = 1.3 Hz), 130.8 (d, J = 2.6 Hz), 130.5, 120.4 (d, J = 23.9 Hz), 129.8, 129.6 (br m, $BAr^{F}{}_4$), 129.3 (br m, $BAr^{F}{}_4$), 129.1, 128.7, 128.6, 128.0, 127.9, 127.5, 127.1, 125.2 (q, J_{CF} = 270 Hz, $BAr^{F}{}_4$) 118.0 (br m, $BAr^{F}{}_4$), 62.7 (d, J_{CP} = 85 Hz), 45.6, 43.7 (d, J = 2.7 Hz), 38.3 (d, J_{CP} = 22 Hz), 38.0 (d, J_{CP} = 22 Hz), 31.4 (d, J_{CP} = 7 Hz), 31.1 (d, J_{CP} = 8 Hz), 29.0, 28.1. ^{31}P{^{1}H} NMR: δ 64.35. HRMS calc. (found) for $C_{31}H_{41}AuPS$ (M^+): 673.2327 (673.2335).

(*R*,S)-[(P1)AuCHPh(EtSPh)]$^+$ [$BArF_4$]$^-$ [(*R*,S**)-2.7b].** Reaction of (**P1**)AuCHClPh, ethyl phenyl sulfide, and $NaBAr^{F}{}_4$ employing a procedure analogous to that used to synthesize **2.7a** led to isolation of (*S*,R**)-**2.7b** in 71% yield as colorless crystals. (*S*,R**)-**2.7b** isomerized in toluene-d_8 at 25 °C ($t_{1/2}$ = ~25 min) or CD_2Cl_2 to form an equilibrium 2.5:1 (toluene-d_8) or 3.0:1 (CD_2Cl_2) mixture of (*S*,R**)-**2.7b** and (*S*,S**)-**2.7b**

and was analyzed spectroscopically as such a mixture. ^{1}H NMR [(*S**,*R**)-**2.7b**]: δ 7.79 (t, *J* = 8 Hz, 1H), 7.72 (br s, 8H, $BAr^{F}{}_{4}$), 7.67 (t, *J* = 7 Hz, 1 H), 7.59 (t, *J* = 8 Hz, 2 H), 7.56 (br s, 4H, $BAr^{F}{}_{4}$), 7.50 (m, 4H), 7.42 (d, *J* = 8 Hz, 2 H), 7.37 (t, *J* = 8 Hz, 2 H), 7.27 (t, *J* = 8 Hz, 1H), 7.17 (d, *J* = 8 Hz, 3 H), 7.07 (m, 1H), 7.01 (t, *J* = 8 Hz, 1H), 6.95 (m, 1H), 3.30 (d, *J* = 6 Hz, 1H), 3.05 (m, 1H), 2.85 (m, 1H), 1.34 (d, *J* = 15.2 Hz, 9H), 1.04 (t, *J* = 6.8 Hz, 3 H), 0.99 (d, *J* = 15.3 Hz, 9 H). ^{1}H NMR [(*S**,*S**)-**2.7b**]: δ 7.79 (t, *J* = 8 Hz, 1H), 7.72 (br s, 8H, $BAr^{F}{}_{4}$), 7.67 (t, *J* = 7 Hz, 1 H), 7.59 (t, *J* = 8 Hz, 2 H), 7.56 (br s, 4H, $BAr^{F}{}_{4}$), 7.50 (m, 4H), 7.42 (d, *J* = 8 Hz, 2 H), 7.37 (t, *J* = 8 Hz, 2 H), 7.27 (t, *J* = 8 Hz, 1H), 7.17 (d, *J* = 8 Hz, 3 H), 7.07 (m, 1H), 7.01 (t, *J* = 8 Hz, 1H), 6.95 (m, 1H), 3.33 (d, *J* = 6 Hz, 1H), 3.05 (m, 1H), 2.85 (m, 1H), 1.39 (d, *J* = 15.2 Hz, 9H), 1.32 (d, *J* = 15.3 Hz, 9 H), 1.24 (t, *J* = 6.8 Hz, 3 H). ^{13}C{^{1}H} NMR [(*S**,*R**)-**2.7b**+ (*S**,*S**)-**2.7b**]: δ 162.3 (dd, *J* = 99.6, 50.1 Hz), 149.6 (d, *J* = 14.8 Hz), 144.2 (d, *J* = 5.9 Hz), 137.5 (d, *J* = 3.7 Hz), 135.4 (br, $BAr^{F}{}_{4}$) 135.0, 134.6, 133.5 (d, *J* = 7.6 Hz), 131.2, 130.9 (m, $BAr^{F}{}_{4}$) 130.52, 130.47, 130.4, 130.1, 129.8, 129.6 (m, $BAr^{F}{}_{4}$), 129.3 (m, $BArF_{4}$), 129.1, 128.9, 127.87, 127.8 (d, *J* = 6.1 Hz), 127.5, 127.07, 125.2 (q, J_{CF} = 272 Hz, $BAr^{F}{}_{4}$), 118.04 (br m, $BAr^{F}{}_{4}$). ^{13}C{^{1}H} NMR [*S**,*R**)-**2.7b**]: δ 63.6 (d, J_{CP} = 85 Hz), 41.3 (d, *J* = 2.5 Hz), 37.8 (d, J_{CP} = 22 Hz), 37.9 (d, J_{CP} = 22 Hz), 31.4 (d, J_{CP} = 7 Hz), 30.6 (d, J_{CP} = 8 Hz), 9.8. ^{13}C{^{1}H} NMR [(*S**,*S**)-**2.7b**] δ 64.2 (d, J_{CP} = 85 Hz), 41.3 (d, *J* = 2.5 Hz), 38.2 (d, J_{CP} = 22 Hz), 38.0 (d, J_{CP} = 22 Hz), 31.3 (d, J_{CP} = 7 Hz), 31.2 (d, J_{CP} = 8 Hz), 10.1. ^{31}P{^{1}H} NMR [(*S**,*R**)-**2.7b**]:

δ 64.32. $^{31}P\{^{1}H\}$ NMR [(*S**,*S**)-**2.7b**]: 64.68. HRMS calc. (found) for $C_{35}H_{43}AuPS$ (M^+): 723.2483 (723.2481).

[(P1)AuC(H)(SPh$_2$)(Ph)]$^+$ [BAr$^{F}_4$]$^-$ (2.7c). A solution of (**P1**)AuCHClPh (200 mg, 0.32 mmol) and diphenyl sulfide (85 μL, 0.64 mmol) in toluene (2 mL) was added to $NaBArF_4$ (310 mg, 0.35 mmol) in a microwave vial cooled at –78 °C. The resulting suspension was stirred for 30 min and warmed to room temperature. The resulting suspension was allowed to settle and the solution was decanted and added to cold pentane (4 °C). The resulting white suspension was cooled overnight at –20 °C to give a crystalline solid which was dissolved in minimal toluene and cooled at –20 °C overnight to give **2.7c** (210 mg, 39%) as colorless crystals. ^{1}H NMR: δ 7.80 (t, *J* = 7.6 Hz, 1H), 7.75 (br s, 8H BAr^{F}_4), 7.67 (t, *J* = 7.6 Hz, 1H), 7.62 (m, 2H), 7.57 (br s, 4H, BAr^{F}_4), 7.49 (m, 4H), 7.39 (t, *J* = 7.6 Hz, 1H), 7.25 (t, *J* = 7.6 Hz, 1H), 7.18 (m, 3H), 7.09 (c, *J* = 7.7 Hz, 1H), 7.00 (m, 1H), 3.75 (d, *J* = 5.4 Hz, 1H), 1.35 (d, *J* = 15.2 Hz, 9H), 0.94 (d, *J* = 15.2 Hz, 9 H). $^{13}C\{^{1}H\}$ NMR:[S3] δ 162.3 (dd, *J* = 99.4, 50.0 Hz), 149.6 (d, *J* = 14.9 Hz), 144.4 (d, *J* = 6.5 Hz), 137.2 (d, *J* = 3.8 Hz), 135.4 (br s, BAr^{F}_4), 134.5, 134.3, 133.8, 133.5 (d, *J* = 6.3 Hz), 131.41 (d, *J* = 1.8 Hz), 131.37, 131.1 (d, *J* = 6.3 Hz), 130.9 (d, *J* = 3.8 Hz), 130.7 (br s, BAr^{F}_4), 130.5, 130.1, 129.6 (br m, BAr^{F}_4), 129.55, 129.49, 129.44, 129.36, 128.7, 127.9 (d, *J* = 6.3 Hz), 127.6 (d, *J* = 5.0 Hz), 125.8, 125.2 (q, J_{CF} = 273 Hz, BAr^{F}_4) 118.0 (br t, BAr^{F}_4), 66.6 (d, *J* = 84.0 Hz), 37.9 (d, *J* =

22.3 Hz), 37.7 (d, J = 22.2 Hz), 31.5 (d, J = 6.7 Hz), 30.5 (d, J = 6.6 Hz). $^{31}P\{^{1}H\}$ NMR: δ 64.52. HRMS calc. (found) for $C_{35}H_{43}AuPS$ (M^+): 771.2489 (771.2493).

[(P1)AuC(H)(S(*p*-tolyl)$_2$(Ph)][BAr$^{F}_4$] (2.7d) *p*-tolylsulfide[119] (9.8 mg, 4.6×10^{-2} mmol) and **2.7c** (15 mg, 9.2×10^{-3} mmol) were added to a flame-dried NMR under nitrogen. CD_2Cl_2 (600 μL) was added and the solution was allowed to equilibrate for 30 min to form **2.7d**. **2.7d** was characterized in solution without isolation. ^{1}H NMR (CD_2Cl_2, 25 °C): δ 7.80 (t, J = 7.4 Hz, 1H), 7.74 (br s, 8H, BAr$^{F}_4$), 7.62 (t, J = 7.6 Hz, 1H), 7.57 (br s, BAr$^{F}_4$), 7.53 (d, J = 7.9 Hz, 2H), 7.49 (t, J = 7.5 Hz, 1H), 7.41 (d, J = 8.0 Hz, 2H), 7.37–7.29 (m, obscured by free SPh_2), 7.29–7.14 (m, obscured by free S(*p*-tol)$_2$), 7.08 (d, J = 7.9 Hz, 4H), 7.02 (t, J = 7.5 Hz), 6.97 (d, J = 7.6 Hz, 1H), 3.73 (d, J = 5.5 Hz, 1H), 2.40 (s, 3H), 2.32 (s, obscured by free S(*p*-tol)$_2$), 1.35 (d, J = 15.4 Hz, 9H), 0.95 (d, J = 15.4 Hz). $^{13}C\{^{1}H\}$ NMR (CD_2Cl_2, 25 °C): δ 162.3 (dd, J = 99.9, 50.0 Hz), 145.7, 145.1, 144.4 (d, J = 5.0 Hz), 135.4 (br s, BAr$^{F}_4$), 135.0, 133.5 (d, J = 8.8 Hz), 131.9, 131.1 (d, J = 2.5 Hz), 130.8 (BAr$^{F}_4$), 130.1, 129.6 (BAr$^{F}_4$), 129.5, 129.39, 129.36, 129.34, 129.32, 129.29, 129.2, 128.7 (d, J = 2.5 Hz), 128.4, 127.8 (d, J = 6.3 Hz), 127.5 (d, J = 15.1 Hz), 126.5, 125.3 (q, J = 273 Hz, BAr$^{F}_4$), 118.0 (br m, BAr$^{F}_4$), 66.9 (d, J = 84.1 Hz), 37.9 (d, J = 22.1 Hz), 37.6 (d, J = 22.1 Hz), 31.4 (d, J = 6.7 Hz), 30.4 (d, J = 6.7 Hz), 21.8, 21.7. $^{31}P\{^{1}H\}$ NMR (CD_2Cl_2, 25 °C): δ 64.52.

2.6.3 Benzylidene Transfer Reactions

Benzylidene transfer from 1a. A solution of **2.7a** (30 mg, 1.9×10^{-2} mmol, 32 mM), **2.8** (25 μL, 0.19 mmol, 316 mM) and CH_2Br_2 (2.0×10^{-2} mmol; internal standard) in toluene-d_8 was heated at 75 ± 1 °C in a thermostatted oil bath and monitored periodically by cooling the solution and analyzing by ^{1}H NMR spectroscopy. The concentration of **2.7a** was determined by integrating the *tert*-butyl resonance of **2.7a** at δ 1.05 relative to the CH_2Br_2 resonance at δ 3.95. A plot of ln[**2.7a**] versus time was linear to > 3 half-lives with a pseudo-first-order rate constant of $k_{obs} = 2.28 \pm 0.12 \times 10^{-4}$ s^{-1} to give 1-phenyl-2-anisylcyclopropane in 96% yield based on the integration of the methoxy resonances of 1-phenyl-2-anisylcyclopropane at δ 3.36 and 3.19 relative to the resonance of CH_2Br_2 (Figure 20). Employing a similar procedure, the reaction of DMSO (320 mM) with **2.7a** (32 mM) in toluene-d_8 proceeded with a pseudo-first-order rate constant of $k_{obs} = 1.22 \pm 0.5 \times 10^{-4}$ s^{-1} to form benzaldehyde in 78% yield determined by integrating the formyl resonance of benzaldehyde at δ 9.61 versus the resonance of CH_2Br_2 (Figure 21).

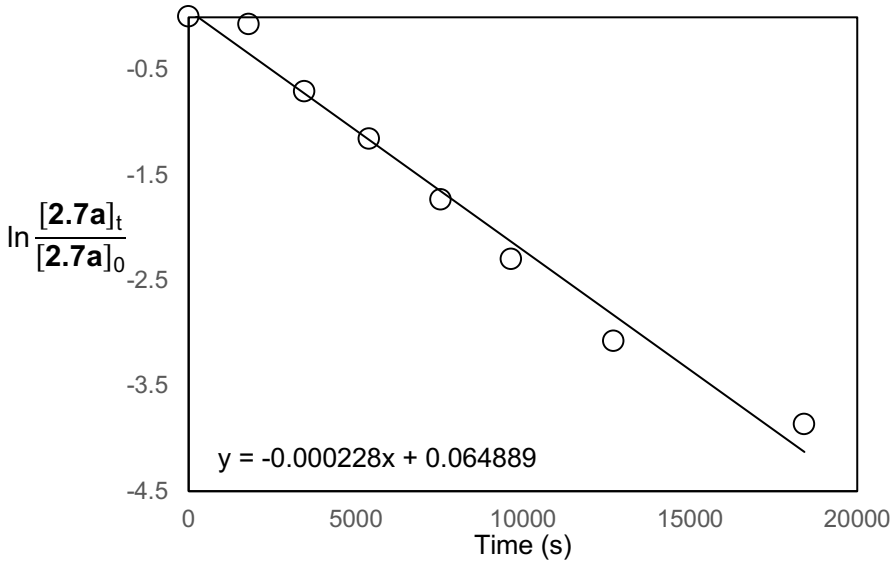

Figure 20. Pseudo-first-order plot of reaction of **2.7a** (32 mM) and *p*-methoxystyrene (320 mM) in toluene-d_8 at 75 °C.

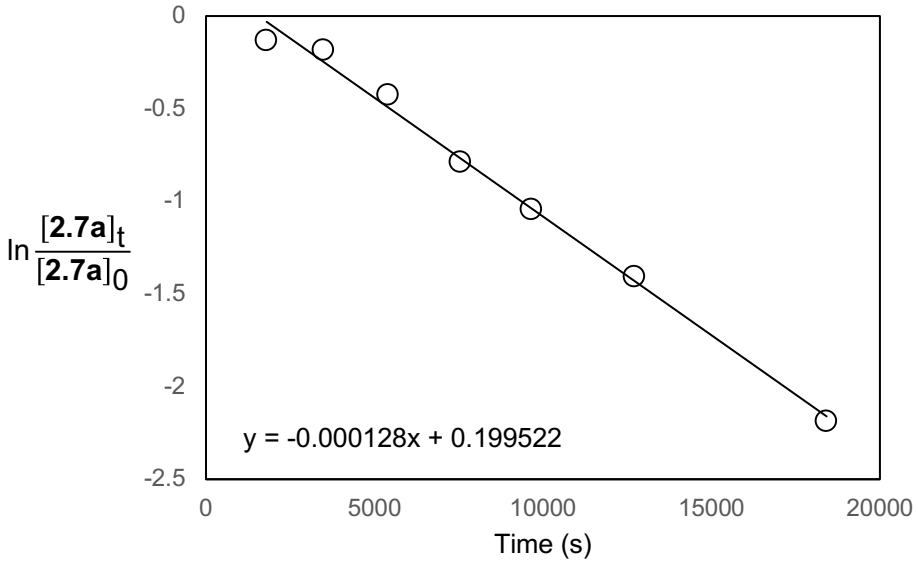

Figure 21. Pseudo-first-order plot of reaction of **2.7a** (32 mM) and DMSO (320 mM) in toluene-d_8 at 75 °C.

Benzylidene transfer from 2.7b. A solution of **2.7b** (21 mg, 1.3×10^{-2} mmol, 22 mM), **2.8** (16 μL, 0.13 mmol, 220 mM) and CH_2Br_2 (8.0×10^{-3} mmol) in tolune-d_8 was heated at 40 ± 1 °C in a thermostatted oil bath and monitored periodically by cooling the solution and analyzing by ^{1}H NMR spectroscopy. The concentration of **2.7b** was determined by integrating the *tert*-butyl resonance of **2.7b** at δ 1.10 relative to the CH_2Br_2 resonance at δ 3.95. A plot of ln[(*S**,*R**)-**2.7b**] versus time was linear to >3 half-lives with a pseudo-first-order rate constant of $k_{obs} = 4.0 \pm 0.3 \times 10^{-4}$ s^{-1} to give 1-phenyl-2-anisylcyclopropane in 95% yield based on the integration of the OMe resonances of 1-phenyl-2-anisylcyclopropane relative to the resonance for CH_2Br_2 (Figure 22). Employing a similar procedure, the reaction of DMSO (220 mM) with **2.7b** (22 mM) proceeded with a pseudo-first-order rate constant of $k_{obs} = 4.0 \pm 0.2 \times 10^{-4}$ s^{-1} to form benzaldehyde in 78% yield determined by integrating the formyl resonance of benzaldehyde at δ 9.61 versus the resonance for CH_2Br_2 (Figure 23).

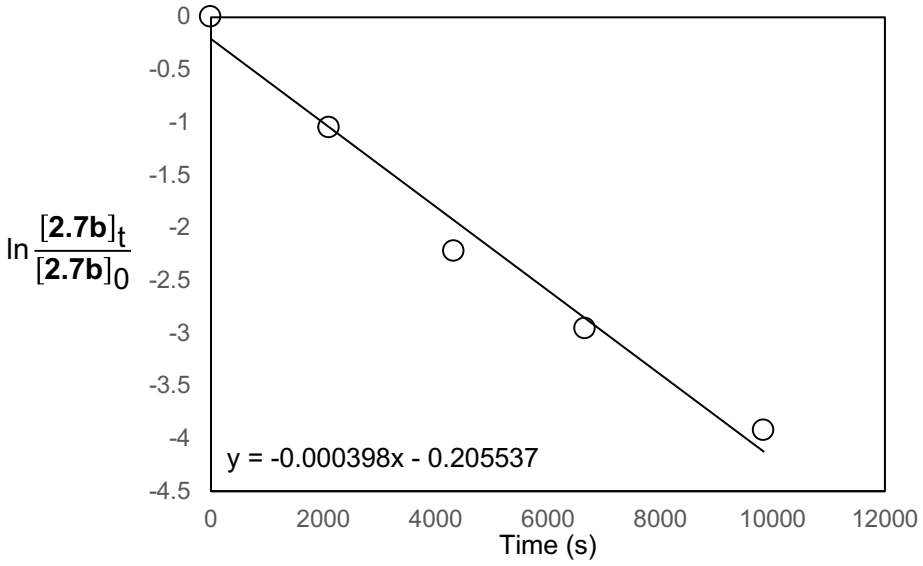

Figure 22. Pseudo-first-order plot of reaction of **2.7b** (22 mM) and *p*-methoxystyrene (220 mM) in toluene-d_8 at 40 °C.

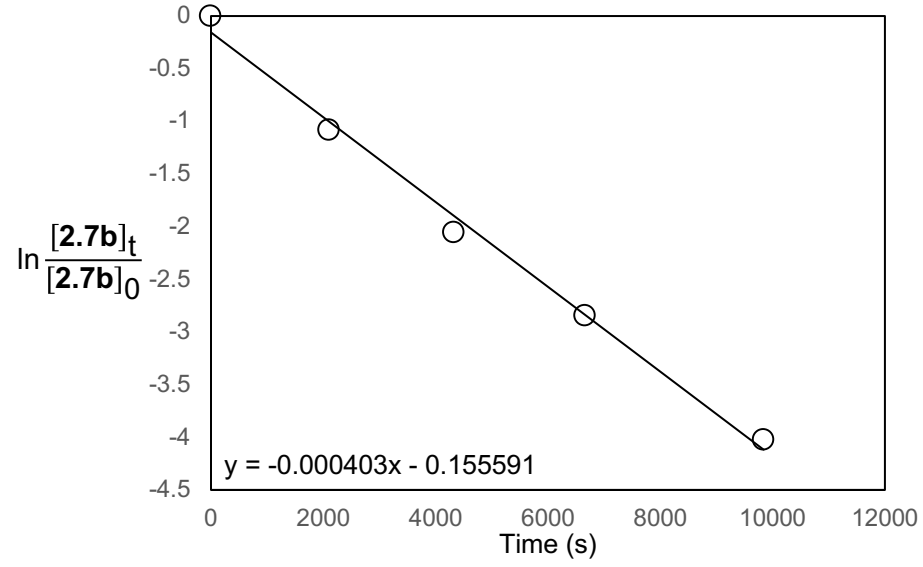

Figure 23. Pseudo-first-order plot of reaction of **2.7b** (22 mM) and DMSO (220 mM) in toluene-d_8 at 40 °C.

Benzylidene transfer from 2.7c. A solution of **2.7c** (15 mg, 9.2×10^{-3} mmol, 15 mM), **2.8** (12 μL, 9.2×10^{-2} mmol, 153 mM) and CH_2Br_2 (2.0×10^{-2} mmol) in toluene-d_8 was placed in an NMR spectrometer maintained at 25 ± 1 °C and analyzed by ^{1}H NMR spectroscopy, recording 4 scans in ~20 s intervals. The concentration of **2.7c** was determined by integrating the *tert*-butyl resonance of **2.7c** at δ 0.67 relative to the CH_2Br_2 resonance at δ 3.95. A plot of ln[**2.7c**] versus time was linear to >3 half-lives with a pseudo-first-order rate constant of $1.8 \pm 0.2 \times 10^{-2}$ s^{-1} to give 1-phenyl-2-anisylcyclopropane in 87% yield as determined by integrating the OMe resonances of 1-phenyl-2-anisylcyclopropane at δ 3.36 and 3.19 relative to the resonance of CH_2Br_2 (Figure 24). Employing a similar procedure, reaction of styrene (150 mM) with **2.7c** (15 mM) in toluene-d_8 at 25 °C proceeded with a pseudo-first-order rate constant of k_{obs} = 1.8 ± 0.2×10^{-2} s^{-1} to form 1,2-diphenylcyclopropane[120S5] in 82% yield as determined by integrating the benzylic resonance at δ 2.18 relative to CH_2Br_2 (Figure 25).

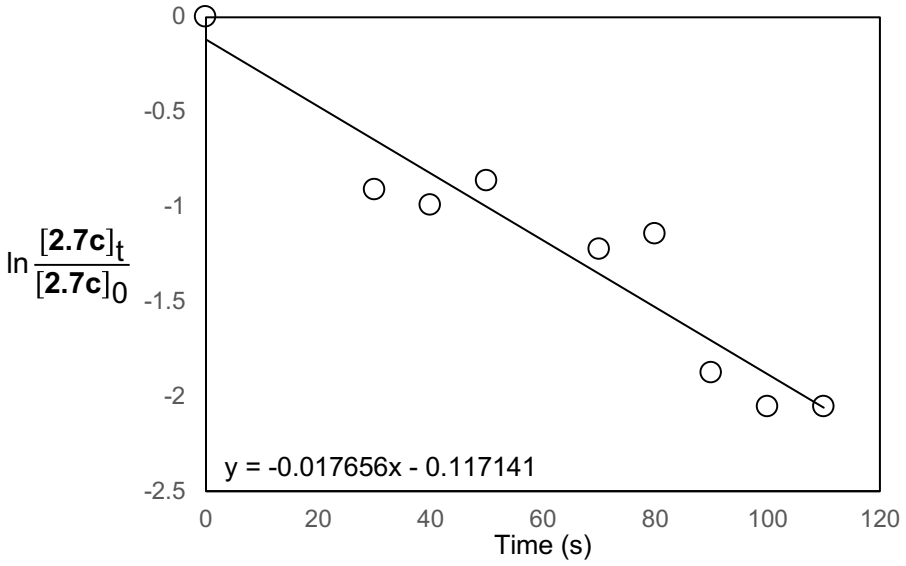

Figure 24. Pseudo-first-order plot of reaction of **2.7c** (15 mM) and *p*-methoxystyrene (150 mM) in toluene-d_8 at 25 °C.

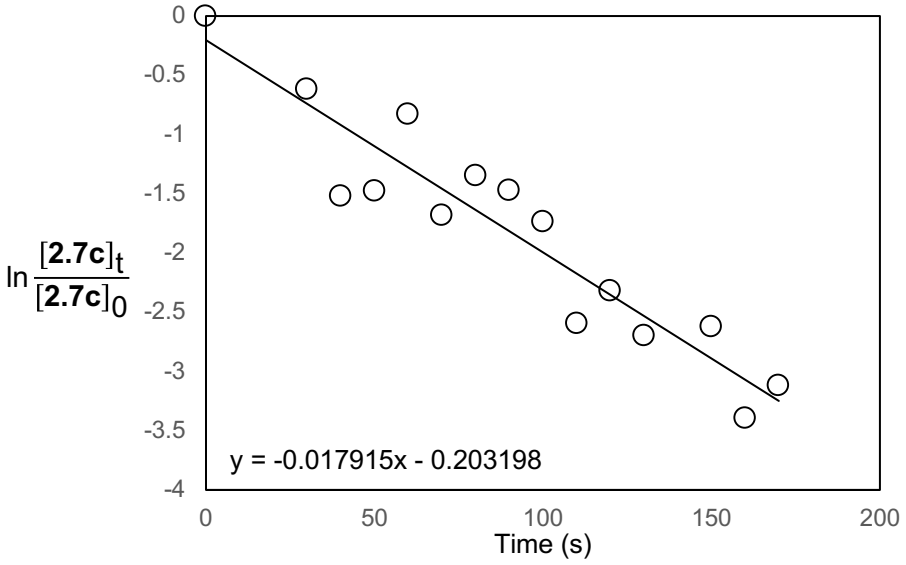

Figure 25. Pseudo-first-order plot of reaction of **2.7c** (15 mM) and styrene (150 mM) in toluene-d_8 at 25 °C.

Benzylidene transfer from 2.7c with DMSO. DMSO (6.4 μL, 9.0×10^{-2} mmol, 0.20 M) and CH_2Br_2 (1.2×10^{-2} mmol) were added via syringe to a solution of **2.7c** (15 mg, 9.0×10^{-3} mmol, 22 mM) in toluene-d_8 at 25 °C and thoroughly mixed. ^{1}H NMR analysis of the resulting solution after 5 min revealed complete consumption of **2.7c** to form benzaldehyde in 65% yield determined by integrating the formyl resonance of benzaldehyde at δ 9.61 versus the resonance of CH_2Br_2 at δ 3.95.

Benzylidene transfer from 2.7c with norbornene. Norbornene (11 mg, 0.12 mmol, 0.20 M) and CH_2Br_2 (1.2×10^{-2} mmol) were added via syringe to a solution of **2.7c** (22 mg, 1.3×10^{-2} mmol, 22 mM) in toluene-d_8 at 25 °C and thoroughly mixed. ^{1}H NMR analysis of the resulting solution after 5 min revealed complete consumption of **2.7c** to form 3-phenyltricyclo[3.2.1.0^{2,4}]octane[121] in 67% yield as determined by integrating the benzylic resonances δ 2.34 relative to the resonance of CH_2Br_2 at δ 3.95.

Benzylidene transfer from 2.7c to cyclohexene and 1-hexene. Cyclohexene (11 μL, 9.0×10^{-2} mmol, 150 mM) and hexadecane (2.6 μL, 9.0×10^{-3} mmol) were added via syringe to a solution of **2.7c** (15 mg, 9.0×10^{-3} mmol, 15 mM) in toluene (600 μL) and the resulting solution was agitated for 5 min. The resulting solution was filtered through a plug of silica gel and eluted with hexanes:EtOAc (*v*/*v* = 9/1). GC analysis of the eluent revealed the formation of 7-phenylbicyclo[4.1.0]heptane[122] in 79% yield as a 4:1 mixture of cis/trans isomers. Employing a similar procedure, reaction of **2.7c** (15 mM) with 1-

hexene in toluene at 25 °C led to formation of (2-butylcyclopropyl)benzene[120] in 76% yield as a 3:1 mixture of cis/trans isomers.

2.6.4 Isomerization of 2.7b

Kinetics of the isomerization of (*S,*R**)-2.7b to (*S**,*S**)-2.7b.** A freshly prepared solution of (*S**,*R**)-**2.7b** (15 mM) in toluene-d_8 was placed in the probe of an NMR spectrometer maintained at 25 ± 1 °C and the solution was monitored periodically in 5 min intervals. The concentrations of (*S**,*R**)-**2.7b** and (*S**,*S**)-**2.7b** were determined by integrating the benzylic resonances of (*S**,*R**)-**2.7b** and (*S**,*S**)-**2.7b** at δ 3.09 and 3.13, respectively (Figure 26). A plot of $\ln([\mathbf{2.7b}]_t - [\mathbf{2.7b}]_\infty)$ versus time was linear to >3 half-lives with an observed rate constant of $k_{obs} = k_f + k_r = 4.67 \pm 0.17 \times 10^{-4}$ s^{-1} (Figure 27). An equilibrium constant for the conversion of (*S**,*R**)-**2.7b** and (*S**,*S**)-**2.7b** of K_{eq} = [(*S**,*R**)-**2.7b**]/[(*S**,*S**)-**2.7b**] = 0.40 ± 0.02 was determined by integrating the benzylic resonances of (*S**,*R**)-**2.7b** and (*S**,*S**)-**2.7b** at ≥ 5 half-lives. From these data, we determined values for the forward and reverse first-order rate constants for the conversion of (*S**,*R**)-**2.7b** and (*S**,*S**)-**2.7b** of $k_f = 1.33 \pm 0.15 \times 10^{-4}$ s^{-1} and $k_r = 3.3 \pm 0.4 \times 10^{-4}$ s^{-1}.

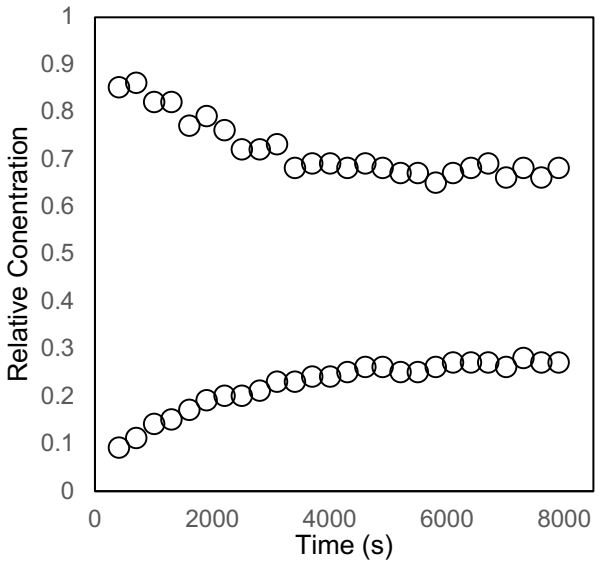

Figure 26. Concentration versus time plots for the isomerization of (S*,R*)-**2.7** (14 mM) to (S*,S*)-**2.7b** in toluene-d_8 at 25 °C.

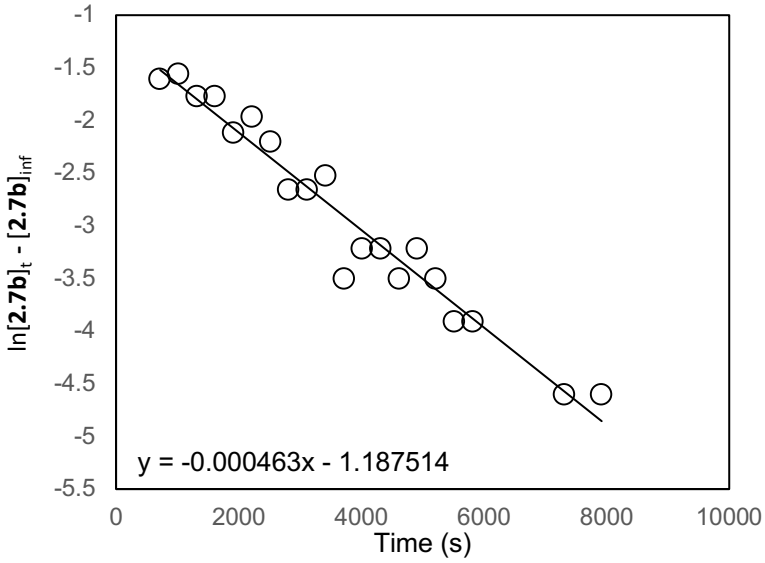

Figure 27. First-order plot of approach to equilibrium for the isomerization of (S*,R*)-**2.7b** (14 mM) to (S*,S*)-**2.7b** in toluene-d_8 at 25 °C.

Isomerization of (*S,*R**)-2.7b to (*S**,*S**)-2.7b in the presence of THT.** A freshly prepared solution of (*S**,*R**)-**2.7b** (12 mg, 7.6×10^{-3} mmol, 13 mM), THT (0.8 μL, 8×10^{-3} mmol, 13 mM) and CH_2Br_2 (8.0×10^{-3} mmol) in toluene-d_8 was monitored periodically by ^{1}H NMR spectroscopy. The concentration of (*S**,*R**)-**2.7b** was determined by integrating the *tert*-butyl resonance of (*S**,*R**)-**2.7b** at δ 0.67 relative to the CH_2Br_2 resonance at δ 3.95. Because the *t*-Bu resonance for (*S**,*S**)-**2.7b** was obscured, the concentration of (*S**,*S**)-**2.7b** was determined from the integration of the *tert*-butyl resonance of (*S**,*R**)-**2.7b** and the benzylic resonances of (*S**,*R**)-**2.7b** and (*S**,*S**)-**2.7b**. A plot of ln[(*S**,*R**)-**2.7b** + (*S**,*S**)-**2.7b**] versus time through ~1 half-life provided the first-order rate constant for the conversion of **2.7b** to **2.7a** of $k = 2.6 \pm 0.5 \times 10^{-5}$ s^{-1} (Figure 28). A plot of ln{[(*S**,*R**)-**2.7b**]$_t$/[(*S**,*R**)-**2.7b** + (*S**,*S**)-**2.7b**]$_t$ – [(*S**,*R**)-**2.7b**]$_{inf}$/[(*S**,*R**)-**2.7b** + (*S**,*S**)-**2.7b**]$_{inf}$ provided the first-order rate constant for approach to equilibrium for the isomerization of (*S**,*R**)-**2.7b** to (*S**,*S**)-**2.7b** of $k_{obs} = k_f + k_r = 5.1 \pm 0.8 \times 10^{-4}$ s^{-1} (Figure 29). From this value and from the equilibrium constant for the conversion of (*S**,*R**)-**2.7b** to (*S**,*S**)-**2.7b** ($K_{eq} = 2.5$) we obtained a first-order rate constant for the conversion of (*S**,*R**)-**1b** to (*S**,*S**)-**2.7b** of $k_f = 1.4 \pm 0.20 \times 10^{-4}$ s^{-1}.

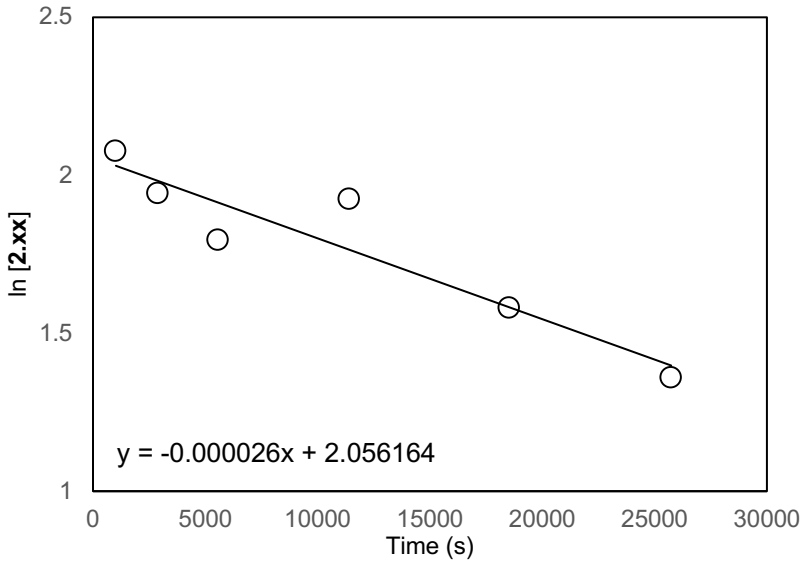

Figure 28. First-order plot of conversion of **2.7b** (13 mM) to **2.7a** in the presence of THT (13 mM) in toluene-d_8 at 25 °C.

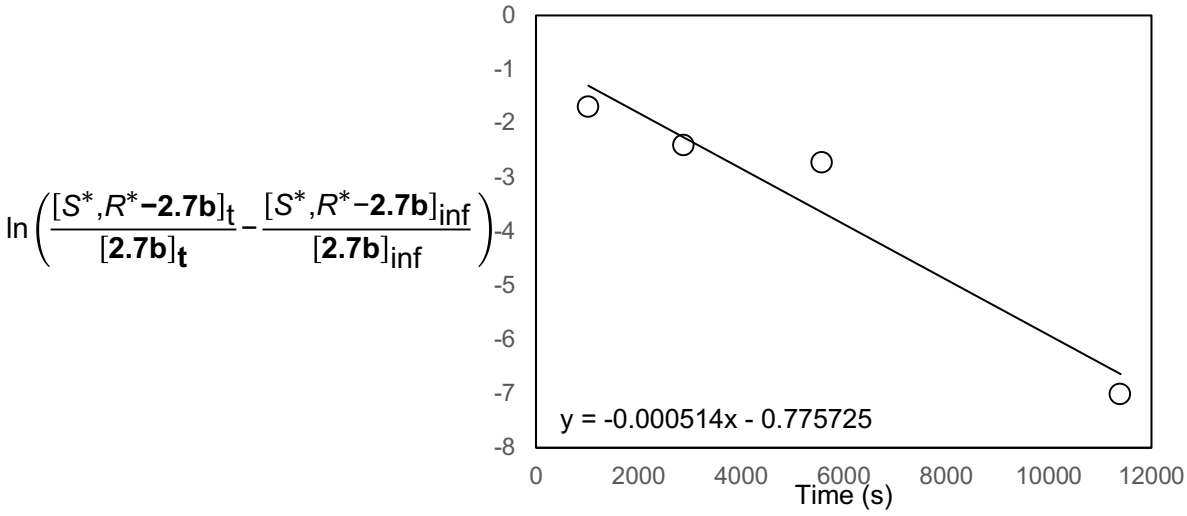

Figure 29. First-order plot for approach to equilibrium for the conversion of (S*,R*)-**2.7b** (13 mM) to (S*,S*)-**2.7b** in the presence of THT (13 mM) in toluene-d_8 at 25 °C.

2.6.4 Sulfide Exchange Experiments

Kinetics of formation of 2.7a from 2.7b. THT (9.1 μL, 9.0×10^{-2} mmol) was added to a solution of **2.7c** (15.0 mg, 9.5×10^{-3} mmol) in toluene-d_8 (600 μL), agitated, and immediately placed in the probe of an NMR spectrometer maintained at 25 °C and the solution was monitored in 5 min intervals. The concentration of **2.7b** was determined by integrating the benzylic resonances of **2.7b** at δ 2.90. A plot of ln[**2.7b**] versus time was linear to >3 half-lives with an observed rate constant of $k_{obs} = 1.14 \pm 0.03 \times 10^{-4}$ s^{-1} (Figure 30).

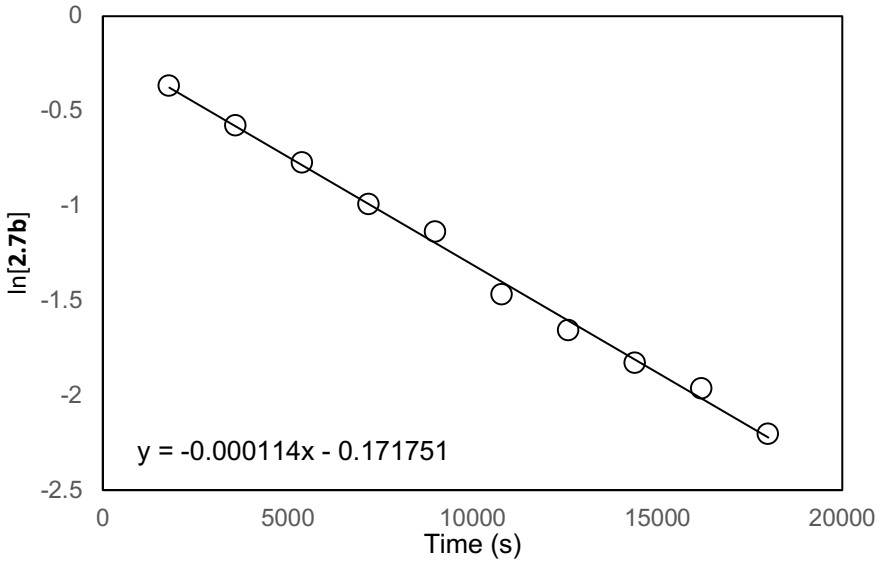

Figure 30. First order plot of conversion of **2.7b** (16 mM) to **2.7a** in the presence of THT (150 mM) in toluene-d_8 at 25 °C.

Kinetics of formation of 2.7d from 2.7c. A solution of *p*-tolylsulfide (50 μL, 7.5×10^{-3} mmol, 15 mM) was added to a solution of **2.7c** (11.3 mg, 6.9×10^{-3} mmol, 12.5 mM) in toluene-d_8 (550 μL), agitated, and immediately placed in the probe of an NMR spectrometer maintained at 25 °C and the solution was monitored in 20 sec intervals. The concentration of **2.7c** and **2.7d** were determined by integrating the benzylic resonances of **2.7c** and **2.7d** at δ 3.44 and 3.51, respectively. A plot of $\ln([\mathbf{2.7c}]_t - [\mathbf{2.7c}]_{inf}$ versus time was linear to >3 half-lives with an observed rate constant of $k_{obs} = k_1 + k_{-1}$ =1.18 ± 0.08×10^{-2} s^{-1} (Figure 31). An equilibrium constant for the conversion of **2.7c** to **2.7d** of K_{eq} = 18.29 was determined by integrating the benzylic resonances of **2.7c** and **2.7d**. From this data, we determined the values of the forward and reverse first-order rate constants for the conversion of **2.7c** to **2.7d** of $k_1 = 1.11 \times 10^{-2}$ s^{-1} and $k_{-1} = 6.11 \times 10^{-4}$ s^{-1}.

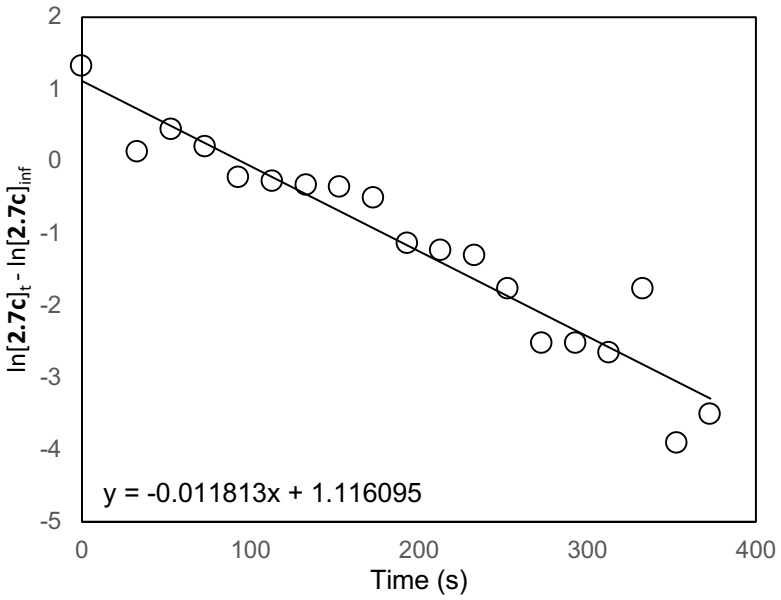

Figure 31. First order plot for approach to equilibrium for the conversion of **2.7v** (13 mM) to **2.7d** in the presence of THT (13 mM) in toluene-d_8 at 25 °C.

2.6.5 Kinetic Experiments

Kinetics of reaction of 2.7c with styrene in the presence of diphenyl sulfide. A solution of **2.7c** (15 mg, 9.2×10^{-3} mmol, 15 mM), styrene (11 μL, 9.2×10^{-2} mmol, 153 mM), diphenyl sulfide (16 μL, 9.2×10^{-2} mmol, 153 mM) and CH_2Br_2 (2.0×10^{-2} mmol) in toluene-d_8 was monitored at 25 °C periodically by ^{1}H NMR spectroscopy. The concentration of **2.7c** was determined by integrating the *tert*-butyl resonance of **2.7c** at δ 0.55 relative to the CH_2Br_2 resonance at δ 3.95. A plot of ln[**2.7c**] versus time was linear to >3 half-lives with a pseudo first-order rate constant of $k_{obs} = 3.02 \pm 0.05 \times 10^{-3}$ s^{-1} (Table 4, entry 2; Figure 32). An analogous procedure was used to determine k_{obs} as a function

of [Ph_2S] and [styrene] (Table 4, entries 3 – 9; Figures 33–39). A plot of $1/k_{obs}$ versus [Ph_2S]/[stryene] was linear with a slope of $2.7 \pm 1.3 \times 10^2$ s and an intercept of $0.78 \pm 26 \times 10^2$ s (Figure 16), which provided the values $k_1 = 1.3 \pm 0.5 \times 10^{-2}$ s^{-1} ($\Delta G^{\ddagger} = 20.3 \pm 0.2$ kcal/mol) and $k_{-1}/k_2 = 3.5 \pm 1.4$.

Table 4. Pseudo first-order rate constants for the reaction of **2.7c** with styrene in toluene-d_8 at 95 °C as a function of [Ph_2S] and [styrene].

entry	Figure	[Ph_2S] (mM)	[styrene] (mM)	(10^3) k_{obs} (s^{-1})
1	25	0	150	17.9 ± 2.3
2	32	150	150	3.02 ± 0.05
3	33	150	310	3.58 ± 0.09
4	34	150	460	6.98 ± 0.22
5	35	150	600	6.27 ± 0.19
6	36	150	1530	9.38 ± 0.26
7	37	310	150	1.77 ± 0.05
8	38	460	150	9.14 ± 0.02
9	39	610	150	0.81 ± 0.02

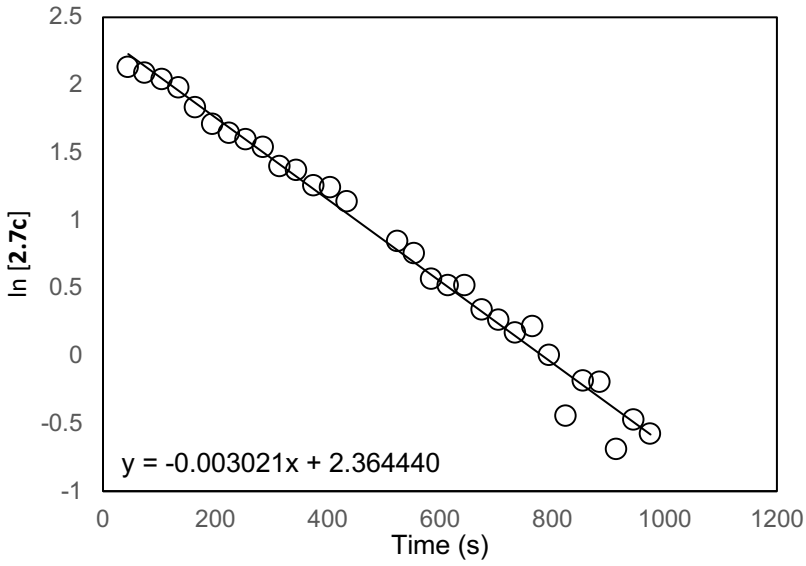

Figure 32. Pseudo first-order plot of reaction of **2.7c** (15 mM), styrene (150 mM) and diphenyl sulfide (150 mM) in toluene-d_8 at 25 °C.

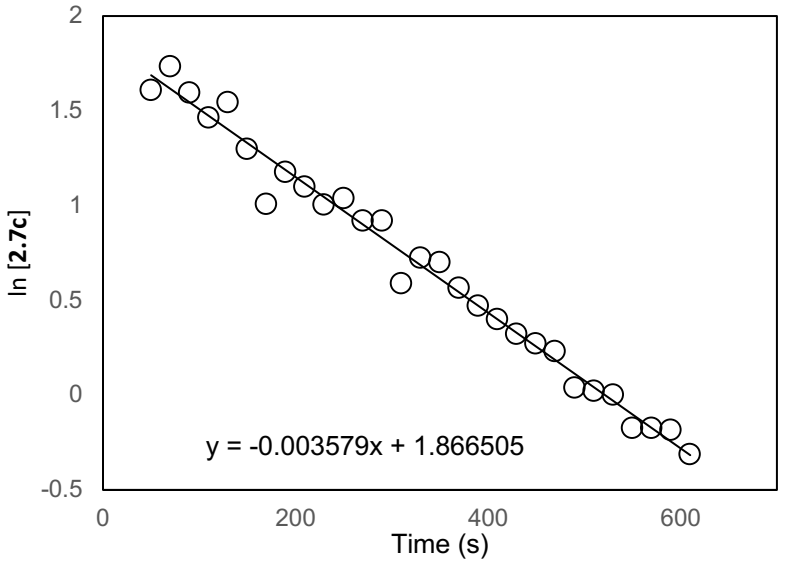

Figure 33. Pseudo first-order plot of reaction of **2.7c** (15 mM), styrene (310 mM) and diphenyl sulfide (150 mM) in toluene-d_8 at 25 °C.

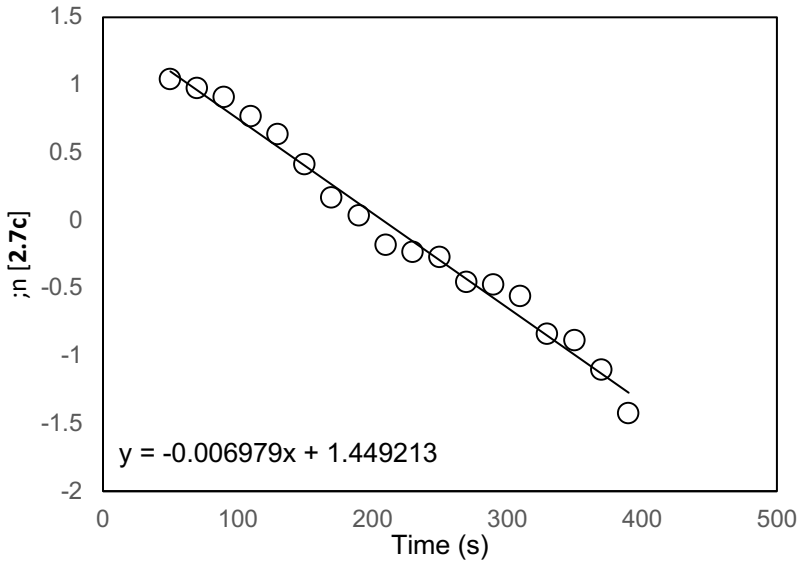

Figure 34. Pseudo first-order plot of reaction of **2.7c** (15 mM), styrene (460 mM) and diphenyl sulfide (150 mM) in toluene-d_8 at 25 °C.

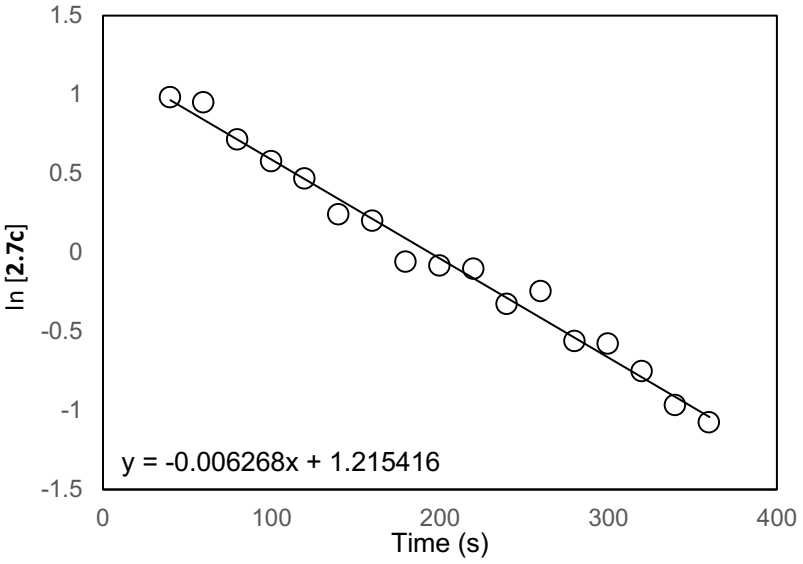

Figure 35. Pseudo first-order plot of reaction of **2.7c** (15 mM), styrene (310 mM) and diphenyl sulfide (600 mM) in toluene-d_8 at 25 °C.

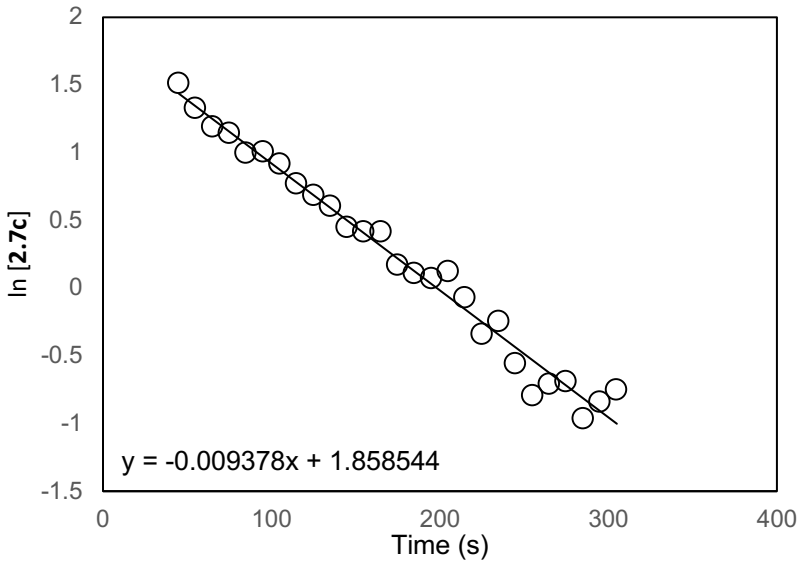

Figure 36. Pseudo first-order plot of reaction of **2.7c** (15 mM), styrene (310 mM) and diphenyl sulfide (1530 mM) in toluene-d_8 at 25 °C.

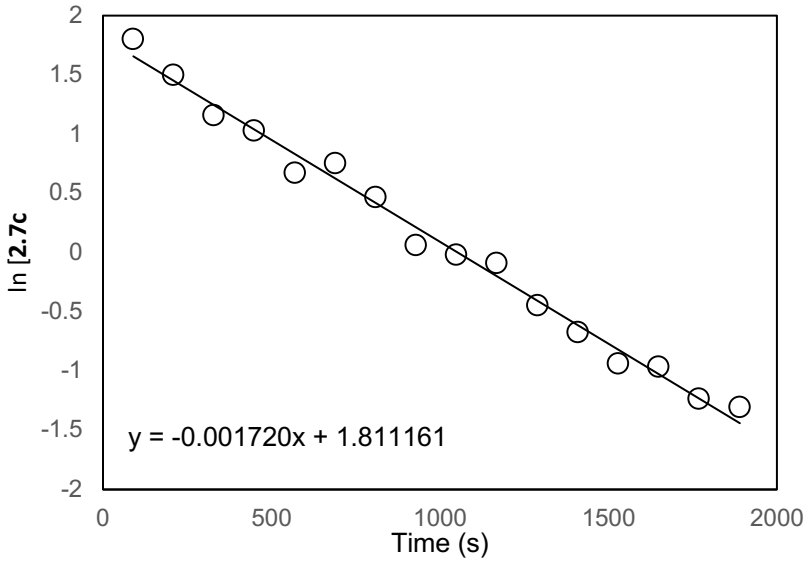

Figure 37. Pseudo first-order plot of reaction of **2.7c** (15 mM), styrene (310 mM) and diphenyl sulfide (310 mM) in toluene-d_8 at 25 °C.

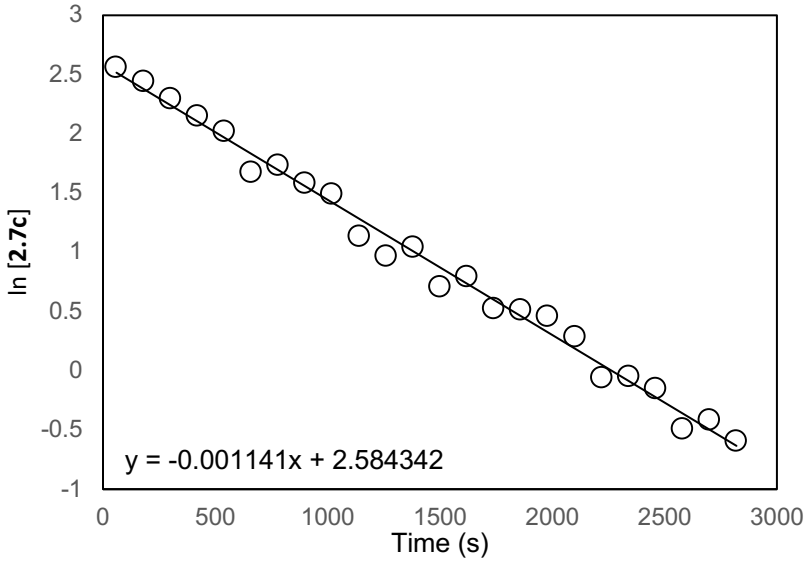

Figure 38. Pseudo first-order plot of reaction of **2.7c** (15 mM), styrene (310 mM) and diphenyl sulfide (460 mM) in toluene-d_8 at 25 °C.

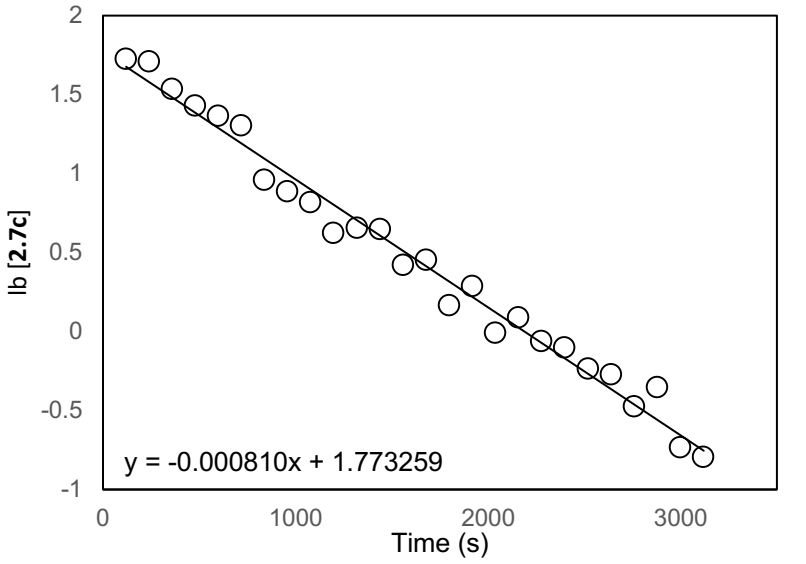

Figure 39. Pseudo first-order plot of reaction of **2.7c** (15 mM), styrene (310 mM) and diphenyl sulfide (610 mM) in toluene-d_8 at 25 °C.

Kinetics of reaction of 2.7a with 2.8 and THT. A solution of **2.7a** (15 mg, 9.8×10^{-3} mmol, 16 mM), **2.8** (13 μL, 9.8×10^{-2} mmol, 163 mM), tetrahydrothiophene (8.7 μL, 9.8×10^{-2} mmol, 163 mM) and CH_2Br_2 (2.0×10^{-2} mmol) in tolune-d_8 was placed in an NMR spectrometer heated to 95 °C and analyzed periodically by ^{1}H NMR spectroscopy. The concentration of **2.7a** was determined by integrating the *tert*-butyl resonance of **2.7a** at δ 1.05 relative to the CH_2Br_2 resonance at δ 3.95. A plot of ln[**2.7a**] versus time was linear to > 3 half-lives with a pseudo-first-order rate constant of $k_{obs} = 5.04 \pm 0.20 \times 10^{-4}$ s^{-1} (Table 5, entry 2). An analogous procedure was used to determine k_{obs} as a function of both [THT] and [**2.8**] (Table 5). A plot of $1/k_{obs}$ versus [THT]/[**2.8**] was linear with a slope of $1.52 \pm 0.06 \times 10^3$ s and an intercept of $3.7 \pm 1.2 \times 10^2$ s (Figure 40), which provided the values $k_1 = 2.7 \pm 0.9 \times 10^{-3}$ s^{-1} ($\Delta G^{\ddagger} = 26.0 \pm 0.2$ kcal/mol) and $k_{-1}/k_2 = 4.1 \pm 1.3$.

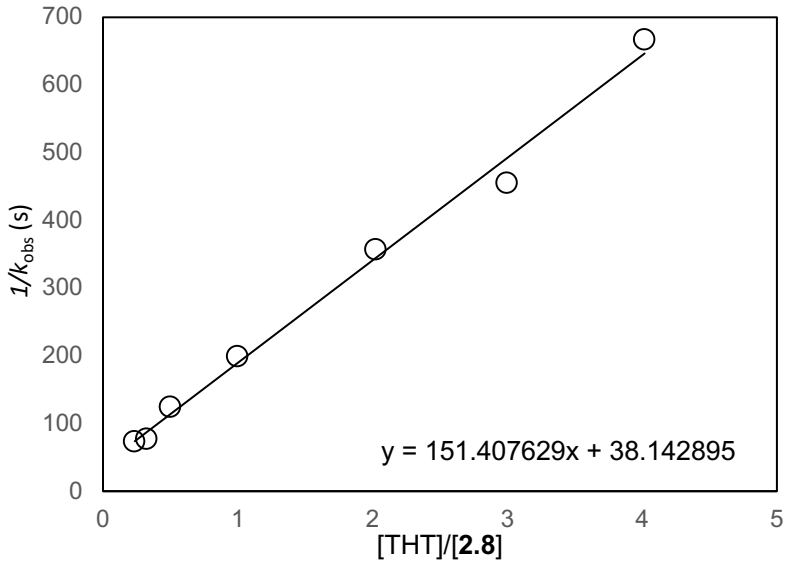

Figure 40. Plot of 1/kobs versus [THT]/[**2.8**] for the reaction of **2.7a** with **2.8** in toluene-d_8 at 95 °C.

Table 5. Pseudo-first-order rate constants for the reaction of **2.7a** with **2.8** in toluene-d_8 at 95 °C as a function of [THT] and [**2.8**].

entry	Figure	[THT] (mM)	[**2.8**] (mM)	(10^3) k_{obs} (s^{-1})
1	41	0	163	12.3±0.3
2	42	163	163	5.04±0.20
3	42	330	163	2.81±0.27
4	44	489	163	2.20±0.13
5	45	655	163	1.50±0.05
6	46	163	326	8.07±0.54
7	47	163	502	13.1±0.7
8	48	163	690	13.8±1.2

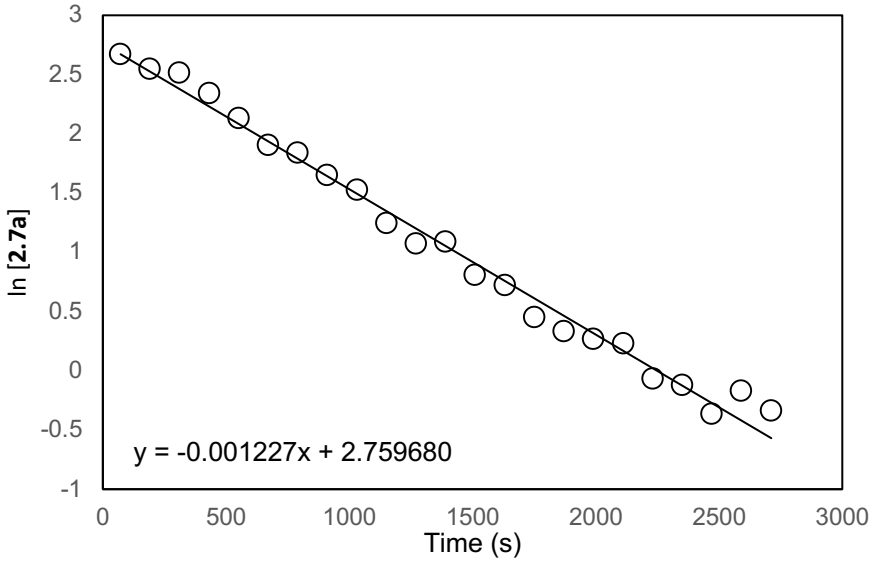

Figure 41. Pseudo first-order plot of reaction of **2.7a** (16 mM) and **2.8** (163 mM) in toluene-d_8 at 95 °C.

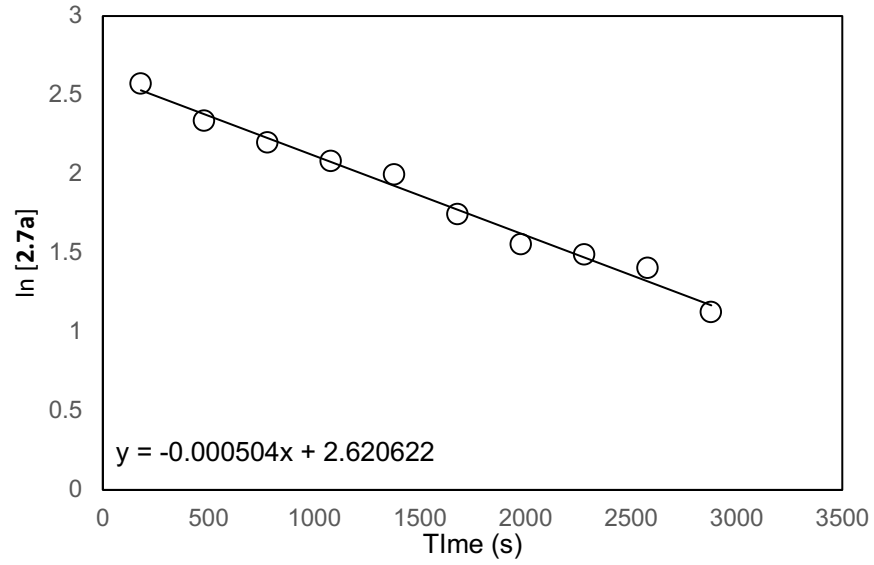

Figure 42. Pseudo first-order plot of reaction of **2.7a** (16 mM) and **2.8** (163 mM) and THT (163 mM) in toluene-d_8 at 95 °C.

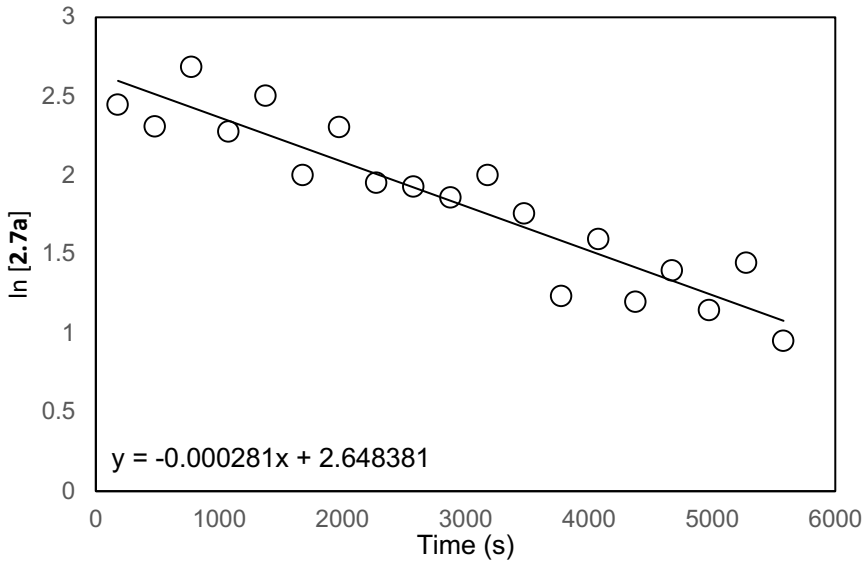

Figure 43. Pseudo first-order plot of reaction of **2.7a** (16 mM) and **2.8** (163 mM) and THT (330 mM) in toluene-d_8 at 95 °C.

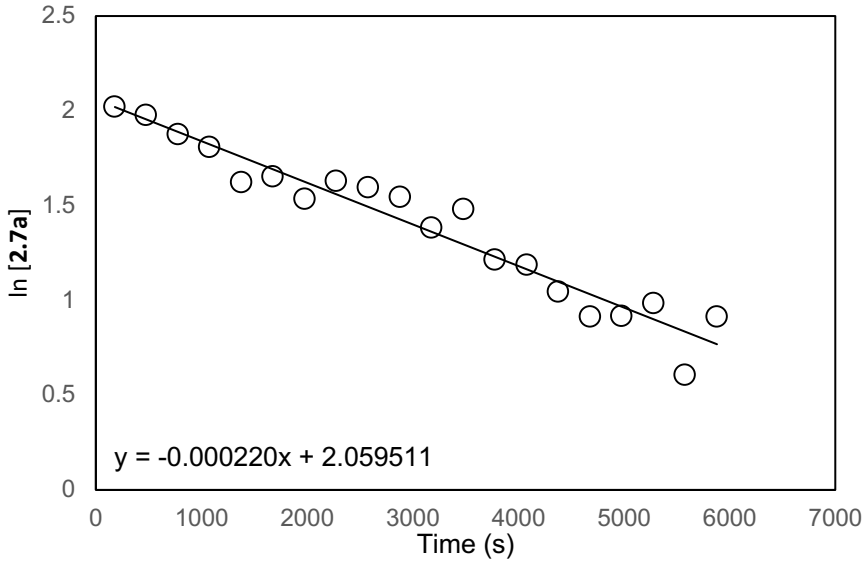

Figure 44. Pseudo first-order plot of reaction of **2.7a** (16 mM) and **2.8** (163 mM) and THT (489 mM) in toluene-d_8 at 95 °C.

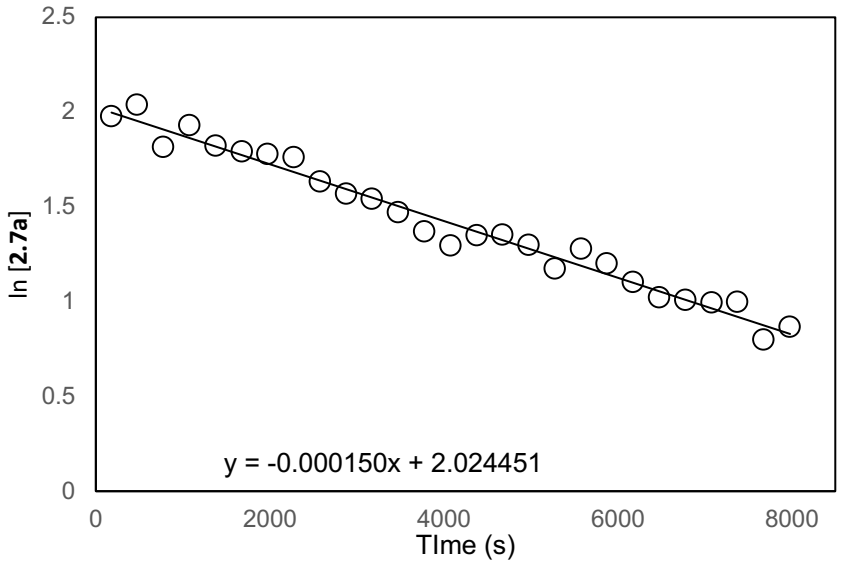

Figure 45. Pseudo first-order plot of reaction of **2.7a** (16 mM) and **2.8** (163 mM) and THT (655 mM) in toluene-d_8 at 95 °C.

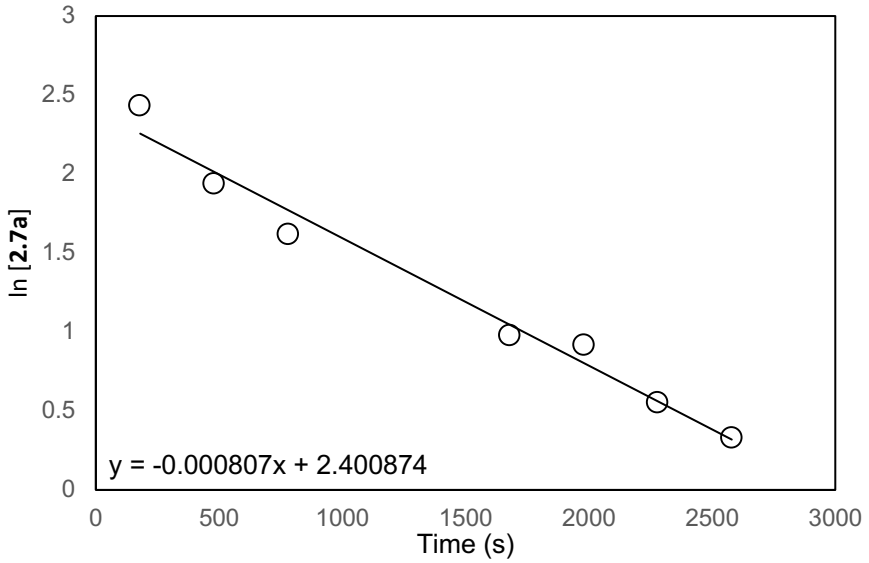

Figure 46. Pseudo first-order plot of reaction of **2.7a** (16 mM) and **2.8** (326 mM) and THT (330 mM) in toluene-d_8 at 95 °C.

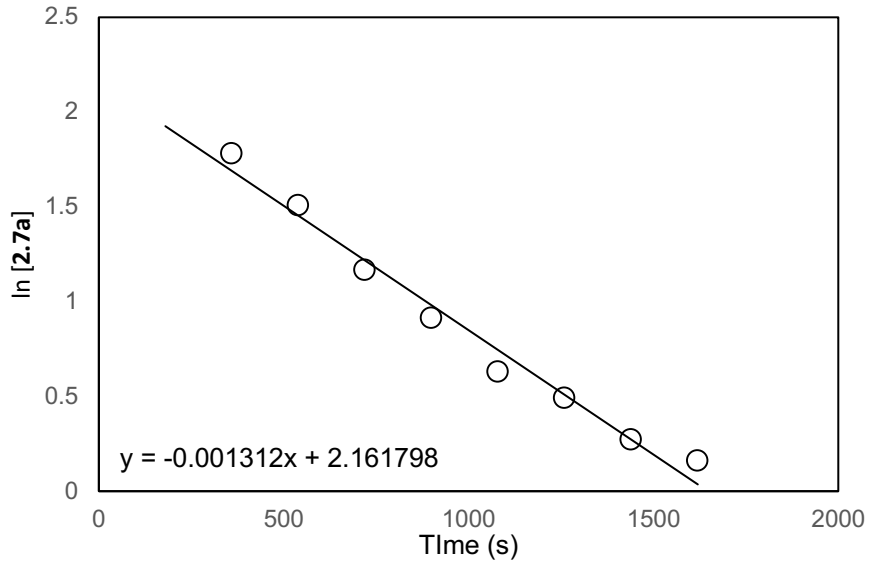

Figure 47. Pseudo first-order plot of reaction of **2.7a** (16 mM) and **2.8** (502 mM) and THT (330 mM) in toluene-d_8 at 95 °C.

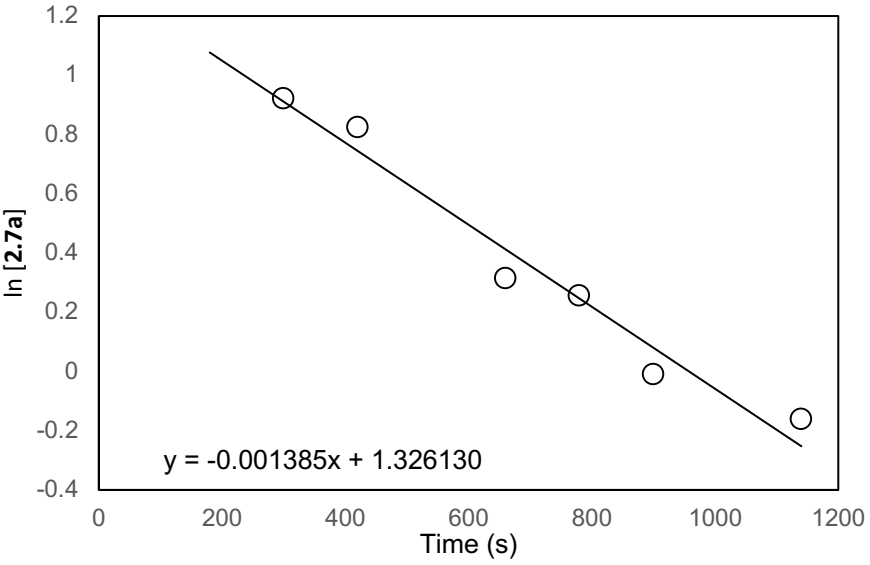

Figure 48. Pseudo first-order plot of reaction of **2.7a** (16 mM) and **2.8** (690 mM) and THT (330 mM) in toluene-d_8 at 95 °C.

2.6.5 Hammett Analysis

A solution of **2.7c** (15 mg, 9.2×10^{-3} mmol, 15 mM), **2.8** (11 μL, 9.2×10^{-2} mmol, 153 mM), diphenyl sulfide (16 μL, 9.2×10^{-2} mmol, 153 mM) and CH_2Br_2 (2.0×10^{-2} mmol) in toluene-d_8 was monitored at 25 °C periodically by ^{1}H NMR spectroscopy. The concentration of **2.7c** was determined by integrating the *tert*-butyl resonance of **2.7c** at δ 0.55 relative to the CH_2Br_2 resonance at δ 3.95. A plot of ln[**2.7c**] versus time was linear to >3 half-lives with a pseudo first-order rate constant of $k_{obs} = 6.53 \pm 0.22 \times 10^{-3}$ s^{-1} (Table 6, entry 1; Figure 50). An analogous procedure was used to determine k_{obs} as a function of [Ph_2S] and [styrene] for each styrene derivative (Tables 6–9). Plots of $1/k_{obs}$ versus [Ph_2S]/[stryene] were linear for each styrene derivative (Figures 49, 55, 60, and 65). The slope of each line was compared with the slope of line in Figure 2.8, to determine the value of k_X/k_H, which was compared with Hammett σ parameters to establish the rho value for the gold(I) benzylidene transfer.

Table 6. Pseudo-first-order rate constants for the reaction of **2.7c** with **2.8** in toluene-d_8 at 25 °C as a function of [Ph_2S] and [styrene].

entry	Figure	[Ph_2S] (mM)	[styrene] (mM)	(10^3) k_{obs} (s^{-1})
1	50	150	150	6.53 ± 0.22
2	51	310	150	4.17 ± 0.07
3	52	460	150	2.37 ± 0.11
4	53	610	150	1.83 ± 0.06
5	54	150	310	9.70 ± 0.27

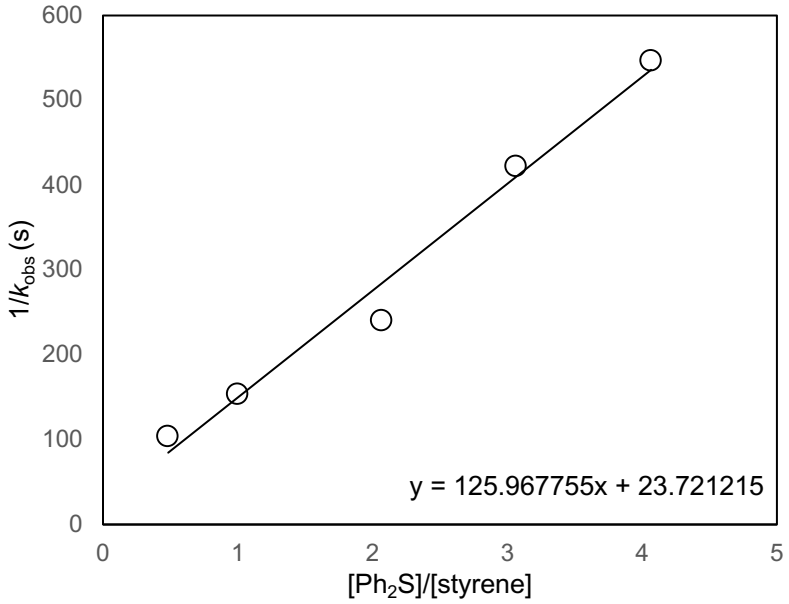

Figure 49. Plot of $1/k_{obs}$ versus [Ph_2S]/[styrene] for the reaction of **2.7c** with **2.8** in toluene-d_8 at 25 °C

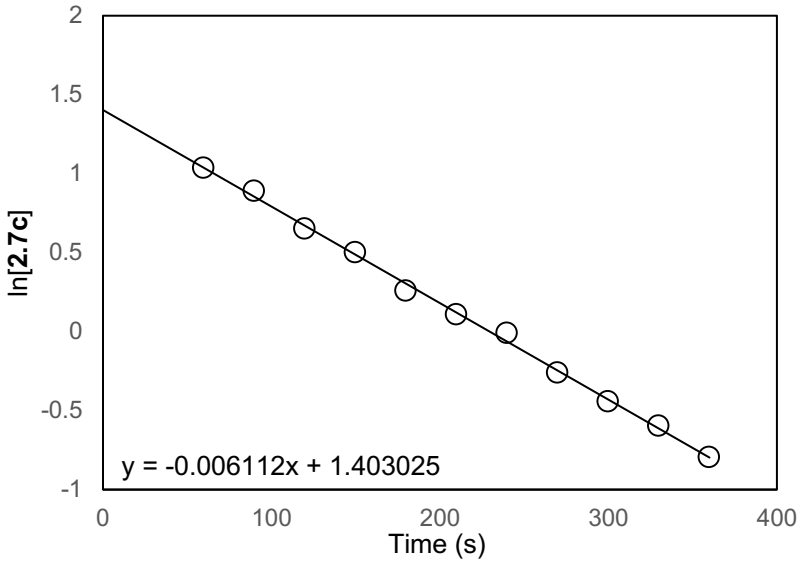

Figure 50. Pseudo-first-order plot of reaction of **2.7c** (15 mM) and **2.8** (150 mM) and Ph_2S (150 mM) in toluene-d_8 at 25 °C.

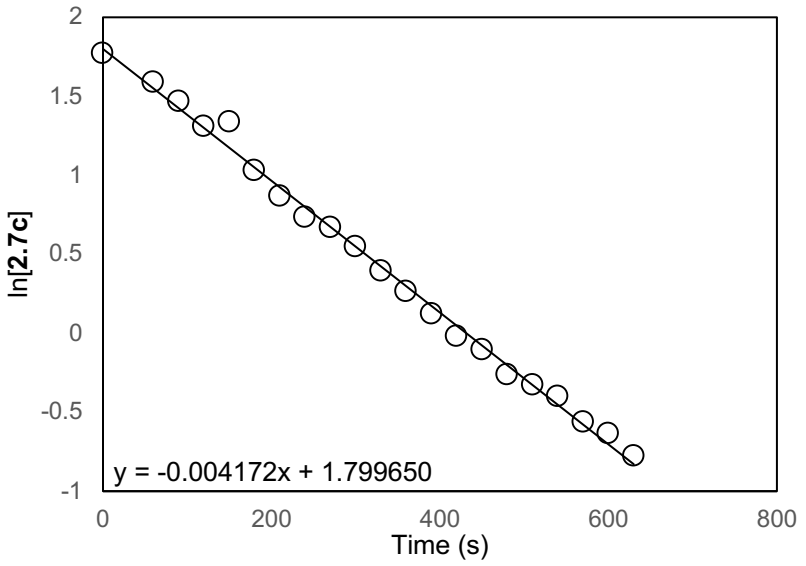

Figure 51. Pseudo-first-order plot of reaction of **2.7c** (15 mM) and **2.8** (150 mM) and Ph_2S (310 mM) in toluene-d_8 at 25 °C.

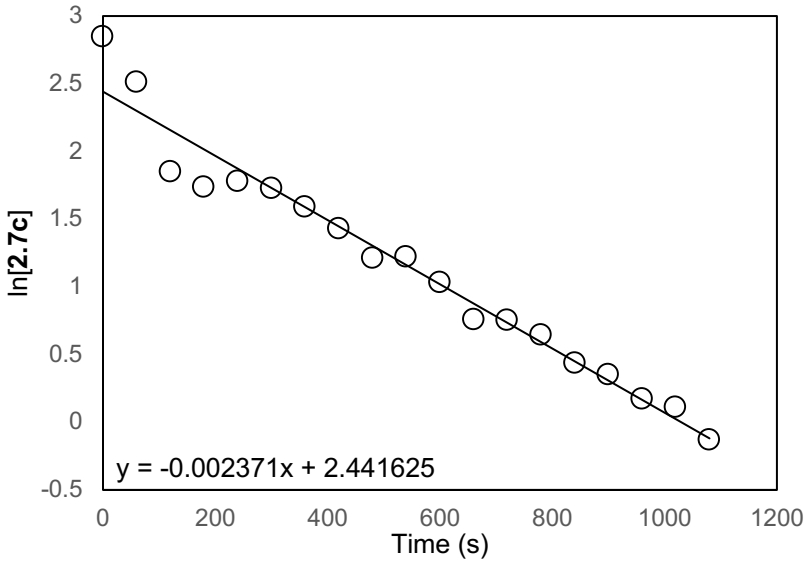

Figure 52. Pseudo-first-order plot of reaction of **2.7c** (15 mM) and **2.8** (150 mM) and Ph_2S (460 mM) in toluene-d_8 at 25 °C.

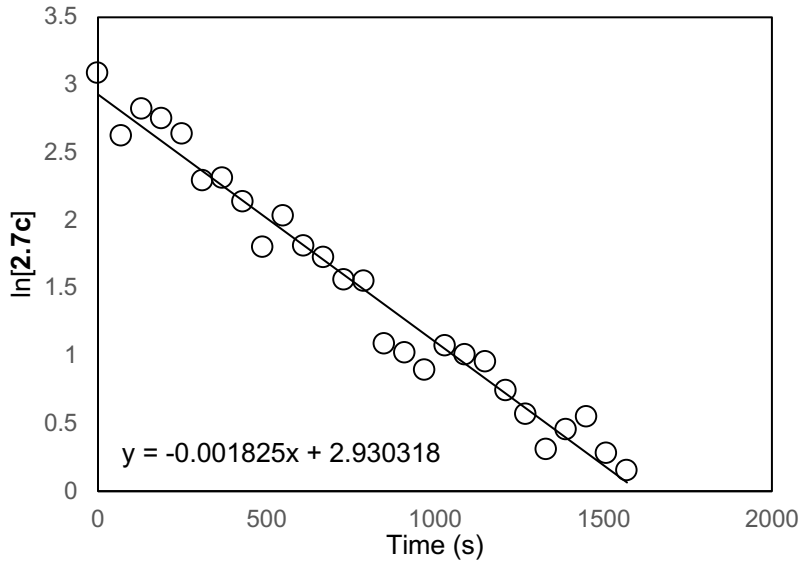

Figure 53. Pseudo-first-order plot of reaction of **2.7c** (15 mM) and **2.8** (150 mM) and Ph_2S (610 mM) in toluene-d_8 at 25 °C.

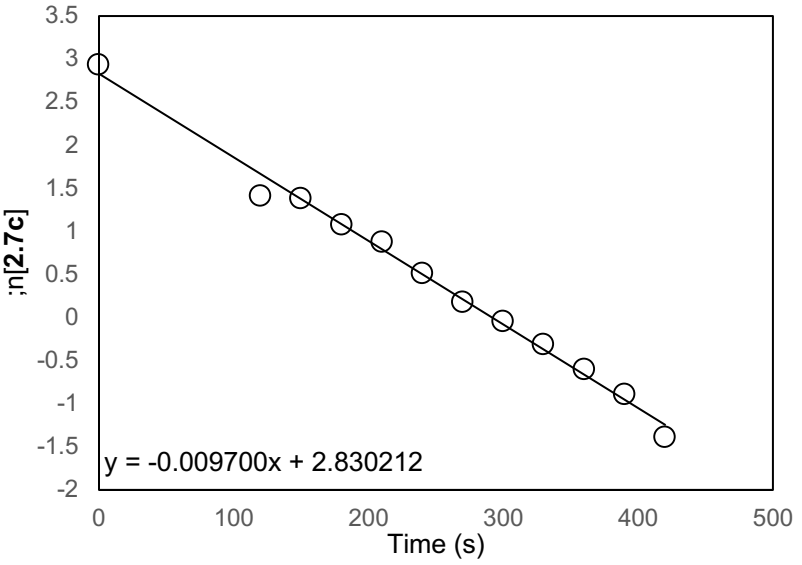

Figure 54. Pseudo-first-order plot of reaction of **2.7c** (15 mM) and **2.8** (310 mM) and Ph_2S (150 mM) in toluene-d_8 at 25 °C.

Table 7. Pseudo-first-order rate constants for the reaction of **2.7c** with *p*-methylstyrene in toluene-d_8 at 25 °C as a function of [Ph_2S] and [styrene].

entry	Figure	[Ph_2S] (mM)	[styrene] (mM)	(10^3) k_{obs} (s^{-1})
1	56	150	150	4.16 ± 0.08
2	57	310	150	2.28 ± 0.05
3	58	610	150	1.41 ± 0.08
4	59	150	310	7.25 ± 0.21

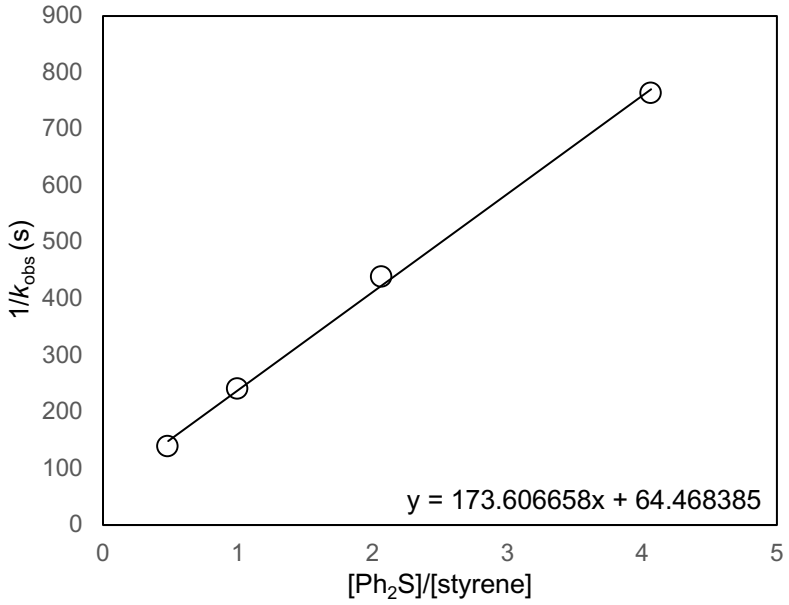

Figure 55. Plot of $1/k_{obs}$ versus [Ph_2S]/[styrene] for the reaction of **2.7c** with *p*-methylstyrene in toluene-d_8 at 25 °C

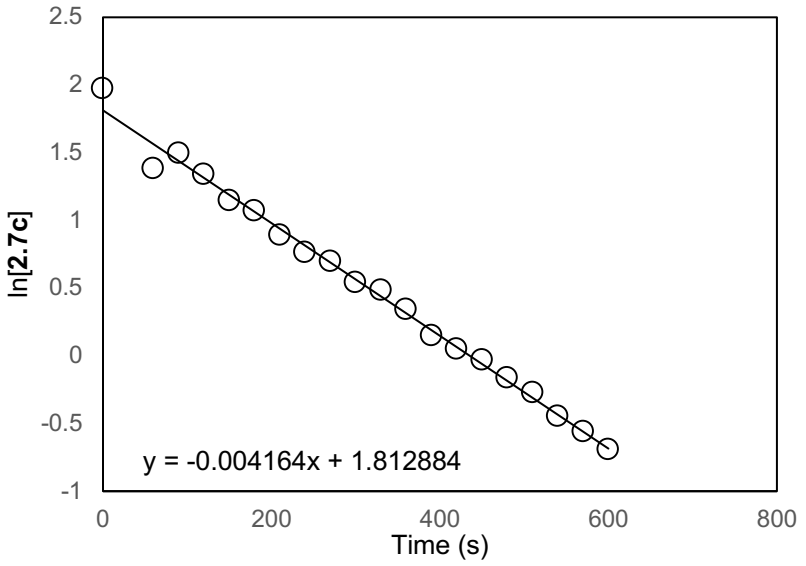

Figure 56. Pseudo-first-order plot of reaction of **2.7c** (15 mM) and *p*-methylstyrene (150 mM) and Ph_2S (150 mM) in toluene-d_8 at 25 °C.

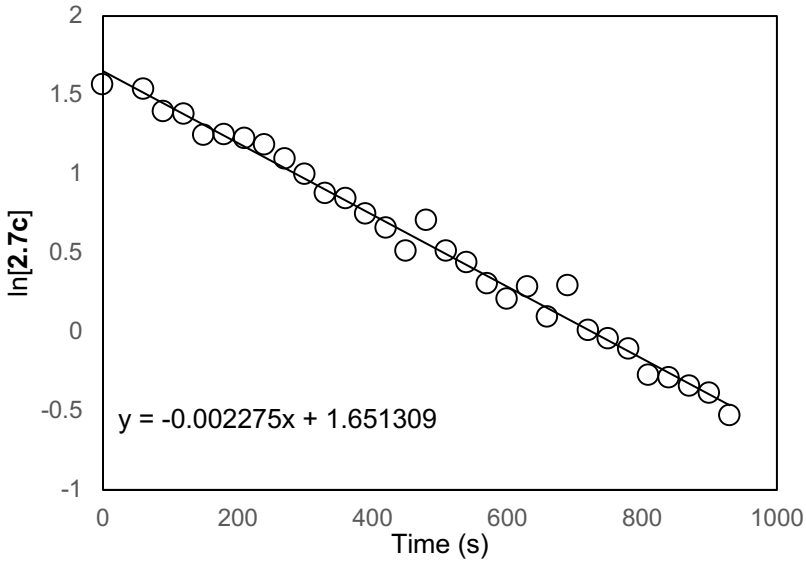

Figure 57. Pseudo-first-order plot of reaction of **2.7c** (15 mM) and *p*-methylstyrene (150 mM) and Ph_2S (310 mM) in toluene-d_8 at 25 °C.

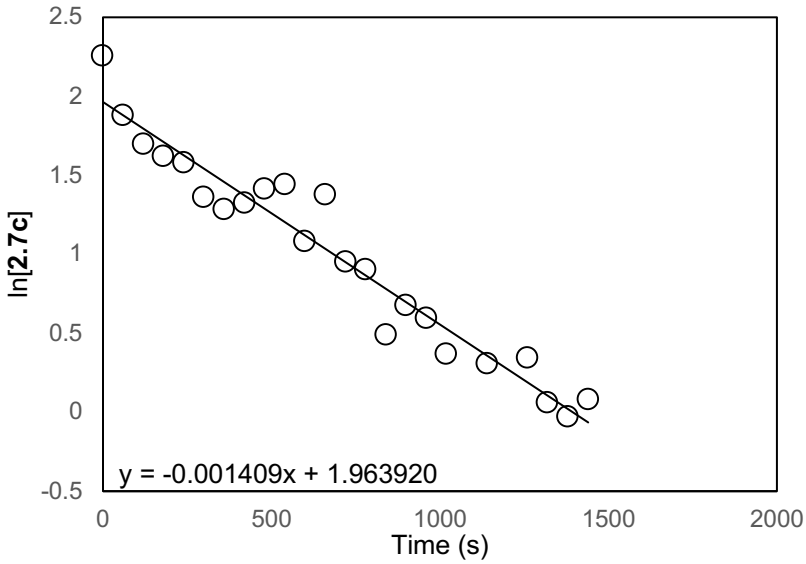

Figure 58. Pseudo-first-order plot of reaction of **2.7c** (15 mM) and *p*-methylstyrene (150 mM) and Ph_2S (610 mM) in toluene-d_8 at 25 °C.

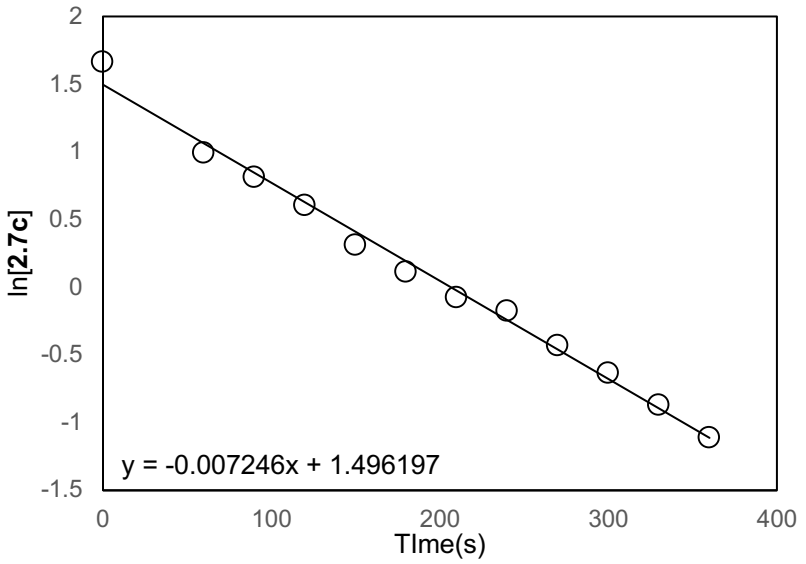

Figure 59. Pseudo-first-order plot of reaction of **2.7c** (15 mM) and *p*-methylstyrene (1310 mM) and Ph_2S (150 mM) in toluene-d_8 at 25 °C.

Table 8. Pseudo-first-order rate constants for the reaction of **2.7c** with *p*-chlorostyrene in toluene-d_8 at 25 °C as a function of [Ph_2S] and [styrene].

entry	Figure	[Ph_2S] (mM)	[styrene] (mM)	(10^3) k_{obs} (s^{-1})
1	61	150	150	1.17 ± 0.03
2	62	310	150	0.75 ± 0.01
3	63	460	150	0.43 ± 0.01
4	64	150	310	2.32 ± 0.05

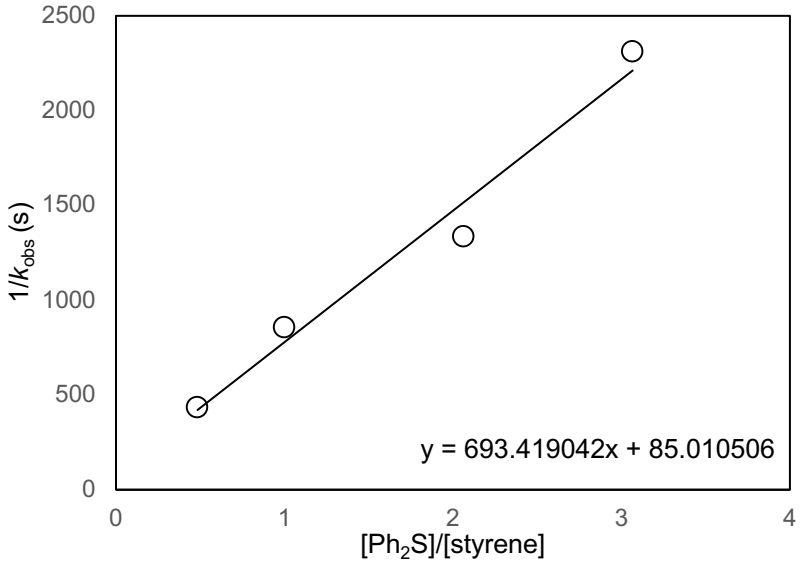

Figure 60. Plot of 1/k_{obs} versus [Ph_2S]/[styrene] for the reaction of **2.7c** with *p*-chlorostyrene in toluene-d_8 at 25 °C

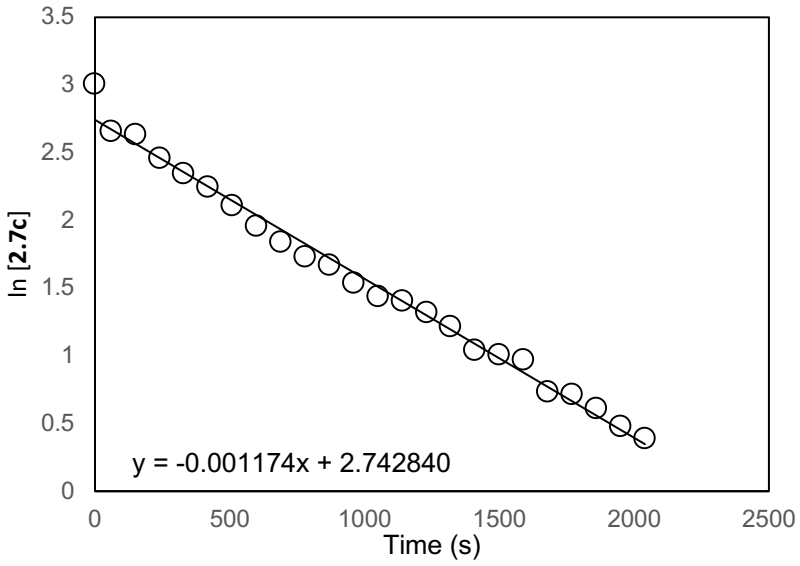

Figure 61. Pseudo-first-order plot of reaction of **2.7c** (15 mM) and *p*-chlorostyrene (150 mM) and Ph_2S (150 mM) in toluene-d_8 at 25 °C.

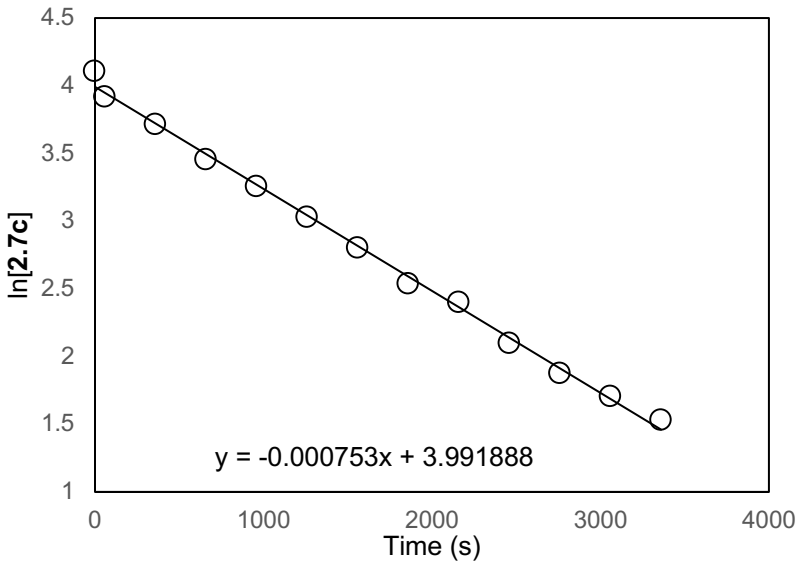

Figure 62. Pseudo first-order plot of reaction of **2.7c** (15 mM) and *p*-chlorostyrene (150 mM) and Ph_2S (310 mM) in toluene-d_8 at 25 °C.

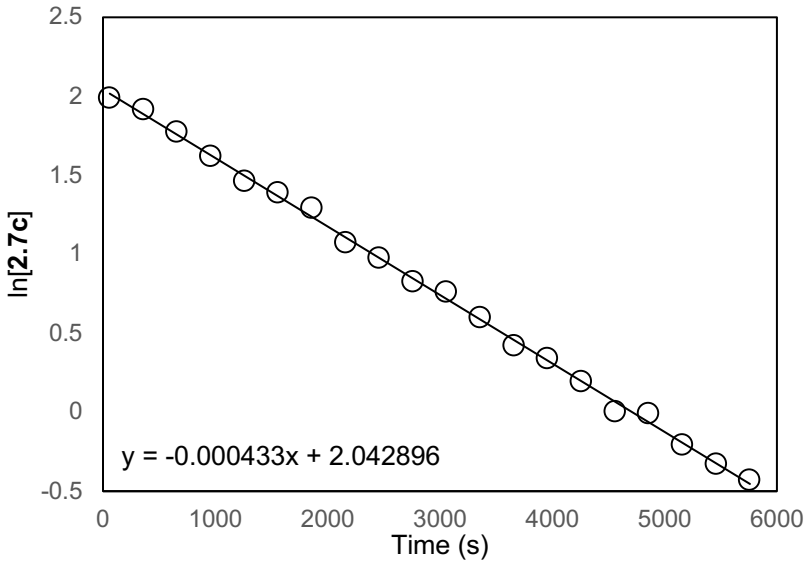

Figure 63. Pseudo first-order plot of reaction of **2.7c** (15 mM) and *p*-chlorostyrene (150 mM) and Ph_2S (460 mM) in toluene-d_8 at 25 °C.

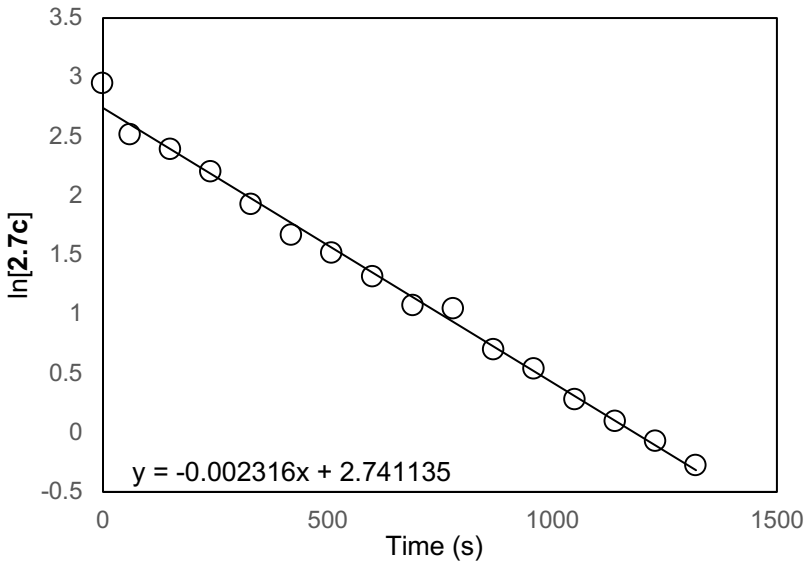

Figure 64. Pseudo first-order plot of reaction of **2.7c** (15 mM) and *p*-chlorostyrene (310 mM) and Ph_2S (150 mM) in toluene-d_8 at 25 °C.

Table 9. Pseudo-first-order rate constants for the reaction of **2.7c** with *p*-cyanostyrene in toluene-d_8 at 25 °C as a function of [Ph_2S] and [styrene].

entry	Figure	[Ph_2S] (mM)	[styrene] (mM)	(10^4) k_{obs} (s^{-1})
1	66	150	150	1.66 ± 0.09
2	67	310	150	0.77 ± 0.03
3	68	460	150	0.67 ± 0.02
4	69	150	310	3.41 ± 0.26

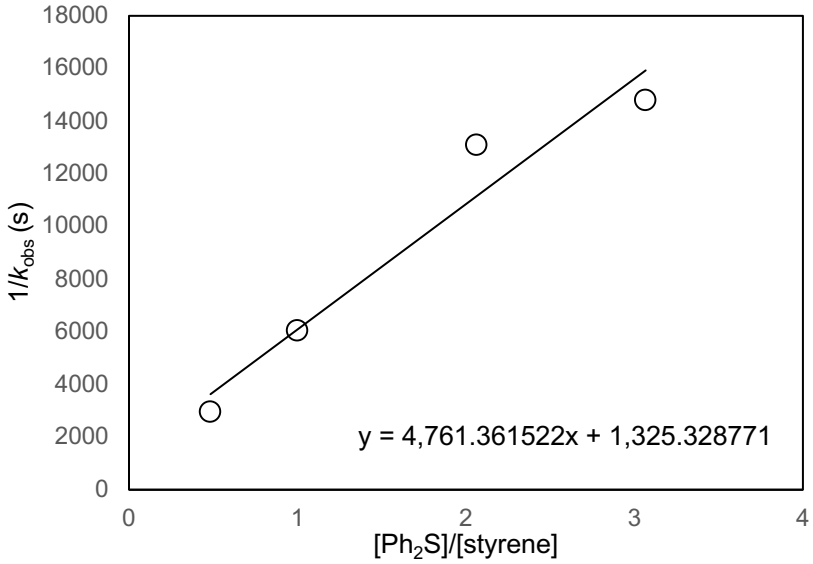

Figure 65. Plot of 1/k_{obs} versus [Ph_2S]/[styrene] for the reaction of **2.7c** with *p*-cyanostyrene in toluene-d_8 at 25 °C.

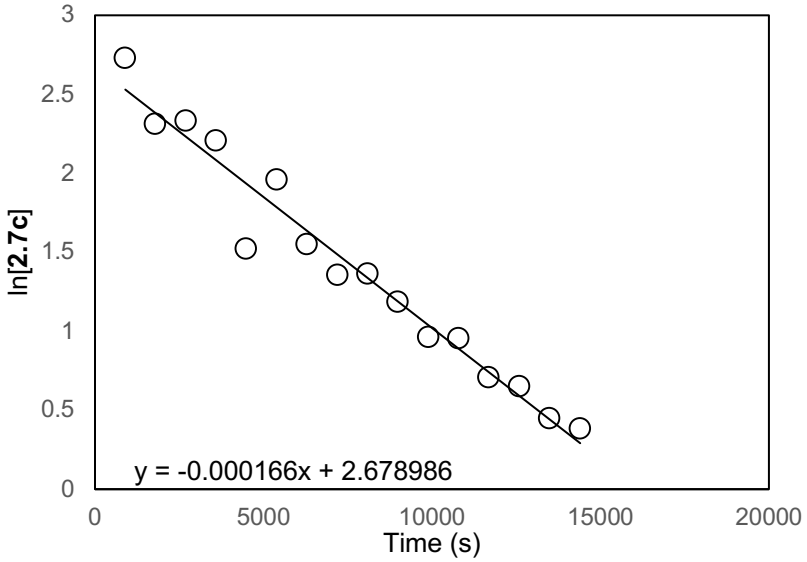

Figure 66. Pseudo-first-order plot of reaction of **2.7c** (15 mM) and *p*-cyanostyrene (150 mM) and Ph_2S (150 mM) in toluene-d_8 at 25 °C.

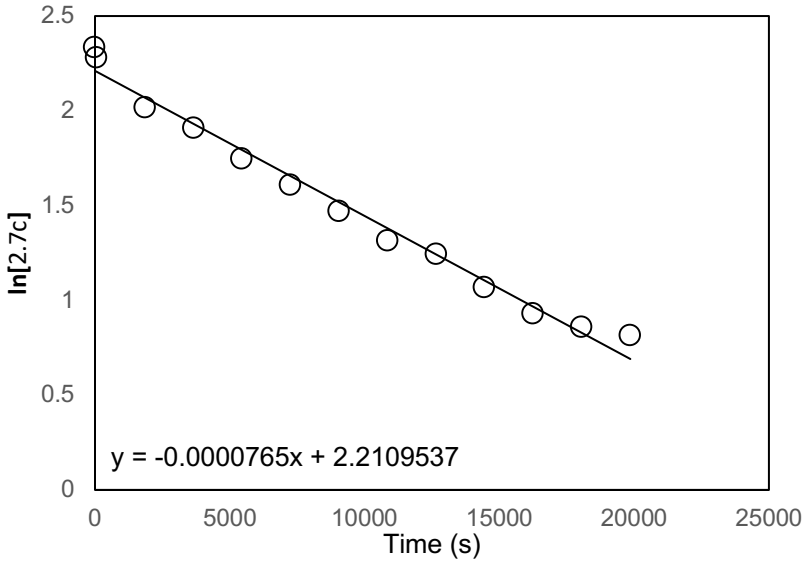

Figure 67. Pseudo-first-order plot of reaction of **2.7c** (15 mM) and *p*-cyanostyrene (150 mM) and Ph_2S (310 mM) in toluene-d_8 at 25 °C.

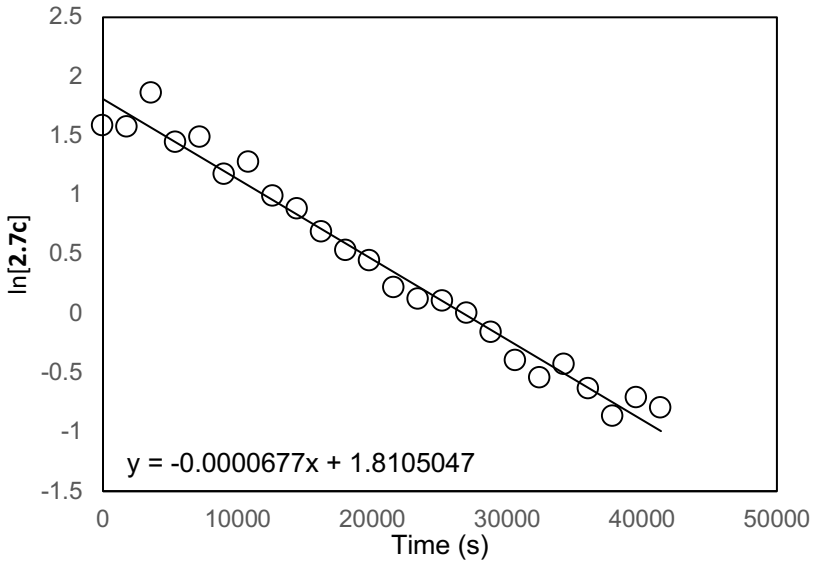

Figure 68. Pseudo-first-order plot of reaction of **2.7c** (15 mM) and *p*-cyanostyrene (150 mM) and Ph_2S (460 mM) in toluene-d_8 at 25 °C.

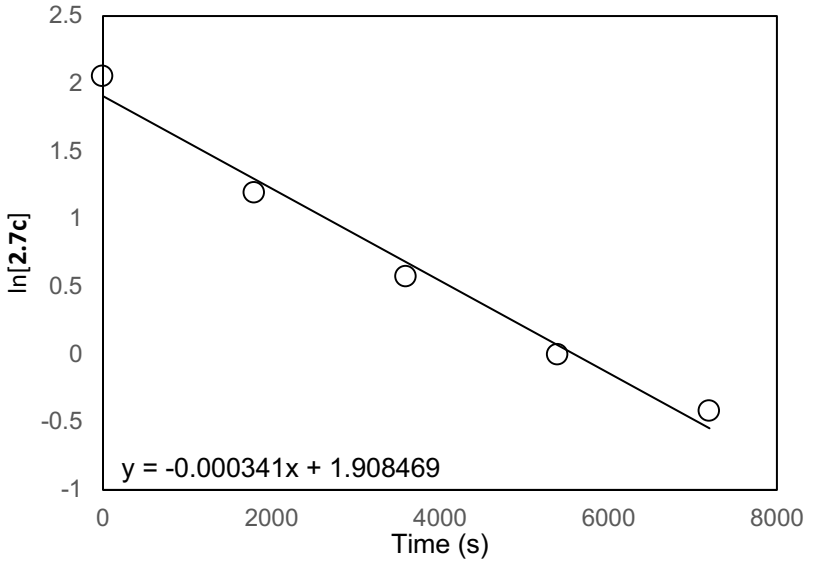

Figure 69. Pseudo-first-order plot of reaction of **2.7c** (15 mM) and *p*-cyanostyrene (310 mM) and Ph_2S (150 mM) in toluene-d_8 at 25 °C.

2.6.6 Kinetic Isotope Experiments

Kinetics of reaction of 2.7c with α-deuterio-4-methoxystyrene in the presence of diphenyl sulfide. A solution of **2.7c** (15 mg, 9.2×10^{-3} mmol, 15 mM), α-deuterio-4-methoxystyrene (11 μL, 9.2×10^{-2} mmol, 153 mM), diphenyl sulfide (16 μL, 9.2×10^{-2} mmol, 153 mM) and CH_2Br_2 (2.0×10^{-2} mmol) in toluene-d_8 was monitored at 25 °C periodically by ^{1}H NMR spectroscopy. The concentration of **2.7c** was determined by integrating the *tert*-butyl resonance of **2.7c** at δ 0.55 relative to the CH_2Br_2 resonance at δ 3.95. A plot of ln[**2.7c**] versus time was linear to >3 half-lives with a pseudo first-order rate constant of $k_{obs} = 4.36 \pm 0.08 \times 10^{-3}$ s^{-1} (Table 10, entry 1; Figure 71). An analogous procedure was used to determine k_{obs} as a function of [Ph_2S] and [styrene] (Table 10, entries 2 – 5; Figure 72 – 75). A plot of $1/k_{obs}$ versus [Ph_2S]/[stryene] was linear with a slope of $1.35 \pm 0.09 \times 10^2$ s and an intercept of $0.65 \pm 0.23 \times 10^2$ s (Figure 70), which provided a kinetic isotope effect of 1.07 ± 0.11.

Table 10. Pseudo-first-order rate constants for the reaction of **2.7c** with *p*-cyanostyrene in toluene-d_8 at 25 °C as a function of [Ph_2S] and [styrene].

entry	Figure	[Ph_2S] (mM)	[styrene] (mM)	(10^3) k_{obs} (s^{-1})
1	71	150	150	4.36 ± 0.08
2	72	310	150	3.16 ± 0.06
3	73	460	150	2.16 ± 0.02
4	74	620	150	1.59 ± 0.04
5	75	150	310	8.15 ± 0.30

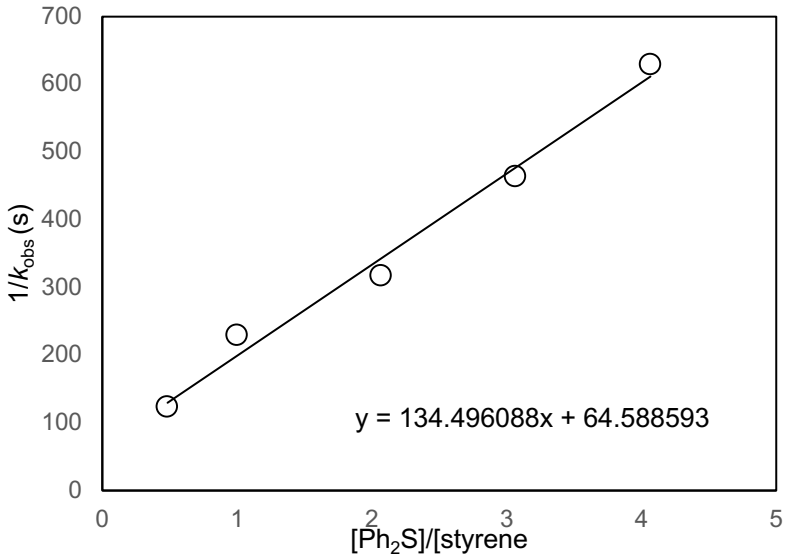

Figure 70. Plot of $1/k_{obs}$ versus [Ph_2S]/[styrene] for the reaction of **2.7c** with α-deuterio-4-methoxystyrene in toluene-d_8 at 25 °C.

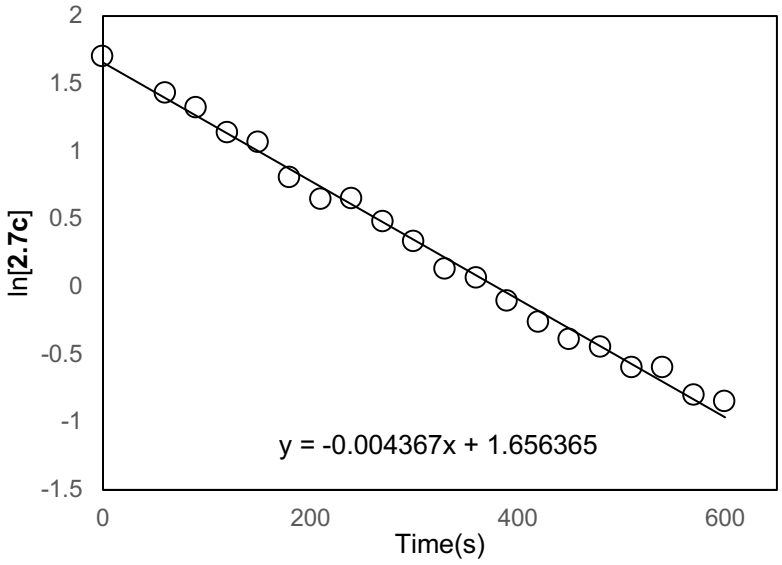

Figure 71. Pseudo-first-order plot of reaction of **2.7c** (15 mM) and α-deuterio-4-methoxystyrene (150 mM) and Ph_2S (150 mM) in toluene-d_8 at 25 °C.

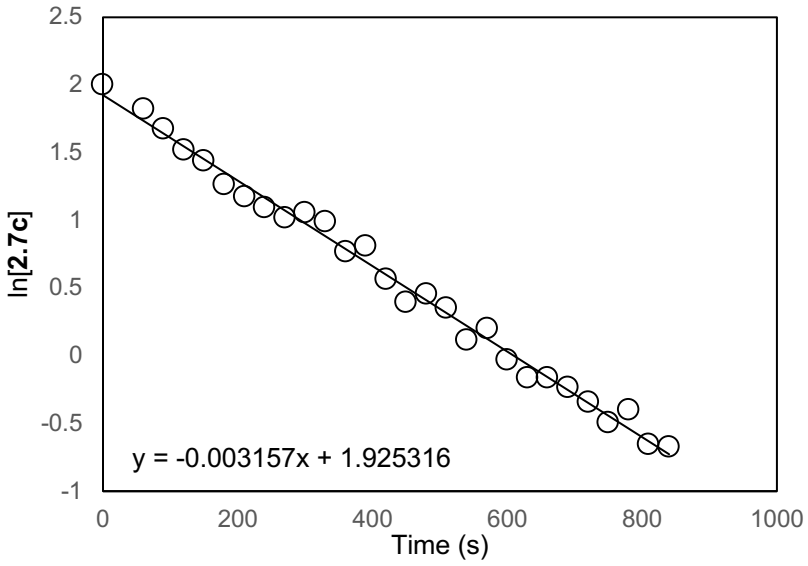

Figure 72. Pseudo-first-order plot of reaction of **2.7c** (15 mM) and α-deuterio-4-methoxystyrene (150 mM) and Ph_2S (310 mM) in toluene-d_8 at 25 °C.

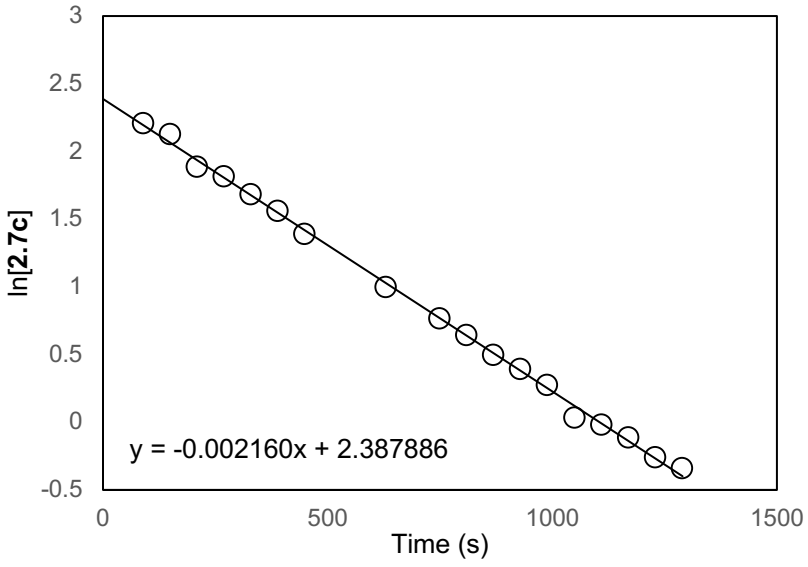

Figure 73. Pseudo-first-order plot of reaction of **2.7c** (15 mM) and α-deuterio-4-methoxystyrene (150 mM) and Ph_2S (460 mM) in toluene-d_8 at 25 °C.

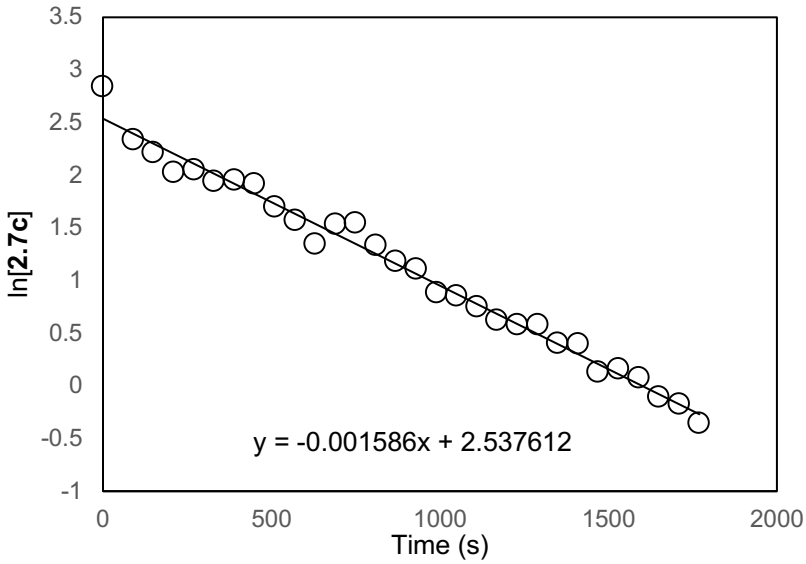

Figure 74. Pseudo-first-order plot of reaction of **2.7c** (15 mM) and α-deuterio-4-methoxystyrene (150 mM) and Ph_2S (610 mM) in toluene-d_8 at 25 °C.

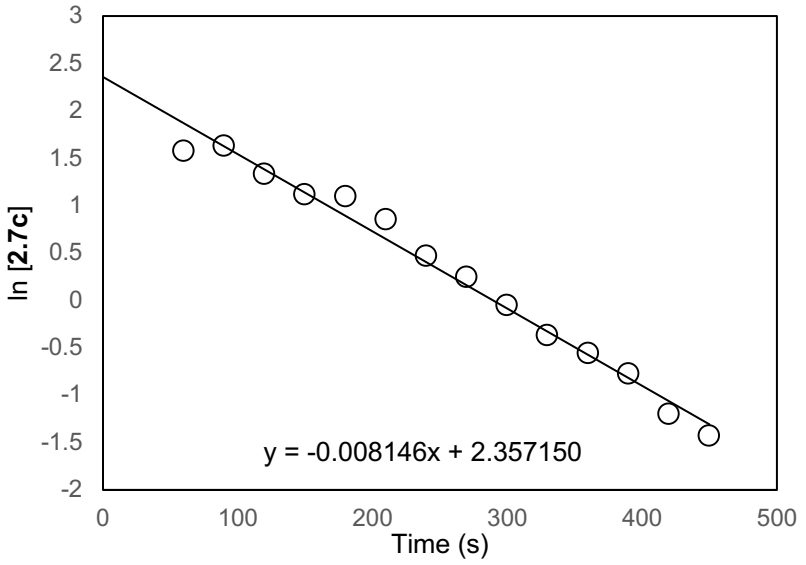

Figure 75. Pseudo-first-order plot of reaction of **2.7c** (15 mM) and α-deuterio-4-methoxystyrene (310 mM) and Ph_2S (150 mM) in toluene-d_8 at 25 °C.

Kinetics of reaction of 2.7c with β-dideuterio-4-methoxystyrene in the presence of diphenyl sulfide. A solution of **2.7c** (15 mg, 9.2×10^{-3} mmol, 15 mM), β-dideuterio-4-methoxystyrene (11 μL, 9.2×10^{-2} mmol, 153 mM), diphenyl sulfide (16 μL, 9.2×10^{-2} mmol, 153 mM) and CH_2Br_2 (2.0×10^{-2} mmol) in toluene-d_8 was monitored at 25 °C periodically by ^{1}H NMR spectroscopy. The concentration of **2.7c** was determined by integrating the *tert*-butyl resonance of **2.7c** at δ 0.55 relative to the CH_2Br_2 resonance at δ 3.95. A plot of ln[**2.7c**] versus time was linear to >3 half-lives with a pseudo first-order rate constant of $k_{obs} = 4.36 \pm 0.08 \times 10^{-3}$ s^{-1} (Table 11, entry 1; Figure 32). An analogous procedure was used to determine k_{obs} as a function of [Ph_2S] and [styrene] (Table 11, entries 2 – 4; Figure 77–80). A plot of $1/k_{obs}$ versus [Ph_2S]/[stryene] was linear with a slope of $1.46 \pm 0.04 \times 10^2$ s and an intercept of $0.63 \pm 0.08 \times 10^2$ s (Figure 76), which provided a kinetic isotope effect of 1.16 ± 0.09.

Table 11. Pseudo-first-order rate constants for the reaction of **2.7c** with *p*-cyanostyrene in toluene-d_8 at 25 °C as a function of [Ph_2S] and [styrene].

entry	Figure	[Ph_2S] (mM)	[styrene] (mM)	(10^3) k_{obs} (s^{-1})
1	77	150	150	4.57 ± 0.03
2	78	310	150	2.75 ± 0.04
4	79	610	150	1.53 ± 0.01
5	80	150	310	8.03 ± 0.41

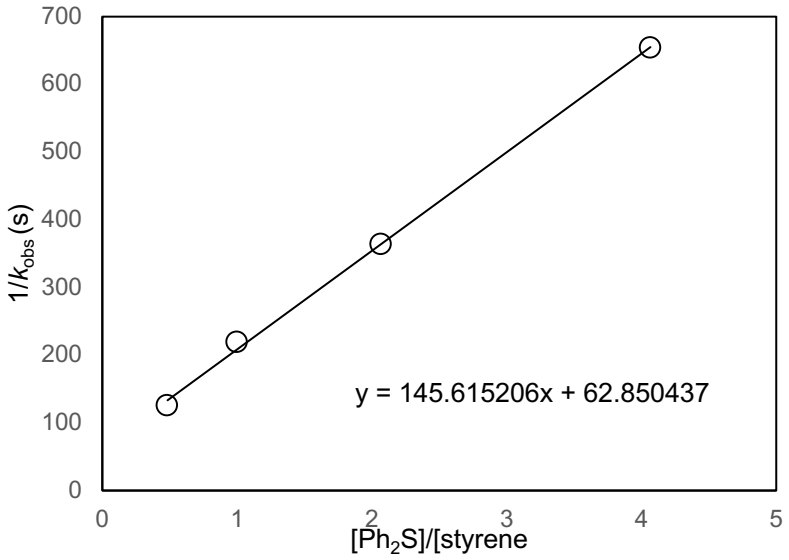

Figure 76. Plot of $1/k_{obs}$ versus [Ph_2S]/[styrene] for the reaction of **2.7c** with β-dideuterio-4-methoxystyrene in toluene-d_8 at 25 °C.

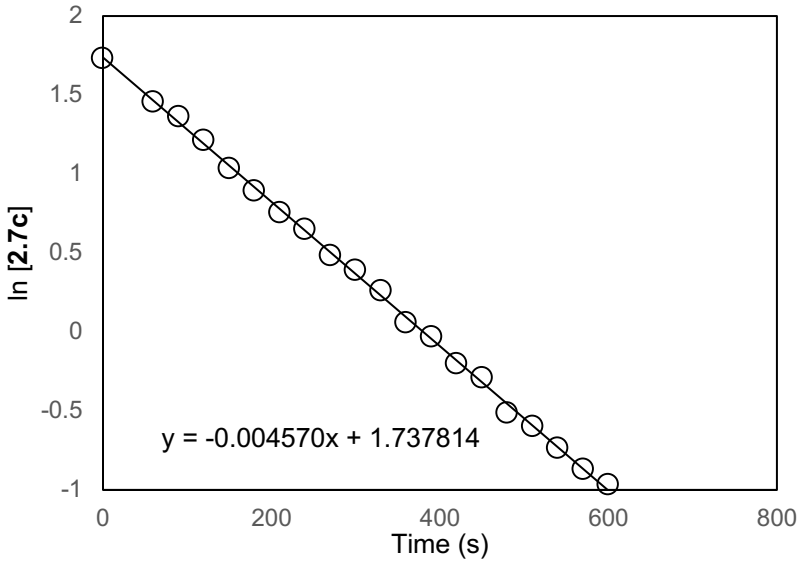

Figure 77. Pseudo-first-order plot of reaction of **2.7c** (15 mM) and β-dideuterio-4-methoxystyrene (150 mM) and Ph_2S (150 mM) in toluene-d_8 at 25 °C.

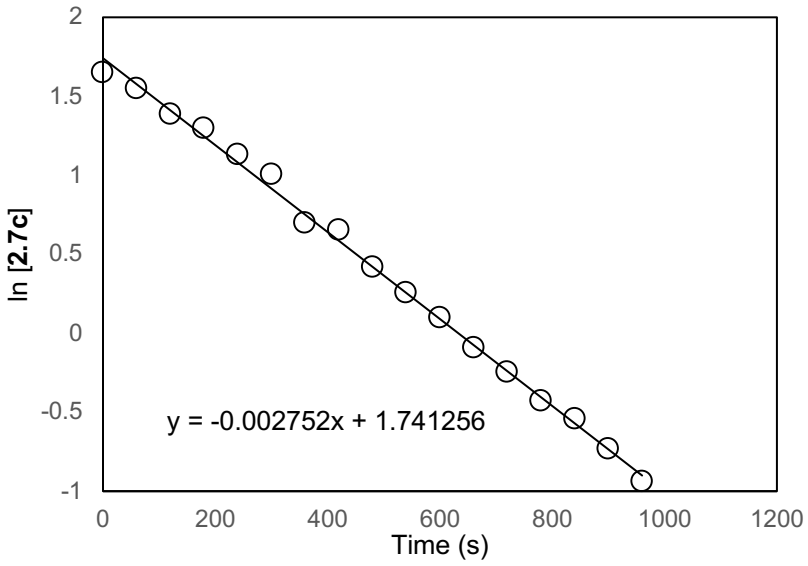

Figure 78. Pseudo-first-order plot of reaction of **2.7c** (15 mM) and β-dideuterio-4-methoxystyrene (150 mM) and Ph_2S (310 mM) in toluene-d_8 at 25 °C.

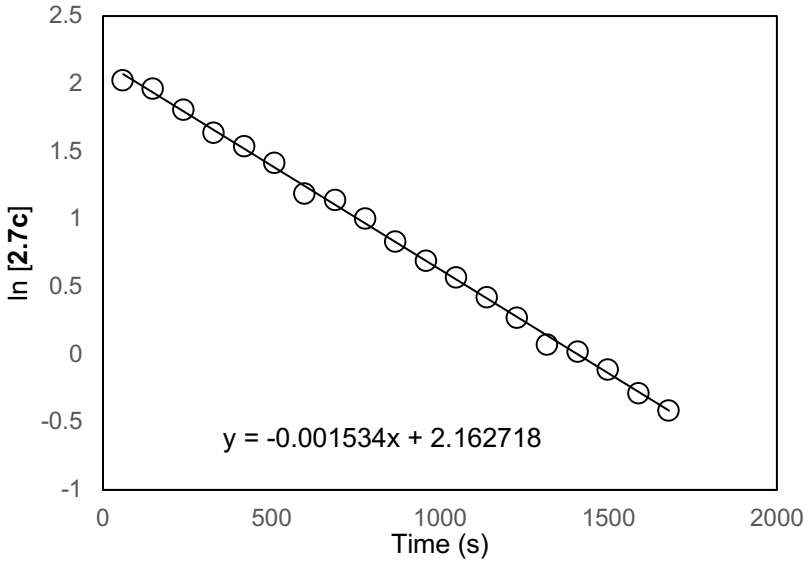

Figure 79. Pseudo-first-order plot of reaction of **2.7c** (15 mM) and β-dideuterio-4-methoxystyrene (150 mM) and Ph_2S (610 mM) in toluene-d_8 at 25 °C.

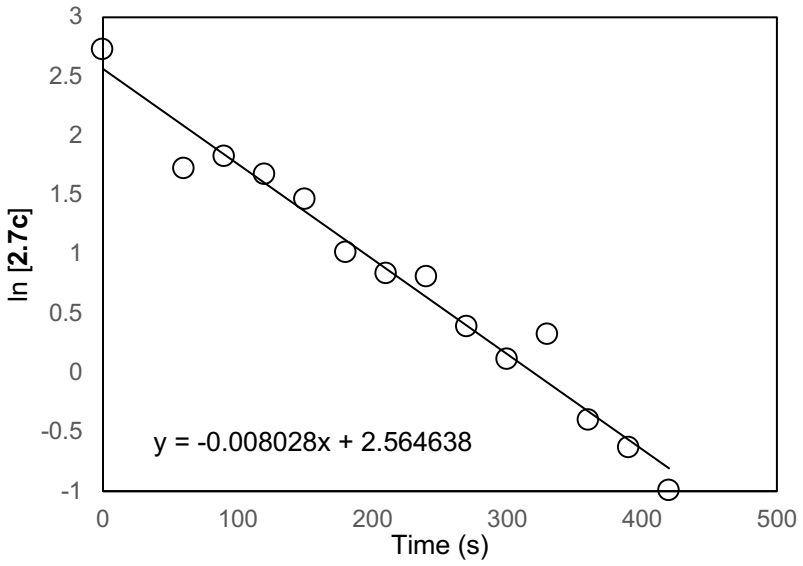

Figure 80. Pseudo-first-order plot of reaction of **2.7c** (15 mM) and β-dideuterio-4-methoxystyrene (310 mM) and Ph_2S (150 mM) in toluene-d_8 at 25 °C.

2.6.7 Crystallographic Data

Molecular structure data for 2.7a. A concentrated solution of **1a** was layered with hexanes at 4 °C and maintained at that temperature overnight to afford colorless crystals suitable for X-ray analysis. A colorless block-like specimen of $C_{63}H_{53}AuBF_{24}PS$, approximate dimensions 0.266 mm × 0.341 mm × 0.446 mm, was used for the X-ray crystallographic analysis. The X-ray intensity data were measured on a Bruker-Nonius X8 Kappa APEX II system equipped with a fine-focus sealed tube (MoKα, λ = 0.71073 Å) and a graphite monochromator. The total exposure time was 11.28 hours. The frames were integrated with the Bruker SAINT software package using a narrow-frame

algorithm. The integration of the data using a triclinic unit cell yielded a total of 556435 reflections to a maximum θ angle of 36.58° (0.60 Å resolution), of which 60571 were independent (average redundancy 9.186, completeness = 99.4%, R_{int} = 4.49%, R_{sig} = 2.67%) and 49543 (81.79%) were greater than $2\sigma(F^2)$. The final cell constants of a = 15.1721(4) Å, b = 20.7402(5) Å, c = 22.0070(5) Å, α = 64.3030(10)°, β = 85.7140(10)°, γ = 81.4250(10)°, volume = 6170.0(3) $Å^3$, are based upon the refinement of the XYZ-centroids of 9754 reflections above 20 σ(I) with 4.660° < 2θ < 67.47°. Data were corrected for absorption effects using the Numerical Mu Calculated method (SADABS). The ratio of minimum to maximum apparent transmission was 0.732. The calculated minimum and maximum transmission coefficients (based on crystal size) are 0.2215 and 0.3025. The final anisotropic full-matrix least-squares refinement on F^2 with 1703 variables converged at R1 = 3.76%, for the observed data and wR2 = 9.05% for all data. The goodness-of-fit was 1.153. The largest peak in the final difference electron density synthesis was 7.043 $e^-/Å^3$ and the largest hole was -2.038 $e^-/Å^3$ with an RMS deviation of 0.130 $e^-/Å^3$. On the basis of the final model, the calculated density was 1.654 g/cm^3 and F(000), 3048 e^-.

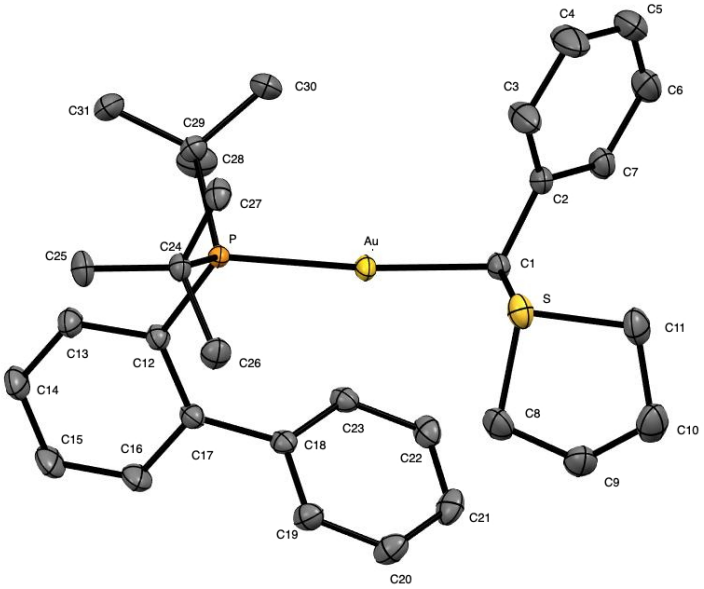

Figure 81. ORTEP diagram of gold(I) benzylide complex **2.7a** with ellipsoids shown at 50% probability level and with counterion, solvent and hydrogen atoms omitted.

Table 12. Bond Lengths for **2.7a**.

Bond	Length (Å)	Bond	Length (Å)	Bond	Length (Å)
Au1-C1	2.0963(19)	Au1-P1	2.2921(5)	C22-H22	0.95
S1-C1	1.796(2)	S1-C11	1.817(2)	C24-C26	1.531(3)
S1-C8	1.827(2)	P1-C12	1.827(2)	C24-C25	1.536(3)
P1-C24	1.877(2)	P1-C28	1.887(2)	C20-H20	0.95
C1-C2	1.507(3)	C1-H1	1.0	C21-H21	0.95
C2-C3	1.395(3)	C2-C7	1.397(3)	C26-H26	0.98
C3-C4	1.390(3)	C3-H3	0.95	C23-H23	0.95
C4-C5	1.387(4)	C4-H4	0.95	C24-C27	1.532(3)
C5-C6	1.387(4)	C5-H5	0.95	C25-H25A	0.98
C6-C7	1.389(3)	C6-H6	0.95	C21-C22	1.389(4)
C7-H7	0.95	C8-C9	1.517(3)	C22-C23	1.385(3)
C8-H8A	0.99	C8-H8B	0.99	C27-H27A	0.98
C9-C10	1.519(4)	C9-H9A	0.99	C28-C30	1.525(3)
C9-H9B	0.99	C10-C11	1.516(3)	C28-C31	1.537(3)
C10-H10	0.99	C10-H10B	0.99	C29-H29	0.98
C11-H11	0.99	C11-H11B	0.99	C30-H30	0.98
C12-C17	1.405(3)	C12-C13	1.406(3)	C30-H30	0.98
C13-C14	1.382(3)	C13-H13	0.95	C31-H31	0.98
C14-C15	1.381(4)	C14-H14	0.95	C28-C29	1.535(3)
C15-C16	1.386(4)	C15-H15	0.95	C29-H29A	0.98
C16-C17	1.398(3)	C16-H16	0.95	C29-H29C	0.98
C17-C18	1.493(3)	C18-C19	1.395(3)	C30-H30B	0.98
C18-C23	1.398(3)	C19-C20	1.390(3)	C31-H31A	0.98
C19-H19	0.95	C20-C21	1.382(4)	C31-H31C	0.98

Table 13. Bond Angles for **2.7a**

Bond	Angle (°)	Bond	Angle (°)	Bond	Angle (°)
C1-Au1-P1	174.62(5)	C1-S1-C11	106.77(10)	C13-C12-P1	118.94(16)
C1-S1-C8	108.56(10)	C11-S1-C8	93.97(11)	C14-C13-H13	119.1
C12-P1-C24	105.13(9)	C12-P1-C28	107.65(10)	C15-C14-C13	119.9(2)
C24-P1-C28	113.87(10)	C12-P1-Au1	115.01(7)	C13-C14-H14	120.0
C24-P1-Au1	107.55(6)	C28-P1-Au1	107.82(7)	C14-C15-H15	120.4
C2-C1-S1	114.62(14)	C2-C1-Au1	116.64(14)	C15-C16-C17	122.1(2)
S1-C1-Au1	105.32(9)	C2-C1-H1	106.5	C17-C16-H16	119.0
S1-C1-H1	106.5	Au1-C1-H1	106.5	C16-C17-C18	114.94(19)
C3-C2-C7	118.0(2)	C3-C2-C1	122.24(18)	C19-C18-C23	118.7(2)
C7-C2-C1	119.76(19)	C4-C3-C2	120.7(2)	C23-C18-C17	120.7(2)
C4-C3-H3	119.6	C2-C3-H3	119.6	C20-C19-H19	119.6
C5-C4-C3	120.5(3)	C5-C4-H4	119.7	C21-C20-C19	120.1(2)
C3-C4-H4	119.7	C6-C5-C4	119.4(2)	C19-C20-H20	119.9

C6-C5-H5	120.3	C4-C5-H5	120.3	C20-C21-H21	120.2
C5-C6-C7	120.0(2)	C5-C6-H6	120.0	C23-C22-C21	120.4(2)
C7-C6-H6	120.0	C6-C7-C2	121.3(2)	C21-C22-H22	119.8
C6-C7-H7	119.3	C2-C7-H7	119.3	C22-C23-H23	119.8
C9-C8-S1	106.48(16)	C9-C8-H8A	110.4	C26-C24-C27	109.63(18)
S1-C8-H8A	110.4	C9-C8-H8B	110.4	C27-C24-C25	107.91(17)
S1-C8-H8B	110.4	H8A-C8-H8B	108.6	C27-C24-P1	116.21(15)
C8-C9-C10	106.3(2)	C8-C9-H9A	110.5	C24-C25H25A	109.5
C10-C9-H9A	110.5	C8-C9-H9B	110.5	H25A-C25H25B	109.5
C10-C9-H9B	110.5	H9A-C9-H9B	108.7	H25A-C25-H25C	109.5
C11-C10-C9	106.48(19)	C11-C10-H10A	110.4	C24-C26H26A	109.5
C9-C10-H10A	110.4	C11-C10-H10B	110.4	H26A-C26H26B	109.5
C9-C10-H10B	110.4	H10A-C10-H10B	108.6	H26A-C26H26C	109.5
C10-C11-S1	105.81(16)	C10-C11-H11A	110.6	C24-C27H27A	109.5
S1-C11-H11A	110.6	C10-C11-H11B	110.6	H27A-C27H27B	109.5
S1-C11-H11B	110.6	H11A-C11-H11B	108.7	H27A-C27-H27C	109.5
C17-C12-C13	118.32(19)	C17-C12-P1	122.70(15)	C30-C28-C29	110.3(2)
C14-C13-C12	121.8(2)	C29-C28-C31	107.9(2)	C30-C28-P1	116.75(15)
C12-C13-H13	119.1	C29-C28-P1	105.54(15)	C31-C28-P1	108.21(15)
C15-C14-H14	120.0	C28-C29-H29A	109.5	C28-C29-H29B	109.5
C14-C15-C16	119.1(2)	H29A-C29-H29B	109.5	C28-C29-H29C	109.5
C16-C15-H15	120.4	H29A-C29H-29C	109.5	H29B-C29-H29C	109.5
C15-C16-H16	119.0	C28-C30-H30A	109.5	C28-C30-H30B	109.5
C16-C17-C12	118.7(2)	H30A-C30-H30B	109.5	C28-C30-H30C	109.5
C12-C17-C18	126.29(18)	H30A-C30-H30C	109.5	H30B-C30-H30C	109.5
C19-C18-C17	120.1(2)	C28-C31-H31A	109.5	C28-C31-H31B	109.5
C20-C19-C18	120.7(2)	H31A-C31-H31B	109.5	C28-C31-H31C	109.5
C18-C19-H19	119.6	H31A-C31-H31C	109.5	H31B-C31-H31C	109.5
C21-C20-H20	119.9	C26-C24-P1	108.99(14)	C24-C26-H26C	109.5
C20-C21-C22	119.7(2)	C25-C24-P1	104.91(14)	H26B-C26-H26C	109.5
C22-C21-H21	120.2	C24-C25-H25B	109.5	C24-C27-H27B	109.5
C23-C22-H22	119.8	C24-C25-H25C	109.5	C24-C27-H27C	109.5
C22-C23-C18	120.3(2)	H25B-C25-H25C	109.5	H27B-C27-H27C	109.5
C18-C23-H23	119.8	C24-C26-H26B	109.5	C30-C28-C31	107.80(19)
C26-C24-C25	108.90(19)				

Molecular structure data for 2.7b. A concentrated solution of **2.7b** was layered with hexanes at 4 °C and maintained at that temperature overnight to afford colorless crystals suitable for X-ray analysis. A colorless block-like specimen of $C_{67}H_{55}AuBF_{24}PS$, approximate dimensions 0.159 mm × 0.196 mm × 0.334 mm, was used for the X-ray crystallographic analysis. The X-ray intensity data were measured on a Bruker-Nonius X8 Kappa APEX II system equipped with a fine-focus sealed tube (MoKα, λ = 0.71073 Å) and a graphite monochromator. The total exposure time was 4.27 hours. The frames were integrated with the Bruker SAINT software package using a narrow-frame algorithm. The integration of the data using a triclinic unit cell yielded a total of 112324 reflections to a maximum θ angle of 35.09° (0.62 Å resolution), of which 28935 were independent (average redundancy 3.882, completeness = 99.8%, R_{int} = 4.04%, R_{sig} = 4.04%) and 28738 (99.32%) were greater than $2\sigma(F^2)$. The final cell constants of a = 9.9146(7) Å, b = 12.2594(8) Å, c = 14.1211(8) Å, α = 97.946(2)°, β = 102.376(2)°, γ = 96.979(2)°, volume = 1640.01(18) $Å^3$, are based upon the refinement of the XYZ-centroids of 9633 reflections above 20 σ(I) with 4.900° < 2θ < 59.68°. Data were corrected for absorption effects using the Multi-Scan method (SADABS). The ratio of minimum to maximum apparent transmission was 0.879. The calculated minimum and maximum transmission coefficients (based on crystal size) are 0.6568 and 0.7469.

The structure was solved and refined using the Bruker SHELXTL Software Package,

using the space group P 1, with Z = 1 for the formula unit, $C_{67}H_{55}AuBF_{24}PS$. The final anisotropic full-matrix least-squares refinement on F^2 with 922 variables converged at R1 = 2.60%, for the observed data and wR2 = 5.15% for all data. The goodness-of-fit was 1.011. The largest peak in the final difference electron density synthesis was 0.912 $e^-/Å^3$ and the largest hole was -0.521 $e^-/Å^3$ with an RMS deviation of 0.077 $e^-/Å^3$. On the basis of the final model, the calculated density was 1.607 g/cm^3 and F(000), 788 e^-.

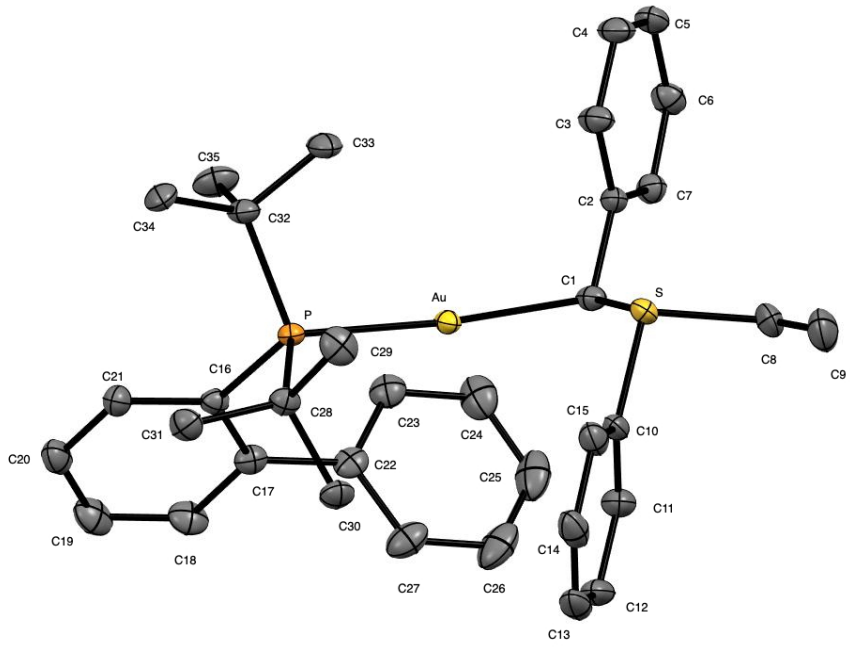

Figure 82. ORTEP diagram of gold(I) benzylide complex **2.7b** with ellipsoids shown at 50% probability level and with counterion, solvent and hydrogen atoms omitted.

Table 14. Bond Lengths for **2.7b**

Bond	Length (Å)	Bond	Length (Å)	Bond	Length (Å)
Au1-C1	2.095(4)	Au1-P1	2.2941(9)	C28-C31	1.527(4)
S1-C10	1.774(3)	S1-C1	1.787(4)	C28-C30	1.539(4)
S1-C8	1.814(3)	P1-C16	1.832(3)	C29-H29	0.98
P1-C32	1.876(3)	P1-C28	1.878(3)	C30-H30	0.98
C1-C2	1.513(4)	C1-H1	1.0	C30-H30	0.98
C2-C7	1.392(4)	C2-C3	1.399(4)	C31-H31B	0.98
C3-C4	1.391(4)	C3-H3	0.95	C32-C34	1.532(4)
C4-C5	1.385(4)	C4-H4	0.95	C32-C33	1.548(4)
C5-C6	1.381(4)	C5-H5	0.95	C33-H33	0.98
C6-C7	1.392(4)	C6-H6	0.95	C34-H34A	0.98
C7-H7	0.95	C8-C9	1.514(5)	C34-H34C	0.98
C8-H8A	0.99	C8-H8B	0.99	C35-H35B	0.98
C9-H9A	0.98	C9-H9B	0.98	C28-C29	1.535(4)
C9-H9C	0.98	C10-C11	1.385(4)	C29-H29	0.98
C10-C15	1.390(4)	C11-C12	1.394(4)	C29-H29	0.98
C11-H11	0.95	C12-C13	1.383(5)	C30-H30	0.98
C12-H12	0.95	C13-C14	1.380(5)	C31-H31	0.98
C13-H13	0.95	C14-C15	1.390(4)	C31-H31	0.98
C14-H14	0.95	C15-H15	0.95	C32-C35	1.535(4)
C16-C21	1.404(4)	C16-C17	1.410(4)	C33-H33	0.98
C17-C18	1.407(4)	C17-C22	1.488(4)	C33-H33	0.98
C18-C19	1.375(5)	C18-H18	0.95	C34-H34B	0.98
C19-C20	1.379(5)	C19-H19	0.95	C35-H35A	0.98
C20-C21	1.390(4)	C20-H20	0.95	C35-H35C	0.98
C21-H21	0.95	C22-C27	1.389(4)		
C22-C23	1.390(4)	C23-C24	1.392(5)		
C23-H23	0.95	C24-C25	1.382(6)		
C24-H24	0.95	C25-C26	1.372(6)		
C25-H25	0.95	C26-C27	1.389(5)		
C26-H26	0.95	C27-H27	0.95		

Table 15. Bond Angles (°) for **2.7b**

Bond	Angle (°)	Bond	Angle (°)	Bond	Angle (°)
C1-Au1-P1	171.87(10)	C10-S1-C1	105.83(15)	C18-C19-C20	119.8(3)
C10-S1-C8	101.72(13)	C1-S1-C8	105.65(16)	C20-C19-H19	120.1
C16-P1-C32	107.77(12)	C16-P1-C28	103.70(12)	C19-C20-H20	120.2
C32-P1-C28	113.73(12)	C16-P1-Au1	118.12(9)	C20-C21-C16	121.7(3)
C32-P1-Au1	106.98(9)	C28-P1-Au1	106.79(9)	C16-C21-H21	119.1
C2-C1-S1	108.0(2)	C2-C1-Au1	113.3(2)	C27-C22-C17	120.8(3)
S1-C1-Au1	106.25(16)	C2-C1-H1	109.7	C22-C23-C24	120.6(3)
S1-C1-H1	109.7	Au1-C1-H1	109.7	C24-C23-H23	119.7
C7-C2-C3	118.5(2)	C7-C2-C1	119.5(2)	C25-C24-H24	120.2
C3-C2-C1	122.0(3)	C4-C3-C2	120.6(3)	C26-C25-C24	120.4(3)
C4-C3-H3	119.7	C2-C3-H3	119.7	C24-C25-H25	119.8
C5-C4-C3	120.1(3)	C5-C4-H4	119.9	C25-C26-H26	119.9
C3-C4-H4	119.9	C6-C5-C4	119.8(3)	C22-C27-C26	120.5(3)
C6-C5-H5	120.1	C4-C5-H5	120.1	C26-C27-H27	119.7
C5-C6-C7	120.3(3)	C5-C6-H6	119.9	C31-C28-C30	108.4(2)
C7-C6-H6	119.9	C2-C7-C6	120.7(3)	C31-C28-P1	116.10(19)
C2-C7-H7	119.7	C6-C7-H7	119.7	C30-C28-P1	105.07(18)
C9-C8-S1	111.1(2)	C9-C8-H8A	109.4	C28-C29-H29B	109.5
S1-C8-H8A	109.4	C9-C8-H8B	109.4	C28-C29-H29C	109.5
S1-C8-H8B	109.4	H8A-C8-H8B	108.0	H29B-C29-H29C	109.5
C8-C9-H9A	109.5	C8-C9-H9B	109.5	C28-C30-H30B	109.5
H9A-C9-H9B	109.5	C8-C9-H9C	109.5	C28-C30-H30C	109.5
H9A-C9-H9C	109.5	H9B-C9-H9C	109.5	H30B-C30-H30C	109.5
C11-C10-C15	121.9(3)	C11-C10-S1	121.5(2)	C28-C31-H31B	109.5
C15-C10-S1	116.5(2)	C10-C11-C12	118.5(3)	C28-C31-H31C	109.5
C10-C11-H11	120.8	C12-C11-H11	120.8	H31B-C31-H31C	109.5
C13-C12-C11	120.1(3)	C13-C12-H12	120.0	C34-C32-C33	107.8(2)
C11-C12-H12	120.0	C14-C13-C12	120.9(3)	C34-C32-P1	115.86(19)
C14-C13-H13	119.6	C12-C13-H13	119.6	C33-C32-P1	108.12(19)
C13-C14-C15	120.0(3)	C13-C14-H14	120.0	C32-C33-H33B	109.5
C15-C14-H14	120.0	C10-C15-C14	118.7(3)	C32-C33-H33C	109.5
C10-C15-H15	120.7	C14-C15-H15	120.7	H33B-C33-H33C	109.5
C21-C16-C17	118.3(2)	C21-C16-P1	119.3(2)	C32-C34-H34B	109.5
C17-C16-P1	122.20(19)	C18-C17-C16	118.5(3)	C32-C34-H34C	109.5
C18-C17-C22	116.4(2)	C16-C17-C22	125.1(2)	H34B-C34-H34C	109.5
C19-C18-C17	122.0(3)	C19-C18-H18	119.0	C32-C35-H35B	109.5
C17-C18-H18	119.0	C31-C28-C29	109.8(2)	C32-C35-H35C	109.5
C18-C19-H19	120.1	C29-C28-C30	108.8(2)	H35B-C35-H35C	109.5
C19-C20-C21	119.6(3)	C29-C28-P1	108.47(18)	C35-C32-P1	107.08(19)
C21-C20-H20	120.2	C28-C29-H29A	109.5	C32-C33-H33A	109.5
C20-C21-H21	119.1	H29A-C29-H29B	109.5	H33A-C33-H33B	109.5
C27-C22-C23	118.8(3)	H29A-C29-H29C	109.5	H33A-C33-H33C	109.5
C23-C22-C17	120.3(3)	C28-C30-H30A	109.5	C32-C34-H34A	109.5

C22-C23-H23	119.7	H30A-C30-H30B	109.5	H34A-C34-H34B	109.5
C25-C24-C23	119.6(3)	H30A-C30-H30C	109.5	H34A-C34-H34C	109.5
C23-C24-H24	120.2	C28-C31-H31A	109.5	C32-C35-H35A	109.5
C26-C25-H25	119.8	H31A-C31-H31B	109.5	H35A-C35-H35B	109.5
C25-C26-C27	120.1(3)	H31A-C31-H31C	109.5	H35A-C35-H35C	109.5
C27-C26-H26	119.9	C34-C32-C35	110.0(3)		
C22-C27-H27	119.7	C35-C32-C33	107.7(2)		

Molecular structure data for 2.7c. A concentrated solution of **2.7c** in toluene was cooled to –20 °C and maintained at that temperature overnight to afford colorless crystals suitable for X-ray analysis. A colorless block-like specimen of $C_{78}H_{62.51}AuBF_{24}PS$, approximate dimensions 0.094 mm × 0.160 mm × 0.230 mm, was used for the X-ray crystallographic analysis. The X-ray intensity data were measured on a Bruker-Nonius X8 Kappa APEX II system equipped with a fine-focus sealed tube (MoKα, λ = 0.71073 Å) and a graphite monochromator. The total exposure time was 22.68 hours. The frames were integrated with the Bruker SAINT software package using a narrow-frame algorithm. The integration of the data using a triclinic unit cell yielded a total of 172348 reflections to a maximum θ angle of 29.71° (0.72 Å resolution), of which 20862 were independent (average redundancy 8.261, completeness = 99.4%, R_{int} = 4.42%, R_{sig} = 2.92%) and 15047 (72.13%) were greater than $2\sigma(F^2)$. The final cell constants of a = 12.3231(8) Å, b = 17.1500(10) Å, c = 17.7972(11) Å, α = 82.835(2)°, β = 85.871(2)°, γ = 82.226(2)°, volume = 3691.8(4) $Å^3$, are based upon the refinement of the XYZ-centroids of 9643 reflections above 20 σ(I) with 4.625° < 2θ < 53.81°. Data were corrected for absorption effects using

the numerical method (SADABS). The ratio of minimum to maximum apparent transmission was 0.836. The calculated minimum and maximum transmission coefficients (based on crystal size) are 0.7072 and 0.8464. The final anisotropic full-matrix least-squares refinement on F^2 with 1270 variables converged at R1 = 3.46%, for the observed data and wR2 = 9.76% for all data. The goodness-of-fit was 1.055. The largest peak in the final difference electron density synthesis was 1.775 $e^-/Å^3$ and the largest hole was -0.626 $e^-/Å^3$ with an RMS deviation of 0.080 $e^-/Å^3$. On the basis of the final model, the calculated density was 1.553 g/cm^3 and F(000), 1723 e^-.

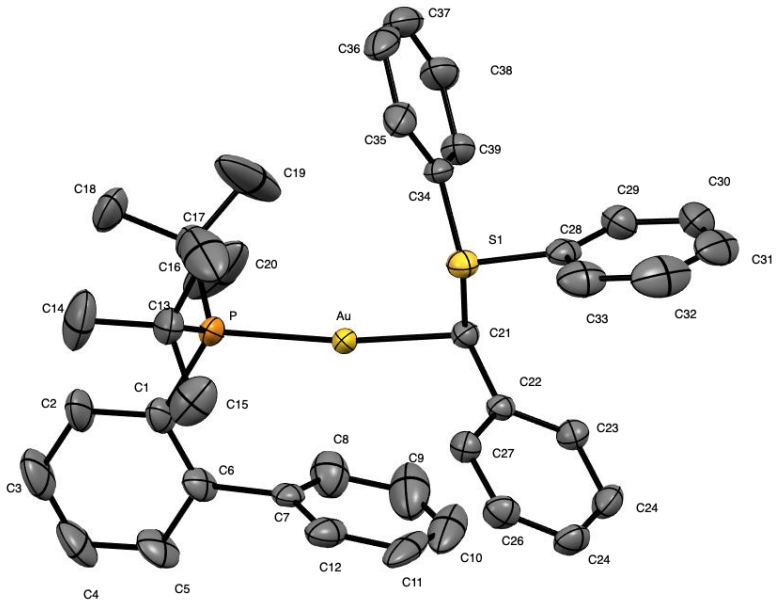

Figure 83. ORTEP diagram of gold(I) benzylide complex **2.7c** with ellipsoids shown at 50% probability level and with counterion, solvent and hydrogen atoms omitted.

Table 16. Bond Lengths for **2.7c**

Bond	Length (Å)	Bond	Length (Å)	Bond	Length (Å)
Au1-C21	2.125(2)	Au1-P1	2.2983(14)	C19A-H19D	0.98
P1-C1	1.856(4)	P1-C17	1.888(6)	C19A-H19F	0.98
P1-C13	1.895(7)	C1-C2	1.39	C20A-H20E	0.98
C1-C6	1.39	C2-C3	1.39	S1-C34	1.783(3)
C2-H2	0.95	C3-C4	1.39	S1-C21	1.813(3)
C3-H3	0.95	C4-C5	1.39	C21-H21	1.0
C4-H4	0.95	C5-C6	1.39	C22-C27	1.387(4)
C5-H5	0.95	C6-C7	1.511(5)	C23-C24	1.398(4)
C7-C8	1.39	C7-C12	1.39	C24-C25	1.372(5)
C8-C9	1.39	C8-H8	0.95	C25-C26	1.376(4)
C9-C10	1.39	C9-H9	0.95	C26-C27	1.387(4)
C10-C11	1.39	C10-H10	0.95	C27-H27	0.95
C11-C12	1.39	C11-H11	0.95	C28-C33	1.376(4)
C12-H12	0.95	C13-C15	1.506(8)	C29-H29	0.95
C13-C16	1.523(8)	C13-C14	1.524(8)	C30-H30	0.95
C14-H14A	0.98	C14-H14B	0.98	C31-H31	0.95
C14-H14C	0.98	C15-H15A	0.98	C32-H32	0.95
C15-H15B	0.98	C15-H15C	0.98	C34-C39	1.377(4)
C16-H16A	0.98	C16-H16B	0.98	C35-C36	1.408(5)
C16-H16C	0.98	C17-C19	1.508(9)	C36-C37	1.369(6)
C17-C18	1.513(11)	C17-C20	1.522(11)	C37-C38	1.359(6)
C18-H18A	0.98	C18-H18B	0.98	C38-C39	1.386(4)
C18-H18C	0.98	C19-H19A	0.98	C39-H39	0.95
C19-H19B	0.98	C19-H19C	0.98	C19A-H19E	0.98
C20-H20A	0.98	C20-H20B	0.98	C20A-H20D	0.98
C20-H20C	0.98	Au1A-C21	2.070(2)	C20A-H20F	0.98
Au1A-P1A	2.3195(15)	P1A-C1A	1.863(4)	S1-C28	1.795(3)
P1A-C13A	1.877(7)	P1A-C17A	1.877(7)	C21-C22	1.513(3)
C1A-C2A	1.39	C1A-C6A	1.39	C21-H21A	1.0
C2A-C3A	1.39	C2A-H2A	0.95	C22-C23	1.392(4)
C3A-C4A	1.39	C3A-H3A	0.95	C23-H23	0.95
C4A-C5A	1.39	C4A-H4A	0.95	C24-H24	0.95
C5A-C6A	1.39	C5A-H5A	0.95	C25-H25	0.95
C6A-C7A	1.513(4)	C7A-C8A	1.39	C26-H26	0.95
C7A-C12A	1.39	C8A-C9A	1.39	C28-C29	1.362(5)
C8A-H8A	0.95	C9A-C10A	1.39	C29-C30	1.386(5)
C9A-H9A	0.95	C10A-C11A	1.39	C30-C31z	1.357(7)
C10A-H10A	0.95	C11A-C12A	1.39	C31-C32	1.351(7)
C11A-H11A	0.95	C12A-H12A	0.95	C32-C33	1.409(6)
C13A-C16A	1.524(10)	C13A-C15A	1.535(9)	C33-H33	0.95
C13A-C14A	1.566(10)	C14A-H14D	0.98	C34-C35	1.395(4)
C14A-H14E	0.98	C14A-H14F	0.98	C35-H35	0.95
C15A-H15D	0.98	C15A-H15E	0.98	C36-H36	0.95

C15A-H15F	0.98	C16A-H16D	0.98	C37-H37	0.95
C16A-H16E	0.98	C16A-H16F	0.98	C38-H38	0.95
C17A-C18A	1.520(13)	C17A-C20A	1.535(9)		
C17A-C19A	1.544(8)	C18A-H18D	0.98		
C18A-H18E	0.98	C18A-H18F	0.98		

Table 17. Bond Angles (°) for **2.7c**

Bond	Angle (°)	Bond	Angle (°)	Bond	Angle (°)
C21-Au1-P1	171.38(8)	C1-P1-C17	105.9(3)	C17-C20-H20A	109.5
C1-P1-C13	104.5(3)	C17-P1-C13	115.6(3)	H20A-C20-H20B	109.5
C1-P1-Au1	118.44(15)	C17-P1-Au1	109.3(2)	H20A-C20-H20C	109.5
C13-P1-Au1	103.49(19)	C2-C1-C6	120.0	C21-Au1A-P1A	170.87(8)
C2-C1-P1	117.6(3)	C6-C1-P1	122.2(3)	C1A-P1A-C17A	107.4(3)
C3-C2-C1	120.0	C3-C2-H2	120.0	C1A-P1A-Au1A	118.21(14)
C1-C2-H2	120.0	C2-C3-C4	120.0	C17A-P1A-Au1A	106.8(2)
C2-C3-H3	120.0	C4-C3-H3	120.0	C2A-C1A-P1A	117.1(3)
C5-C4-C3	120.0	C5-C4-H4	120.0	C3A-C2A-C1A	120.0
C3-C4-H4	120.0	C4-C5-C6	120.0	C1A-C2A-H2A	120.0
C4-C5-H5	120.0	C6-C5-H5	120.0	C2A-C3A-H3A	120.0
C5-C6-C1	120.0	C5-C6-C7	115.2(4)	C5A-C4A-C3A	120.0
C1-C6-C7	124.6(4)	C8-C7-C12	120.0	C3A-C4A-H4A	120.0
C8-C7-C6	117.6(4)	C12-C7-C6	122.0(4)	C6A-C5A-H5A	120.0
C7-C8-C9	120.0	C7-C8-H8	120.0	C5A-C6A-C1A	120.0
C9-C8-H8	120.0	C10-C9-C8	120.0	C1A-C6A-C7A	127.2(4)
C10-C9-H9	120.0	C8-C9-H9	120.0	C8A-C7A-C6A	121.6(4)
C9-C10-C11	120.0	C9-C10-H10	120.0	C9A-C8A-C7A	120.0
C11-C10-H10	120.0	C10-C11-C12	120.0	C7A-C8A-H8A	120.0
C10-C11-H11	120.0	C12-C11-H11	120.0	C8A-C9A-H9A	120.0
C11-C12-C7	120.0	C11-C12-H12	120.0	C9A-C10A-C11A	120.0
C7-C12-H12	120.0	C15-C13-C16	108.0(6)	C11A-C10A-H10A	120.0
C15-C13-C14	109.5(7)	C16-C13-C14	109.0(6)	C12A-C11A-H11A	120.0
C15-C13-P1	105.4(4)	C16-C13-P1	116.5(5)	C11A-C12A-C7A	120.0
C14-C13-P1	108.2(5)	C13-C14-H14A	109.5	C7A-C12A-H12A	120.0
C13-C14-H14B	109.5	H14A-C14-H14B	109.5	C16A-C13A-C14A	108.7(6)
C13-C14-H14C	109.5	H14A-C14-H14C	109.5	C16A-C13A-P1A	107.6(4)
H14B-C14-H14C	109.5	C13-C15-H15A	109.5	C14A-C13A-P1A	107.6(5)
C13-C15-H15B	109.5	H15A-C15-H15B	109.5	C13A-C14A-H14E	109.5
C13-C15-H15C	109.5	H15A-C15-H15C	109.5	C13A-C14A-H14F	109.5
H15B-C15-H15C	109.5	C13-C16-H16A	109.5	H14E-C14A-H14F	109.5
C13-C16-H16B	109.5	H16A-C16-H16B	109.5	C13A-C15A-H15E	109.5
C13-C16-H16C	109.5	H16A-C16-H16C	109.5	C13A-C15A-H15F	109.5

H16B-C16-H16C	109.5	C19-C17-C18	108.6(10)	H15E-C15A-H15F	109.5
C19-C17-C20	106.3(10)	C18-C17-C20	106.9(12)	H19B-C19-H19C	109.5
C19-C17-P1	108.9(5)	C18-C17-P1	120.4(11)	C17-C20-H20B	109.5
C20-C17-P1	104.9(5)	C17-C18-H18A	109.5	C17-C20-H20C	109.5
C17-C18-H18B	109.5	H18A-C18-H18B	109.5	H20B-C20-H20C	109.5
C17-C18-H18C	109.5	H18A-C18-H18C	109.5	C1A-P1A-C13A	104.0(3)
H18B-C18-H18C	109.5	C17-C19-H19A	109.5	C13A-P1A-C17A	112.4(3)
C17-C19-H19B	109.5	H19A-C19-H19B	109.5	C13A-P1A-Au1A	108.2(2)
C17-C19-H19C	109.5	H19A-C19-H19C	109.5	C2A-C1A-C6A	120.0
C6A-C1A-P1A	122.7(3)	C13A-C16A-H16E	109.5	C22-C21-Au1A	122.25(17)
C3A-C2A-H2A	120.0	C13A-C16A-H16F	109.5	C22-C21-Au1	116.49(17)
C2A-C3A-C4A	120.0	H16E-C16A-H16F	109.5	C22-C21-H21	111.4
C4A-C3A-H3A	120.0	C18A-C17A-C19A	106.9(10)	Au1-C21-H21	111.4
C5A-C4A-H4A	120.0	C18A-C17A-P1A	117.3(11)	S1-C21-H21A	106.3
C6A-C5A-C4A	120.0	C19A-C17A-P1A	109.3(4)	C27-C22-C23	118.6(2)
C4A-C5A-H5A	120.0	C17A-C18A-H18E	109.5	C23-C22-C21	118.8(2)
C5A-C6A-C7A	112.8(4)	C17A-C18A-H18F	109.5	C22-C23-H23	119.7
C8A-C7A-C12A	120.0	H18E-C18A-H18F	109.5	C25-C24-C23	119.9(3)
C12A-C7A-C6A	118.2(4)	C17A-C19A-H19E	109.5	C23-C24-H24	120.0
C9A-C8A-H8A	120.0	C17A-C19A-H19F	109.5	C24-C25-H25	120.1
C8A-C9A-C10A	120.0	H19E-C19A-H19F	109.5	C25-C26-C27	120.6(3)
C10A-C9A-H9A	120.0	C17A-C20A-H20E	109.5	C27-C26-H26	119.7
C9A-C10A-H10A	120.0	C17A-C20A-H20F	109.5	C26-C27-H27	119.8
C12A-C11A-C10A	120.0	H20E-C20A-H20F	109.5	C29-C28-C33	122.1(3)
C10A-C11A-H11A	120.0	C34-S1-C21	107.20(13)	C33-C28-S1	114.8(3)
C11A-C12A-H12A	120.0	C22-C21-S1	104.11(17)	C28-C29-H29	120.6
C16A-C13A-C15A	107.5(7)	S1-C21-Au1A	110.60(13)	C31-C30-C29	120.3(4)
C15A-C13A-C14A	109.1(6)	S1-C21-Au1	101.46(12)	C29-C30-H30	119.9
C15A-C13A-P1A	116.1(5)	S1-C21-H21	111.4	C32-C31-H31	119.5
C13A-C14A-H14D	109.5	C22-C21-H21A	106.3	C31-C32-C33	120.4(4)
H14D-C14A-H14E	109.5	Au1A-C21-H21A	106.3	C33-C32-H32	119.8
H14D-C14A-H14F	109.5	C27-C22-C21	122.5(2)	C28-C33-H33	121.3
C13A-C15A-H15D	109.5	C22-C23-C24	120.5(3)	C39-C34-C35	121.9(3)
H15D-C15A-H15E	109.5	C24-C23-H23	119.7	C35-C34-S1	114.5(2)
H15D-C15A-H15F	109.5	C25-C24-H24	120.0	C34-C35-H35	121.2
C13A-C16A-H16D	109.5	C24-C25-C26	119.9(3)	C37-C36-C35	120.0(3)
H16D-C16A-H16E	109.5	C26-C25-H25	120.1	C35-C36-H36	120.0
H16D-C16A-H16F	109.5	C25-C26-H26	119.7	C38-C37-H37	119.4
C18A-C17A-C20A	109.0(12)	C26-C27-C22	120.4(3)	C37-C38-C39	120.8(4)
C20A-C17A-C19A	107.5(7)	C22-C27-H27	119.8	C39-C38-H38	119.6
C20A-C17A-P1A	106.5(4)	C29-C28-S1	123.0(2)	C34-C39-H39	120.7
C17A-C18A-H18D	109.5	C28-C29-C30	118.8(4)	C37-C36-H36	120.0
H18D-C18A-H18E	109.5	C30-C29-H29	120.6	C38-C37-C36	121.2(3)

H18D-C18A-H18F	109.5	C31-C30-H30	119.9	C36-C37-H37	119.4
C17A-C19A-H19D	109.5	C32-C31-C30	120.9(4)	C37-C38-H38	119.6
H19D-C19A-H19E	109.5	C30-C31-H31	119.5	C34-C39-C38	118.5(3)
H19D-C19A-H19F	109.5	C31-C32-H32	119.8	C38-C39-H39	120.7
C17A-C20A-H20D	109.5	C28-C33-C32	117.4(4)		
H20D-C20A-H20E	109.5	C32-C33-H33	121.3		
H20D-C20A-H20F	109.5	C39-C34-S1	123.6(2)		
C34-S1-C28	103.00(12)	C34-C35-C36	117.6(3)		
C28-S1-C21	104.71(12)	C36-C35-H35	121.2		

3. Experimental Evaluation of (L)Au Electron-Donor Ability in Cationic Gold Carbene Complexes

Portions of the chapter have been published: Carden, R. G.; Lam, Nathan; Widenhoefer, R. A. *Chem. Eur. J.* **2017**, *23*, 17992–1800

3.1 Background

3.1.1 Bonding in gold(I) carbenes

Cationic gold carbene complexes have been widely invoked as intermediates in a diverse range of gold(I)-catalyzed reactions, most notably enyne cycloisomerizations and alkene cyclopropanations.[11,36,62] Although the intermediacy of gold carbenes in these transformations is supported by a wealth of experimental and computational data, there is still much debate regarding the nature of the gold–carbon bond, specifically the extent of d→π back-bonding and, more generally, the extent of electron donation from the (L)Au fragment to the electron-deficient C1 carbon atom.[36,62] For example, Fürstner concluded that the stabilization of the γ,γ-dialkoxy allylic cation by the gold phosphine fragment in complex **3.1** was "marginal" on the basis of low C2–C3 rotational barriers.[123] However, DFT analysis of complex **3.2** by Toste and Goddard suggested that stabilization of a tertiary allylic carbocation by a (Me_3P)Au group is similar to that provided by a methoxy group (Figure 84).[21]

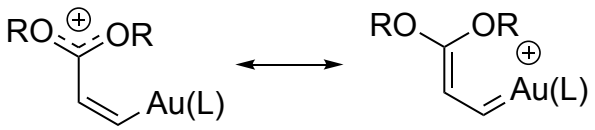

3.1

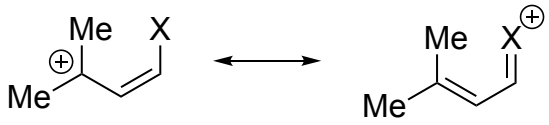

3.2 [X = Au(PMe_3), OMe]

Figure 84. Cationic gold carbene complexes

Straub attributed the relatively short Au–C(Mes)$_2$ bond (2.014 Å) of the structurally characterization bis(mesityl)carbene complex **3.3** to the significant, but not predominant, double bond character Au=C(Mes)$_2$.[124] Similarly, structural analysis of the gold cyclopropyl(methoxy)carbene complex **3.4** suggested that the extent of (L)Au→C electron donation was similar that that provided by a cyclopropyl group.[125] Conversely, Fürstner concluded that there is only little back donation of electron density from gold

to the carbene center in the structurally characterized bis(anisyl)carbene complex **3.5** (Figure 85).[45]

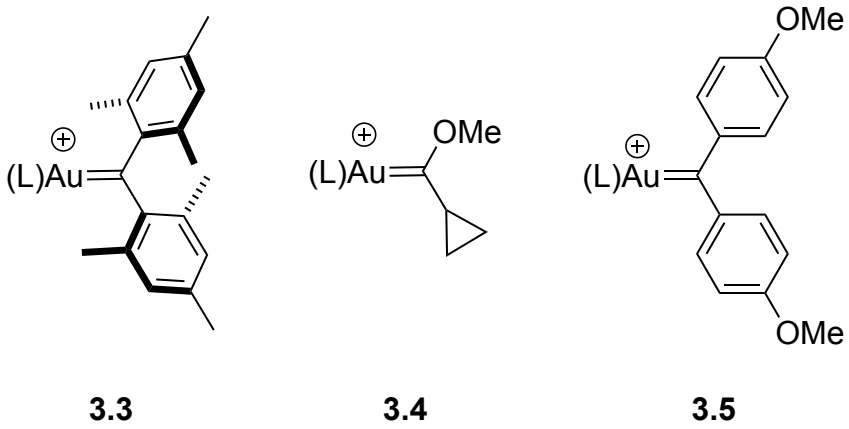

3.3 **3.4** **3.5**

Figure 85. Structurally characterized gold carbene complexes

Embedded within the debate regarding the extent of (L)Au→C electron donation in gold carbene complexes is the role of the supporting ligand in modulating the electron-donor ability of the (L)Au fragment.[11,36,62] In particular, the computationally-derived bonding model for gold carbene complexes proposed by Toste and Goddard invokes an L–Au–C bonding network consisting of a three-center, four-electron σ-hyperbond and two orthogonal π-bonds involving donation of electron density from filled metal 5d orbitals to π-acceptor orbitals on the ligand and carbene carbon atom (Figure 86).[21] Owing to the nature of these orbitals and the competition for electron

density, the better the sigma donor L, the weaker the sigma components of the Au–C1 bond, and similarly, the more π-acidic L is, the weaker the Au→C1 back-donation.

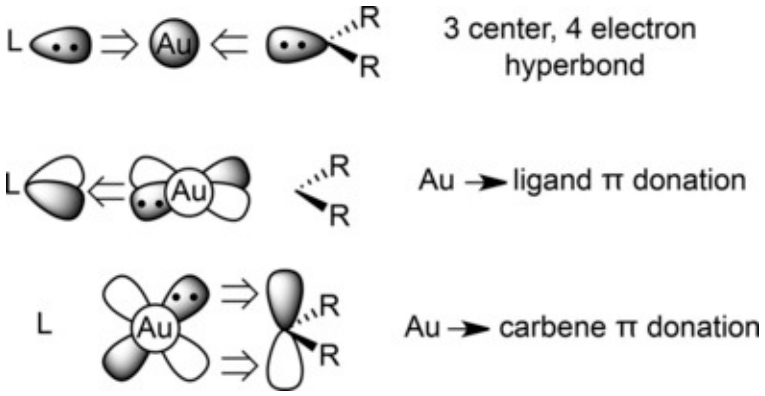

Figure 86. Proposed bonding model for gold carbene complexes.[21]

3.1.2 Ligand effect in gold(I)-catalyzed reactions

The pronounced effect of the supporting ligand on the catalytic behavior of gold(I) carbene complexes is well-documented,[12,126] including the notable difference between *N*-heterocyclic carbene (NHC) ligands and dialkyl(*o*-biphenyl) phosphine ligands, which are among the most important supporting ligands employed in gold(I) catalysis, and which are both considered to be strong σ-donors and weak π-acceptor ligands.[12,126] For example, Echavarren has shown that the product ratio in the cycloaddition/arylation of enyne **3.6** with indole catalyzed by [(L)AuNCMe]SbF_6 complexes changed from 80:20 favoring product **3.7a** when L=P(t-Bu)$_2$-*o*-biphenyl (**P1**) to

75:25 favoring product **3.7b** when L = IPr (Scheme 16).[127] Similarly, Barriault documented the reversal of 6-endo/5-exo selectivity in the gold(I)-catalyzed cycloisomerization of 1,6 enyne **3.8** employing either IPr of *o*-biphenylphosphine **P2** as supporting ligand (Scheme 17).[128]

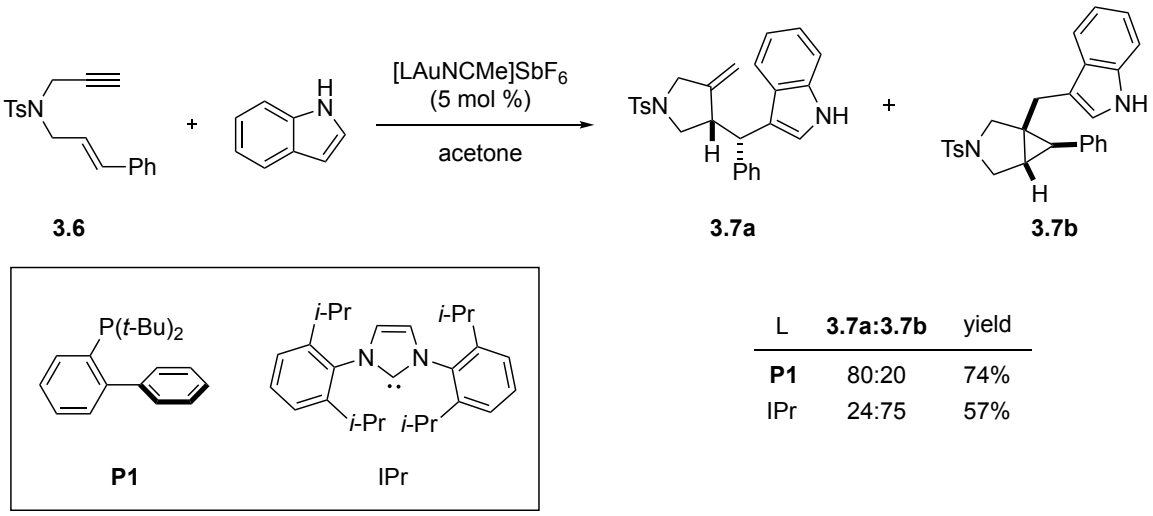

L	**3.7a:3.7b**	yield
P1	80:20	74%
IPr	24:75	57%

Scheme 16. Ligand-controlled selectivity of the gold(I)-catalyzed cyclization/arylation of enyne **3.6**

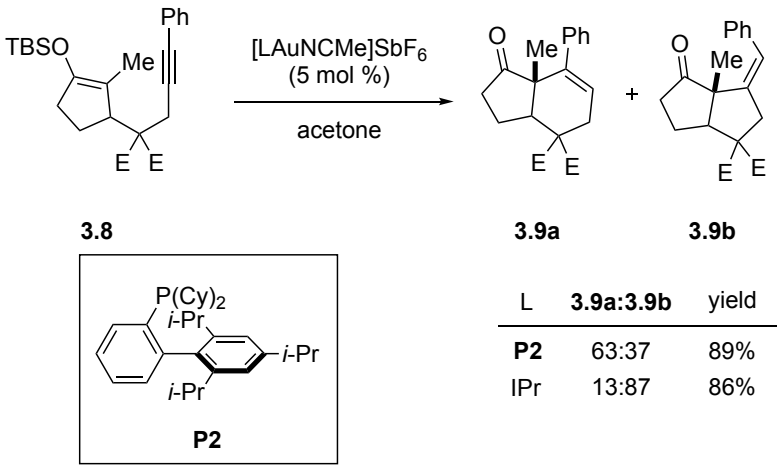

Scheme 17. Ligand-controlled selectivity of gold(I)-catalyzed cyclization of **3.8**.

In contrast to the study of ligand effects in gold(I)- πcatalysis, experimental quantification of the effect of supporting ligand on the electron donor properties of (L)Au fragments, particularly those in cationic gold(I) carbene complexes, is largely absent.[129-131] For example, Belpassi measured the ligand-dependent activation barriers for rotation about the C–N(pyrollidine) bond of gold NHC complexes **3.10** and correlated these values to the computationally derived extent of d→π backbonding, although a direct comparison of alkyl phosphine and NHC ligands was not feasible (Scheme 18).[132] Hashmi investigated the ligand-dependent hydrolytic cleavage of γ,γ-dialkoxy gold carbene complexes **3.11** and correlated these reaction rates with the ligand-dependent LUMO energies of the carbene complex (Scheme 18).[133] The rate of hydrolysis was found

to track inversely with the σ-donor ability of the (L)Au fragment, which increased in the order $P(OR)_3$<PPh_3<**P2**<IPr.

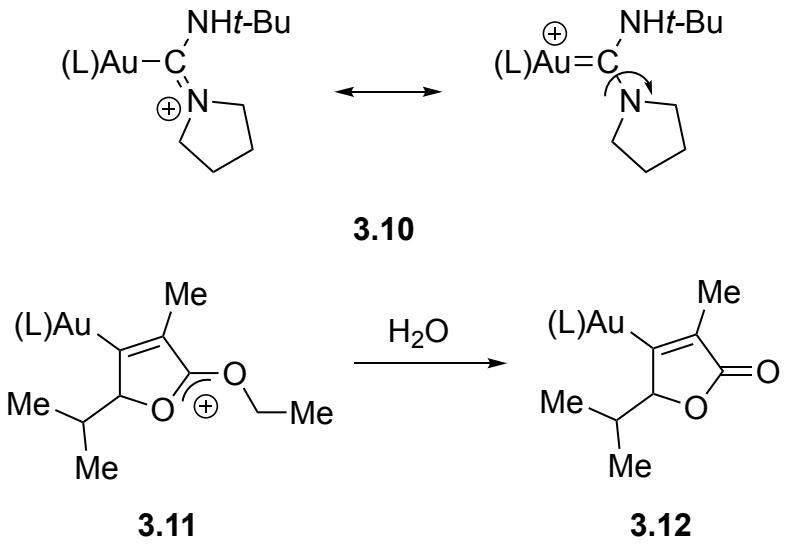

Scheme 18. Experimental evaluation of supporting ligand on the electron donor properties of (L)Au fragments in gold carbene complexes.

More directly, Chen has evaluated the ligand-dependent stabilization of cationic gold(I) carbene complexes by measuring the energy barriers for the formation of gold arylidene complexes **3.14a** and **3.14b** through the collision-induced dissociation (CID) of the corresponding gold sulfonium-imidazolylidene precursors (**3.13**) in the gas phase (Scheme 19).[48] Quantitative CID threshold analysis for the formation of **3.14a** and **3.14b** indicated that the IPr ligand stabilized the carbene by 2.3±2.7 kcal mol^{-1} relative to **P1**,

which, despite the error in this analysis, correlated well with the predicted value of 1.8 kcal mol^{-1} from DFT calcualtions.[48]

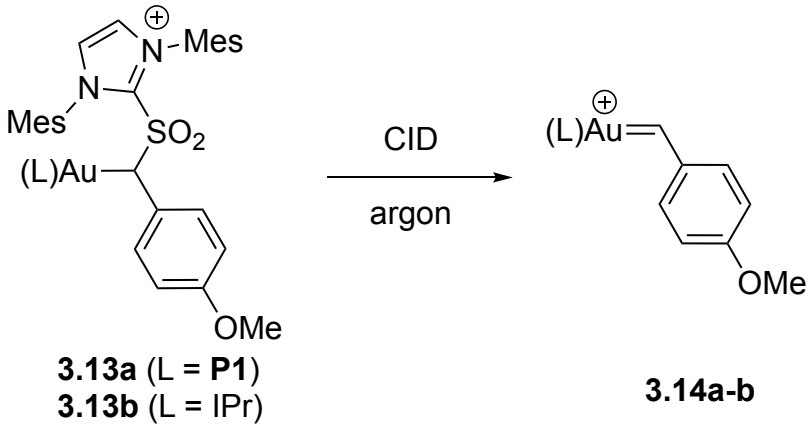

Scheme 19. Quantitative determination of the ligand-dependent stabilization of gold(I) carbene complexes in the gas phase.

3.1.3. Project goals and scope

We therefore sought to experimentally evaluate the ligand-dependent electron-donor ability of (L)Au fragments in cationic gold carbene complexes, including an assessment of the relative contributions of σ- and π-donation from the (L)Au fragment. Previous efforts directed towards this goal analyzed the charge-dependence perturbation of C–C bond lengths in the cyclopropyl group of the cyclopropyl(methoxy) carbene complex **3.4** relative to protonated cyclopropyl ketones (Figure 74).[125] However, this approach suffered from the large experimental error in the C–C bond lengths

relative to the extent of perturbation and the necessity of obtaining suitable crystals of both the carbene complexes and oxocarbenium model compounds for analysis. To circumvent these limitations, we sought to exploit the large dispersion and charge-dependent chemical shifts of heteronuclear NMR to evaluate charge distribution and (L)Au→C electron donation in cationic gold carbene complexes. This chapter reports both ^{29}Si and ^{19}F NMR analysis of both gold(I) carbene complexes and relevant organic model compounds to evaluate the electron-donor ability of (L)Au fragments with phosphine and NHC ligands.

3.2 ^{29}Si NMR Studies

3.2.1 Cationic gold (β,β-disilyl)vinylidene complexes

Guided by the work of Müller,[134-139] our group previously reported that the low-temperature hydride abstraction from gold acetylide complex **3.15a** with triphenylcarbenium tetrakis(pentafluorophenyl)borate leads to selective formation of the thermally unstable cationic gold (β,β-disilyl) vinylidene complex **3.16a** (Scheme 20).[140-163] In the ^{13}C NMR, resonances at δ 206 and 112 ppm were assigned to the C1 and C2 vinylidene carbon atoms, respectively (Table 18). A significant decrease in the one bond C1–C2 coupling constant of **3.16a** ($^{1}J_{CC}$ = 60 Hz) relative to the neutral acetylide precursors **3.15a** ($^{1}J_{CC}$ = 91 Hz) is observed, which is consistent with the diminished s-character of the C2 atom of **3.16a** relative to **3.15a**.[164,165] Detection of the C1 and C2 vinylidene carbon atoms was complicated by the facile interconversion ($\Delta G^{\ddagger}$ = 9.7 kcal mol^{-1}) of these atoms, presumably through the gold π-disilacyclohexyne intermediate **I**.

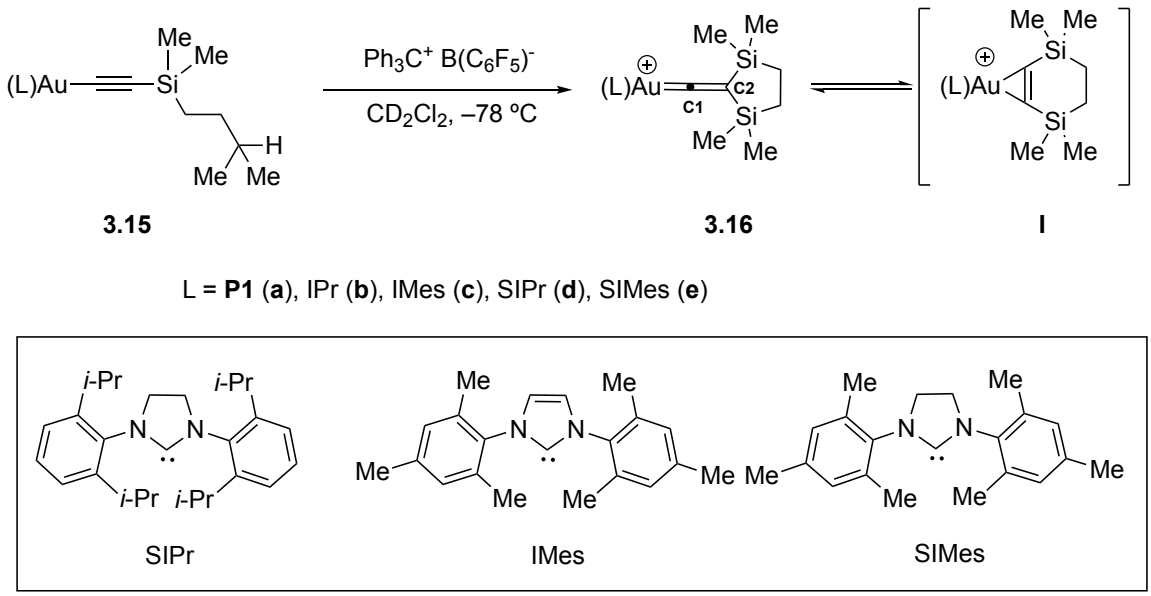

Scheme 20. Generation of gold (β,β-disilyl)vinylidene complexes **3.16** from gold acetylide complexes **3.15**.

The propensity of a silicon atom to stabilize a carbenium ion at the β-position through hyperconjugation (β-affect) is well documented.[166] The β-Si hyperconjugation, in turn, leads to the depletion of electron density from the silicon atom, which is evidenced by a number of spectroscopic features, most notably the deshielding of the silicon atom in the ^{29}Si NMR spectrum.[134-139,167-172] A ^{29}Si NMR spectrum (–80 °C) of **3.16** has a sharp resonance at δ = 33.5 ppm which is significantly deshielded ($\Delta\delta^{29}$Si = +54.1 ppm) relative to the ^{29}Si NMR resonance of the C(sp)-bound silicon atom of the acetylide complex **3.15** (δ = –20.6 ppm; Table 18) owing to the β-Si hyperconjugation as represented by resonance structures **C** and **D** (Figure 87). All of the spectroscopy of gold(I) vinylidene

complexes **3.16** is consistent with a symmetric Y-shaped or rapidly equilibrating distorted Y-shaped ground state structure, both of which have been validated for α-substituted-β,β-disilyl vinyl cations.[135-139]

Table 18. Select ^{13}C and ^{29}Si NMR data for gold(β,β-disilyl)vinylidene complexes **3.16** and α-aryl-β,β-disilyl vinyl cations **3.18**

entry	Compound	α-Substituent	$\delta^{13}C$ (*C1*)	$\delta^{13}C$ (*C2*)	$\delta^{29}Si$	$\Delta\delta^{29}Si$[a]
1	**3.16a**	**P1**	206	112	33.5	+54.1
2	**3.16b**	IPr	203.5	111.8	35.8	+56.7
3	**3.16c**	IMes	202.8	112.3	36.2	+55.2
4	**3.16d**	SIPr	198.5	114.2	36.2	+57.9
5	**3.16e**	SIMes	202.8	115.2	34.5	+55.3
6	**3.18a**	4-C_6H_5Me	183.9	83.6	56.0	+70.2
7	**3.18b**	4-C_6H_5OPh	185.8	84.5	52.3	+66.6
8	**3.18c**	4-C_6H_5OMe	187.2	84.0	50.2	+65.0
9	**3.18d**	4-$C_6H_5NMe_2$	194.9	85.9	37.3	+52.2

[a] $\Delta\delta^{29}Si$ refers to the chemical shift difference between $\delta^{29}Si$ of the vinylidene complex or vinyl cation and the $\delta^{29}Si$ of the C(sp)-bound silicon atom of the neutral acetylide precursor.

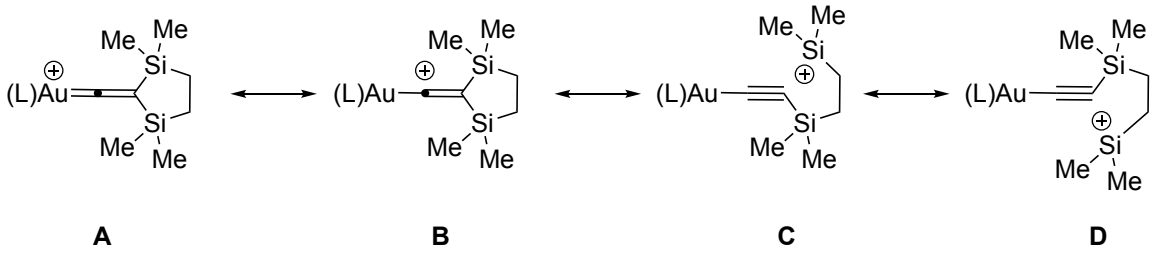

Figure 87. Relevant resonance contributors for gold vinylidene complexes **3.16**

It has been shown that the extent of β-Si hyperconjugation across a range of β-silyl substituted carbenium ions is not constant, but increases with the increasing electron demand of the electron-deficient carbon atom.[134,136,170-172] Notably, Müller quantified this relationship in the context of α-aryl-β,β-disilyl vinyl cations **3.17** containing a six-membered disilacycle by establishing a correlation between the ^{29}Si NMR chemical shift and the Hammett-Brown σ^+ parameter of the *p*-substituent of the α-aryl group. [135] The Hammett-Brown σ^+ parameter has been employed to characterize the electron donor/acceptor properties of substituents that can effectively delocalize positive charge from the reaction center through conjugation with more negative values indicating greater stabilization of the positive charge.[173] We therefore reasoned that ^{29}Si NMR chemical shifts could be similarly employed to evaluate the electron donor ability of the (L)Au fragment in the cationic gold (β,β-disilyl)vinylidene complex **3.15** and related derivatives, provided that a similar correlation could be established between the electron donor ability of the α-substituent and the ^{29}Si NMR chemical shift of the α-aryl-β,β-disilyl vinyl cations **3.18** containing a five-membered disilacycle (Figure 88).[174]

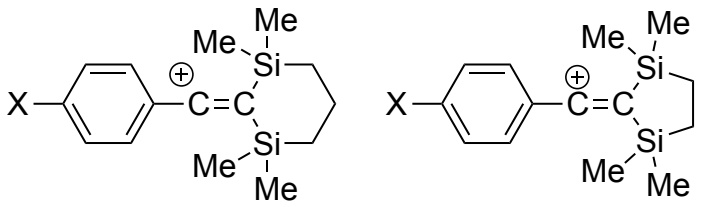

3.17 **3.18**

Figure 88. α-Aryl-β,β-disilyl vinyl cations synthesized by Müller and Widenhoefer, respectively.

Toward this objective of evaluating the electron-donor ability of the (L)Au fragment in gold (β,β-disilyl)vinylidene complexes, we first sought to expand the scope of gold vinylidene complexes with respect to supporting ligand. To achieve this, we synthesized the thermally unstable gold (β,β-disilyl)vinylidene complexes **3.16 b-e** with NHC supporting ligands. Conversely, the attempted synthesis of gold (β,β-disilyl)vinylidene complexes with less electron-donating ligands, like PPh_3 and P(*t*-Bu)$_3$, proved unsuccessful. Complexes **3.16 b-e** were characterized at –80 °C by ^{1}H, ^{13}C and ^{29}Si NMR spectroscopy (Table 18). The ^{13}C NMR spectra of complexes **3.16 b-e** displayed vinylidene resonances at δ = 203–198 ppm and δ = 112–115 ppm, respectively, which, unlike **3.16a**, showed no broadening at –80 °C. This observation suggested a higher energy barrier for the C2/C1 interconversion relative to **3.16a**. Indeed, a spin-saturation transfer analysis of the IPr-supported gold (β,β-disilyl)vinylidene complex **3.16b** provided an energy barrier of ($\Delta G^{\ddagger} = 11.4 \pm 0.3$ kcal mol^{-1}) for the interconversion of the

C1 and C2 vinylidene carbon atoms. Each of the complexes **3.16 b-e** displayed a single sharp resonance in the ^{29}Si NMR spectrum at –80 °C. The ^{29}Si NMR chemical shifts (δ^{29}Si) showed only slight dependence on the nature of the supporting ligand and ranged from δ^{29}Si = 34.5 ppm (L = SIMes) for **3.16e** to δ^{29}Si = 36.2 ppm for **3.16d** (L = SIPr), all of which were slightly deshielded relative to phosphine derivative **3.16a** (δ = 33.5 ppm, Table 18).

3.2.2 α-Aryl-β,β-Disilyl Vinyl Cations

We next sought to establish a correlation between the ^{29}Si NMR chemical shifts (δ^{29}Si) and the electron donor ability of the α-substituent in the α-aryl-β,β-disilyl vinyl cations **3.18**. To this end, the thermally unstable vinyl cations **3.18** were generated *in situ* through treatment of the corresponding aryl acetylenes **3.19** with triphenylcarbenium tetrakis(pentafluorophenyl)borate at –78 °C in CD_2Cl_2, and upon attempted isolation the vinyl cations decomposed and, therefore, were characterized without isolation by ^{1}H, ^{13}C and ^{29}Si NMR spectroscopy at 0 °C (Scheme 21).

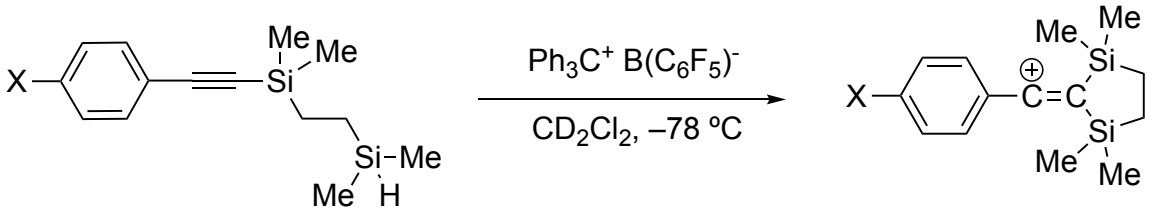

3.19 **3.18**

R = Me (**a**), OPh (**b**), OMe (**c**), NMe_2 (**d**)

Scheme 21. Generation of α-aryl-β,β-disilyl vinyl cations **3.18** by hydride abstraction from aryl acetylenes **3.19**.

The ^{13}C NMR spectra of cations **3.18 a-d** displayed diagnostic resonances at δ = 184–195 ppm and δ = 84–86 ppm assigned to the C1 and C2 vinyl carbon atoms, respectively (Table 18). In the ^{29}Si NMR spectra of the vinyl cations **3.18**, $\delta^{29}Si$ depended strongly on the electron donor ability of the α-aryl group and ranged from δ = 56.0 ppm for the *p*-tolyl substituted vinyl cation **3.18a** to δ = 37.3 ppm for the *p*-(dimethylamino)phenyl substituted vinyl cation **3.18d**, all of which were significantly deshielded relative to the C(sp)-bound silicon atom of the aryl acetylene precursors **3.19** (δ = –14.1–14.9 ppm). A plot of the $\delta^{29}Si$ versus Hammett-Brown σ^+ parameter was linear (R^2 = 0.99),[173] which established a correlation between the ^{29}Si NMR chemical shift and the electron donor ability of the α-aryl group of vinyl cations **3.18** (Figure 89).

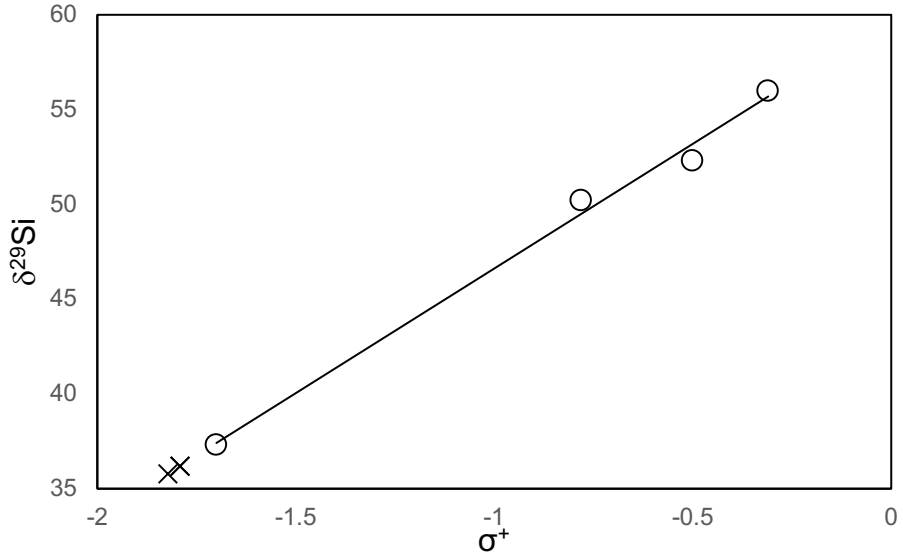

Figure 89. Linear correlation between $\delta^{29}Si$ and Hammett-Brown σ + parameter for vinyl cations 3.**18** (○) with calculated values for gold(I) vinylidene complexes **3.16** (×).

3.2.3 Discussion

From the ^{29}Si NMR data for gold(β,β-disilyl)vinylidene complexes **3.16** and α-aryl-β,β-disilyl vinyl cations **3.18**, a number of conclusions can be drawn, with varying levels of confidence. First, the correlation between σ^+ and δ^{29}Si for α-aryl-β,β-disilyl vinyl cations **3.18** established that ^{29}Si NMR chemical shift is sensitive to and dependent on the electron-donor ability of the α-substituent. Therefore, we can reasonably conclude that the ^{29}Si NMR chemical shift of gold vinylidene complexes **3.16** likewise reflects similar sensitivity with the electron-donor ability of the (L)Au fragment. Therefore, these data indicate that the electron donor ability of the (L)Au fragments decreases in the order (**P1**)Au > (IMes)Au ≈ (SIMes)Au > (IPr)Au > (SIPr)Au, although the magnitude of the difference between the most and least electron-donating fragment is small, and less than the difference between a *p*-tolyl group and a *p*-phenoxy group.

Taking the δ^{29}Si of vinylidene complexes **3.16** and vinyl cations **3.18** as a measure of electron-donor ability of the α-substituent leads to the somewhat unexpected conclusion that all of the (L)Au fragments investigated (δ^{29}Si = 36.2–34.5 ppm) are more electron donating than the *p*-(dimethylamino)phenyl group of **3.18d** (δ^{29}Si = 37.3 ppm). A number of considerations support the validity of this comparison. First, the spectroscopy of both gold vinylidene complexes **3.16** and vinyl cations **3.18** are consistent with Y-shaped vinyl cations structures, and therefore **3.16** and **3.18** differ only in the α-

substituent. Second, although a number of factors in addition to electron density are known to affect ^{29}Si NMR chemical shifts, the similar structures and identical counterions of the complexes and the identical medium for ^{29}Si NMR analysis suggest that these other factors are largely mitigated. Third, because the silicon atoms of **3.16** and **3.18** are far removed from the α-substituent, steric or through-space perturbation of δ^{29}Si by the α-substituent appears unlikely.

As noted by Müller, the α-substituent of an α-substituted β,β-disilyl vinyl cation stabilizes the C1 carbon atom through a combination of inductive effects and resonance electron donation.[134] The strong correlation between for α-aryl-β,β-disilyl vinyl cations **3.18** indicated that for these compounds, the C1 stabilization from the aryl group is predominantly that of π-donation. This does not, however, require or imply that the electronic stabilization of the C1 atom in the gold vinylidene complexes **3.16** by the (L)Au fragment is also predominantly that of π-donation. Here it is important to note that sp carbenium ions are more sensitive to inductive effects than are sp^2 carbenium ions, owing to the greater s character and higher electronegativity of the sp carbenium ion relative to the sp^2 carbenium ion.[175-180] For example, *ab initio* calculations suggest that, although a single α-CH_3 stabilizes an alkyl cation by ≈1.3 kcal mol^{-1} more than α-trimethylsilyl group, the α-trimethylsilyl group stabilizes a vinyl cation by ≈8.3 kcal mol^{-1} more than an α-CH_3 group.[180] In the former case, the superior hyperconjugation of the

C–H bonds outweighs the lower electronegativity of the silicon atom, whereas the latter case, electronegativity differences take precedence.

Given the sensitivity of an sp carbenium ion to inductive stabilization, we considered that the apparent greater electron donor ability of the (L)Au fragments in gold vinylidene complexes **3.16** relative to the *p*-(dimethylamino)phenyl group of vinyl cation **3.18d**, might be due to the greater inductive electron releasing ability of the (L)Au fragments relative to the *p*-(dimethylamino)phenyl group. Here it should be noted that Müller's analysis of β-SiC hyperconjugation in α-aryl-β,β-disilyl vinyl cations **3.17** established a correlation between the $\Delta\delta^{29}$Si versus Hammett-Brown σ^+ parameter, where $\Delta\delta^{29}$Si represents the difference betweenδ^{29}Si of **3.17** and that of the C(sp)-bound silicon atom of the corresponding neutral aryl silyl alkyne precursor.[134] Because σ-donation from the α-aryl group would be felt in both the silyl alkyne moiety and the vinyl cation, whereas π-donation from the α-aryl group would be felt only in the vinyl cation, the $\Delta\delta^{29}$Si values presumably reflect the π-donor ability of the α-aryl group to a greater extent than does δ^{29}Si. However, because δ^{29}Si of the silyl alkynes was largely invariant of the nature of the α-aryl group, similarly strong correlations exist between the Hammett-Brown σ^+ parameter and either δ^{29}Si or $\Delta\delta^{29}$Si for vinyl cations **3.17**.

As was the case for vinyl cations **3.17** and their neutral silyl acetylene precursors, the δ^{29}Si of the C(sp)-bound silicon atom of the aryl silyl alkynes **3.19** was largely

invariant of the nature of the α-aryl group and α-aryl-β,β-disilyl vinyl cations **3.18** displayed equally good correlation between the Hammett-Brown σ^+ parameter and either δ^{29}Si (R^2 = 0.99) or $\Delta\delta^{29}$Si (R^2 = 0.99, Figure 90). Likewise, the δ^{29}Si of the C(sp)-bound silicon atom of the gold acetylide complex **3.15** differed by <0.4 ppm. However, the δ^{29}Si of the C(sp)-bound silicon atom of the aryl silyl acetylenes **3.19** are deshielded by ≈ 6 ppm relative to the δ^{29}Si of the C(sp)-bound silicon atom of gold acetylide complexes **3.15**. Because there is no net π-bonding in the Au–C bond of the gold acetylide complex,[181] these differences in the δ^{29}Si of the aryl acetylene **3.19** relative to the gold acetylide complexes **3.15** can presumably be attributed to the greater inductive electron releasing ability of the (L)Au fragments of **3.15** relative to the *p*-substituted aryl group of **3.19**. It therefore follows that σ-donation from the (L)Au fragment likewise represents a significant component of the net (L)Au→C1 electron donation in gold vinylidene complexes **3.16**, as reflected by the representative δ^{29}Si values. In this context, comparison of the $\Delta\delta^{29}$Si values is instructive (Table 18, Figure 90). In particular, the $\Delta\delta^{29}$Si for vinyl cation **3.18d** (+52.2) is smaller than the $\Delta\delta^{29}$Si for any of the gold vinylidene complexes **3.16** (≥+54.1), suggesting that the *p*-(dimethylamino)phenyl is a stronger π-donor than any of the (L)Au fragments.

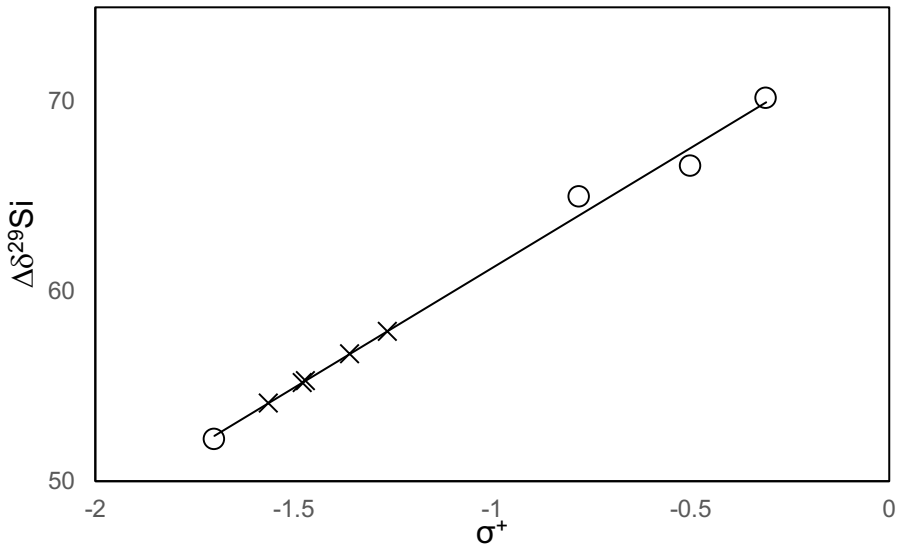

Figure 90. Linear correlation between $\Delta\delta^{29}Si$ and Hammett-Brown σ^+ parameter for vinyl cations **3.18** (○) with calculated values for gold(I) vinylidene complexes **3.16** (×).

3.3 ^{19}F NMR Studies

The analysis of ^{29}Si NMR spectroscopy of gold vinylidene complexes **3.16**, vinyl cations **3.18** and their neutral acetylenic precursors pointed to the greater inductive electron-donating ability of the (L)Au fragments compared to *p*-substututed aryl groups. To gain better insight into the ligand-dependent σ- and π-donor properties of the (L)Au fragment, we sought to determine the inductive (σ_i) and resonance (σ_r) substituent parameters of (L)Au fragments employing the ^{19}F NMR method developed by Taft.[182-184] The ^{19}F NMR chemical shifts of *m*- and *p*-substituted fluorobenzene derivatives (FC_6H_4X) represent a sensitive probe of the electron donor/acceptor properties of the substituent X.[182-184] For a substituent X, the ^{19}F chemical shift of *m*-FC_6H_4X (δ_m) and *p*- FC_6H_4X (δ_p) relative to fluorobenzene internal standard are empirically related to the inductive (σ_i) and resonance (σ_r) substituent parameters according to the relationships $\sigma_i = (\delta_m - 0.60)/-7.1$ and $\sigma_r = (\delta_m - \delta_p)/-29.5$. The inductive parameter reflects the through-space and inductive electron donating/accepting properties of the substituent, whereas the resonance parameter reflects the π-donor acceptor properties of the substituent. A negative σ_I or σ_r value indicates that the substituent is electron donating relative to a hydrogen atom. This method has been employed to determine the inductive and resonance donor/acceptor properties of hundreds of substituent groups[185] and has been extended to include numerous transition-metal fragments[186-192] including a handful of

gold(I)-ligand fragments. However, data for (PR_3)Au and (NHC)Au fragments relevant to gold(I) catalysis are absent.[193,194]

3.3.1 Neutral Gold Fluorophenyl Complexes

To determine the inductive (σ_I) and resonance (σ_r) substituent parameters for (L)Au fragments, we synthesized an eight-membered family of gold *m*- and *p*-fluorophenyl complexes (L)Au(C_6H_4F) [*m*-**3.20**/*p*-**3.20**; L = **P1** (**a**), IPr (**b**), PPh_3 (**c**), P(*t*-Bu)$_3$ (**d**)] though transmetallation of *m*- and *p*-fluorophenylboronic acid with (L)AuCl (Table 17).[194] The ^{19}F chemical shifts (δ_m and δ_p) and the associated inductive (σ_i) and resonance (σ_r) substituent parameters of complexes **3.20**, and values for L = $P(OPh)_3$ taken from the literature are compiled in Table 19. As expected, this data indicates that the gold fragments (**P1**)Au and (IPr)Au fragments are much more inductively electron-donating than are the triarylphosphine and triaryl phosphite fragments (Ph_3P)Au and [$P(PhO)_3$]Au, and are likewise much more inductively electron-donating than a simple aryl group. For comparison, the inductive and resonance substituent parameter for a phenyl group are $\sigma_i = 0.14$ and $\sigma_r = 0.01$.[182] Also worth noting is that these data revealed no detectable difference between the σ- and π-electron donor/acceptor properties of (**P1**)Au and (IPr)Au.

Table 19. ^{19}F Chemical shift data and inductive and resonance parameters for gold *m*- and *p*-flurorophenyl complexes **3.20**

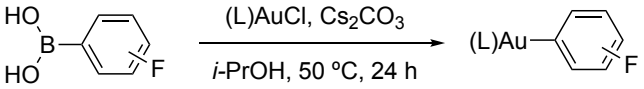

			m/p-**3.20**			
entry	Compound	L	δ_m[a]	δ_p[a]	σ_I	σ_r
1	**3.20a**	**P1**	3.71	5.71	–0.44	–0.07
2	**3.20b**	IPr	3.74	5.85	–0.44	–0.07
3	**3.20c**	PPh_3	2.43	3.51	–0.26	–0.04
4	**3.20d**	P(*t*-Bu)$_3$	3.65	4.51	–0.43	+0.01
5	**--**[b]	$P(OPh)_3$	2.10	2.95	–0.21	–0.02

[a] Chemical shift relative to C_6H_5F, with positive increments indicating more negative chemical shifts.
[b] Taken from ref. 79

3.3.2 Gold Fluorophenyl(methoxy)carbene Complexes

^{19}F NMR analysis of gold fluorophenyl complexes **3.20** revealed the strong inductive electron-donating ability and modest π-donor properties of the (L)Au (L = IPr, **P1**) fragments. We were concerned, however, that the relatively low-electron demands of the fluorophenyl group in compounds **3.20** may mask both the π-donor potential of the (L)Au fragments and subtle differences between the σ/π electron donor properties of the (**P1**)Au and (IPr)Au fragments that might be revealed under the conditions of higher electron demand found in cationic carbene complexes. Toward the evaluation of the σ- and π-electron donor properties of the (**P1**)Au and (IPr)Au fragments in cationic gold carbene complexes, we first determined the inductive and resonance parameters for the

(L)AuC(OMe) (L = **P1**, IPr) substituent groups of the cationic gold fluoromethyl(methoxy)carbene complexes $[(L)AuC(OMe)(C_6H_4F)]^+SbF_6^-$ [L = **P1** (*m*/*p*-**3.22a**, IPr (*m*/*p*-**3.22b**)] through ^{19}F NMR analysis. We targeted the methoxycarbene complexes **3.22** as previous analysis of the gold(methoxy)cyclopropyl)carbene complex **3.4** established that the C1 methoxy group provided needed stabilization to the complex without masking the electron donor effects of the (L)Au fragment.[125]

The requisite fluorophenyl(methoxy)carbene complexes **3.22** were isolated as thermally unstable yellow microcrystalline solids in 32–58% yield by metathesis of the chromium fluorophenyl(methoxy carbene complexes $(CO)_5CrC(OMe)(C_6H_4F)$ (*m*/*p*-**3.21**) with a 1:1 mixture of (L)AuCl and $AgSbF_6$ in CH_2Cl_2 at room temperature followed by recrystallization from CH_2Cl_2:pentane at –20 °C (Scheme 22). As was observed with the cationic gold vinylidene complexes **3.16**, the synthesis of the corresponding triphenylphosphine carbene complexes $(Ph_3P)AuC(OMe)(C_6H_4F)$ was unsuccessful. Complexes **3.22** were characterized by ^1H, ^{13}C, and ^{19}F NMR spectroscopy. Notably, the C1 carbene resonances of the complexes **3.22** appeared at δ = 282–292 ppm in the ^{13}C NMR spectra, which is typical of gold Fisher carbene complexes.[45,152,195-197] ^{19}F NMR analysis of complexes **3.22** provided the inductive and resonance parameters for the respective (L)AuC(OMe) groups of σ_I = +0.60 and σ_r = +0.61 for L = **P1** and σ_I = +0.62 and σ_r = +0.62 for L = IPr (Table 20). The large positive values indicate that the (L)AuCOMe

substituent group is highly electron withdrawing, as would be expected owing to the net positive charge on the carbene C1 atom.

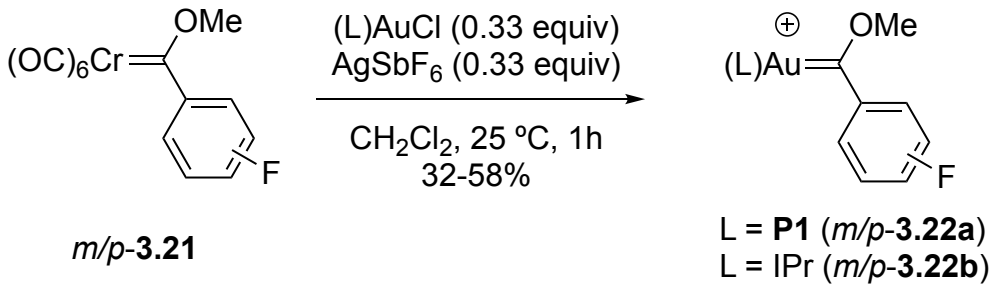

Scheme 22. Synthesis of **3.22** via metathesis with **3.21**

Table 20. ^{19}F NMR chemical shift data and inductive and resonance parameters for **3.22** and **3.24.**

entry	Compound	Substituent	δ_m[a]	δ_p[a]	σ_I	σ_r
1	**3.22a**	**P1**AuC(OMe)	–3.69	–21.58	+0.60	+0.61
2	**3.22b**	IPrAuC(OMe)	–3.78	–21.92	+0.62	+0.62
3	**3.24a**	(Ph)C(OH)	–6.55	–30.11	+1.01	+0.80
4	**3.24b**	(*p*-C_6H_4Br)C(OH)	–6.77	–29.58	+1.04	+0.77
5	**3.24c**	(*p*-C_6H_4Me)C(OH)	–6.22	–27.27	+0.96	+0.71
6	**3.24d**	(*p*-C_6H_4OPh)C(OH)	–5.82	–23.71	+0.90	+0.61
7	**3.24e**	(*p*-C_6H_4OMe)C(OH)	–5.85	–22.05	+0.91	+0.55

[a] Chemical shift relative to C_6H_5F, with positive increments indicating more negative chemical shifts.

3.3.3 Protonated Monofluorobenzophenones

The substituent parameters determined for the (L)AuC(OMe) fragments of gold carbene complexes **3.22** reflect the electron demand of the C1 carbene atom, which is stabilized by electron donation from both the (L)Au fragment and the OMe moiety. To evaluate the contribution of the (L)Au fragment to the electronic stabilization of the C1 carbon atom of complexes **3.22**, we determined the inductive and resonance parameters for the (*p*-C_6H_4X)C(OH) substituent groups of the protonated benzophenone derivatives [(*p*-C_6H_4X)(C_6H_4F)C(OH)]$^+$OTf$^-$ (*m*/*p*-**3.24**) [X = H (**a**), Br (**b**), Me (**c**), OPh (**d**), OMe (**e**)] using ^{19}F NMR analysis.[198] These protonated benzophenone derivatives were used due to the inability to generate the methylated benzophenones (*p*-C_6H_4X)(C_6H_4F)C(OMe)]$^+$OTf$^-$ directly analogous to **3.22**. However, Olah has shown previously that there is no significant difference in the C=O bond polarization of protonated and methylated ketones,[199] and potential hydrogen bonding between OTf$^-$ and the protonated ketone becomes insignificant at high HOTf concentrations, such as those employed in these reactions.[200] Therefore, we reasoned if that a correlation could be established between the inductive electron releasing ability and π-donor ability of the C1 aryl groups with the σ_i and σ_r parameters, respectively, of the (*p*-C_6H_4X)(C_6H_4F)C(OH) substituents, then meaningful comparisons could be made

between the inductive electron releasing ability and π-donor ability of the (L)Au fragments of **3.22** relative to the *p*-substituted groups of **3.24**.

The requisite protonated monofluorobenzophenones **3.24** were generated *in situ* via protonation of the corresponding monofluorobenzophenones **3.23** with excess triflic acid (>10 equiv.) in CD_2Cl_2 (Scheme 23). Formation of the oxocarbenium ions **3.24** was established by the significant deshielding of the oxygen bound carbon atom ($\Delta\delta \approx 23$ ppm) of **3.24** relative to **3.23** in the ^{13}C NMR spectra. Complete conversion of **3.23** to **3.24** was established by titrating **3.23** with HOTf until no further change in the NMR spectra was observed. The ^{19}F NMR chemical shifts (δ_m and δ_p) and the associated inductive (σ_i) and resonance (σ_r) parameters for the (*p*-C_6H_4X)C(OH) substituent are shown in Table 20. The inductive parameters for the (*p*-C_6H_4X)C(OH) substituent ranged from $\sigma_I = +1.04$ for X = Br to $\sigma_I = +0.90$ for X = OPh, all of which are significantly more positive than the inductive parameters for the (L)AuC(OMe) substituents ($\sigma_I = +0.60 – +0.62$). The resonance parameters for (*p*-C_6H_4X)C(OH) were more sensitive to the nature of the *p*-C_6H_4X group and ranged from $\sigma_r = +0.80$ for X = H to $\sigma_r = +0.55$ for X = OMe, as compared to the values of $\sigma_r = +0.61 – +0.62$ for the (L)AuC(OMe) substituents.

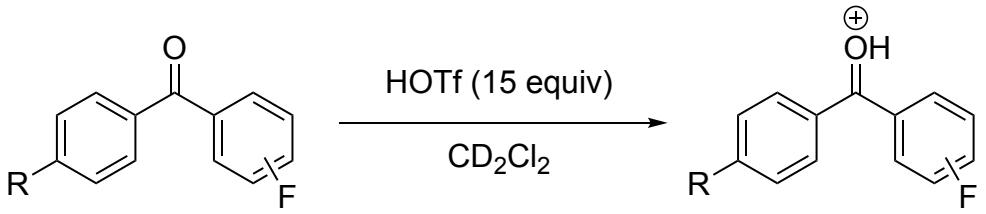

m/p-**3.23** *m/p*-**3.24**

R = H (**a**), Br (**b**), Me (**c**), OPh (**d**), OMe (**e**)

Scheme 23. Protonation of **3.23** with triflic acid.

Interpretation of the σ_r parameter for the (*p*-C_6H_4X)C(OH) groups of **3.24** in comparison to those of **3.22** requires consideration of the structures of protonated benzophenones. It has been shown that the log(pK_a) of protonated monosubstituted benzophenones derivatives display a linear correlation with the Hammett-Brown σ^+ parameter ($\rho^+ = 1.09$),[200] but the reaction constant is attenuated relative to those obtained for the correlation of log(pK_a) with σ^+ for protonated benzaldehyde ($\rho^+ = 1.86$)[201] and acetophenone ($\rho^+ = 2.17$)[202] derivatives. These differences can be attributed in part to twisting of the aryl rings of the benzophenones to minimize the unfavorable van der Walls interactions of the *ortho* hydrogen atoms,[203] which attenuates the π-overlap between the aryl groups and the electron deficient carbon atom. Nevertheless, the much lower values relative to σ_i for (*p*-C_6H_4X)C(OH) substituents and the greater sensitivity of

σ_r ($\Delta\sigma_r = 0.25$) relative to σ_i ($\Delta\sigma_i = 0.14$) suggests that the electron deficient carbon atom of **3.24** is stabilized primarily through π-donation.

A plot of the Hammett σ parameter for the aryl substituent X versus σ_i for the (*p*-C_6H_4X)C(OH) substituent of protonated monofluorobenzophenone **3.24** established a correlation between these parameters [$\sigma_i = (0.26\pm0.03)\sigma + (0.99\pm0.01)$; $R^2 = 0.96$; Figure 91] that was clearly superior to the Hammett-Brown σ^+ parameter and σ_i ($R^2 = 0.88$). Similarly, a plot of the Hammett-Brown σ^+ parameter for aryl substituent X versus σ_r for the (*p*-C_6H_4X)C(OH) substituent established a modest correlation between the parameters [$\sigma_r = (0.27\pm0.5)\sigma^+ + (0.77\pm0.02)$; $R^2 = 0.92$; Figure 92], whereas no correlation was observed between σ and σ_r. These correlations indicate the differences in the σ_i of the (*p*-C_6H_4X)C(OH) substituent are primarily caused by the inductive electron releasing ability of the *p*-C_6H_4X aryl group, and, likewise, the differences in σ_r of the (*p*-C_6H_4X)C(OH) substituent are primarily determined by the π-donor ability of the *p*-C_6H_4X aryl group.

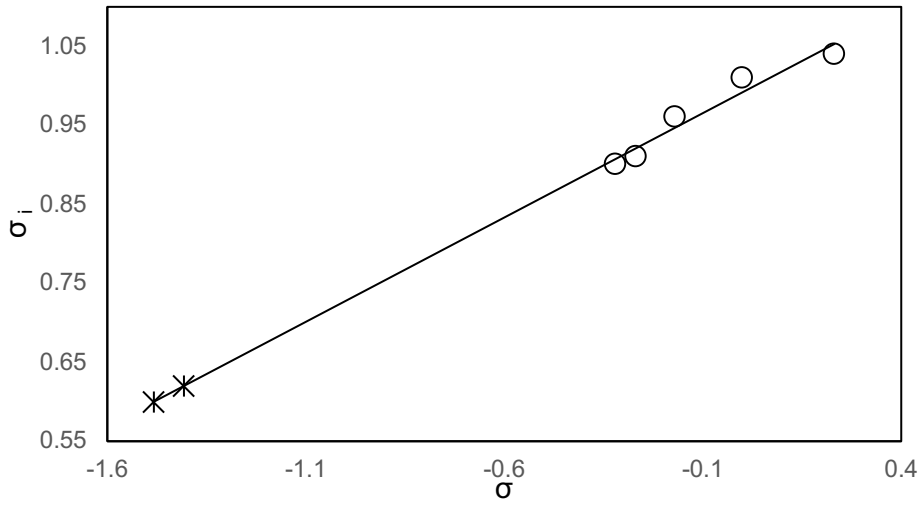

Figure 91. Correlation between σ_i and Hammett σ parameters for protonated monofluorobenzophenones **3.24** (○) with calculated values for gold(I) carbene complexes **3.2** (×) superimposed.

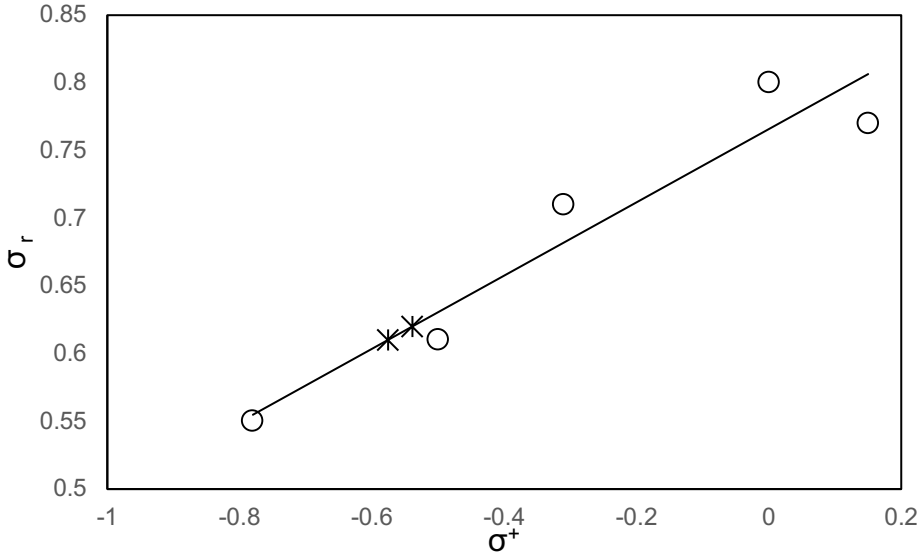

Figure 92. Correlation between σ_r and Hammett-Brown σ^+ parameters for protonated monofluorobenzophenones **3.24** (○) with calculated values for gold(I) carbene complexes **3.2** (×) superimposed.

3.3.4 Discussion

From the observed correlation between the σ and σ_i and between σ^+ and σ_r for the (*p*-C_6H_4X)C(OH) substituents of protonated monofluorobenzophenones **3.24**, it follows that any significant differences in the σ_i and σ_r values for the (L)AuC(OMe) (L = **P1**, IPr) fragments of **3.22** or between (L)AuC(OMe) and (*p*-C_6H_4X)C(OH) substituents can be attributed to differences in the inductive electron releasing ability and π-donor ability, respectively, of the corresponding (L)Au and or *p*-C_6H_4X groups. Therefore, several conclusions can be reasonably drawn from this data. First, (**P1**)Au has a nominally greater inductive electron releasing ability and π-donor ability than does (IPr)Au, although the differences are less than those between a phenyl group and *p*-bromophenyl group. Second, the significantly larger (more positive) inductive parameters of (*p*-C_6H_4X)C(OH) substituents (σ_i = +1.04–0.90) relative to those of the (L)AuC(OMe) substituents (σ_i = +0.62–0.60) further supports the conclusion that the (L)Au fragments are significantly more inductively electron releasing that are *p*-substituted aryl groups. The observed correlation between σ and σ_i predicts a σ_i value of +0.78 for a hypothetical (*p*-$C_6H_4NMe_2$)C(OH) substituent, which suggests that the (L)Au fragments are significantly more electron-donating than a *p*-dimethylamino phenyl group. Third, a comparison of the resonance parameters for the (*p*-C_6H_4X)C(OH) and (L)AuC(OMe) substituents indicates that the π-donor ability of the (L)Au fragment is lower than that of

a *p*-methoxyphenyl group but comparable to the *p*-phenoxyphenyl group. Given the potential attenuation of π-overlap of the aryl rings in **3.24**, these comparisons suggest that the (L)Au groups are modest π-donors relative to *p*-substituted aryl groups.

3.4 Summary and Conclusions

We have analyzed the spectroscopy of cationic gold (β,β-disilyl)vinyilidene complexes **3.16**, neutral fluorophenyl gold complexes **3.20**, cationic gold fluorophenyl(methoxy)carbene complexes **3.24**, and relevant organic model compounds to evaluate the ligand-dependent electron donor ability of the (L)Au fragments in gold carbene complexes relative to *p*-substituted aryl groups. The first conclusion drawn from these experiments is that the (**P1**)Au fragment is a nominally stronger electron donor than the (IPr)Au fragment in cationic gold carbene complexes. For example, ^{29}Si NMR analysis of the cationic gold vinylidene complex **3.16** suggests that the (**P1**)Au fragment is more electron donating than (IPr)Au, but the difference is less than that between a *p*-tolyl goup and a *p*-phenoxyphenyl group. Similarly, ^{19}F NMR analysis of the cationic gold fluorophenyl(methoxy)carbene complexes **3.24** suggests that (**P1**)Au is both more inductively releasing and a better π-donor than (IPr)Au, although this difference is less than that between a phenyl group and a *p*-bromophenyl group. ^{19}F NMR analysis of neutral fluorophenyl gold complexes **3.20** showed no detectable difference between either the inductive electron releasing ability or π-donor ability of the (**P1**)Au and (IPr)Au fragments. Although the contention that the (**P1**)Au fragment is more inductively electron releasing than is the (IPr)Au fragment seems to contradict the general perceptions of IPr as a strong donor ligand to gold,[204-209] Widenhoefer's analysis

of the kinetics of gold(I)-catalyzed allene racemization[210] and Belpassi's computational analysis of the electronic structure of cationic gold carbonyl complexes[132] support this conclusion.

Regarding the electron donor ability of the (L)Au fragments relative to *p*-substituted aryl groups, ^{29}Si NMR analysis of the gold (β,β-disilyl)vinyilidene complexes **3.16**, and the α-aryl-β,β-disilyl vinyl cations **3.18** suggests that the electron donor ability of the (L)Au (L = **P1**, IPr) fragment exceeds that of a *p*-(dimethylamino)phenyl group. Given the sensitivity of sp carbenium ions to inductive effects,[174] comparative ^{29}Si NMR analysis of the neutral gold acetylide complexes **3.15** and aryl acetylenes **3.19** suggests that σ-donation represents a major component of the net (L)Au→C electron donation in gold vinylidene complexes **3.16**. This hypothesis was corroborated through ^{19}F NMR analysis of gold fluorophenyl complexes **3.20** and comparative analysis of gold fluorophenyl(methoxy)carbene complexes **3.22** and the protonated monofluorobenzophenones **3.24**. Theses analyses revealed that the inductive electron donating ability of the (L)Au (L = **P1**, IPr) fragments significantly exceed that of a *p*-(dimethylamino)phenyl group whereas the π-electron donor ability of the (L)Au fragment was equal to or less than that provided by a *p*-phenoxyphenyl group.

Taken together, a picture emerges from these studies of (L)Au (L = **P1**, IPr) fragments as strong inductively electron donating, and modest π-donors, with very

similar electron-donor properties between the two fragments. These subtle differences in electron-donor ability, coupled with the different steric profiles of the ligands, are apparently sufficient to lead to the sometimes disparate catalytic behavior observed for (**P1**) and (IPr)Au complexes. The recognition of these (L)Au fragments as strongly inductively electron donating is significant because extant discussions of the (L)Au→C electron donation in the context of cationic gold carbene complexes have focused nearly exclusively on d→p backbonding represents a minor component of the total (L)Au→C donation in gold carbene complexes. It therefore follows that any evaluation of the electron donor ability of (L)Au fragments in cationic gold carbene complexes that considers only d→p backbonding will likely underestimate the full extent of (L)Au→C electron donation.

3.5 Experimental Details

3.5.1 General Methods

Reactions were performed under a nitrogen atmosphere employing standard Schlenk and glovebox techniques unless specified otherwise. NMR Spectra were obtained on a Varian spectrometer operating at 500 MHz for ^{1}H NMR, 125 MHz for ^{13}C NMR, 99 MHz for ^{29}Si NMR, and 101 MHz for ^{31}P NMR in CD_2Cl_2 at 25 °C unless noted otherwise. ^{1}H and ^{13}C were referenced to residual solvent signal, ^{29}Si was referenced to an external tetramethylsilane standard ($\delta = 0.0$) and ^{31}P was referenced to an external phosphoric acid (neat) standard ($\delta = 0.0$). Flash chromatography was performed employing 200-400 mesh silica gel 60 F 254. CD_2Cl_2 was dried over CaH_2, distilled and stored over 3Å molecular sieves in a glove box prior to use. Diethyl ether, methylene chloride, and THF were purified by passage through columns of activated alumina under nitrogen. All other reagents were obtained through major chemical suppliers and used as received. [2-Dimethylsilyl(ethyl)]dimethylsilylacetylene was prepared employing a published procedure.

3.5.2 Gold Acetylide Complexes

(P1)Au[η^1-C≡CSi(Me)$_2$CH$_2$CH$_2$SiMe$_2$H] (3.15a). A solution of [2-dimethylsilyl(ethyl)]dimethylsilylacetylene (211 mg, 1.2 mmol) in THF (3 mL) was treated with *n*-butyllithium (2.5 M, 0.44 mL, 1.1 mmol) at –78 °C and the reaction

mixture was stirred for 30 min. A solution of (**P1**)AuCl [**P1** = P(*t*-Bu)$_2$*o*-biphenyl; 531 mg, 1.00 mmol] in THF (8 mL) was added dropwise and the resulting mixture was warmed to room temperature, stirred for 1 h, opened to air, and stirred for 10 min. THF was evaporated under vacuum and the residue was extracted with hexanes and concentrated to dryness to give pure **13.15a** (242 mg, 36%) as a white, microcrystalline solid. ^{1}H NMR ($CDCl_3$): δ 7.84 (td, *J* = 7.3, 1.5 Hz, 1 H), 7.50-7.40 (m, 5 H), 7.28-7.23 (m, 1 H), 7.14 (d, *J* = 6.8 Hz, 1H), 3.88 (septet, *J* = 3.4 Hz, 1 H) 1.38 (d, *J* = 14.9 Hz, 18 H), 0.61 (m, 4 H), 0.16 (s, 6 H), 0.10 (d, *J* = 3.6 Hz, 6 H). ^{13}C{^{1}H] NMR: δ 153.1 (d, J_{CP} = 123), 150.3 (d, J_{CP} = 15 Hz), 142.2 (d, J_{CP} = 5.8 Hz),134.3, 133.0 (d, J_{CP} = 6.9 Hz), 130.0, 129.1, 128.9, 128.1, 127.5 (d, J_{CP} = 38 Hz), 126.5, (d, J_{CP} = 5.8 Hz), 105.1 (d, J_{CP} = 18.9 Hz), 37.4 (d, J_{CP} = 22.1 Hz), 31.0, 10.2, 6.6, –1.2, –4.7. ^{31}P{^{1}H} NMR: δ 58.3. ^{29}Si{^{1}H} NMR: δ –13.7 (–$SiMe_2H$), –20.6 (–C≡CSi). HRMS (ESI); calc. (found) for $C_{28}H_{45}AuPSi_2$ (MH^+): 665.2463 (665.2458).

All remaining gold acetylide complexes were synthesized employing methods analogous to that used to synthesize **3.15a**.

(IPr)Au(η^1-C≡CSi(Me$_2$)CH$_2$CH$_2$SiMe$_2$H (3.15b). White microcrystalline solid, 72%. ^{1}H NMR: δ 7.62 (t, *J* = 7.8 Hz, 2 H), 7.42 (d, *J* = 7.8 Hz, 4 H), 7.22 (s, 2 H), 3.82 - 3.76 (m, 1 H), 2.60 (hept, *J* = 6.6 Hz, 4 H), 1.38 (d, *J* = 6.8 Hz, 12 H), 1.26 (d, *J* = 6.8 Hz, 12 H), 0.56 - 0.38 (m, 4H) 0.04 (d, *J* = 3.6 Hz, 6 H), 0.00 (s, 6 H). ^{13}C{^{1}H} NMR: δ 191.3, 149.5,

145.7, 134.5, 130.5, 124.3, 123.3, 107.4, 28.9, 24.6, 24.2, 10.1, 6.5, –1.1, –4.6; ^{29}Si NMR: δ –9.9 (d, *J* = 25 Hz, $SiMe_2H$), –20.9 (C≡CSi). HRMS calc. (found) for $C_{35}H_{53}AuN_2Si_2$ (MH^+): 705.1831 (705.1816).

(SIPr)Au(η^1-C≡CSi(Me$_2$)CH$_2$CH$_2$SiMe$_2$H (3.15c). White solid, 36%. ^{1}H NMR: δ 7.52 (t, *J* = 7.7 Hz, 2 H), 7.33 (d, *J* = 7.8 Hz, 4 H), 4.02 (s, 4 H), 3.78 - 3.75 (m, 1 H), 3.09 (hept, *J* = 7.0 Hz, 4 H), 1.44 (d, *J* = 6.8 Hz, 12 H), 1.37 (d, 6.8 Hz, 12 H), 0.52 - 0.36 (m, 4H) 0.02 (d, *J* = 3.6 Hz, 6 H), –0.02 (s, 6 H). ^{13}C{^{1}H} NMR: δ 211.2, 150.0, 147.4, 134.9, 130.3, 125.1, 108.0, 54.4, 29.5, 25.5, 24.4, 10.3, 6.9, –1.3, –4.6. ^{29}Si NMR: δ –10.0 ($SiMe_2H$), –20.8 (C≡CSi). HRMS calc. (found) for $C_{35}H_{55}AuN_2Si_2$ (MH^+): 707.3642 (707.3630).

(IMes)Au(η^1-C≡CSi(Me$_2$)CH$_2$CH$_2$SiMe$_2$H (3.15d). White solid, 44%. ^{1}H NMR: δ 7.11 (s, 2 H), 7.08 (s, 4 H) 3.78 - 3.74 (m, 1 H), 2.40 (s, 6 H), 2.11 (s, 12 H), 0.51 - 0.35, (m, 4H) 0.02 (d, *J* = 3.6 Hz, 6 H), –0.02 (s, 6 H). ^{13}C{^{1}H} NMR (Figure S32): δ 189.6, 150.7, 140.4, 135.5, 129.8, 122.9, 107.7, 21.5, 18.1, 10.4, 6.9, –1.3, –4.6. ^{29}Si NMR: δ –9.8 ($SiMe_2H$), –20.6 (C≡CSi). HRMS calc. (found) for $C_{35}H_{41}AuN_2Si_2$ (MH^+): 671.2546 (671.2537).

(SIMes)Au(η^1-C≡CSi(Me$_2$)CH$_2$CH$_2$SiMe$_2$H (3.15e). White solid, 91%. ^{1}H NMR (Figure S33): δ 7.03 (s, 4 H), 3.95 (s, 4 H), 3.78 - 3.74 (m, 1 H), 2.35 (s, 6 H), 2.33 (s, 12 H), 0.48 - 0.36, (m, 4H) 0.02 (d, *J* = 3.6 Hz, 6 H), –0.04 (s, 6 H). ^{13}C{^{1}H} NMR: δ 210.4, 150.9, 139.5, 136.4, 135.5, 130.1, 107.9, 51.5, 21.5, 18.3, 10.3, 6.9, –1.3, –4.6. ^{29}Si NMR: δ –9.9 (–

$SiMe_2H$), –20.8 (–C≡CSi). HRMS calc. (found) for $C_{35}H_{43}AuN_2Si_2$ (MH^+): 673.2703 (673.2766).

3.5.3 Gold Vinylidene Complexes

3.16a. A solution of **3.15a** (20 mg, 0.025 mmol) in CD_2Cl_2 (200 μL) was added dropwise to a flame-dried NMR tube containing a solution of triphenylcarbenium tetra(pentaflurophenyl)borate (26 mg, 0.28 mmol) in CD_2Cl_2 (400 μL) at –78 °C. The tube was shaken to thoroughly mix the contents and then placed in the probe of an NMR spectrometer precooled at –20 °C. Quantitative formation of **3.16a** was observed within 10 min as evidenced by the loss of the silyl hydride peak at δ 3.7 of **3.15a** in the ^{1}H NMR spectrum. Complex **3.16a** was thermally unstable and was characterized in solution without isolation. ^{1}H NMR (–80 °C): δ 2.33 (br m, 4 H), 1.21 (br d, J = 6.5 Hz, 12 H), 1.18 (br d, J = 6.5 Hz, 12 H), 0.98 (s, 4 H), 0.11 (s, 12 H), aromatic/vinyl resonances obscured by triphenylmethane/trityl cation resonances. ^{13}C{^{1}H} NMR (–80 °C): δ 203.5, 181.2, 147.2 (d, $^1J_{CF}$ = 239 Hz [$B(C_6F_5)_4^-$]), 145.2, 137.5 (d, $^1J_{CF}$ = 242 Hz [$B(C_6F_5)_4^-$]), 135.5 (d, $^1J_{CF}$ = 241 Hz [$B(C_6F_5)_4^-$]), 134.6, 132.6, 130.6, 124.1, 124 - 122 (br m, [$B(C_6F_5)_4^-$]), 111.8, 28.4, 24.8, 22.9, 12.0, 0.5. ^{31}P{^{1}H} NMR (–80 °C): δ◎ 58.3. ^{29}Si NMR (–80 °C): δ 35.8.

All remaining gold vinylidene complexes were synthesized employing methods analogous to that used to synthesize **3.16a**.

3.16b. ^{1}H NMR (–80 °C): δ 4.10 (s, 4 H), 2.92 (br s, 4 H), 1.29 (br s, 24H), 0.97 (s, 4 H), 0.09 (s, 12 H), aromatic resonances obscured by triphenylmethane/trityl cation resonances. ^{13}C{^{1}H} NMR (–80 °C): δ 204.7, 202.8, 147.2 (d, $^{1}J_{CF}$ = 239 Hz [B(C$_6$F$_5$)$_4^-$]), 146.3, 137.5 (d, $^{1}J_{CF}$ = 242 Hz [B(C$_6$F$_5$)$_4^-$]), 135.5 (d, $^{1}J_{CF}$ = 241 Hz [B(C$_6$F$_5$)$_4^-$]), 134.6, 132.7, 129.9, 124 - 122 (br m, [B(C$_6$F$_5$)$_4^-$]), 112.3, 28.5, 25.3, 23.1, 12.1, 0.5. ^{29}Si NMR (–80 °C): δ 36.2.

3.16c. ^{1}H NMR (–80 °C): δ 2.29 (s, 6 H), 2.08 (s, 12 H), 1.05 (s, 4 H), 0.20 (s, 12 H), aromatic/vinyl resonances obscured by triphenylmethane/trityl cation resonances. ^{13}C{^{1}H} NMR (–80 °C): δ 198.5, 179.9, 147.2 (d, $^{1}J_{CF}$ = 239 Hz [B(C$_6$F$_5$)$_4^-$]), 139.9, 137.5 (d, $^{1}J_{CF}$ = 242 Hz [B(C$_6$F$_5$)$_4^-$]), 135.5 (d, $^{1}J_{CF}$ = 241 Hz [B(C$_6$F$_5$)$_4^-$]), 134.6, 133.6, 128.9, 124 - 122 (br m, [B(C$_6$F$_5$)$_4^-$]), 123.1, 114.2, 20.8, 17.4, 12.2, 0.6. ^{29}Si NMR (–80 °C): δ 34.6.

3.16d ^{1}H NMR (–80 °C): δ 4.06 (s, 6 H), 2.25 (s, 18 H), 1.01 (s, 4 H), 0.13 (s, 12 H), aromatic resonances obscured by triphenylmethane/trityl cation resonances. ^{13}C{^{1}H} NMR (–80 °C): δ 201.8, 196.8, 147.2 (d, $^{1}J_{CF}$ = 239 Hz [B(C$_6$F$_5$)$_4^-$]), 139.1, 137.5 (d, $^{1}J_{CF}$ = 242 Hz [B(C$_6$F$_5$)$_4^-$]), 135.6, 135.5 (d, $^{1}J_{CF}$ = 241 Hz [B(C$_6$F$_5$)$_4^-$]), 133.4, 129.1, 124 - 122 (br m, [B(C$_6$F$_5$)$_4^-$]), 115.2, 50.6, 20.7, 17.6, 12.2, 0.46. ^{29}Si NMR (–80 °C): δ 34.5.

3.16e ^{1}H NMR (–80 °C): δ 4.10 (s, 4 H), 2.92 (br s, 4 H), 1.29 (br s, 24H), 0.97 (s, 4 H), 0.09 (s, 12 H), aromatic resonances obscured by triphenylmethane/trityl cation resonances. ^{13}C{^{1}H} NMR (–80 °C): δ 204.7, 202.8, 147.2 (d, $^{1}J_{CF}$ = 239 Hz [B(C$_6$F$_5$)$_4^-$]), 146.3,

137.5 (d, $^1J_{CF}$ = 242 Hz [$B(C_6F_5)_4^-$]), 135.5 (d, $^1J_{CF}$ = 241 Hz [$B(C_6F_5)_4^-$]), 134.6, 132.7, 129.9, 124 - 122 (br m, [$B(C_6F_5)_4^-$]), 112.3, 28.5, 25.3, 23.1, 12.1, 0.5. ^{29}Si NMR (–80 °C): δ 36.2.

3.5.4 ^{13}C-Spin Saturation Transfer Analysis of 3.16b

An NMR tube containing complex **3.16b** (0.16M) in CD_2Cl_2 was synthesized as described above and placed in the probe of an NMR spectrometer cooled at –80 °C. Spin-lattice relaxation time (T_1) were determined for the vinylidene carbon resonances at δ 204 (C_A; T_1 = 0.2298) and δ 112 (C_B; T_1 = 0.2694). Integration of the C_A resonance (δ 204) with (S) and without (S_0) saturation of the C_B resonance showed a 12.9% decrease in the intensity of the C_A resonance. Using this information, the first-order rate constant for the intramolecular exchange of C_A and C_B of k_{obs} = 0.64 ± 0.03 s^{-1} was calculated. [ref]

$$k_{obs} = \frac{1}{T_{1C_A}}\left(\frac{S_0}{S} - 1\right) = 0.64\ s^{-1} \rightarrow 11.2\frac{kcal}{mol}$$

3.5.5 Aryl Acetylenes

4-C_6H_4MeC≡CSi(Me)$_2$(CH_2)$_2$SiMe$_2$H (3.19a). 4-Ethylnyltoluene (1.02 g, 10 mmol) was added dropwise to a solution of phenylmagnesium bromide (11 mL, 1.0 M in THF, 11 mmol) in THF (20 mL) at 0 °C and stirred for 30 min. The resulting solution was added slowly over 2 h to a solution of 1,2-bis(chlorodimethylsilyl)ethane (2.80 g, 13 mmol) in THF (30 mL) at 60 °C in a flask equipped with a reflux condenser and the resulting solution was stirred for 16 h. Lithium aluminum hydride (0.53 g, 14 mol) was added to the resulting solution in several portions and the reaction mixture was stirred

for an additional 4 h at 60 °C. The resulting suspension was cooled to 0 °C and treated sequentially with 10% (w/w) NaOH (0.5 mL) and denionzied water (3 mL). The resulting mixture was filtered through Celite® and the aqueous layer was extracted with diethyl ether (3 × 15 mL). The organic solution was dried ($MgSO_4$) and concentrated under vacuum. Flash chromatography of the residue (SiO_2: hexanes) gave **3.19a** (0.94 g, 38%) as a colorless oil. TLC (hexanes): R_f = 0.33. ^{1}H NMR ($CDCl_3$): δ 7.42 - 7.29 (m, 2 H), 7.16 - 7.06 (m, 2H), 3.90 - 3.83 (m, 1 H), 2.34 (s, 3 H), 0.63 (m, 4 H), 0.21 (s, 6 H), 0.08 (d, *J* = 3.6 Hz, 6H). ^{13}C{^{1}H} NMR ($CDCl_3$): 138.7, 132.0, 129.1, 120.3, 105.9, 92.6, 21.6, 9.4, 6.6, –2.0, –4.6. ^{29}Si NMR: δ –14.2 (C≡CSi), –9.8 (d, *J* = 23 Hz, $SiMe_2H$). HRMS calc. (found) for $C_{15}H_{29}Si_2$ (MH^+): 261.1489 (261.1485).

The remaining silyl acetylene complexes were synthesized employing procedures analogous to that used to synthesize **3.19a**.

4-C_6H_4OPhC≡CSi(Me)$_2$(CH_2)$_2$$SiMe_2H$ (3.19b). Colorless oil, 63%. TLC (hexanes–EtOAc = 96:4): R_f = 0.50. ^{1}H NMR: δ 7.63 - 7.34 (m, 9 H), 3.89 (m, 1 H), 0.68 (s, 4 H), 0.24 (s, 6 H), 0.12 (d, *J* = 3.6 Hz, 6 H). ^{13}C{^{1}H} NMR: δ 158.4, 156.9, 134.1, 130.5, 124.5, 118.8, 118.4, 105.6, 93.2, 9.7, 6.9, –1.9, –4.5. ^{29}Si NMR: δ –9.7 ($SiMe_2H$), –14.1 (C≡CSi). HRMS calculated (found) for $C_{20}H_{26}OSi_2$ (MH^+): 339.1595 (339.1589).

4-C_6H_4OMeC≡CSi(Me)$_2$(CH_2)$_2$$SiMe_2H$ (3.19c). Colorless oil, 60%. TLC (hexanes–EtOAc = 95:5): R_f = 0.35. ^{1}H NMR ($CDCl_3$): δ 7.49 - 7.31 (m 2 H), 6.91 - 6.73 (m, 2H), 3.83

(m, 1 H), 3.81 (s, 3 H) 0.63 (m, 4 H), 0.21 (s, 6 H), 0.09 (d, *J* = 3.6 Hz, 6H). $^{13}C\{^{1}H\}$ NMR ($CDCl_3$): δ 159.7, 133.5, 135.4, 113.2, 55.3, 9.3, 6.6, –2.1, –4.8. ^{29}Si NMR: δ –9.8 (d, *J* = 23 Hz, $SiMe_2H$), –14.3 (C≡CSi). HRMS calc. (found) for $C_{15}H_{29}OSi_2$ (MH^+): 277.1438 (277.1434).

4-$C_6H_4NMe_2C{\equiv}CSi(Me)_2(CH_2)_2SiMe_2H$ (3.19d). Colorless oil, 44%. TLC (hexanes–EtOAc = 95:5): R_f = 0.42. ^{1}H NMR: δ 7.37 - 7.29 (m 2 H), 6.69 - 6.48 (m, 2H), 3.95 - 3.84 (m, 1 H), 2.97 (s, 6 H), 0.79 - 0.57 (m, 4 H), 0.21 (s, 6 H), 0.11 (d, *J* = 3.6 Hz, 6H). $^{13}C\{^{1}H\}$ NMR (Figure S8): 150.9, 133.6, 112.2, 110.3, 107.5, 90.9, 40.5, 9.9, 7.1, –1.7, –4.5. ^{29}Si NMR: δ –9.8 (d, *J* = 23 Hz, $SiMe_2H$), –14.9 (C≡CSi). HRMS calc. (found) for $C_{16}H_{27}NSi_2$ (MH^+): 290.1755 (290.1757).

3.5.6 α-Aryl-β,β-Disilyl Vinyl Cations

3.18a. A solution of **16a** (40 mg, 0.15 mmol) in CD_2Cl_2 (200 μL) was added dropwise at –78 °C to a flame-dried NMR tube containing a solution of triphenylcarbenium tetra(pentaflurophenyl)borate (0.14 g, 0.15 mmol) in CD_2Cl_2 (400 μL). The NMR tube was shaken to thoroughly mix the contents and placed in the probe of an NMR spectrometer precooled at 0 °C. Formation of **15a** was observed immediately as evidenced by the complete loss of the silyl hydride peak at δ 3.8 of **16a** in the ^{1}H NMR spectrum. Compound **15a** was thermally unstable and was characterized in solution without isolation. ^{1}H NMR (0 °C): δ 2.62 (s, 3H), 1.38 (s, 4H), 0.69 (s, 12H) aromatic/vinyl resonances obscured by triphenylmethane/trityl cation. $^{13}C\{^{1}H\}$ NMR (0 °C): δ 183.9,

157.5, 148.4 (d, $^{1}J_{CF}$ = 239 Hz [$B(C_6F_5)_4^-$]), 141.9 (d, J_{CH} = 25.6 Hz), 138.6 (d, $^{1}J_{CF}$ = 242 Hz [$B(C_6F_5)_4^-$]), 136.6 (d, $^{1}J_{CF}$ = 241 Hz [$B(C_6F_5)_4^-$]), 132.3 (d, J_{CH} = 28.6 Hz), 125 - 123 (br m, [$B(C_6F_5)_4^-$]), 111.3, 84.0, 23.7 (d, J_{CH} = 20.5 Hz), 13.1 (d, J_{CH} = 16.4 Hz), 0.5 (q, J_{CH} = 15.9 Hz). ^{29}Si NMR (0 °C): δ 56.0.

All remaining α-aryl-β,β-disilyl vinyl cations were synthesized employing an analogous procedure.

3.18b. ^{1}H NMR (0 °C): δ 1.31 (s, 4H), 0.63 (s, 12H), aromatic/vinyl resonances obscured by triphenylmethane/trityl cation. ^{13}C{^{1}H} NMR (0 °C): δ 185.8, 15171.0, 153.0, 148.4 (d, $^{1}J_{CF}$ = 239 Hz [$B(C_6F_5)_4^-$]), 140.2, 138.6 (d, $^{1}J_{CF}$ = 242 Hz [$B(C_6F_5)_4^-$]), 136.6 (d, $^{1}J_{CF}$ = 241 Hz [$B(C_6F_5)_4^-$]),131.22, 127.5 125–123 (br m, [$B(C_6F_5)_4^-$]), 121.3, 119.3, 106.9, 84.5, 12.9, 0.35. ^{29}Si NMR (0 °C): δ 52.3.

3.18c. ^{1}H NMR: δ 4.06 (s, 3H), 1.32 (s, 4H), 0.64 (s, 12H), aromatic/vinyl resonances obscured by triphenylmethane/trityl cation. ^{13}C{^{1}H} NMR: δ 187.2, 172.6, 148.8 (d, $^{1}J_{CF}$ = 239 Hz [$B(C_6F_5)_4^-$]), 144.6 (d, J_{CH} = 18.9 Hz), 138.8 (d, $^{1}J_{CF}$ = 242 Hz [$B(C_6F_5)_4^-$]), 136.9 (d, $^{1}J_{CF}$ = 241 Hz [$B(C_6F_5)_4^-$]), 125.5 - 123.5 (br m, [$B(C_6F_5)_4^-$]), 117.9 (d, J_{CH} = 25.3 Hz) 105.9, 84.9, 57.8 (d, J_{CH} = 21.4 Hz), 13.0 (d, J_{CH} = 16.2 Hz), 0.4 (q, J_{CH} = 16.4 Hz); ^{29}Si NMR (0 °C): δ 50.6.

3.18d. ^{1}H NMR (0 °C): δ 3.29 (s, 6H), 1.17 (s, 4H), 0.52 (s, 12H), aromatic/vinyl resonances obscured by triphenylmethane/trityl cation. ^{13}C{^{1}H} NMR (0 °C): δ 194.9,

158.6, 148.4 (d, $^{1}J_{CF}$ = 239 Hz [$B(C_6F_5)_4^-$]), 138.6 (d, $^{1}J_{CF}$ = 242 Hz [$B(C_6F_5)_4^-$]), 136.6 (d, $^{1}J_{CF}$ = 241 Hz [$B(C_6F_5)_4^-$]), 125 - 123 (br m, [$B(C_6F_5)_4^-$]), 119.5, 114.4, 98.7, 85.9, 41.3, 11.9, –0.5; ^{29}Si NMR (0 °C): δ 37.3.

3.5.7 Gold Fluorophenyl Complexes

$Ph_3PAu(3\text{-}C_6H_4F)$ (*m*-3.20a). Cesium carbonate (0.920 g, 2.8 mmol) was added to a solution of Ph_3PAuCl (0.740 g, 1.4 mmol) and 3-flurophenyl boronic acid (0.41 g, 2.9 mmol) in isopropanol (50 mL) under nitrogen and the resulting solution was stirred for 24 h at 50 °C, cooled to room temperature and concentrated under vacuum. The resulting residue was extracted with toluene and filtered through Celite. The resulting solution was concentrated to dryness under vacuum and the resulting residue was washed with pentane, dried under vacuum, and extracted with minimal toluene. The resulting solution was filtered through Celite, washed with pentane, and dried under vacuum to give *m*-**3.20a** (0.55 g, 60%) as a white solid. NMR spectra data matched that reported in the literature.[S3] ^{1}H NMR: δ 7.64 - 7.56 (m, 6H), 7.00 - 6.93 (m, 2H), 7.54 - 7.45 (m, 11H). $^{13}C\{^{1}H\}$ NMR: δ 164.2 (d, J_{CF} = 252 Hz), 140.7 (d, J = 5 Hz), 134.9 (d, J = 14 Hz), 131.8, 131.4, 129.6 (d, J = 11 Hz), 114.4 (dd J = 18.1 Hz, 6 Hz). ^{19}F NMR: δ –117.4 (m). ^{31}P NMR: δ 43.3.

All remaining aryl gold complexes were synthesized employing a procedure analogous to that used to synthesize *m*-**3.20a**.

$Ph_3PAu(4\text{-}C_6H_4F)$ (*p*-3.20a). White solid, 22%. NMR spectra data matched that reported in the literature.[S3] ^1H NMR: δ 7.66-7.60 (m, 7H), 7.57-7.48 (m, 9H), 7.36-7.23 (m, 2H), 6.80-6.72 (m, 1H). ^{13}C {^1H} NMR: δ 176.4 (d, *J* = 117.8 Hz), 164.3 (d, *J* = 248 Hz), 135.6, 135.0 (d, *J* = 14 Hz), 131.9, 131.6 (d, *J* = 50 Hz), 129.7 (d, *J* = 7 Hz), 128.7 - 128.6 (m), 125.6 (d, *J* = 15 Hz), 112.6 (d, *J* = 21 Hz). ^{19}F NMR: δ –116.2 (m). ^{31}P NMR: δ 42.9 (d, *J* = 5 Hz).

(*t*-Bu_3P)$Au(3\text{-}C_6H_4F)$ (*m*-3.20b). White solid, 28%. ^1H NMR: δ 7.22-7.13 (m, 3H), 6.71-6.33 (m, 1H), 1.55 (d, *J* = 13 Hz, 27H). $^{13}C\{^1H\}$ NMR: δ 162.8 (d, *J* = 252 Hz), 139.8 (d, *J* = 12 Hz), 137.4 (d, *J* = 10 Hz), 129.5 (d, *J* = 112 Hz), 127.8 (d, J = 6 Hz), 129.7 (d, *J* = 15 Hz), 38.6 (d, *J* = 13 Hz), 32.2 (d, *J* = 5 Hz); ^{19}F NMR: δ –116.5 (m); ^{31}P NMR: δ 91.8 (*J* = 6 Hz). HRMS calc. (found) for $C_{30}H_{58}Au_2FP_2$ (M^+): 893.3323 (893.3351).[S4]

(*t*-Bu_3P)$Au(4\text{-}C_6H_4F)$ (*p*-3.20b). White solid, 32%. ^1H NMR: δ 7.45-7.37 (m, 2H), 6.94-6.88 (m, 2H), 1.54 (d, *J* = 13 Hz, 27H). $^{13}C\{^1H\}$ NMR: δ 161.4 (d, *J* = 240 Hz), 140.4 (d, *J* = 5 Hz), 114.1 (d, *J* = 6 Hz), 114.0 (d, *J* = 6 Hz), 39.2 (d, *J* = 15 Hz), 32.8 (d, *J* = 4 Hz). ^{19}F NMR: δ –116.5 (m). ^{31}P NMR: δ 94.0. HRMS calc. (found) for $C_{30}H_{58}Au_2FP_2$ (M^+): 893.3323 (893.3344).[S4]

(P1)$Au(3\text{-}C_6H_4F)$ (*m*-3.20c). (white solid, 26%). ^1H NMR: δ 7.98 - 7.93 (m, 1H), 7.53 - 7.46 (m, 2H), 7.38 - 7.32 (m, 2H), 7.27 - 7.20 (m, 4H), 7.09 - 7.03 (m, 2H), 6.86 - 6.79 (m, 2H), 1.46 (d, *J* = 15 Hz, 18H). $^{13}C\{^1H\}$ NMR: δ 161.5 (d, *J* = 241 Hz), 150.9 (d, *J* = 17 Hz), 143.6 (d, *J* = 6 Hz), 140.5 (d, *J* = 5 Hz), 135.8, 133.4 (d, *J* = 7 Hz), 130.5, 130.2, 129.0 (d, *J* = 30

Hz), 128.7, 128.0, 113.5 (d, *J* = 6 Hz), 113.3 (d, *J* = 6Hz), 125.7 (d, *J* = 19.7 Hz), 31.4 (d, *J* = 7Hz); ^{19}F NMR: δ –119.5 (m). ^{31}P NMR: δ 65.2. HRMS calc. (found) for $C_{26}H_{31}AuFP$ (MH^+): 589.1729 (589.1734).

[P(*t*-Bu)$_2$*o*-biphenyl]Au(3-C$_6$H$_4$F) (*p*-3.20c). White solid, 23%. ^{1}H NMR: 7.99-7.92 (m, 1H), 7.56 - 7.46 (m, 2H), 7.41 - 7.34 (m, 2H), 7.34 - 7.29 (m, 4H), 7.13 - 7.05 (m, 1H), 6.89 - 6.79 (m, 2H), 6.65 - 6.57 (m, 1H), 1.46 (d, *J* = 14Hz, 18H). ^{13}C {^{1}H} NMR: δ 177.1 (d, *J* = 113 Hz), 163.4 (dd, *J* = 9, 252 Hz), 150.8 (d, *J* = 19 Hz), 143.6 (d, *J* = 12 Hz), 135.8, 135.6 (d, *J* = 2 Hz), 133.4 (d, *J* = 7 Hz), 130.6 (d, *J* = 2 Hz), 130.1, 129.0, 128.8 128.0, 127.8 - 127.7 (m), 127.2 (d, *J* = 5 Hz), 125.3 (d, *J* = 14 Hz), 111.0 (d, *J* = 21 Hz), 37.8 (d, *J* = 16 Hz), 125.7 (d, *J* = 7 Hz). ^{19}F NMR: δ –117.5 (m). ^{31}P NMR: δ 64.9 (d, *J* = 6 Hz). HRMS calc. (found) for $C_{26}H_{31}AuFP$ (MH^+): 589.1729 (589.1738).

(IPr)Au(3-C$_6$H$_4$F) (*m*-3.20d). White solid, 26%. ^{1}H NMR: δ 7.58 - 7.50 (m, 2H), 7.40 - 7.32 (m, 4H), 7.27 - 7.19 (m, 2H), 7.00 - 6.89 (m, 1H), 6.79 - 6.77 (m, 2H), 6.52 - 6.45 (m, 1H), 2.68 (quint, *J* = 8Hz, 4H), 1.42 (d, *J* = 8Hz, 12H), 1.27 (d, *J* = 8 Hz, 12H). ^{13}C {^{1}H} NMR: δ 173.2, 162.9 (d, *J* = 247 Hz), 146.5, 136.3, 135.1, 130.8, 127.8 (d, *J* = 8 Hz), 126.0 (d, *J* = 13 Hz), 124.6, 123.7, 110. 9 (d, *J* = 22 Hz), 29.37, 24.8, 24.2. ^{19}F NMR: δ –117.6 (m). HRMS calc. (found) for $C_{33}H_{40}AuFN_2$ (MH^+): 681.2914 (681.2902).

(IPr)Au(4-C$_6$H$_4$F) (*p*-3.20d). White solid, 69%. ^{1}H NMR: δ 7.52 (t, *J* = 7 Hz, 2H), 7.34 (d, *J* = 7 Hz, 4H), 7.21 (s, 2H), 6.94 (dd, *J* = 7, 8 Hz, 2H), 6.67 (dd, *J* = 10, 11 Hz, 2H),

2.67 (quint, J = 7 Hz, 4H), 1.40 (d, J = 6 Hz, 12H), 1.25 (d, J = 6 Hz, 12H). $^{13}C\{^{1}H\}$ NMR: δ 163.6 (d, J = 308 Hz), 146.5, 141.1 (d, J = 6 Hz), 135.2, 130.8, 124.5, 123.6, 113.4 (d, J = 17 Hz), 29.4, 24.8, 24.2. ^{19}F NMR: –119.8 (m). HRMS calc. (found) for $C_{33}H_{40}AuFN_2$ (MH^+): 719.2473 (719.2452).

3.5.8 Gold Fluorophenyl(methoxy)carbene Complexes

[(P1)AuC(OMe)(3-C_6H_4F)]$^+$ SbF_6^- (*m*-3.22a). *n*-BuLi (1.0 mL, 2.5 mmol, 2.5 M in hexanes) was added dropwise to a solution of 3-flurorobromobenzene (0.28 mL, 2.5 mmol) in diethyl ether (3 mL) at 0 °C. The resulting solution was stirred at 0 °C for 30 min and transferred via cannula to a stirred suspension of $Cr(CO)_6$ (0.55 g, 2.5 mmol) in diethyl ether (20 mL) at 0 °C. The reaction mixture was stirred at room temperature for 3 h and the resulting dark orange solution was exposed to air, stirred for 10 min, and concentrated under vacuum. The resulting residue was dissolved in degassed, deionized water (15 mL), cooled at 0 °C, and treated with Me_3OBF_4 (0.73 g, 5.0 mmol), added in several portions. The resulting dark red solution was stirred for 15 min, diluted with hexanes (20 mL), and stirred for 1 h. The layers were separated and the aqueous layer was extracted with hexanes (3 × 15 mL). The combined organic extracts were washed with brine, dried ($MgSO_4$), and concentrated under vacuum. The resulting residue was quickly chromatographed (SiO_2: hexanes) and the dark red fraction (R_f = 0.20) was collected and concentrated under vacuum to give $(CO)_5CrC(OMe)(3\text{-}C_6H_4F)$ (*m*-**3.21**).

CH_2Cl_2 (3 mL) was added to a mixture of (**P1**)AuCl (50 mg, 0.094 mmol) and $AgSbF_6$ (32 mg, 0.093 mmol) at 0 °C. A solution of *m*-**3.21** (93 mg, 0.23 mmol) in CH_2Cl_2 (10 mL) was added dropwise to the reaction mixture and the resulting solution was stirred at room temperature for 3 h, filtered through a pad of Celite, and concentrated under vacuum. The resulting residue was dissolved in minimal CH_2Cl_2, diluted with hexanes (25 mL), and cooled at –20 °C for 4 h. The resulting red solution was decanted off the yellow precipitate, which was dissolved in minimal CH_2Cl_2 and recrystallized by vapor diffusion with pentane at –20 °C to give *m*-**3.22a** (30 mg, 52%) as a yellow solid. In the solid state, *m*-**3.22a** decomposed over the course of 6 h at –20 °C to give bisphosphine gold complex, $[L\text{-}Au\text{-}L]^+$.

For *m*-3.21: ^1H NMR ($CDCl_3$): δ 7.9-6.4 (br m, 4H), 4.8 (br s, 3H). $^{13}C\{^1H\}$ NMR ($CDCl_3$): δ 223.9, 215.9, 131.2, 119.5, 116.9, 109.7, 67.4. ^{19}F NMR ($CDCl_3$): δ –111.8 (m).

For *m*-3.22a: ^1H NMR ($CDCl_3$): δ 8.01 - 7.84 (m, 2 H), 7.73 - 7.65 (m, 1H), 7.63 - 7.52 (m, 2H), 7.31 - 7.17 (m, 6H), 6.91 - 6.86 (t, J = 4.3 Hz, 1H), 4.91 (s, 3H), 1.49 (d, J = 15.5 Hz, 18H). $^{13}C\{^1H\}$ NMR ($CDCl_3$): δ 290.0 (d, J_{CP} = 98 Hz), 163.1 d, J_{CF} = 240 Hz), 149.5 (d, J_{CP} = 14 Hz), 144.1 (d, J_{CP} = 7 Hz), 143.4, 135.0, 133.8, 132.2 (d, J_{CF} = 9 Hz), 132.1, 130.2 (d, J_{CP} = 33 Hz), 129.2 (d, J_{CP} = 57 Hz), 128.4 (d, J_{CP} = 8 Hz), 127.9, 127.0 (d, J_{CP} = 21 Hz), 126.1 (d, J_{CP} = 43 Hz), 119.1 (d, J_{CP} = 23 Hz), 75.08, 40.7 (d, J_{CP} = 23 Hz), 31.5 (d, J = 5 Hz). ^{19}F NMR ($CDCl_3$): δ –109.5 (m). ^{31}P NMR ($CDCl_3$): δ 62.2.

The remaining gold fluorophenyl(methoxy)carbene complexes were synthesized employing a procedure analogous to that used to synthesize *m*-**3.22a**.

[(P1)AuC(OMe)(4-C_6H_4F)]$^+$ SbF_6^- (*p*-3.22a). Yellow solid, 58%. ^{1}H NMR ($CDCl_3$): δ 8.12–8.06 (m, 2 H), 7.94 - 7.89 (m, 1H), 7.60 - 7.53 (m, 2H), 7.36 - 7.16 (m, 6H), 6.86 (t, *J* = 4.3 Hz, 1H), 4.81 (s, 3H), 1.48 (d, *J* = 15.5 Hz, 18H). ^{13}C{^{1}H} NMR ($CDCl_3$): δ 286.5 (d, J_{CP} = 99.5 Hz), 169.6 (d, J_{CF} = 269 Hz), 148.9 (d, J_{CP} = 16.4 Hz), 143.5, 138.6 (br m), 137.9, 134.5 (d, J_{CP} = 2.5 Hz), 132.2 (d, J_{CF} = 8.8 Hz), 131.3 (d, J_{CP} = 37.8 Hz), 129.7, 129.4, 127.9 (d, J_{CP} = 6.3 Hz), 127.4, 125.7 (d, J_{CF} = 44.1 Hz), 117.5 (d, J_{CP} = 22.6 Hz), 71.6, 37.8 (d, J_{CP} = 22.6 Hz), 31.1 (d, J_{CP} = 6.3 Hz). ^{19}F NMR ($CDCl_3$): δ –91.6 (m). ^{31}P NMR ($CDCl_3$): δ 62.4.

$(CO)_5$CrC(OMe)(4-C_6H_4F)] (*p*-3.21). ^{1}H NMR ($CDCl_3$): δ 7.5 (br s, 2H), 7.1 (br s, 2H), 4.8 (br s, 3H). ^{13}C{^{1}H} NMR ($CDCl_3$): δ 247.2, 223.8, 216.4, 164.4 (d, *J* = 252 Hz), 150.1, 127.2, 115.5, 67.5. ^{19}F NMR ($CDCl_3$): δ –107.9 (m).

[(IPr)AuC(OMe)(3-C_6H_4F)]$^+$ SbF_6^- (*m*-3.22b). Yellow solid, 32%. ^{1}H NMR ($CDCl_3$): 7.64-7.61 (m, 4 H), 7.59 (s, 2 H), 7.43 (d, *J* = 8 Hz, 4 H), 7.04 (t, *J* = 8 Hz, 2 H), 4.3 (s, 3 H), 2.54 (sept, *J* = 8 Hz, 4 H), 1.30 (d, *J* = 8 Hz, 12 H), 1.26 (d, *J* = 8 Hz, 12 H). ^{13}C{^{1}H} NMR ($CDCl_3$): δ 282.1, 207.2, 186.6, 169.5 (d, J_{CF} = 270 Hz), 146.3, 138.6 (m), 133.2, 125.6, 124.6, 117.2 (*J* = 21 Hz), 70.6, 29.9, 24.9, 29.2. ^{19}F NMR ($CDCl_3$): δ –91.3 (m).

[(IPr)AuC(OMe)(4-C_6H_4F)]$^+$ SbF_6^- (*p*-3.22b). Yellow solid, 35%. ^{1}H NMR ($CDCl_3$): δ 7.65 (t, *J* = 8 Hz, 2 H), 7.53 (s, 1 H), 7.47 - 7.31 (m, 4 H), 7.29 - 7.21 (m, 3 H), 7.14 - 7.04

(m, 1 H), 4.33 (s, 3 H), 2.57 (sept, J = 8 Hz, 4 H), 1.27 (d, J = 2 Hz, 12 H), 1.24 (d, J = 8 Hz, 12 H). $^{13}C\{^{1}H\}$ NMR ($CDCl_3$): δ 285.5, 186.1, 162.6 (d, J_{CF} = 250 Hz), 146.1, 146.7, 145.2, 143.6 (d, J_{CF} = 8 Hz), 139.1, 133.4, 132.1, 131.5, 131.4 (d, J_{CF} = 9 Hz), 130.9, 126.7 (d, J_{CF} = 21 Hz), 125.9, 125.2, 125.5, 119.3 (d, J_{CF} = 21 Hz), 28.9, 24.9, 24.2. ^{19}F NMR ($CDCl_3$): δ –109.38 (m).

3.5.9 Monofluorobenzophenones

(3-Fluorophenyl)(phenyl)methanone (*m*-3.23a). Benzaldehyde (0.53 g, 5.0 mmol) was added dropwise to a solution of 3-fluorophenylmagnesium bromide (5.25 mL, 1.0 M in MeTHF, 5.25 mmol) in THF (10 mL) at 0 °C, stirred for 15 min, and treated with deionized water (4 mL). The layers were separated and the aqueous layer was extracted with diethyl ether (3 × 15 mL). The combined organic extracts were dried ($MgSO_4$) and concentrated under vacuum. The residue was dissolved in CH_2Cl_2 (5 mL) and added dropwise to a stirred suspension of pyridinium dichromate (PDC) (2.2 g, 5.8 mmol) in CH_2Cl_2 (25 mL) at 0 °C. The reaction mixture was stirred for 16 h and filtered through Celite. The filtrate was concentrated under vacuum and the residue was dissolved in hexanes (5 mL) and cooled at –20 °C overnight to give *m*-**3.23a** (0.47 g, 46 %) as a white solid. ^{1}H NMR ($CDCl_3$): δ 7.91 - 7.81 (m, 2 H), 7.81 - 7.70 (m, 2 H), 7.64 - 7.55 (m, 1 H), 7.53 - 7.45 (m, 2 H), 7.20 - 7.12 (m, 2 H). $^{13}C\{^{1}H\}$ NMR ($CDCl_3$): δ 194.2, 165.6 (d, J_{CF} = 252 Hz), 136.3, 133.5, 132.7 (d, J_{CF} = 13 Hz), 131.8, 131.5, 127.7, 115.7 (d, J_{CF} = 25 Hz).

^{19}F NMR ($CDCl_3$): δ –106.0 (m). HRMS calc. (found) for $C_{13}H_9FO$ (MH^+): 201.0710 (201.0710).

All remaining fluorinated benzophenone derivatives were synthesized employing procedures similar to that used to synthesize *m*-**3.23a**.

(4-Fluorophenyl)(phenyl)methanone (*p*-3.23a). ^{1}H NMR ($CDCl_3$): δ 7.66 (q, *J* = 8 Hz, 4H), 7.55 - 7.52 (m, 1 H), 7.50 - 7.43 (m, 3 H), 7.33 - 7.28 (m, 1H). ^{13}C{^{1}H} NMR ($CDCl_3$): δ 194.3, 162.6 (d, J_{CF} = 252 Hz), 139.3 (d, J_{CF} = 8 Hz), 135.9, 131.9, 131.6, 130.3 (d, J_{CF} = 5 Hz), 128.1, 125.8, 119.8 (d, J_{CF} = 21 Hz), 116.7 (d, J_{CF} = 23 Hz). ^{19}F NMR ($CDCl_3$): δ –111.6 (m). HRMS calc. (found) for $C_{13}H_9FO$ (MH^+): 201.0710 (201.0708).

(3-Fluorophenyl)(4-bromophenyl)methanone (*m*-3.23b). ^{1}H NMR ($CDCl_3$): δ 7.81 (d, *J* = 8 Hz, 2 H), 7.64 - 7.56 (m, 2 H), 7.54 - 7.42 (m, 4H), 7.33 - 7.25 (m, 1H); ^{13}C{^{1}H} NMR ($CDCl_3$): δ 195.4, 162.6 (d, J_{CF} = 252 Hz), 139.8 (d, J_{CF} = 126 Hz), 137.1, 132.9, 130.3, 130.1 (d, J_{CF} = 9 Hz), 128.5, 125.9, 119.5 (d, J_{CF} = 25 Hz), 116.9 (d, J_{CF} = 9 Hz). ^{19}F NMR ($CDCl_3$): δ –112.05 (m). HRMS calc. (found) for $C_{13}H_8BrFO$ (MH^+): 278.9815 (278.9810).

(3-Fluorophenyl)(*p*-tolyl)methanone (*m*-3.23c). ^{1}H NMR ($CDCl_3$): δ 7.72 (d, *J* = 8Hz, 2H), 7.57 - 7.42 (m, 4H), 7.30 (d, *J* = 8 Hz, 2H), 2.45 (s, 3H). ^{13}C{^{1}H} NMR ($CDCl_3$): δ 195.2, 165.8 (J_{CF} = 252 Hz), 144.0, 135.3, 134.8, 133.0 (d J_{CF} = 8.8 Hz), 130.6, 129.6, 115.8 (d, J_{CF} = 23 Hz), 21.9. ^{19}F NMR ($CDCl_3$): δ –112.9 (m). HRMS calc. (found) for $C_{14}H_{11}FO$ (MH^+): 215.0867 (215.0869).

(4-Fluorophenyl)(*p*-tolyl)methanone (*p*-3.23c). White solid, 81%. ^{1}H NMR ($CDCl_3$): δ 7.82 (dd, *J* = 5.5, 8.9 Hz, 2 H), 7.68 (d, *J* = 8.9 Hz, 2 H), 7.31 (d, *J* = 8.8 Hz, 2 H), 7.18 (t, *J* = 8.8 Hz, 2 H), 2.44 (s, 3 H). ^{13}C{^{1}H} NMR ($CDCl_3$): δ 195.2, 165.8 (d, J_{CF} = 252 Hz), 144.0, 135.3, 134.8, 133.0 (d, J_{CF} = 8.8 Hz), 130.6, 129.6, 115.8 (d, J_{CF} = 22 Hz), 21.9. ^{19}F NMR ($CDCl_3$): δ –107.6 (m). HRMS calc. (found) for $C_{14}H_{11}FO$ (MH^+): 215.0867 (215.0865).

(3-Fluorophenyl)(4-phenoxyphenyl)methanone (*m*-3.23d). White solid, 89%. ^{1}H NMR ($CDCl_3$): δ 7.82 - 7.8 (m, 2H), 7.52 - 7.38 (m, 5H), 7.25 - 7.18 (m, 2 H), 7.08 (d, *J* = 8 Hz, 2H), 7.02 (d, *J* = 8 Hz, 2 H); ^{13}C{^{1}H} NMR ($CDCl_3$): δ 194.1, 162.6 (d, J_{CF} = 248 Hz), 162.1, 150.5, 140.2, 132.6, 131.4, 130.2, 130.1 (d, J_{CF} = 7.5 Hz), 125.6, 124.9, 120.39 119.2 (d, J_{CF} = 20 Hz), 117.30, 116.7 (d, J_{CF} = 21 Hz). ^{19}F NMR ($CDCl_3$): δ –112.04 (m). HRMS calc. (found) for $C_{14}H_{11}FO_2$ (MH^+): 231.0816 (231.0814).

(4-Fluorophenyl)(4-phenoxyphenyl)methanone (*p*-3.23d). ^{1}H NMR ($CDCl_3$): δ 7.84-7.78 (m, 4H), 7.39 (t, J = 8 Hz, 1H), 7.24-7.00 (m, 8H); ^{13}C{^{1}H} NMR ($CDCl_3$): δ 194.1, 165.3 (d, J_{CF} = 253 Hz), 161.8, 155.6, 134.2, 132.5 (d, *J* = 8.8 Hz), 132.4, 131.9, 130.2, 124.8, 120.3, 117.3, 115.5 (d, J_{CF} = 23 Hz). ^{19}F NMR ($CDCl_3$): δ –106.47 (m). HRMS calc. (found) for $C_{14}H_{11}FO_2$ (MH^+): 231.0816 (231.0815).

(3-Fluorophenyl)(4-methoxyphenyl)methanone (*m*-3.23e). ^{1}H NMR ($CDCl_3$): δ 7.81 (d, *J* = 8 Hz, 2 H), 7.53 - 7.49 (m, 1 H), 7.47-7.40 (m 3H), 6.96 (d, *J* = 8 Hz, 2H). ^{13}C{^{1}H}

NMR ($CDCl_3$): δ 194.2, 165.2 (d, J_{CF} = 254 Hz), 163.4, 134.6, 132.5, 132.4 (d, J_{CF} = 8.8 Hz), 130.12, 115.42 (d, J_{CF} = 21 Hz), 113.8, 55.6. ^{19}F NMR ($CDCl_3$): δ –112.3. HRMS calc. (found) for $C_{19}H_{13}FO_2$ (MH^+): 293.0972 (293.0971).

(4-Fluorophenyl)(4-methoxyphenyl)methanone (*p*-3.23e). White solid, 93%. ^1H NMR ($CDCl_3$): δ 7.82 - 7.76 (m, 4 H), 7.17 (t, *J* = 8.8 Hz, 2 H), 6.98 (d, *J* = 8.8 Hz), 2 H), 3.88 (s, 3 H). $^{13}C\{^1H\}$ NMR ($CDCl_3$): δ 194.1, 163.6, 162.6 (d, J_{CF} = 250 Hz), 140.5 (d, J_{CF} = 6 Hz), 132.7, 130.0 (d, J_{CF} = 8 Hz), 129.7, 125.6, 119.0 (d, J_{CF} = 21 Hz), 116.6 (d, J_{CF} = 23 Hz), 113.8, 55.6. ^{19}F NMR ($CDCl_3$): δ –108.0 (m). HRMS calc. (found) for $C_{19}H_{13}FO_2$ (MH^+): 293.0972 (293.0817).

3.5.10 Protonated Monofluorobenzophenones

$[(4\text{-}C_6H_4Br)(4\text{-}C_6H_4F)COH]^+$ OTf^- (*p*-3.24b). Trifluoromethanesulfonic acid (0.17 g, 1.5 mmol) was added incrementally in five portions (3, 6, 9, 12 and 15 equiv) to a solution of ***p*-3.23b** (20 mg, 0.11 mmol) in CD_2Cl_2 (500 μL) in an NMR tube. After each addition, the solution was thoroughly mixed by shaking and was analyzed by NMR spectroscopy. From this analysis, it was determined that 9 equiv HOTf was sufficient to achieve quantitative formation of *p*-**3.24b** as determined by ^{19}F NMR analysis. ^1H NMR: δ 8.21 (dd, *J* = 4, 8 Hz, 2 H), 8.03 (d, *J* = 8 Hz, 2 H), 7.90 (d, *J* = 8 Hz, 2 H), 7.54 (t, *J* = 12 Hz, 2 H). $^{13}C\{^1H\}$ NMR: δ 205.3, 173.1 (d, J_{CF} = 276 Hz), 141.4, 141.2 (d, J_{CF} = 11 Hz), 137.4,

135.4, 128.7, 126.4, 119.9 (d, J_{CF} = 23 Hz), 119.1 (q, J_{CF} = 318 Hz, OTf). ^{19}F NMR: δ –82.69 (m).

All remaining protonated monofluorobenzophenones were synthesized employing a procedure similar to that used to synthesize *p*-**3.24b**.

[(4-C$_6$H$_4$Br)(3-C$_6$H$_4$F)COH]$^+$ OTf$^-$ (*m*-3,24b). ^{1}H NMR: δ 8.07 - 7.99 (m, 4 H), 7.89 - 7.85 (m, 3 H), 7.79 - 7.74 (m, 1 H). ^{13}C{^{1}H} NMR δ 207.0, 163.7 (d, J_{CF} = 25 Hz), 143.4, 138.4, 135.6, 133.7, 132.8, 131.7, 129.9 (d, J_{CF} = 21 Hz), 128.3, 122.0, 121.8, 119.0 (q, J_{CF} = 318 Hz, OTf). ^{19}F NMR: δ –106.13 (m).

[(Ph)(4-C$_6$H$_4$F)COH]$^+$ OTf$^-$ (*p*-3.24a). ^{1}H NMR: δ 8.26 (dd, *J* = 4, 8 Hz, 2 H), 8.19 (t, *J* = 8 Hz, 1 H), 8.05 (d, *J* = 8 Hz, 2 H), 7.86 (t, *J* = 12 Hz, 2 H), 7.55 (dd, *J* = 4, 8 Hz, 2 H). ^{13}C{^{1}H} NMR δ 206.3, 173.1, (d, J_{CF} = 275 Hz), 142.9, 141.5, 136.4, 131.6, 130.1, 126.4, 119.8, 119.0 (q, J_{CF} = 318 Hz, OTf). ^{19}F NMR: δ –82.78 (m).

[(Ph)(3-C$_6$H$_4$F)COH]$^+$ OTf$^-$ (*m*-3.24a).). ^{1}H NMR: δ 8.28 - 8.13 (m, 1 H), 8.16 (d, *J* = 8 Hz, 2 H), 7.99 - 7.77 (m, 5 H). ^{13}C{^{1}H} NMR: δ 208.1, 163.6 (d, J_{CF} = 256 Hz), 144.2, 137.5, 133.4, 131.7, 130.0, 129.98, 129.7, 122.40 (d, J_{CF} = 15 Hz), 119.0 (q, J_{CF} = 318 Hz, OTf). ^{19}F NMR: δ –106.53 (m).

[(4-C$_6$H$_4$Me)(4-C$_6$H$_4$F)COH]$^+$ OTf$^-$ (*p*-3.24c). ^{1}H NMR: δ 8.20 (dd, *J* = 4, 8 Hz, 2 H), 8.02 (d, *J* = 8 Hz, 2 H), 7.69 (d, *J* = 8 Hz, 2 H), 7.53 (t, *J* = 12 Hz, 2 H), 2.67 (s, 3 H);

$^{13}C\{^{1}H\}$ NMR: δ 204.4, 172.4 (d, J_{CF} = 273 Hz), 158.7, 140.6 (d, J_{CF} = 11 Hz), 137.4, 132.7, 127.4, 126.7, 119.5 (d, J_{CF} = 24 Hz), 119.5 (q, J_{CF} = 318 Hz, OTf), 23.5. ^{19}F NMR: δ –85.79 (m).

[(4-C_6H_4Me)(3-C_6H_4F)COH]$^+$ OTf$^-$ (*m*-3.24c). ^{1}H NMR: δ 8.10 (d, *J* = 8 Hz, 2 H), 7.86 - 7.80 (m, 3 H), 7.77 - 7.67 (m, 3 H). $^{13}C\{^{1}H\}$ NMR: δ 205.6, 163.6 (d, J_{CF} = 252 Hz), 160.5, 134.6, 133.3, 132.9, 132.2, 132.0, 128.7, 128.6, 127.0, 121.7 (d, J_{CF} = 30 Hz), 119.5 (d, J_{CF} = 24 Hz), 23.6. ^{19}F NMR: δ –106.90 (m).

[(4-C_6H_4OPh)(4-C_6H_4F)COH]$^+$ OTf$^-$ (*p*-3.24d). ^{1}H NMR: δ 8.17 (d, J = 8 Hz, 2H), 8.08 – 8.00 (m, 2H), 7.60 – 7.50 (m, 4 H), 7.42 (t, J = 8 Hz, 1H), 7.29 (d, J = 8 Hz, 2H), 7.20 (d, J = 8 Hz, 2H)/ $^{13}C\{^{1}H\}$ NMR: δ 199.6, 173.2, 171.1 (d, J_{CF} = 278 Hz), 153.5, 141.9, 135.5 (d, J_{CF} = 8.8 Hz), 131.6, 128.1, 126.8, 121.5, 119.8, 119.2 (d, J_{CF} = 23 Hz), 119.1 (q, J_{CF} = 318 Hz, OTf). ^{19}F NMR : δ –89.91 (m).

[(4-C_6H_4OPh)(3-C_6H_4F)COH]$^+$ OTf$^-$ (*m*-3.24d). ^{1}H NMR: δ 8.27 (d, J= = 8 Hz, 2 H), 7.84 – 7.68 (m 3 H), 7.63 – 7.52 (m, 3H), 7.43 (t, J = 8 Hz, 1 H), 7.29 (d, J = 8 Hz), 2 H), 7.20 (d, J = 8 Hz, 2 H).$^{13}C\{^{1}H\}$ NMR: δ 200.0, 174.3, 163.6 (d, J_{CF} = 254 Hz), 153.4, 142.9, 133.3 (d, J_{CF} = 7.6 Hz), 132.3 (J_{CF} = 6.3 Hz), 131.6, 130.3, 128.2, 127.0 (d, J_{CF} = 20 Hz), 122.6, 121.5, 120.5, 120.8, 119.1 (q, J_{CF} = 318 Hz, OTf). ^{19}F NMR: δ –108.19 (m).

[(4-C_6H_4OMe)(4-C_6H_4F)COH]$^+$ OTf$^-$ (*p*-3.24e). ^{1}H NMR: δ 8.22 (d, *J* = 8 Hz, 2 H), 8.0 (dd, *J* = 4, 8 Hz, 2 H), 7.49 (t, *J* = 12 Hz, 2 H), 7.32 (d, *J* = 8 Hz), 4.15 (s, 3H). $^{13}C\{^{1}H\}$

NMR: δ 198.9, 174.7, 170.8 (d, J_{CF} = 267 Hz), 142.2, 138.2 (d, J_{CF} = 10.1 Hz), 127.2, 122.1, 119.3 (q, J_{CF} = 318 Hz, OTf) 119.1 (d, J_{CF} = 23 Hz), 118.40, 58.30. ^{19}F NMR: δ –90.81 (m).

[(4-C_6H_4OMe)(3-C_6H_4F)COH]$^+$ OTf$^-$ (*m*-3.24e). ^{1}H NMR: δ 8.28 (d, *J* = 8 Hz, 2 H), 7.82 - 7.57 (m, 4 H), 7.31 (d, *J* = 8 Hz, 2 H), 4.17 (s, 3 H). ^{13}C{^{1}H} NMR: δ 198.5, 175.9, 163.7 (d, J_{CF} = 252 Hz), 143.1, 133.3 (d, J_{CF} = 8.8 Hz), 132.5, 129.9, 126.5 (d, J_{CF} = 21 Hz), 122.6, 120.1 (d, J_{CF} = 25 Hz), 119.2 (q, J_{CF} = 318 Hz, *OTf*), 118.72, 58.6. ^{19}F NMR: δ –107.47 (m).

4. Mechanistic Studies on the Gold(I)-catalyzed Hydrofunctionalization of Allenes

Portions of this chapter have been published: R. J. Harris, R. G. Carden, A. N. Duncan, R. A. Widenhoefer. *ACS Catal.* **2018**, *8*, 8941–8952.

R. J. Harris completed initial kinetic experiments for both the gold(I)-catalyzed hydroalkoxylation of **4.1** with **4.2** and the gold(I)-catalyzed hydroamination of **4.1** with **4.7**.

4.1 Introduction

Recently, the gold(I)-catalyzed hydrofunctionalization of allenes has attracted considerable attention, specifically due to the ease of performing both stereospecific[211-219] and enantioselective[219-222] transformations with a wide range of nucelophiles.[223,224] Due to its accessibility and broad reactivity, gold(I)-catalyzed allene hydrofunctionalization has been applied to the total syntheses of a number of natural products, including (–)-rhaxinilam[225], flinderoles B and C[226], swainsonine[227], bejarol[228], jaspine B[229], indoxamycin[230], and (–)-funebrine[231]. Despite the synthetic advances from gold(I)-catalyzed allene hydrofunctionalization reactions, gaps still exist in our understanding of the mechanism of these reactions.

Recent efforts to understand the mechanism of gold(I)-catalyzed allene hydrofunctionalization reactions have relied mostly on computational analysis.[232-241]

However, recent experimental studies have focused on the synthesis and reactivity of potential intermediates in gold(I)-catalyzed allene hydrofunctionalization, including cationic gold π-allene complexes[242-244], neutral gold vinyl complexes[215,245-269] and *gem*-diaurated vinyl complexes.[250,251,254,258,262-269] Beyond the reactivity of intermediates, experimental studies have established a net *anti* addition of the H–X bond across the C=C of the allene, consistent with outer sphere addition on cationic gold π-allene complexes.[270-276]

Less experimental information is available about the behavior of proposed catalytic intermediates under catalytic conditions, including the identification of catalyst resting states and turnover limiting steps. Furthermore, much of this information is gleaned from intramolecular hydrofunctionalization reactions. For example, Gagné reported that a cationic bis(gold) vinyl complex accumulated in solution during the gold(I)-catalyzed intramolecular hydroarylation of allenes, consistent with turnover limiting protodeauration.[250,251,264] A subsequent study by Widenhoefer and Gangé of the hydroarylation of 2,2-diphenylhexa-4,5-diene-1-ol catalyzed by [P(*t*-Bu)$_2$-*o*-biphenyl]AuOTs supported a mechanisms involving reversible C–O bond formation followed by turnover-limiting protodeauration of mono(gold) vinyl complex that occurred competitively with the formation of an inactive bis(gold) vinyl complex.[258,277-280] In comparison, Lalic's investigation of the intramolecular hydroalkoxylation of γ-

hydroxy allenes catalyzed by a gold(I) carboxylate complex supported a mechanism involving irreversible C–O bond formation followed by turnover-limiting protodeauration of a mono(gold) vinyl complex without competing formation of bis(gold)vinyl complex.[215]

The only kinetic and mechanistic analysis of a gold(I)-catalyzed intermolecular allene hydrofunctionaliztion reaction reported by Toste and Goddard is a combined experimental and computational study of the hydroamination of 1,7-diphenylhepta-3,4-diene with methyl carbazate catalyzed by $(PPh_3)AuNTf_2$. The authors propose a "two-step, no intermediate" mechanism involving turnover-limiting isomerization of a gold π-allene complex to a gold η^1-allylic cation transition state that is trapped by nucleophilic attack by methyl carbazate.[211] This hypothesis was supported by near zero-order dependence of the rate of hydroamination on methyl carbazate concentration and the assignment of the gold π-allene complex as the catalyst resting state based on ^{31}P NMR analysis of reaction mixtures. A subsequent study by Widenhoefer showed that the complex assigned by Toste and Goddard as a gold π-allene complex was instead the catalyst decomposition product $[(PPh_3)_2Au]^+$.[244] Based on these results, turnover-limiting allene isomerization may not necessarily be the rate determining step, since there are other possible mechanistic pathways which could account for a zero-order dependence on the methyl carbazate concentration.

4.2 Gold(I)-catalyzed Intermolecular Hydroalkoxylation of Allenes with Alcohols

4.2.1 Background

The intermolecular gold(I)-catalyzed hydroalkoxylation of **4.1** with **4.2** was targeted to understand the mechanism of intermolecular gold(I)-catalyzed allene hydrofunctionalization with weakly basic nucleophiles due to its high reaction efficiency and high regioselectivity forming **4.3** almost exclusively (Scheme 24). To probe the mechanism, we performed kinetic and spectroscopic analysis of catalytic mixtures, deuterium labeling studies and independently synthesized potential catalytic intermediates. These results are consistent with a mechanism involving reversible, endergonic formation of a cationic gold π-allene complex that undergoes irreversible, outer-sphere attack of alcohol on an η^2-allene complex followed by rapid protodeauration.

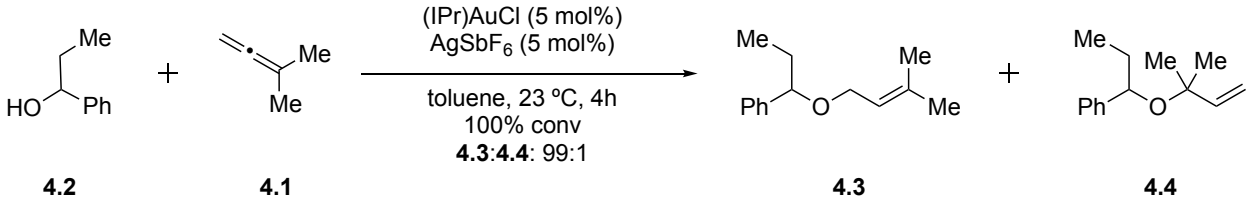

Scheme 24. Regioselective gold(I)-catalyzed hydroalkoxylation of **4.1** with **4.2**

Preliminary experiments by our group, focused on investigating the kinetics of the reaction of **4.1** with **4.2** catalyzed by (IPr)AuOTf in toluene under conditions of excess **4.1**. In one experiment, a toluene solution of **4.1** (1.6 M). **4.2** (0.16 M), hexadecane (internal standard), and a catalytic amount of (IPr)AuOTf (15 mM) was stirred at 30 °C and analyzed periodically by GC. A plot of ln[**4.1**] versus time was linear to > 3 half-lives with a pseudo-first-order rate constant of $9.8 \pm 0.4 \times 10^{-4}$ s^{-1}, establishing first-order dependence of the rate on alcohol concentration (Table 21, entry 1).

Table 21. Pseudo-first-order rate constants for the hydroalkoxylation of **4.1** with **4.2** catalyzed by (IPr)AuOTf in toluene at 30 °C.

Entry	[**4.1**] (M)	[**4.2**] (M)	[cat.] (mM)	Additive (mM)	(10^4) k_{obs} (s^{-1})
1	1.6	0.16	15	–	9.8 ± 0.4
2	0.78	0.16	15	–	5.4 ± 0.2
3	1.2	0.16	15	–	7.1 ± 0.4
4	2.3	0.16	15	–	11.9 ± 0.3
5	3.1	0.16	15	–	12.8 ± 0.5
6	1.6	0.16	8.2	–	5.4 ± 0.4
7	1.6	0.16	30	–	17.1 ± 0.6
8	1.6	0.16	16	Bu_4NOTf (16)	4.0 ± 0.2
9	1.6	0.16	16	Bu_4NOTf (24)	2.4 ± 0.1
10	1.6	0.16	15	Bu_4NOTf (77)	1.9 ± 0.2
11	1.6	0.16	15	HOTf (8.6)	4.4 ± 0.3
12	1.6	0.16	14	**4.3** (75 mM)	10.1 ± 0.4
13[a]	1.6	0.16	15	–	11 ± 1

[a] 1-phenylpropan-1-ol-*O*-*d* (**4.2**-*d1*; ~90% *d*) was used for this reaction.

To determine the dependence of the rate of gold(I)-catalyzed hydroalkoxylation on allene concentration, pseudo-first-order rate constants of **4.1** with **4.2** (0.16 M) were determined as a function of allene concentration from 0.78 M to 3.1 M (Table 21, entries 1–5). A plot of k_{obs} versus [**4.1**] showed a positive, non-linear dependence of the rate on allene concentration (Figure 93). To determine the dependence of the rate of allene hydroalkoxylation on catalyst concentration, pseudo-first-order rate constants for the hydroalkoxylation of **4.1** (1.6 M) with **4.2** (0.16 M) were determined as a function of catalyst concentration from 8.6 mM to 30 mM (Table 21, entries 1, 6–7). A plot of k_{obs} versus [(IPr)AuOTf] was linear (Figure 94), which established the first-order dependence of the rate on catalyst concentration.

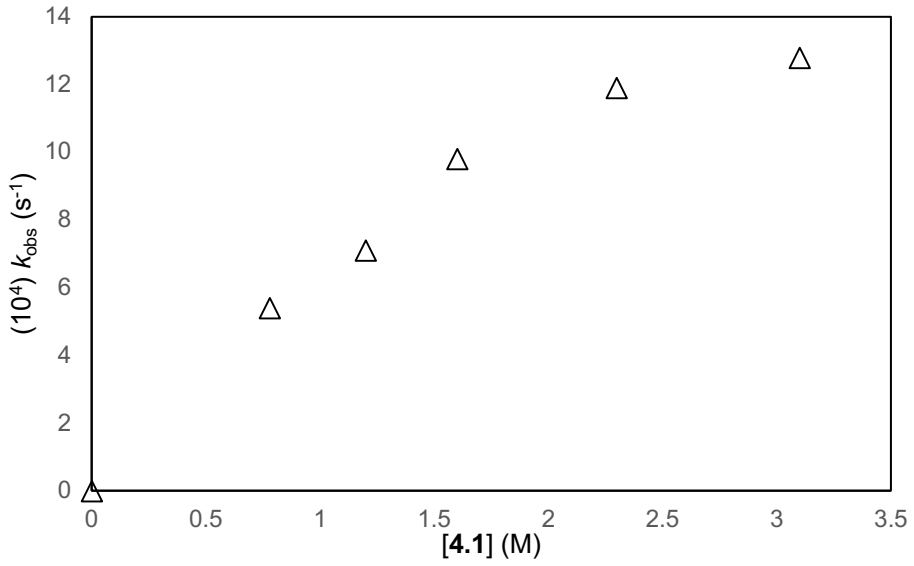

Figure 93. Allene concentration dependence of the rate of hydroalkoxylation of **4.1** (excess) with **4.2** by (IPr)AuOTf in toluene at 30 °C.

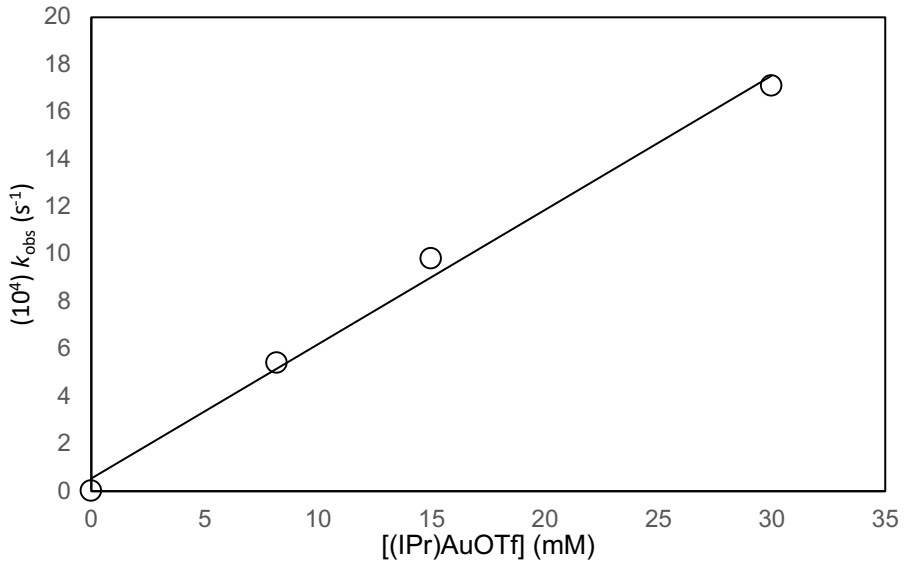

Figure 94. Plot of pseudo-first-order rate constants versus catalyst concentration for hydroalkoxylation of **4.1** (excess) with **4.2** by (IPr)AuOTf in toluene at 30 °C.

The addition of triflic acid (8.6 mM) to the gold(I)-catalyzed reaction of **4.1** with **4.2**, resulted in an ~50% decrease in the rate of the reaction (Table 21, entry 11). To determine the dependence of the rate on of the gold(I)-catalyzed hydroalkoxylation on exogenous triflate ion concentration, pseudo-first-order rate constants for the reaction of **4.1** (1.6 M), **4.2** (0.16 M) catalyzed by (IPr)AuOTf (16 mM) were determined as a function of tetrabutylammonium triflate concentration from 16–77 mM (Table 21, entries 8–10). A plot of k_{obs} versus the concentration of tetrabutylammonium triflate established an inhibition of the rate of hydroalkoxylation by exogenous triflate (Figure 95).

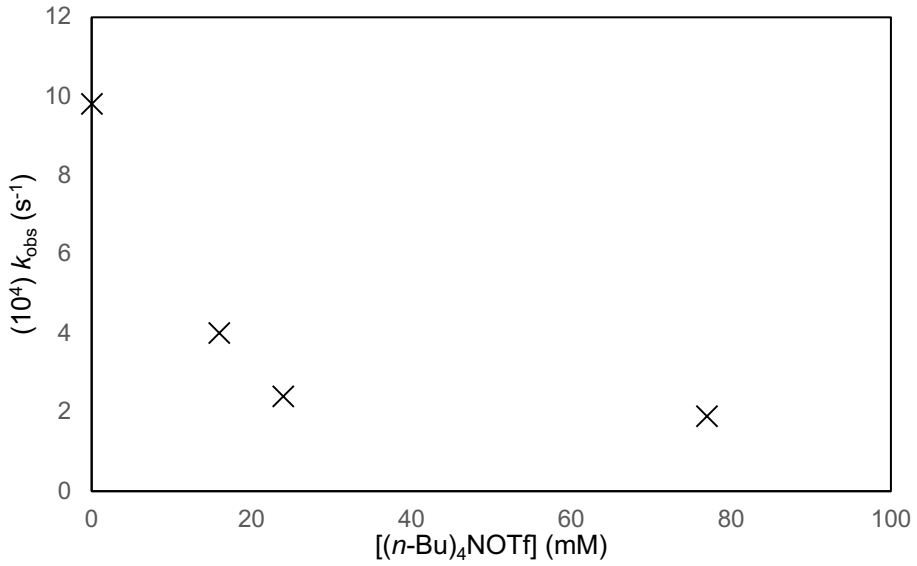

Figure 95. Plot of concentration of k_{obs} versus concentration of tetrabutylammonium triflate for the ratio of **4.1** with **4.2** catalyzed by (IPr)AuOTf.

Product inhibition of the rate of reaction was not observed, since the rate of the gold(I)-catalyzed reaction of **4.2** with excess **4.1** in the presence of allylic ether **4.3** (75 mM) was not significantly slower than the rate hydroalkoxylation in the absence of added **4.3** (Table 21, entry 12). In another experiment, the gold(I)-catalyzed deuterioalkoxylation of **4.1** with 1-phenylpropan-1-ol-*O*-*d* (**4.2**-d_1; ~90% *d*) formed **4.3**-*d* with 77 % deuterium incorporation exclusively at the internal vinylic position of **4.3**-*d* (Scheme 25). A comparison of the pseudo-first-order rate constants of hydroalkoxylation with **4.2** and **4.2**-d_1 revealed no significant deuterium kinetic isotope effect (KIE); k_H/k_D = 1.1 ± 0.1 (Table 21, entries 1 and 13). With this information in hand, we sought to further

our understanding of the mechanism of the gold(I)-catalyzed hydroalkoxylation of **4.1** with **4.2** by performing kinetic analysis of the reaction in the presence of excess **4.2** as well as spectroscopic analysis of the catalytic mixtures.

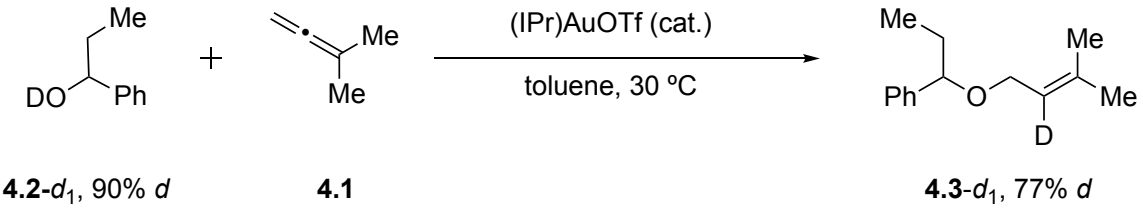

4.2-d_1, 90% d **4.1** **4.3**-d_1, 77% d

Scheme 25. Deuterioalkoxylation of **4.1** with **4.2**-d_1 (90% d) catalyzed by (IPr)AuOTf to give **4.3**-d_1 (77% d).

4.2.2 Results and Discussion

4.2.2.1. Kinetics of Hydroalkoxylation of 4.1 with excess 4.2

Our analysis of the kinetics of the gold(I)-catalzyed hydroalkoxylation of **4.1** with **4.2** under conditions of excess **4.2**, began by analyzing a solution of **4.1** (0.18 M), **4.2** (0.90 M), $CHCl_3$ (internal standard) and (IPr)AuOTf (18 mM) in toluene-d_8 at 30 °C periodically by ^{1}H NMR spectroscopy. A plot of ln[**4.1**] versus time was linear to > 3 half-lives with a pseudo-first-order rate constant of $k_{obs} = 3.39 \pm 0.01 \times 10^{-4}$ s^{-1} (Table 22, entry 1). This established first-order dependence of the rate on allene concentration under conditions of excess **4.2**.

Table 22. Pseudo-first-order rate constants for the hydroalkoxylation of **4.1** with **4.2** catalyzed by (IPr)AuOTf in toluene at 30 °C.

Entry	[**4.1**] (M)	[**4.2**] (M)	[cat.] (mM)	(10^4) k_{obs} (s^{-1})
1	0.18	0.90	18	3.39 ± 0.01
2	0.18	1.8	18	3.06 ± 0.02
3	0.18	2.7	18	2.71 ± 0.01
4	0.14	1.0	6.0	0.834 ± 0.007
5	0.14	1.0	13	2.49 ± 0.03
6	0.14	1.0	15	3.00 ± 0.07
7	0.14	1.0	20	4.06 ± 0.03
8	0.14	1.0	45	8.35 ± 0.15
9[a]	0.14	1.0	15	3.03 ± 0.02

[a] 1-phenylpropan-1-ol-*O*-*d* (**4.2**-*d1*; ~90% *d*) was used for this reaction.

To determine the rate of hydroalkoxylation on alcohol concentration, pseudo-first-order rate constants for the disappearance of **4.1** were determined as a function of [**4.2**] (0.9–2.7 M; Table 22, entries 1–3). A plot of the corresponding pseudo-first order rate constants versus $[\mathbf{4.2}]_0$ showed the rate of hydroalkoxylation displayed near zero-order dependence of the rate of hydroalkoxylation on alcohol concentration, in contrast with the first-order dependence of the rate on alcohol concentration under conditions of excess allene (Figure 96). To determine the dependence of the rate on catalyst concentration, pseudo-first-order rate constants for the hydroalkoxylation of **4.1** (0.15 M) with **4.2** (1.0 M) were determined as a function of catalyst concentration (6.0–45 mM; Table 22, entries 1, 4–8). A plot of k_{obs} versus [(IPr)AuOTf] was linear, establishing first-

order dependence of the rate of hydroalkoxylation on catalyst concentration (Figure 97). This information established an overall second order rate law under conditions of excess alcohol: rate = k'[**4.1**][(IPrAuOTf], where k' = 1.88 ± 0.01 × 10^{-2} M^{-1} s^{-1} at [**4.2**]$_0$ = 0.90 M. Gold-catalyzed deuteroalkoxylation with excess 1-phenylpropan-1-ol-*O*-*d* [**4.2**-d_1; ~90% *d*] occurred with no detectable KIE (k_H/k_D = 1.00 ± 0.03; Table 22, entries 6 and 9).

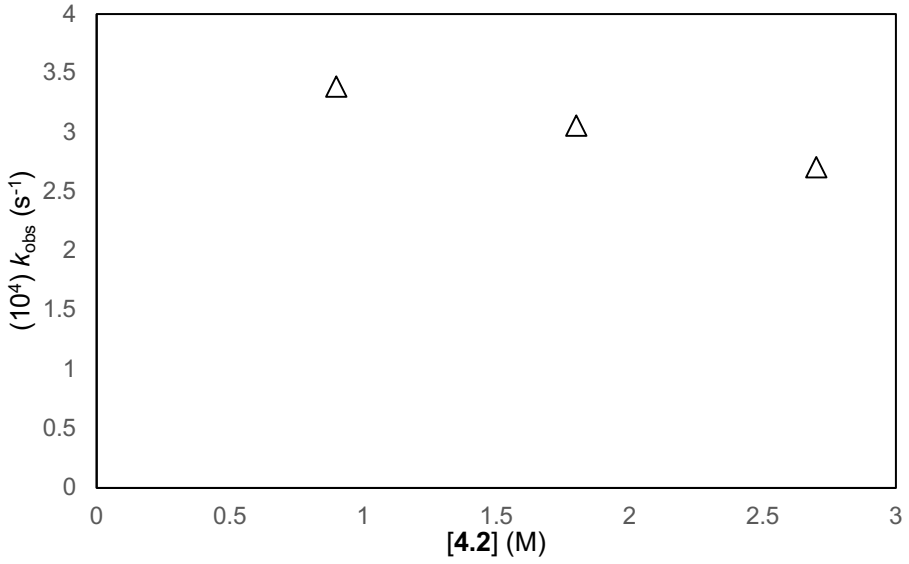

Figure 96. Plot of pseudo-first-order rate constants versus alcohol concentration for hydroalkoxylation of **4.1** with **4.2** (excess) by (IPr)AuOTf in toluene at 30 °C.

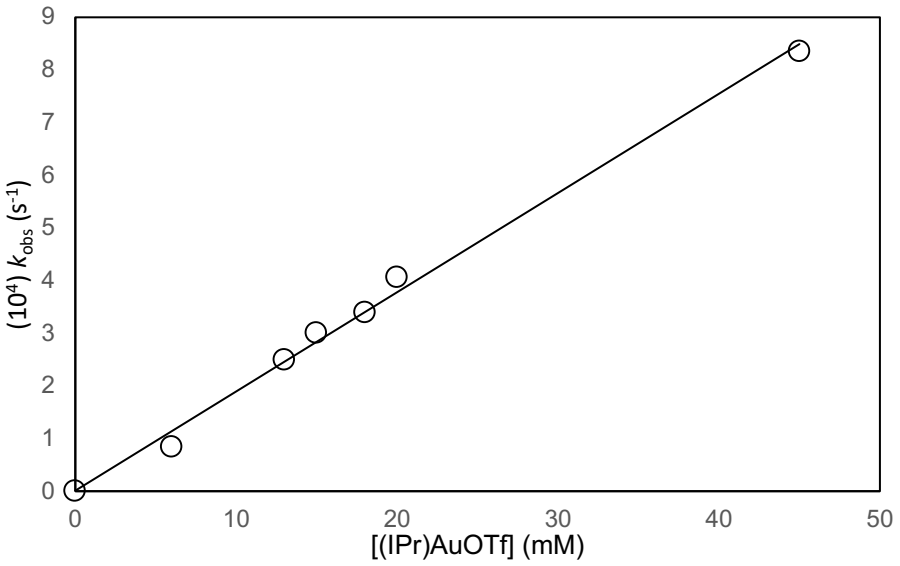

Figure 97. Plot of pseudo-first-order rate constants versus catalyst concentration for hydroalkoxylation of **4.1** with **4.2** (excess) by (IPr)AuOTf in toluene at 30 °C.

4.1.2.2 Spectroscopic Analysis of Reaction Mixtures

Beyond information gleaned from kinetic experiments, the *in situ* analysis of the reaction mixture allows for the observation of potential catalytic resting states for the gold(I)-catalyzed hydroalkoxylation of **4.1** with **4.2**. In order to allow for such observation, a spectroscopic handle was required. Unfortunately, the absence of a phosphine supporting ligand precluded analysis of the catalytic reaction by ^{31}P NMR spectroscopy and excessive broadening and low chemical shift dispersion made ^{1}H NMR spectroscopy also unsuitable. We therefore employed the gold complex (IPr-^{13}C)AuOTf, with the carbene carbon on the IPr ligand labeled with carbon-13, which

displays diagnostic carbene C1 resonances in the ^{13}C NMR for potential reaction intermediates. For examples, the carbene C1 resonance of (IPr-^{13}C)AuOTf appears at δ 163 in the ^{13}C NMR spectrum, compared to δ ~ 180 for gold π-allene complexes[242,244,281] and δ ~ 200 for neutral IPr gold σ-vinyl[282] and cationic IPr bis(gold) vinyl complexes.[283]

In one experiment, allene **4.1** was added incrementally (0.5, 1.0, 1.5, 2.0 M) to (IPr-^{13}C)AuOTf (30 mM) in toluene-d_8 at 30 °C and analyzed after each addition by ^{13}C NMR spectroscopy (Scheme 26). As the concentration of **4.1** increased, the carbene ^{13}C resonance of (IPr-^{13}C)AuOTf broadened and shifted slightly downfield, and when the concertation of **4.1** reached ~2 M, a broad resonance at δ ~ 180, assigned gold π-allene complex **4.5**-[^{13}C], was observed along with the resonance of (IPr-^{13}C)AuOTf at δ 165. Due to excessive broadening, we were unable to determine the relative concentrations needed to measure K_{eq} for allene binding. These observations, however, are consistent with (1) endergonic conversion of (IPr-^{13}C)AuOTf and **4.1** to **4.5**-[^{13}C] and (2) the formation of kinetically relevant concentrations of **4.5**-[^{13}C] in the presence of excess **4.1**. The resulting solution of (IPr-^{13}C)AuOTf (30 mM) and excess **4.1** (~ 2 M) was then treated with alcohol **4.2** (0.14 M) and monitored periodically by ^{13}C NMR spectroscopy at 30 °C. The broad resonance at δ 165 and 180 persisted through the conversion of **4.1** and **4.2** to **4.3** ($t_{1/2}$ = 20 min) without the appearance of any additional carbene resonances. These

observations established that (IPr-^{13}C)AuOTf and gold π-allene complex **4.5** are the predominant gold complexes present under catalytic conditions.

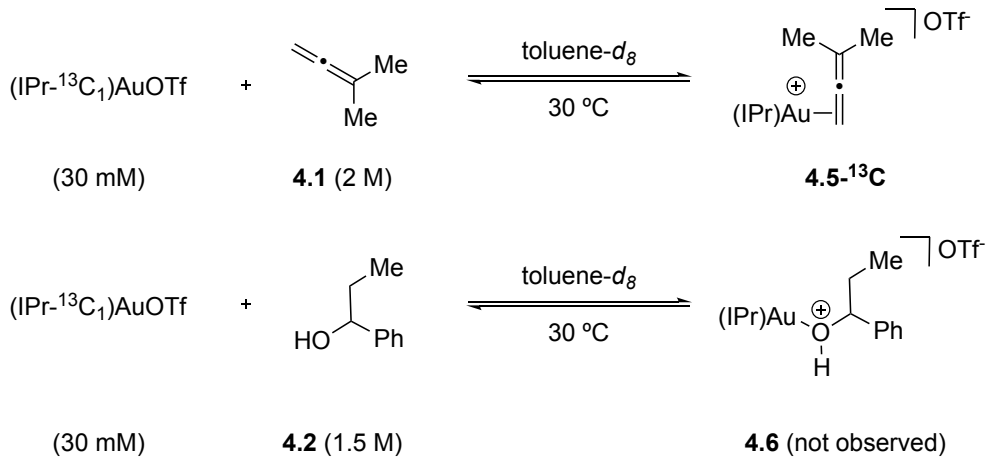

Scheme 26. Equilibria for binding of **4.1** (top) and **4.2** (bottom) to (IPr-^{13}C)AuOTf in toluene-d_8 at 30 °C.

In a second experiment, alcohol **4.2** was added incrementally to a toluene-d_8 solution of (IPr-^{13}C)AuOTf at 30 °C and analyzed after each addition by ^{13}C NMR spectroscopy (Scheme 26). No detectable change of the ^{13}C NMR resonances of (IPr-^{13}C)AuOTf (δ 163) was observed even at high excess of alcohol **4.2** (~ 1.5 M) and no additional carbene resonances were observed. These observations indicate that the equilibrium constant for the conversion of (IPr-^{13}C)AuOTf to gold alcohol complex **4.6** is small.[284] The resulting solution was then treated with allene **4.1** (0.14 M) and the solution was monitored by ^{13}C NMR spectroscopy at 30 °C. The sharp resonance of (IPr-^{13}C)AuOTf at δ 163 broadened slightly upon the addition of allene, but otherwise

remained unchanged throughout the conversion of **4.1** and **4.2** to **4.3** without the appearance of any additional carbene resonance, establishing (IPr-^{13}C)AuOTf as the predominant gold-containing species present during catalysis under conditions of excess alcohol.

4.1.2.3 Proposed Kinetic Model

Interpretation of the kinetics of the gold(I)-catalyzed hydroalkoxylation of **4.1** with **4.2** catalyzed by (IPr)AuOTf leads to the mechanism in Figure 98 involving a reversible reaction of **4.1** with (IPr)AuOTf to form gold π-allene complex **4.5**,[242,243] outer-sphere addition of alcohol **4.2** to **4.5** to form the O-protonated gold σ-vinyl intermediate **II**, followed by rapid protodeauration to form gold π-allylic ether complex **III** that collapses to release **4.3** and close the catalytic cycle. To derive the rate law for the reaction, three key assumptions were made: (1) protodeauration (**II** → **III**), and hence hydroalkoxylation, is irreversible, (2) IPrAuOTf and gold π-allene complex **4.5** are the only complexes that accumulate under catalytic conditions ($[Au]_{tot}$= [(IPr)AuOTf] + [**4.5**]), and (3) cationic π-complex **4.5** exists as the tight ion pair with OTf^- in the nonpolar reaction medium.

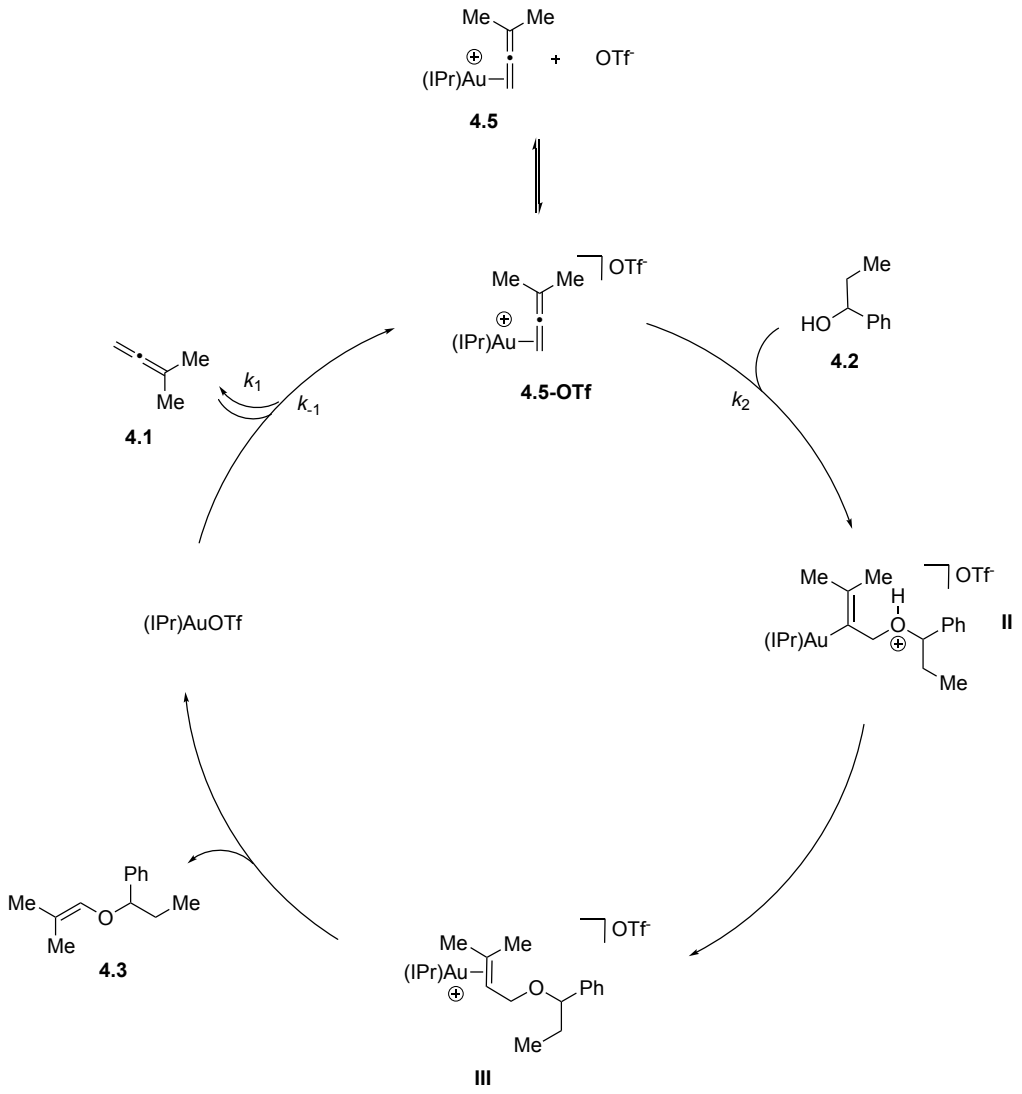

Figure 98. Proposed mechanism of gold(I)-catalyzed hydroalkoxylation of **4.1** with **4.2**

For the mechanism in Figure 98, kinetic scenarios involving turnover-limiting protodeauration or deprotonation of **II** can be discounted based on the absence of a large deuterium kinetic isotope effect (KIE) in experimental observations. Reversible C–

O bond formation followed by turnover-limiting protodeauration or deprotonation would likely display significant deuterium KIEs for deuterioalkoxylation and first order dependence on [**4.2**] under all conditions, neither of which was observed experimentally. Widenhoefer[258] and Lalic[215] have observed large KIEs ($k_H/k_D > 5$) for gold-catalyzed intramolecular hydroalkoxylation of allenes under conditions of turnover-limiting protodeauration. Similarly, mechanisms involving irreversible C–O bond formation followed by turnover-limiting protodeauration would also display significant deuterium KIEs for deuterioalkoxylation, as well as zero order dependence on both [**4.1**] and [**4.2**] under all conditions, and the accumulation of mono(gold) and bis(gold) vinyl complexes under catalytic conditions, none of which we observed experimentally.

The observed change in the kinetic order of the gold-catalyzed hydroalkoxylation of **4.1** with **4.2** as a function of the **4.1**:**4.2** ratio points to a change in the resting state catalyst composition and/or the turnover-limiting step of the catalytic cycle, which would require two or more microscopic steps within the catalytic cycle to occur at similar rates. Application of the pre-equilibrium assumption to the reversible formation of gold π-allene complex **4.5**, which is often assumed valid for gold-catalyzed hydrofunctionalization processes, appears overly restrictive. Rather, application of the Bodenstein (steady state) approximation to gold π-allene complex **4.5** with no additional restrictions generates the rate law given in rate equation 1.[285]

$$\text{rate} = \frac{k_1 k_2 [\mathbf{4.1}][\mathbf{4.2}][\text{Au}]_{\text{tot}}}{k_{-1} + k_1[\mathbf{4.1}] + k_2[\mathbf{4.2}]} \qquad \text{(eq 1)}$$

From rate equation 1, two rate limiting kinetic scenarios are based on the relationship between the rate of C–O bond formation (k_2[**4.2**]) and the rates of interconversion of (IPr)AuOTf and **4.5** (k_1[**4.1**] and k_{-1}). In the case where C–O bond formation is much slower than is the interconversions of (IPr)AuOTf and **4.5** (k_2[**4.2**] ≪ k_1[**4.1**] + k_{-1}), the rate law simplifies to rate equation 2, which predicts first-order rate dependence on [**4.2**] and $[\text{Au}]_{\text{tot}}$ and between zero- and first-order dependence on [**4.1**]. This rate equation matches the experimentally determined rate law for gold-catalyzed reaction of **4.1**and **4.2** under conditions of excess allene **4.1**. In the case where C–O bond formation is much faster than is the interconversions of (IPr)AuOTf and **4.5** (k_2[**4.2**] ≫ k_1[**4.1**] + k_{-1}), rate equation 1 simplifies to the second-order rate equation represented by rate equation 3, which predicts first-order dependence in both [**4.1**] and $[\text{Au}]_{\text{tot}}$ and zero-order dependence on [**4.2**]. This rate equation matches the experimentally determined rate law for gold-catalyzed reaction of **4.1** and **4.2** under conditions of excess alcohol **4.2** where rate = k'[**4.2**][(IPr)AuOTf], and where the macroscopic rate constant k' corresponds directly to microscopic rate constant k_1.

$$\text{rate} = \frac{k_1 k_2[\mathbf{4.1}][\mathbf{4.2}][\text{Au}]_{tot}}{k_{-1} + k_1[\mathbf{4.1}]} \text{ when } k_2 \ll k_{-1} + k_1[\mathbf{4.1}] \qquad \text{(eq 2)}$$

$$\text{rate} = k_1[\mathbf{4.2}][\text{Au}]_{tot} \text{ when } k_2 \gg k_{-1} + k_1[\mathbf{4.1}] \qquad \text{(eq 3)}$$

Rate equation 2, which describes rate behavior for the catalytic hydroalkoxylation reaction under conditions of excess allene, can be rewritten as rate equation 4. Taking the reciprocal of the equation describing k_{obs} gives rate equation 5, which predicts a linear relationship between $1/k_{obs}$ and 1/[**4.1**] under conditions of excess allene at constant catalyst concentration with slope = $k_{-1}/k_1k_2[\text{Au}]_{tot}$ and with intercept $1/k_2[\text{Au}]_{tot}$. Indeed, a plot of the reciprocal of the experimentally determined pseudo-first-order rate constants for the hydrokoxylation of **4.1** under conditions of excess allene at constant catalyst concentration ([cat.] = 16 mM) versus 1/[**4.1**] was linear with a slope = $1.15 \pm 0.05 \times 10^3$ M s and intercept = $3.9 \pm 0.4 \times 10^2$ s (Figure 99), from which the microscopic rate constant $k_2 = 0.17 \pm 0.02$ M^{-1} s^{-1} and equilibrium constant $k_1/k_{-1} = 0.34 \pm 0.02$ M^{-1} were derived. Using the value for k_i, which corresponds to the second-order rate constant for hydroalkoxylation under conditions of excess alcohol ($k' = k_1 = 1.88 \pm 0.01$ M^{-1} s^{-1}), the value for k_{-1} was derived ($k_{-1} = 5.6 \pm 0.5 \times 10^{-2}$ s^{-1}).

$$\text{rate} = k_{obs}[\mathbf{4.2}] \text{ when } k_{obs} = \frac{k_1 k_2[\mathbf{4.1}][\text{Au}]_{tot}}{k_{-1} + k_1[\mathbf{4.1}]} \qquad \text{(eq 4)}$$

$$\frac{1}{k_{obs}} = \frac{k_{-1}}{k_1 k_2 [\mathbf{4.1}][\mathrm{Au}]_{tot}} + \frac{1}{k_2 [\mathrm{Au}]_{tot}} \qquad \text{(eq 5)}$$

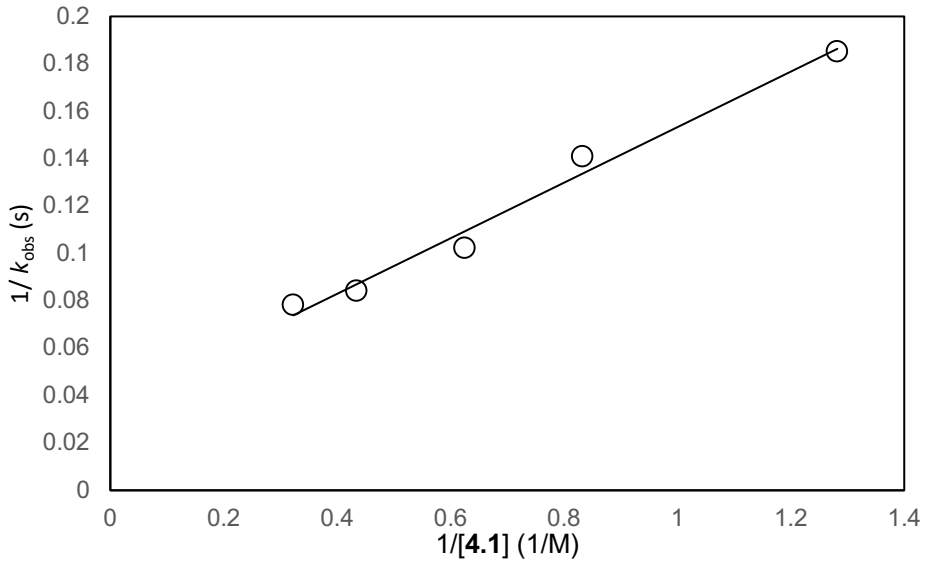

Figure 99. Plot of $1/k_{obs}$ versus 1/[**4.1**] for the hydroalkoxylation of **4.1** with **4.2** catalyzed by (IPr)AuOTf (15 mM) in toluene at 30 °C.

The equilibrium constant $K_1 = 0.34\ M^{-1}$ determined from this analysis predicts an equilibrium ratio of (IPr)AuOTf:**4.5** ≈ 1.5:1 at [**4.1**] = 2 M and $[Au]_{tot}$ = 30 mM according the relationship K_1 = [**4.5**]/[(IPr)AuOTf][**4.1**]. This value is consistent with our experimental observations, considering the low sensitivity of our ^{13}C NMR measurements. Less clear is that the values determined for the microscopic rate constant k_1, k_{-1}, and k_2 validate the limiting conditions (k_2[**4.2**] ≪ k_1[**4.1**] + k_{-1}) and (k_2[**4.2**] ≫ k_1[**4.1**] + k_{-1}), corresponding to the experimental conditions of excess allene and excess

alcohol, respectively. The calculated values for k_1[**4.1**]. k_{-1}, and k_2[**4.2**] under conditions of excess allene ([**4.1**] = 1.6 M, [**4.2**] = 0.16 M) are 0.034, 0.056 and 0.027 s^{-1}, respectively, and the calculated values for k_1[**4.1**]. k_{-1}, and k_2[**4.2**] under conditions of excess alcohol ([**4.1**] = 0.18 M, [**4.2**] = 1.8 M) are 0.0034, 0.056, and 0.31 s^{-1}, respectively. It should be noted, however, that the value for k_1 in this analysis was determined under conditions of excess alcohol, whereas the values for k_2 and k_1 were determined under condition of excess allene, under the assumption that the magnitude of these microscopic rate constants are invariant with the reaction conditions. One observation that suggests this may not be the case is the observed decrease in k_{obs}, where $k_{obs}/[Au]_{tot} = k_1$, with increasing [**4.2**] under conditions of excess alcohol (Figure 85), suggesting that the k_1 may be larger under conditions of excess allene, though it is unclear how this phenomenon may arise.

4.1.2.4 Role of Ion Pairing and Exogenous Triflate

The formation of ion pars between noncoordinating anions and cationic transition metals,[286,287] including cationic gold π complexes,[288-290] is well established, with association constants that typically exceed 1×10^4 in CH_2Cl_2.[291,292] Furthermore, because log K_A for ion pair association typically scales with the reciprocal of the dielectric constant of the medium (1/ε),[293] ion pairing of **4.5** with OTf^- is anticipated to be exceptionally strong in the nonpolar reaction medium employed in the catalytic hydroalkoxylation of **4.1** with **4.2** (ε(CH_2Cl_2) = 8.93; ε(toluene) = 2.38).[294,295] Importantly,

ligand substitution of cationic transition-metal complexes with strongly associated anionic ligands occurs through an interchange mechanism and displays a zero-order rate dependence on the concentration of the anionic ligand.[286,287,291,292,296-298] In the context of gold(I)-catalyzed allene hydroalkoxylation, the presence of strong ion paring between **4.5** and OTf^- is constant, with the absence of any significant curvature of the plot of k_{obs} versus [(IPr)AuOTf)] at constant, excess [**4.1**] (Figure 94). For example, under conditions of negligible ion pairing between **4.5** and OTf^- ($K_A[OTf^-] \ll 1$) rate equation 2 becomes rate equation 6, containing the term $k_{-1}K_A[OTf]$ in the denominator, assuming ligand exchange occurs via interchange through a tight ion pair. Because [OTf] would increase with the increasing $[Au]_{tot}$ under conditions of negligible ion pairing, the rate dependence on catalyst concentration under such conditions would approach half order, which was not observed (Figure 94).

$$\text{rate} = \frac{k_1 k_2[\mathbf{4.1}][\mathbf{4.2}][\text{Au}]_{\text{tot}}}{k_{-1}K_A[\text{OTf}] + k_1[\mathbf{4.1}]} \qquad \text{(eq 6)}$$

Under conditions of strong ion paring between **4.5** and OTf, the observed inhibition of the rate of hydroalkoxylation by tetrabutylammonium triflate (Figure 95) points to the presence of an additional triflate-dependent pathway for the reversion of **4.5** to (IPr)AuOTf. Relaxing the condition of strong ion pairing between **4.5** and OTf ($K_A[OTf^-] \gg 1$) does not account for the observed rate dependence on both catalyst and tetrabutylammonium triflate concentration, particularly in the case of a modest

association constant for ion pairing between **4.5** and OTf. In this case, the rate dependence on triflate concentration would be most pronounced at the lowest triflate concentration, such as in the determination of the rate dependence on (IPr)AuOTf concentration, however, no deviation for linearity was observed for a plot of k_{obs} versus [(IPr)AuOTf] from 0–30 mM (Figure 94). Also, owing to the strong ion pairing between tetrabutylammonium and triflate in nonpolar reaction medium[299,300] and the higher concentrations of triflate employed in these experiments relative to catalytic conditions (16–77 mM versus ≤ 30 mM, respectively), it is unlikely that this triflate-dependent pathway is relevant under conditions of catalytic hydroalkoxylation.

4.2.3 Summary

In summary, this section reports an investigation of the kinetics and mechanism of the intramolecular hydroalkoxylation of 3-methyl-1,2-butadiene (**4.1**) with 1-phenylpropan-1-ol (**4.2**) catalyzed by (IPr)AuOTf in toluene. All of our data are consistent with the mechanism depicted in Figure 87 involving endergonic formation of the cationic gold π-allene complex **4.5**, which exists as the tight ion pair **4.5**·OTf in the nonpolar reaction medium. Outer-sphere addition of **4.2** to **4.5**·OTf followed by rapid protodemetalation and collapse of the resulting gold π-allene complex **III** releases the primary allylic ether **4.3** as the kinetic product and regenerates (IPr)AuOTf. The microscopic rate constants for the conversion of (IPr)AuOTf and **4.1** to **4.5**·OTf (k_1[**4.1**]),

the collapse of **4.5**·OTf to (IPr)AuOTf and **4.1** (k_{-1}), and the rate of attack of **4.2** on **4.5**·OTf (k_2[**4.2**]) are similar enough such that (1) application of the pre-equilibrium assumption to the formation of **4.5**·OTf is not valid and (2) the rate behavior of catalytic hydroalkoxylation changes as a function of the relative and absolute concentrations of **4.1** and **4.2**. Under conditions of excess allene **4.1**, the reaction rate displayed first-order dependence on [(IPr)AuOTf] and [**4.2**] and between zero- and first-order dependence on [**4.1**], while under conditions of excess alcohol **4.2**, the reaction rate displayed first-order dependence on [(IPr)AuOTf] and [**4.1**] and zero-order dependence on [**4.2**].

There has been considerable speculation and debate concerning the role of the counterion in gold(I)-catalyzed hydrofunctionalization reactions, in particular whether the outer-sphere C–X (X = N, O) bond formation is assisted by hydrogen bonding between the incoming nucleophile and the counterion.[301-303] Indeed, we have obtained evidence for counterion-assisted C–O bond formation in our investigation of gold-catalyzed intramolecular allene hydroalkoxylation.[304] The present investigation of the mechanism of the gold(I)-catalyzed hydroalkoxylation of **4.1** with **4.2** provides little additional insight in this regard. However, our data do show that potential triflate/alcohol hydrogen bonding cannot lead to significant O–H bond cleavage in the transition state for C–O bond formation, which would have been revealed by the

presence of a KIE for the deuterioalkoxylation of **4.1** with **4.2**-*O*-*d*, which was not observed.

In comparison to counterion effects, there has been much less discussion regarding the effect of reaction medium on the kinetic behavior and mechanism of gold(I)-catalyzed hydrofunctionalization, and the present investigation points to the potential importance of such medium effects. In particular, the kinetics of catalytic hydroalkoxylation of **4.1** in toluene are dominated by the slow and endergonic conversion of (IPr)AuOTf to gold π-allene complex **4.5**·OTf, which was corroborated by in situ ^{13}C NMR analysis of the reaction of **4.1** with (IPr*)AuOTf. This behavior stands in sharp contrast to the reaction of **4.1** with (IPr)AuOTf in CD_2Cl_2, which forms **4.5** quantitatively with <2 equiv of allene.[242,243] Therefore, it is quite reasonable to assume that very different kinetic behavior of the gold-catalyzed hydroalkoxylation of **4.1** with **4.2** would be observed in more polar solvents, although predictions beyond this point are unwarranted owing to the absence of information regarding medium effects on the rate of C–O bond formation and/or on the equilibrium constants for the potentially competing formation of gold–nucleophile complexes.

4.3 Gold(I)-catalyzed Intermolecular Hydroamination of Allenes with Aromatic Amines

4.3.1 Background

In addition to the gold(I)-catalyzed hydroalkoxylation of **4.1** with **4.2**, we were also interested in studying the kinetics of the gold(I)-catalyzed hydroamination of **4.1** with *N*-methylaniline (**4.7**) (Scheme 27). The relative nucleophilicity of **4.7** compared to **4.2** likely renders the mechanism of gold(I)-catalyzed hydroamination distinct from gold(I)-catalyzed hydrofunctionalization with poorer, less coordinating nucleophiles. Previous work by members of our group has established some key pieces of mechanistic information, which will be further expanded though *in situ* analysis of the reaction mixtures.

In a previous experiment, a solution of **4.1** (1.7 M), (IPr)AuOTf (8.4 mM) and **4.7** (0.17 M) in dioxane at 40 °C was monitored periodically by HPLC (Scheme 4.4). Monitoring the formation of hydroamination product **4.8** showed a zero-order dependence of on the concentration of **4.7**, with a plot of the [**4.7**] versus time being linear with a pseudo-zero-order rate constant of $1.66 \pm 0.06 \times 10^{-5}$ M s^{-1} (Table 23, entry 1).

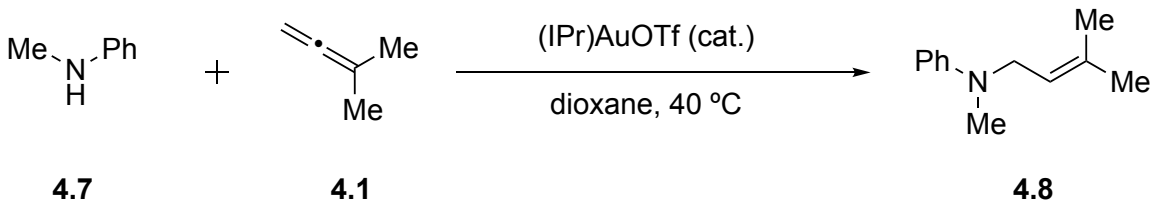

4.7 **4.1** **4.8**

Scheme 27. Gold(I)-catalyzed hydroamination of **4.1** with **4.7** to form **4.8** catalyzed by (IPr)AuOTf.

Table 23. Pseudo-zero-order rate constants for the hydramination of **4.1** with **4.7** catalyzed by (IPr)AuOTf in dioxane at 40 °C.

entry	[**4.1**] (M)	[(IPr)AuOTf] (mM)	(10^5) k_{obs} ($M\ s^{-1}$)
1	1.7	8.4	1.66 ± 0.06
2	1.7	4.3	0.87 ± 0.02
3	1.7	16	3.7 ± 0.3
4	0.83	8.3	1.26 ± 0.05
5	3.3	8.1	3.7 ± 0.1
6	5	8.1	5.3 ± 0.1
7[a]	1.7	8.3	1.66 ± 0.05

[a] *N*-methylaniline-*N*-d_1 (**4.7**-d_1) was used in this reaction.

To established the dependence of the rate of hydroamination on both catalyst concentration and allene concentration a series of experiments were performed at varied catalyst and allene concentration (Table 23, entries 2–6). A plot of k_{obs} versus [(IPr)AuOTf] was linear, establishing a first-order dependence of the rate of gold(I)-catalyzed hydroamination **4.1** with **4.7** on catalyst concentrations (Figure 100). A plot of k_{obs} versus [**4.1**] was linear, which established first-order dependence on the rate of the gold(I)

catalyzed hydroamination of **4.1** with **4.7** on [**4.1**] (Figure 101). With this information in hand, we sought to perform stoichiometric experiments of the gold(I)-catalyzed hydroamination of **4.1** with **4.7** to gain further insight into the mechanism.

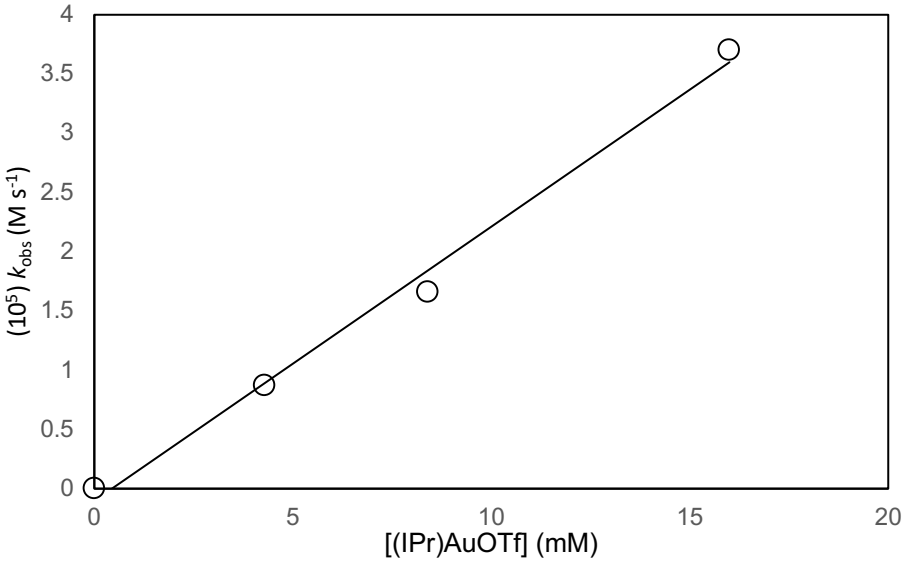

Figure 100. Catalyst concentration dependence of the rate of gold(I)-catalyzed hydroamination of **4.1** with **4.7**.

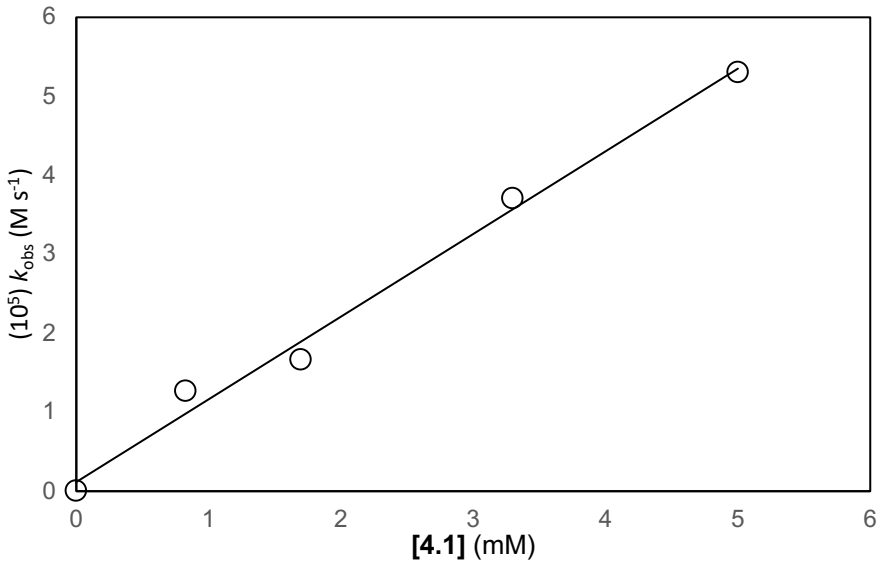

Figure 101. Allene concentration dependence of the rate of gold(I)-catalyzed hydroamination of **4.1** with **4.7**.

4.3.2 Results and Discussion

4.3.2.1 Spectroscopic analysis of reaction mixtures

In an initial experiment, **4.7** (33 mM) was added to a solution of (IPr)AuOTf-[^{13}C] (33 mM; δ 162.8) in dioxane-d_8 at 25 °C which led to quantitative conversion to a new ^{13}C NMR resonance at δ 170.5 which was assigned as *N*-bound gold(I) *N*-methylaniline complex **4.9** (Scheme 28). Treatment of the resulting solution with excess **4.1** led to the formation of a new ^{13}C NMR resonance at δ 187.2 after 120 min as the major gold(I) species. Analysis of the ^{1}H NMR spectrum revealed the formation of two new doublets

at δ 5.07 and 4.32 assigned bis(gold) σ-vinyl complex **4.10**. Upon treatment with an additional equivalent of *N*-methylaniline, the ^{13}C NMR resonance at δ 187.2 disappeared to form *N*-bound gold(I) *N*-methylaniline complex **4.9** and allylic amine product.

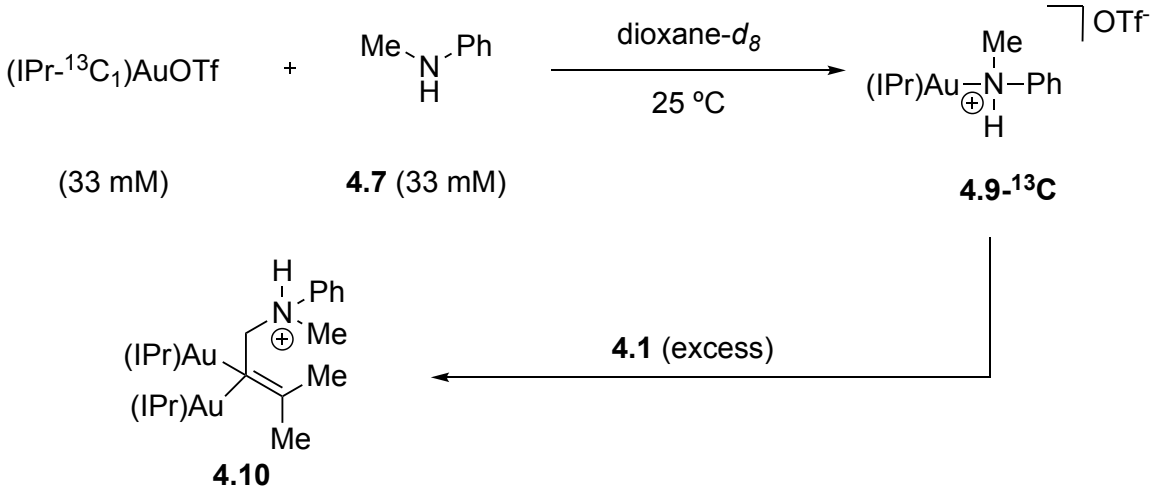

Scheme 28. Generation of **4.9-^{13}C** and **4.10-^{13}C** in dioxane-d_8.

In a similar experiment, **4.1** (33 mM) was added to a solution of (IPr)AuOTf-[^{13}C] (33 mM) in dioxane-d_8 at 25 °C, with no detection of bound allene complex **4.5**. Then, the concentration of **4.1** was incrementally increased (33 – 1200 mM), until the ^{13}C NMR resonance at δ 162.8 has disappeared and was replaced by a new ^{13}C NMR resonance at δ 185.2, corresponding to gold π-allene complex **4.5**. Upon the addition of **4.7** (33 mM), the ^{13}C NMR resonance for gold π-allene complex **4.5** was quantitatively converted to bound gold(I) *N*-methylaniline complex **4.9**, with the formation of **4.8** observed by ^{1}H NMR.

Until ~95% conversion, the ^{13}C NMR resonance for gold(I) *N*-methylaniline complex **4.9** persisted, until eventually forming a 1:1.4:1.3 mixture of ^{13}C NMR resonances corresponding to gold π-allene complex **4.5** (δ 185.2), bis(gold) vinyl complex **4.10** (δ 187.2) and *N*-bound product gold(I) complex **4.11** (δ 167.2).

The assignment of *N*-bound product gold(I) complex **4.11** was confirmed in a separate experiment where **4.8** was mixed (IPr)AuOTf in dioxane-d_8 to give one ^{13}C NMR resonance at δ 167.2. Treatment of this solution with *N*-bound product gold(I) complex **4.11** (1 equivalent), led to the formation of *N*-bound gold(I) *N*-methylaniline complex **4.9**. Analysis of the ^{1}H NMR spectrum allowed for the determination of the K_{eq} for the ligand exchange (K_{eq} = 142.7).

In addition to the stoichiometric experiments described above, the catalytic gold(I)-catalyzed hydroamination of **4.1** was also analyzed by NMR spectroscopy. Periodic ^{1}H and ^{13}C NMR analysis of a solution containing **4.1** (1.2 M), **4.7** (170 mM) and (IPr)AuOTf (35 mM) revealed *N*-bound gold(I) *N*-methylaniline complex **4.9** as the resting state for the gold(I)-catalyzed hydroamination of **4.1** with **4.7**. At ~75% conversion, the ^{13}C NMR resonance for gold σ-vinyl complex **4.10** began to appear and persisted until the end of the reaction.

4.3.2.2. Proposed Kinetic Model

Combining the results from catalytic and stoichiometric studies on the gold(I)-catalyzed hydroamination of **4.1** with **4.7**, a picture of the mechanism for the transformation begins to emerge (Figure 102). *N*-bound gold(I) *N*-methylaniline complex **4.9** is initially formed *in situ* from reaction of (IPr)AuOTf and *N*-methylaniline in solution, and is the active catalyst for the gold(I)-catalyzed hydroamination of **4.1** with **4.7**. Upon ligand exchanged with **4.1**, gold(I) π-allene complex **4.5** is formed. Outer-sphere nucleophilic attack on π-allene complex **4.5** with *N*-methylaniline generates gold(I) σ-vinyl intermediate **IV**. Protodeauration affords allylic amine **4.8** and the active gold(I) catalyst, *N*-bound gold(I) *N*-methylaniline complex **4.9**.

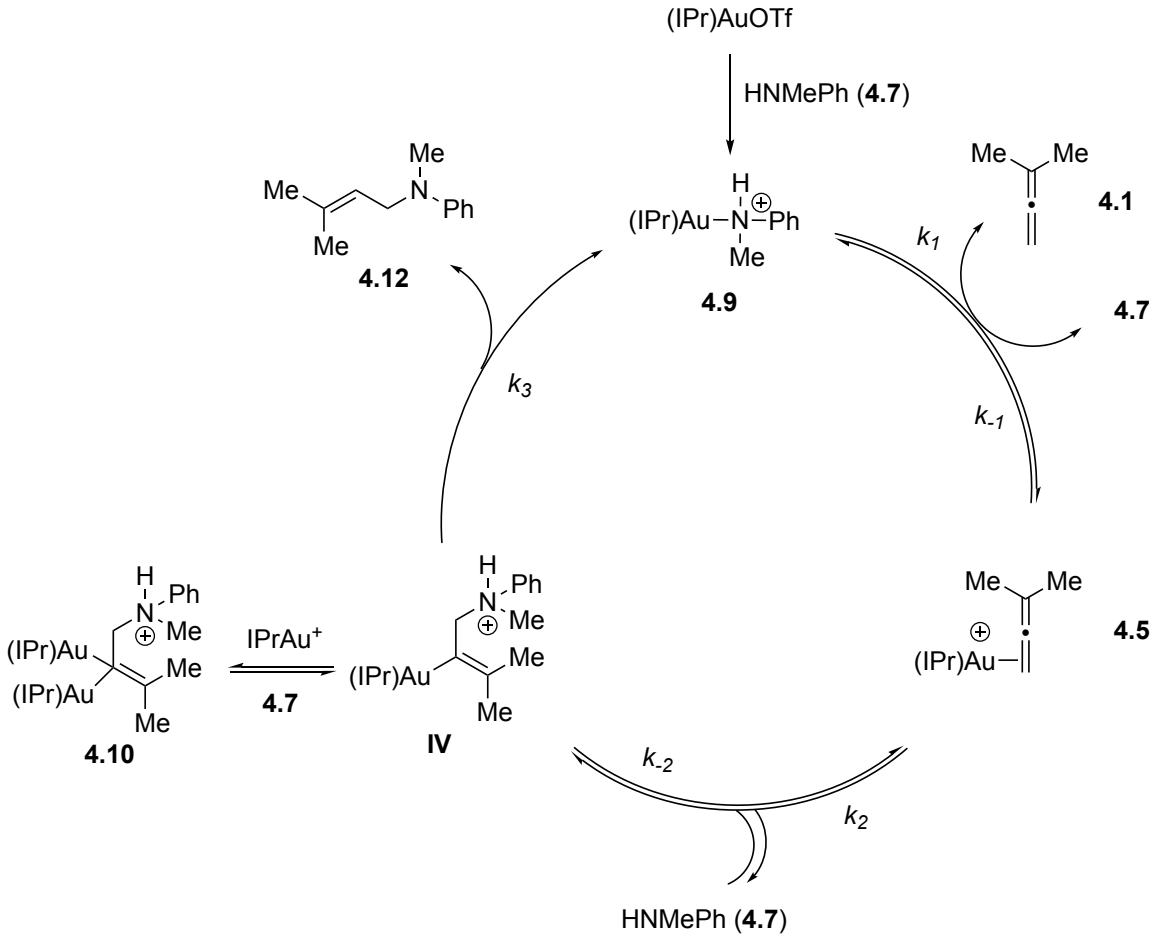

Figure 102. Proposed mechanism for the gold(I)-catalyzed hydroamination of **4.1** with **4.7**. (OTf^- counterions removed for clarity.)

Spectroscopic analysis of the gold(I)-catalyzed hydroamination of **4.1** with **4.7** under catalytic conditions revealed *N*-bound gold(I) *N*-methylaniline complex **4.9** as the resting state in the catalytic cycle. Under both catalytic and stoichiometric conditions, the concentration of bis(gold) vinyl complex **4.10** increased as the reaction progressed, and does not turn over to product in the absence of additional **4.7**, suggesting that

bis(gold) vinyl complex **4.10** forms when there is no more suitable ligand for the (IPr)Au⁻ fragment. Upon introduction of more ligand into the reaction mixture, protodeauration can then occur. This is consistent with our observation that, under stoichiometric conditions, and upon the addition of **4.7**, bis(gold) vinyl complex **4.10** is converted quantitatively to *N*-bound gold(I) *N*-methylaniline complex **4.9** and allylic amine **4.8**.

To derive a rate law for the proposed mechanism two key assumptions are made: (1) protodemetallation, and hence hydroamination, is irreversible and (2) C–N bond formation is rapid and reversible. With these assumptions in place, rate equation 7 can be derived for the mechanism proposed in Figure 102. If $k_1 \ll k_{-1}$, then rate equation 7 can be simplified to rate equation 8, which is consistent with our experimental observation that even in the presence of a large excess (>30 equiv.) of allene **4.1**, *N*-bound gold(I) *N*-methylaniline complex **4.9** persists as the only labeled gold(I) complex in solution based on ^{13}C NMR analysis. Rate equation 8 predicts first-order dependence on the rate for both **4.1** and catalyst concentration and a zero-order dependence on the rate for *N*-methylaniline concentration, which is in accord with experimental observations from previous kinetic analysis of the gold(I)-catalyzed hydroamination of **4.1** with **4.7**.

$$\text{rate} = \frac{k_1 k_2 k_3 [\mathbf{4.1}][\mathbf{4.7}][\text{Au}]_{\text{tot}}}{k_{-1} k_{-2} [\mathbf{4.7}] + k_1 k_{-2} [\mathbf{4.1}]} \qquad \text{(eq 7)}$$

$$\text{rate} = \frac{k_1 k_2 k_3}{k_{-1} k_{-2}}[\mathbf{4.1}][\text{Au}]_{\text{tot}} = k_{\text{obs}}[\mathbf{4.1}][\text{Au}]_{\text{tot}}\text{ , if } k_1 \ll k_{-1} \qquad \text{(eq 8)}$$

4.3.3 Summary

In summary, we report a kinetic and mechanistic analysis of the gold(I)-catalyzed hydroamination of **4.1** with **4.7** catalyzed by (IPr)AuOTf in dioxane. Our kinetic data and the results of spectroscopic analysis of reaction mixtures are consistent with the mechanism depicted in Figure 91. The active catalyst is *N*-bound gold(I) *N*-methylaniline complex **4.9** which undergoes ligand exchange with **4.1** to form gold(I) π-allene complex **4.5.** This intermediate is trapped by outer-sphere nucleophilic addition of **4.7** forming intermediate **IV**, which then undergoes irreversible protodeauration to give primary allylic amine **4.8** as the major product. At low nucleophile concentrations, bis(gold) vinyl complex **4.10** forms in high concentrations and is unable to undergo protodeuaration. Treatment of a solution of bis(gold) vinyl complex **4.10** with **4.7** converts to allylic amine **4.8** and -bound gold(I) *N*-methylaniline complex **4.9**.

4.4 Experimental Details

4.3.1 General Methods

Reactions were performed under an atmosphere of nitrogen in flame- or oven-dried glassware utilizing standard dry box and/or Schlenk line techniques unless specified otherwise. NMR spectra were obtained on Varian spectrometers operating at 400 MHz for ^{1}H NMR and 101 MHz for $^{13}C\{^{1}H\}$ NMR, in $CDCl_3$ unless otherwise noted. GC traces were obtained using an Hewlett Packard 5890 Series II Gas Chromatograph equipped with a Agilent Technologies 25 m Å~ 0.2 mm polydimethylsiloxane column and an FID detector. All solvents and reagents were used as received unless otherwise noted. IPrAuOTf was synthesized using published procedures. Errors reported for rate constants represent one standard deviation of the linear regression and do not reflect systematic errors.

4.3.2 Synthesis of Isotopically Labelled Compounds

(IPr-^{13}C)AuOTf. A solution of chlorotrimethylsilane (700 μL, 5.5 mmol) in ethyl acetate (2 mL) was added dropwise to a stirred solution of *N,N'*-bis(2,6-diisopropylphenyl)etheylenediimine (1.9 g, 5.0 mmol) and paraformaldehyde-^{13}C (150 mg, 5.0 mmol) in ethyl acetate (40 mL) at 70 °C. The resulting suspension was stirred at 70 °C for 2 h, cooled to room temperatures, and then maintained at 4 °C overnight. The resulting precipitate was collected, washed with ethyl acetate (2 x 20 mL) and diethyl

ether (2 x 20 mL), and dried under vacuum to give IPr-^{13}C•HCl (1.42 g, 67%) as a white solid. Dichloromethane (15 mL) was added to a mixture of IPr-^{13}C•HCl (265 mg, 0.62 mmol) and (tht)AuCl (200 mg, 0.62 mmol) and the resulting mixture was stirred at 4 °C for 30 min, treated with finely ground K_2CO_3 (1.2 g, 8.7 mmol), and stirred overnight at 4 °C. The reaction mixture was filtered through Celite and the solvent was evaporated under vacuum. The resulting residue was dissolved in minimal CH_2Cl_2 and precipitated with diethyl ether to give (IPr-^{13}C)AuCl (160 mg, 35%) as a white solid. Dichloromethane (5 mL) was added to a mixture of (IPr-^{13}C)AuCl (100 mg, 0.16 mmol) and AgOTf (50 mg, 0.19 mmol) and the resulting suspension was stirred for 45 min, filtered through Celite, and concentrated under vacuum to give (IPr-^{13}C)AuOTf (94 mg, 80%) as a white solid.

For IPr-^{13}C•HCl: $^{13}C\{^1H\}$ NMR ($CDCl_3$, labeled carbon only): δ 138.6.

For (IPr-^{13}C)AuCl: $^{13}C\{^1H\}$ NMR ($CDCl_3$, labeled carbon only): δ 175.5.

For (IPr-^{13}C)AuOTf: $^{13}C\{^1H\}$ NMR ($CDCl_3$, labeled carbon only): δ 162.2.

1-Phenyl-1-propanol-O-*d* (4.2-*O*-*d*). 1-Phenyl-1-propanol (700 μL, 5.1 mmol) was refluxed in MeOD (5 mL) overnight and then concentrated under vacuum. This process was repeated three times to give **4.2**-O-*d* with ~90% deuterium incorporation as determined by ^{1}H NMR analysis.

4.3.3 Kinetic Experiments

Kinetic analysis of the reaction of 4.1 with 4.2 (excess 4.1). A microwave tube containing IPrAuOTf (14 mg, 1.9×10^{-2} mmol), tetradecane (10.2 μL), 3-methyl-1,2-butadiene (1, 139 mg, 2.0 mmol), and toluene (1.0 mL; total volume = 1.25 mL) was placed in a thermostatted oil bath at 30 ±1 °C for 5 min. 1-Phenylpropan-1-ol (2, 28 mg, 0.20 mmol) was added to the solution via syringe and reaction progress was analyzed as a function of time. To this end, 15-30 μL aliquots were removed periodically via syringe, filtered through a silica gel plug, and analyzed by GC. The concentration of **4.2** was determined by integrating the peak for **4.2** relative to that for tetradecane in the GC spectrum. A plot of ln[**4.2**] versus time was linear through >3 half-lives with a pseudo first-order rate constant of $k_{obs} = 9.8 \pm 0.4 \times 10^{-4}$ s^{-1} (Table 19, entry 1). Pseudo first-order rate constants for the disappearance of **4.2** were likewise determined for the hydroalkoxylation of **4.1** with **4.2** as a function of [(IPr)AuOTf], [**4.1**], [(*n*-Bu)$_4$N][OTf], [HOTf], and [**4.3**] and for the deuterioalkoxylation of **4.1** with **4.2**-O-*d* employing analogous procedures (Table 19, entries 2–13).

Kinetic analysis of the reaction of 4.1 with 4.2 (excess 4.2). Toluene-d_8 (480 μL) was added to an NMR tube containing (IPr)AuOTf (7.4 mg, 1.0×10^{-2} mmol), 1-phenylpropan-1-ol (70 μL, 69 mg, 0.50 mmol), and $CHCl_3$ (6 μL, internal standard) to achieve a total volume of 0.56 mL. The tube was capped with a rubber septum, placed in

probe of an NMR spectrometer preheated at 30 °C and allowed to thermally equilibrate (~5 min). The tube was removed from the spectrometer, 3-methyl-1,2-butadiene (10 μL, 6.9 mg, 0.10 mmol) was added via syringe, the tube was placed back in the spectrometer, and reaction progress was monitored by 1H NMR spectroscopy at 103 s intervals. The concentration of **4.1** was determined by integrating the vinylic resonance of **4.1** (δ 4.13) relative to the resonance for $CHCl_3$ (δ 6.16). A plot of ln[**4.1**] versus time was linear to >3 half-lives with a pseudo first-order rate constant of $k_{obs} = 3.39 \pm 0.01 \times 10^{-4}$ s^{-1} (Table 20, entry 1). Pseudo first-order rate constants were likewise determined as a function of [**4.2**] and (IPr)AuOTf for the hydroalkoxylation of **4.1** with **4.2** and for the deuterioalkoxylation of **4.1** with **4.2**-O-*d* employing analogous procedures (Table 20, entries 2–9).

5. Conclusion

Cationic gold(I) complexes have been recognized as efficient catalysts for a wide array of transformations, including carbene transfers to form cyclopropanes and hydrofunctionalization reactions. Experimental studies of the mechanism for these transformations have been less studied. From the outset, the goal of this research has been to expand our current knowledge of the mechanisms of these transformations. This dissertation reports kinetic and mechanistic studies of two classes of gold(I)-catalyzed reactions as well as the synthesis of cationic gold(I) carbene complexes used to interrogate the ligand donor ability of different (L)Au fragments, which have been shown to affect reactivity of cationic gold(I) complexes.

A series of gold(I) benzylide complexes were synthesized by nucleophilic substitution of α-chloro gold(I) carbenoid complexes with sulfides. These complexes reacted efficiently with alkenes and dimethylsulfoxide to form cyclopropanes and benzaldehyde, respectively. Kinetic analysis of these reactions is consistent with the intermediacy of cationic gold(I) benzylidene complexes. Further mechanistic analysis revealed that alkene stereochemistry is preserved during cyclopropanation and a Hammett analysis of the reaction suggest a concerted mechanism for cyclopropanation.

To evaluate the electron donor ability of (L)Au fragments in cationic gold(I) carbene complexes, a series of cationic gold (β,β-disilyl)vinylidene complexes and

cationic gold (fluorophenyl)methoxycarbene complexes were synthesized. ^{29}Si and ^{19}F NMR analysis of these complexes compared to organic model compounds revealed that (L)Au fragments are significantly more inductively donating and comparable π-donors to *p*-substituted aryl groups. A comparison of various ligands showed that (P(*t*-Bu)$_2$-*o*-biphenyl)Au fragments are nominally stronger electron donors than (IPr)Au fragments, both of which are significantly more electron donating that (PPh$_3$)Au and [P(OMe)$_3$]Au fragments.

Kinetic and mechanistic analysis of the gold(I)-catalyzed hydrofunctionalization of 3-methyl-1,2-butadiene with alcohols and anilines was performed. Experimental data suggest a mechanism for the gold(I)-catalyzed hydroalkoxylation involving endergonic allene displacement of triflate, followed by an outer-sphere attack of alcohol on gold(I)-π-allene complex, followed by rapid protodeauration. In contrast, for the gold(I)-catalyzed hydroamination, the active catalyst is the gold(I) bound nucleophile complex and buildup a bis(gold) vinyl complex suggests a slow protodeauration.

As a whole, this work represents a small step forward in gaining a more complete understanding of the mechanisms of various gold(I)-catalyzed transformations. One key contribution is the establishment of a model system with which to study gold(I) carbene transfer reactions, which merit further study. We have also established a key relationship between (L)Au fragment donor ability. Combined,

this work provides a framework with which to experimentally probe and evaluate proposed mechanisms of gold(I)0catalzyed reactions.

Appendix A. A Single Reaction Thread Ties Together Core Concepts in a General Chemistry Course

Portions of this chapter have been published: M. H. Barbee[†]; R. G. Carden[†]; J. H. R. Johnson; C. L. Brown; D. A. Canelas; S. L. Craig**.** *J. Chem. Educ.* **2018**, *95*, 939–946. This work is co-authored by M. H. Barbee, who is co-first author, and J. H. R. Johnson, C. L. Brown, D. A. Canelas, and S. L. Craig and is adapted from a publication in the *J. Chem. Educ.*

A-1 Introduction

Recent revisions to the guidelines from the American Chemical Society Committee on Professional Training (ACS-CPT) have sparked interest in innovative approaches to the structure of foundation-level chemistry courses.[305,306] In particular, calls have been made to rethink chemical education in the context of an increasingly interdisciplinary world.[305,306] Additionally, specific recommendations have recently been made to include polymer chemistry content in the introductory sequence,[307,308] as the field is often overlooked or underrepresented in undergraduate general chemistry, despite the fact that roughly 50% of all chemists work with polymers at some point in their careers.[309] Some have called for a complete redesign of the chemistry curriculum in an attempt to integrate the traditional domains of chemistry, effectively eliminating courses in discrete disciplines and replacing them with basic, intermediate, or advanced chemistry.[310] Courses in synthesis, analysis, or theory development have been proposed

to better prepare students for future careers;[311] however, because many departments might be reluctant to restructure the chemistry curriculum, others suggest modifying traditional courses so that they are more integrated.[312,313] Historically, a standard general chemistry course attempts to introduce students to this integrated network of chemical sciences by discussing seemingly disconnected topics such as chemical equilibria, molecular-orbital theory, and the thermodynamics associated with work throughout a semester. Here, we describe efforts to improve our general chemistry course by framing the content of multiple units and a laboratory around a single reaction from organic chemistry. The structure of this series of exercises takes advantage of the associative learning principle[7] to draw connections between diverse topics in general chemistry (molecular orbital theory, quantum mechanics, equilibrium, hydrogen bonding, mechanical work and polymer chemistry).

Our choice of organic chemical reaction is the interconversion of spiropyran (SP) to the highly colored and fluorescent merocyanine (MC), a reaction that occurs in response to changes in solvent or various thermal, photochemical, or mechanochemical stimuli (Figure 103).[314-316] The chromic nature of this reaction provides an extremely versatile framework through which to integrate and move between a wide array of topics typically covered in a general chemistry course. Many colleges in the United States have transitioned to a 1-2-1 introductory course sequence,[317] with a single, college-

level general chemistry course, then two organic chemistry courses, then a second general chemistry course. Due to this change in structure, the choice to employ an organic molecule to illustrate concepts in the context of a general chemistry setting provides learners with an opportunity to become familiar with working with carbon-based molecular structure and properties before transitioning into an organic chemistry classroom. The SP-to-MC conversion also involves a substantial change in molecular shape, providing an accessible and valuable entry point into the practice of molecular visualization—a common barrier for success in organic chemistry.[318,319] Furthermore, because SP has been developed by Moore, Sottos, and White as a signature mechanophore (mechanically active functional unit)[315] in the nascent field of polymer mechanochemistry,[320,321] it functions as a bridge between the concepts of classical thermodynamics/chemical kinetics and polymer chemistry by demonstrating the direct coupling of mechanical work and chemical potential. Ongoing research with SP in the Craig Lab[316,322] inspired the development of this exercise as a way to gently encourage first year undergraduate knowledge of and curiosity about local research opportunities. Finally, the use of a reaction that has a visible output allows facile integration into the complementary laboratory portion of the course; this has been shown to increase student investment and understanding of the material.[323] We have implemented the sequence of activities described here in the context of a team-based learning (TBL)

classroom, but it is similarly well suited to a traditional lecture and/or hybrid classroom models. To test the efficacy of these newly developed spiropyran-based applications, we assessed student demonstration of mastery of the course learning objectives that are central to these applications in comparison to a control group who performed more traditional applications centered on the same learning objectives.

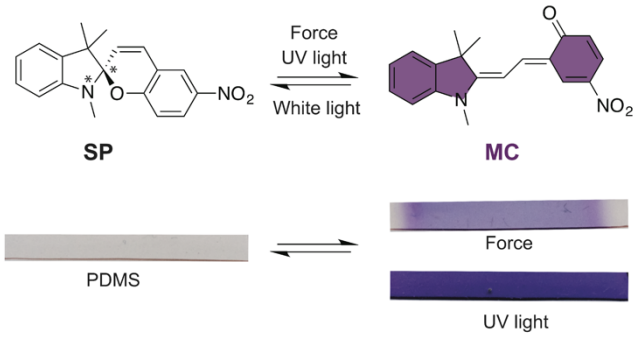

Figure 103. Spiropyran (SP) undergoes a ring-opening reaction to give the highly colored and fluorescent merocyanine (MC) in response to stimuli.

Herein we (1) report information about the course structure through which these spiropyran-applications were first implemented, (2) describe the spiropyran-based classroom module and lab, and (3) present experimental results from a classroom-based study that compared the SP-based approach to a different, more-traditional inorganic approach to obtaining the same general desired learning outcomes.

A-2 Course Structure

The course for which this material was initially designed was taught in an interactive, cooperative classroom structure. Each year this class is composed of 100-120 students, the vast majority (>98%) of whom are first-semester undergraduates. At our university, first year students place into their initial chemistry course based upon a combination of high school chemistry experience, math SAT scores, and chemistry AP scores. There are 4 different classes that students can place into:[324] an introductory class which assumes no prior background in chemistry,[325] the first semester of a traditional 2-semester general chemistry sequence, an organic chemistry class (AP score of 5, or equivalent, is required for this initial placement), and the course described here. This course is called "Honors Chemistry," and it is a one-semester version of general chemistry for students who have completed AP chemistry and scored either a 4 or 5 on the AP exam. We employ a team-based learning (TBL)[326] classroom model, in which the students work together in teams of 4-6 members for the entire semester. In line with previous studies,[326] we have found that keeping teams intact throughout the semester increases the students' trust in each other and allows for the development of a positive group dynamic.

Class periods are twice per week for one hour and fifteen minutes. Digital course materials, organized in terms of the learning objectives for each unit and accompanied

by self-assessment exercises, are provided at the start of the semester via an online course management site; there is no required textbook for the course. All students also participate in an accompanying laboratory section that meets once per week for three hours; the laboratory score is incorporated as part of the overall score used to determine course letter grades. In addition, an optional class meeting period is available each week prior to the start of each unit and again midway through the longer units. At this optional "discussion" meeting (formerly called recitation), questions regarding the core learning objectives or assigned homework problems can be discussed with the instructor or course teaching assistants, and the concepts associated with the online problems most frequently answered incorrectly by students in the course are clarified.

The semester-long course is divided into 8 units; a description of the units, and the order in which they are presented, is provided in Table 24. Each unit follows the same pattern: students are expected to use the unit plans with online materials, graded online homework, and the optional class discussion period to learn or review basic concepts at their own pace prior to the class meeting, and then the first required class period on the unit begins with an ~20 min 10 question multiple choice Individual Readiness Assurance Test (IRAT). This is immediately followed by a team discussion of the same problems and Team Readiness Assurance Test (TRAT). The TRAT allows students to take the IRAT as a group using Immediate Feedback-Assessment Techniques

(IF-AT) scratch cards so that all students finish the team exercises with full awareness of the correct answers.

Table 24. CHEM 110 course structure

Unit	Topics	Dedicated Class Periods
1	Energy, Enthalpy, Thermochemistry	2
2	Atomic Electronic Structure	2
3	Molecular Structure	3
4	Molecular Orbital Theory	4
5	Chemical Equilibrium	2
6	Entropy and Free Energy	2
7	Acids and Bases	2
8	Kinetics and Catalysis	4

Following the TRAT, the remainder of the unit (1.5 – 3.5 class periods) is spent on application problems that are worked by the teams as the instructor and TA's circulate in the room. There are periodic opportunities for reporting answers and class-wide discussion and brainstorming, but most of the class time is spent with the students working in their small teams. It is within the context of these team-based application problems that the activities reported and discussed here are employed. These application problems and RATS are available in the Supporting Information. Other course unit exercises are available upon request.

A-3 Spiropyran Application Activities

In the structure of the semester, we introduce the reversible structural transformation between SP and MC during Unit 4: Molecular Orbital Theory. This chemical reaction is introduced through a demonstration with an accompanying team application problem worksheet (see supporting information) that shows the molecular structures of both SP and MC. First, the students are shown a clear, colorless solution of commercially available SP in toluene. Then, the solution is irradiated with a blue LED light, and, during this perturbation, the solution briefly turns a deep blue/purple. Students are told that the MC compound's structure gives rise to this color. In an application problem completed by the teams during class, the students are first asked to consider the reaction in the context of molecular shape – the teams are asked to explain the relationship between the change in hybridization of the central carbon atom and the ensuing change in the geometry of the molecule. The questions asked in the application rapidly segue into a discussion of the importance that conjugation has on extended molecular geometry and the color change of the reaction, including using the particle-in-a-box model to connect the Schrödinger equation to the energy gap between electronic energy levels and associated color change. Concurrently during the weeks of these in-class discussions, students conduct a laboratory experiment focused on probing the chemical equilibrium, solvatochromism, and impact of solution polarity and hydrogen

bonding on the equilibrium of the SP-to-MC conversion, which leads into Unit 5: Chemical Equilibrium.

We finish our discussion of the SP/MC reaction by tying it to mechanical work through a hands-on activity that illustrates the ability to physically pull on the sides of the molecule embedded in a polymer film and force the opening of the ring. This provides an opportunity to revisit concepts from the first unit in the course (Energy, Enthalpy and Thermochemistry), but in a very visual context of a chemical reaction system, as opposed to the compression and expansion of ideal gases. More specifically, polydimethylsiloxane (PDMS) films with mechanochemically active SP are shown to the class and some students are given small samples to manipulate and share with their teams. The films change color either by pulling on the ends of the film in a stretching deformation or upon UV irradiation (Figure 103). Generally, two class periods are spent working on the SP-to-MC module. The experimental details of the demonstration, the application problem, and the lab exercise can be found in the Supporting Information.

A-4 Learning Objectives

The utility of the SP-to-MC module is that it ties together a wide range of learning objectives (LO's). The LO's for the course, organized by unit, are provided in the Supporting Information, with the specific LO's addressed in this module highlighted

for reference. The LO's that were assessed in a post-activity pop quiz focused on molecular orbital theory, quantum mechanics, equilibrium, hydrogen bonding, work, and polymer chemistry (Figure 104).

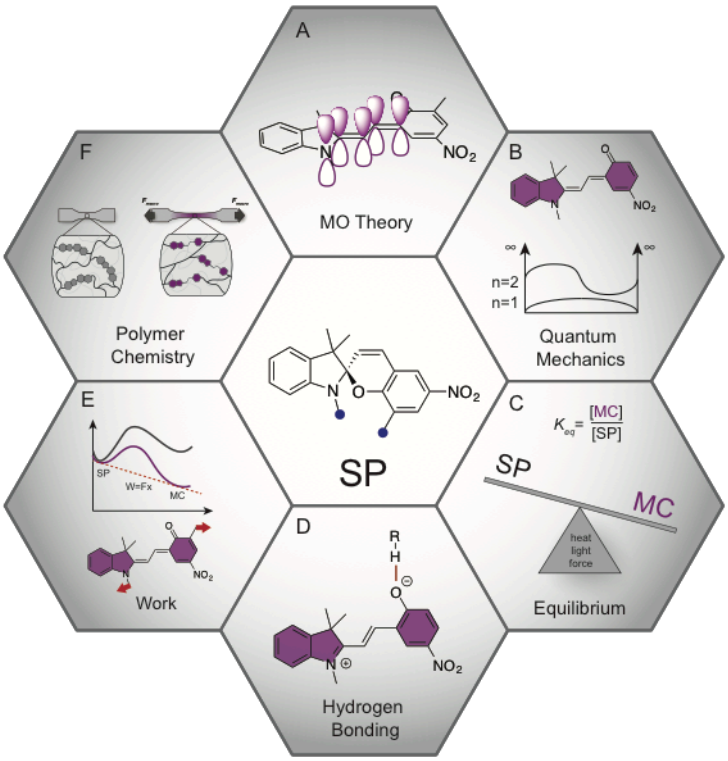

Figure 104. The new applications are structured around a single reaction from organic chemistry to connect diverse topics in general chemistry.

Molecular Orbital Theory. Novice students often initially identify conjugated bonds as a double bond-single bond-double bond pattern from observing presented

example structures without fully grasping the aspects of the molecule that make a conjugated system. The SP-to-MC reaction allows the instructor to emphasize the molecular orbital features that make a molecule conjugated. When discussing this problem, we first ask the students to consider the geometry and hybridization of each of the atoms in the structures of both SP and MC (Figure 104A). Next, learners are asked to identify geometry and hybridization changes that occur as a result of the breaking of the C-O spirocycle bond. As part of this in-class assignment, students are informed that the geometry about N1, denoted by a * in Figure 103, in SP is trigonal planar, and they are asked to classify the hybridization of the N and the surrounding atoms. The student teams quickly identify that only the central carbon, C1, denoted by a * in Figure 103, changes hybridization during the transformation between the two molecules. Indeed, C1 changes from sp^3 hybridization in SP to sp^2 hybridization in MC. It is helpful for the students to visualize the three-dimensional geometry and associated atomic orbitals surrounding the C1 in these two configurations. We find that molecular modeling software, if available, can facilitate this visualization (our students use Spartan Student).[17] Students are encouraged to build the compound on the computer outside of class to prepare for the application problem; this could also be done in the lab during the week prior to the application. We find it instructive to emphasize that this local change in hybridization (rupture of a single bond and rehybridization of a single atom) brings

about a global change in molecular structure – the rightmost side of the MC becomes co-planar with the leftmost side, because of conjugation that is continuous across the molecule. The key point is that the change to sp^2 hybridization provides an unhybridized *p* orbital that can connect two conjugated π systems that are initially separated on either side of the spirocycle connection – a very dramatic consequence of delocalized, molecular orbitals that cannot be explained by localized bonding models such as valence shell electron pair repulsion.

Quantum Mechanics. The change in conjugation provides a smooth transition into a tangible application of the Schrödinger equation and its relationship to color and conjugation (Figure 104B). After highlighting and discussing the concepts of hybridization and conjugation in the SP and MC molecules, the students are challenged to explain why SP is colorless and MC exhibits a purple color. They are prompted specifically to invoke the particle in a box model during their explanation. The key connections include: first, that the color of the molecules relates to whether or not they absorb light in the visible spectrum; second, that the wavelengths absorbed correspond to energies of associated electronic transitions (longer wavelengths means smaller HOMO-LUMO gap); third, that the spacing between orbital energies decreases as the size of the box increases in the particle-in-a-box model; and, fourth, that the size of the

"box" corresponds not to the size of the molecule, but to the size of the conjugated π system in the molecule.

The consequence of increased conjugation in MC is therefore that the gap between the orbital energy levels in MC is smaller than in SP, and less energy is needed to promote an electron to the excited state of MC than is required for SP. This lower energy corresponds to a longer wavelength in the MC molecule (absorbance in the visible) when compared to SP (absorbance almost entirely in the UV).

Equilibrium and Hydrogen Bonding. Through this exercise, students are also challenged to connect molecular structure and resonance to polarity. The teams are tasked with drawing two resonance structures for MC, one of which has formal charge on the nitrogen in the ring structure and one of which does not. They are then asked to consider the resonance structures and predict the polarity of MC relative to SP. Having identified that MC is more polar because of the additional charge separation found in one resonance structure, they are then asked to predict how solvent polarity will influence the amount of MC relative to SP at equilibrium.

The groups determine that, due to it being a more polar molecule with greater charge separation, MC will be stabilized in more polar solvents (Figure 104C). This provides the foundation for a subsequent laboratory exercise, in which students are provided a solution of SP in toluene and given a set of co-solvents (methanol, ethanol,

acetonitrile, acetone, and THF) to add. They are given the dielectric constant of each solvent and the dipole moment of each solvent molecule, and then they are asked to predict which co-solvent will result in the greatest conversion of SP to MC, and hence the greatest color change. Invariably, students predict that, because it has the highest dielectric constant, acetonitrile will generate the greatest color change. Different lab groups add different amounts of the various co-solvents and record the changes in absorbance at 540 nm. The results of all lab groups are compiled and presented in class (representative data shown in Figure 94), verifying what most groups concluded from their own observations: that despite having lower dielectric constants than other co-solvents, methanol and ethanol are the most effective co-solvents at shifting the SP/MC equilibrium toward MC.

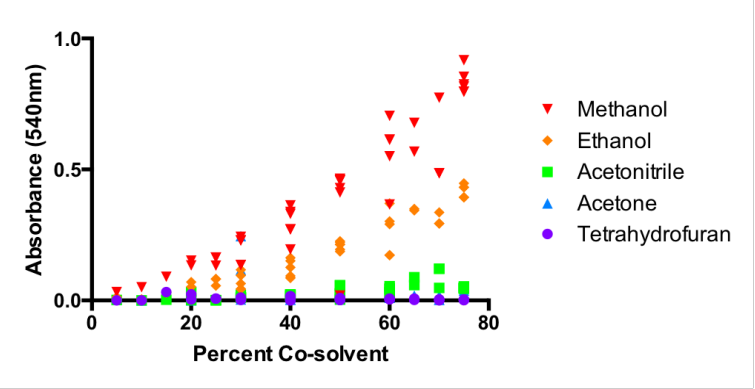

Figure 105. Representative student data for a plot of absorbance (540 nm) of the SP-to-MC conversion vs. percent co-solvent added to a solution of SP in toluene.

When asked about this in class, a few students will have speculated (correctly) that the reason is hydrogen bonding – a concept familiar to them from high school, but also presented in our Unit 3. The negatively charged oxygen atom generated by the conversion of SP to MC is a strong hydrogen bond acceptor, as shown in Figure 78D. Some students will hypothesize that the lone pairs of electrons on the oxygen atom in methanol and ethanol might help to stabilize the positive charge that develops on N1 in MC, providing an opportunity to discuss THF as a control that contradicts that hypothesis. The demonstration highlights in a visible manner the importance of hydrogen bonding as a strong intermolecular force in determining molecular behavior by providing the energy required to "pull" SP sufficiently to convert it into MC.

Work and Polymer Mechanochemistry. To this point, students have seen how the energy necessary to convert SP to MC can be provided by light and by solvation interactions, particularly hydrogen bonding. We conclude the module by demonstrating how mechanical work can similarly provide the necessary energy input for the transformation. The specific mechanism of doing work on the system is polymer mechanochemistry, in which the work is delivered by applying a force across a distance (change in molecular length) as opposed to pressure across a change in volume (Figure 104E).[320] We find this to be a compelling and captivating example of work for a chemistry course, as it involves actual chemical change – the paradigmatic conversion of

SP to MC. Since mechanical force is generally applied to the mechanophore via polymer 'handles,' this provides natural segue into a more general discussion of polymer chemistry. We begin by pointing out that it is effectively impossible to use our human hands to hold the carbon and oxygen atoms in the scissile bond. So, to apply a force directly to the SP, we need to form a covalent bond between the SP and something that is large enough to hold with our fingers.

The mechanism for accomplishing this that the instructor describes is to form bonds between SP and a chemically cross-linked PDMS elastomer (Figure 104F),[316] This provides an opportunity to discuss the molecular structure of polymers and cross-linked polymer networks, including the fact that a piece of a cross-linked rubber is largely a single molecule. For our class, we bring in strips of PDMS film into which SP has been appropriately cross-linked, using a simple formulation that can be repurposed effectively for outreach demonstrations.[327] We prompt the class to vote as to whether or not a person is strong enough to break a chemical bond (in our experience, most students think not). Then, the instructor describes the film composition and invites volunteers to come forward to stretch the films with their fingers. Upon stretching, the film changes color as a result of the mechanical work being channeled directly into the SP-to-MC conversion. In the context of polymer education, this demonstration drives home the point that polymers are made up of molecules, and that the behavior of the

material is intrinsically coupled to the behavior and properties of the molecular constituents.

After demonstrating how the work done by a person's fingers can convert the colorless polymer to purple, we discuss how one would choose which bonds in SP to replace with bonds to the polymer. There are two considerations. First, the substitution must not disrupt the conjugation in the MC, and so replacing a sigma bond (for example, to a hydrogen atom) that is outside the conjugated π system is discussed as the best strategy. Second, the chosen positions must couple to the ring opening reaction (that is, they must move away from each other after the C-O bond breaks). Because work is force•distance, the further the substitution positions move away from each other, the less force is required to provide the necessary work. If available, using a computer modeling program to determine the distance between points and calculating the force needed to break the bond gives students an early opportunity to attempt molecular visualization – for some students, a barrier to success in subsequent organic chemistry courses.[318,319] Molecular model kits could be used to aid in visualization as well.

This exercise ties a chemical reaction to the seemingly abstract physical concepts of work and its relationship to internal energy (these were covered in the first unit of the

course). It also allows for a discussion of what a polymer is and how polymers can have molecular functionality embedded within them for desired chemical effects.

Extension to Organic Chemistry Courses. Although we use the SP-to-MC module in an accelerated general chemistry course, we recognize that not all universities have an equivalent course. We think this module could easily be adapted to an organic chemistry setting. In fact, many of the concepts presented in this general chemistry module are often covered in the introductory chapters of an organic chemistry textbook.[328,329] The details are beyond the scope of this paper, but the SP-to-MC conversion provides additional opportunities to discuss substituent effects in aromatic systems. Many SP derivatives have been synthesized, and they have different photochromic properties as a result of the substituent patterns.[330]

A-5 Methods

A-5.1 Team Formation Process

Prior to the beginning of the semester, an effort was made to create balanced cooperative-learning teams that each were comprised of learners with low, medium, and high relative prior chemistry experience and demonstrated math skills. To this end, students were placed into "semi-random" teams of four (or five) individuals based primarily on rankings from relative self-reported AP Chemistry exam scores. Math SAT scores are known to highly correlate with performance in college-level general chemistry

courses,[324,325,331,332] so Math SAT scores were used as a secondary ranking. Teams were randomly assigned team numbers (1-24) that were used to track team scores over the entire course of the semester. More detail on the formation of teams can be found in the Supporting Information.

A-5.2 Experimental Design

To determine whether or not the SP applications work as well in guiding students towards meeting desired unit learning outcomes when compared to more traditional, small molecule-based applications we had previously used in Unit 4, a random trial was devised. For Unit 4 only, the instructor drew a random number that resulted in the odd-numbered teams being the control group and the even-numbered teams being the experimental group. To exclude bias, the researchers who initially developed the application problems did not teach the course during the semester that the formal assessment of its implementation in the classroom was performed.

At the beginning of the unit on Molecular Orbital Theory, both groups met at the same time and took the same IRAT and TRAT. Next, to examine the effectiveness of the new SP-based applications, the control and experimental groups initially completed two unique sets of applications in the subsequent class meetings. In unique class periods, the control group teams completed the original applications problems, while the experimental group teams completed the re-designed SP-based applications. After

completing each set of applications, each team completed a Strategy Analyst report where, as a team, they ranked both the difficulty of and their interest in the application problems on a five point Likert-type scale. Teams also had the opportunity to provide written feedback about the strengths and areas for improvement for the set of applications they completed on the Strategy Analyst report. The Likert-type scale numeric values were tabulated and the written responses were transcribed by a staff assistant not involved with the study. Averages, standard deviations, and standard errors were calculated for each data set, and an unpaired *t*-test was performed on the two group's numerical responses to test for statistical significance.

After both groups met, separately, to complete the control and experimental applications, the groups were remerged for the next class period and all individuals in both groups completed the same unannounced "pop" quiz. This quiz was a LO-driven assessment composed of ten multiple choice problems. Each problem was coded to specific course learning objectives with a focus on those covered in the Unit 4 applications. Following the individual LO Assessment (pop quiz), each team completed the set of applications they had not previously seen to ensure all students were exposed to all the same application activities by the end of the unit. Scores on the LO Assessment were combined for each group and averages, standard deviations, and standard errors

were calculated. An unpaired *t*-test was performed on the two sets of scores to test for statistical significance.

A-6 Results

Before comparing the results of the application-based IRAT, the results of the previous IRATs were compared for the experimental and control groups. For the first three IRATs taken as part of Units 1, 2, and 3, there was no significant difference in scores between the control and experimental groups ($0.39 < p < 0.70$). A comparison of results on the control and experimental group on both the initial IRAT for Unit 4 and LO Assessment (pop quiz) showed no statistical significance between the two groups, $p = 0.30$ and $p = 0.10$, respectively (Figure 106).

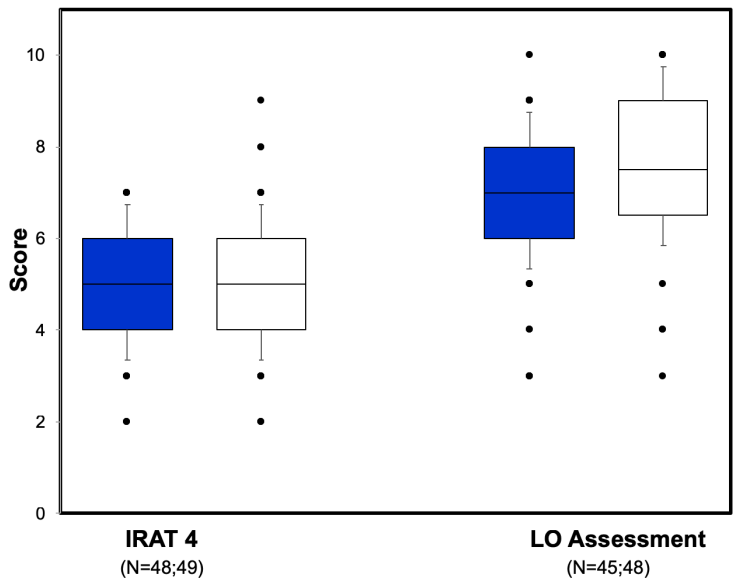

Figure 106. Initial Unit 4 IRAT and LO Assessment scores for control (blue) and experimental group (white).

In addition to the assessment, students' responses to the Likert-type scale items and their written free-response feedback on the applications were analyzed. For the Likert-type scale questions, near the end of each class period, teams were asked to compare the day's applications to those completed for previous units and assess the relative difficulty of and their interest in the applications with 5 representing more difficult/more interested and 1 representing less difficult/less interested (Figure 107). The unpaired t-test showed no statistical difference between the control and experimental groups, $p = 0.2757$ and $p = 0.4154$, respectively. Additionally, teams provided written

feedback on the strengths of the applications as well as areas for improvement. Representative student feedback is shown in Table 25. Complete student feedback is available in the Supporting Information.

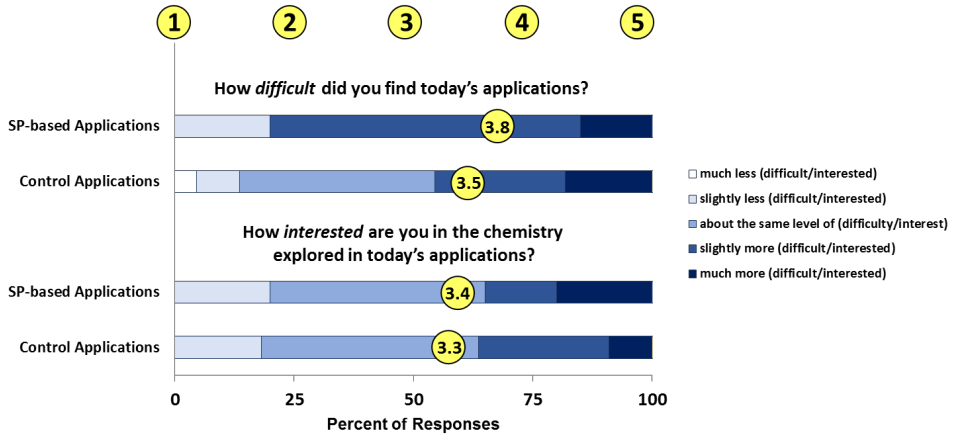

Figure 107. Student Likert-type scale feedback after completing each set of applications.

Table 25. Representative initial student reactions to control and SP-based applications

Prompt	Group	Representative Responses
List at least one strength of today's application	Control	"It combined the topics we have learned in topic 2 and th one we are learning"
		"Makes to link molecular orbital to actual properties of th molecule"
		"We achieved a better understanding of MO Theory"
	Experimental	"Ability to understand concepts of resonance and delocalization"
		"The exercises built on each other and connected to our lal
List at least one possible improvement to today's application	Control	"Questions more related to each other"
		"They could have been more in depth"
	Experimental	"Understanding applying force energetically"
		"The questions should be more clear. For example, the las application should have indicated that the Spartan mode was needed."

A-7 Discussion

A comparison of the initial Molecular Orbital Theory IRAT showed no statistical difference between the Control and Experimental groups. Therefore, prior to completing the application problems, both groups start from a similar initial baseline. After completing the different sets of application problems, both groups showed similar level of mastery of the course learning objectives, based on the LO Assessment, with no statistical difference between the Experimental and Control groups. Students also provided similar feedback on the difficulty level and their interest in the chemistry

content of both sets of applications problems, with generally neutral feelings towards the difficulty and their interest in the chemistry.

Even though there is little difference in the quantitative measures, students expressed unique written feedback on the application problems, with some students in the Control group noticing the disconnection between the application problems while some students in the Experimental group noticed connection within the application set and in the laboratory experiment they had recently performed.

A-8 Limitations

Limitations in this study were present in both the size of the sample as well as the method used to assess student learning outcomes. Due to the class size, the control and experimental group were limited to approximately 50 students each, which limits our ability to observe statistical differences given the small sample size. Maintaining consistency within the course format, only one strategy analyst sheet is collected per team, which shows only the team's net assessment on the difficulty and interest in the SP-based applications. This team-based feedback does not take into account individual students' assessments of the application problems, which may have differed somewhat from that of the whole team. Additionally, the LO Assessment was administered as a multiple choice quiz, similar to the IRATs the students had been previously exposed to,

which could allow students to make an informed guess of the correct answer without a deeper understanding of underlying concepts.

A-9 Summary and Perspectives

The SP/MC module described here directly addresses several learning objectives commonly covered in general chemistry courses, but in the context of polymers and introductory organic chemistry principles. The use of one reaction as a common thread by which to tie together concepts typically presented as disparate entities allows the students to explore the factors that contribute to the organic transformation between SP and MC, highlighting Molecular Orbital theory, quantum mechanics, equilibrium, hydrogen-bonding, and work while also introducing basic concepts of polymer chemistry. We have found this exercise to be a useful way to structure a portion of a general chemistry course in order to address the interdisciplinary nature of chemistry and enhance student's understanding of real-world applications of general chemistry topics. The Craig group's initial interest in the SP-to-MC conversion inspired this work, and students seem to enjoy learning about research at their university. We hope our experience encourages other researchers and educators to adapt their scientific interests to the courses that they teach.

References

(1) Teles, J. H.; Brode, S.; Chabanas, M. *Angew. Chem., Int. Ed.* **1998,** *37* (10), 1415.

(2) Fructos, M. R.; Belderrain, T. R.; de Frémont, P.; Scott, N. M.; Nolan, S. P.; Díaz-Requejo, M. M.; Pérez, P. J.. *Angew. Chem., Int. Ed.* **2005,** *44* (33), 5284.

(3) Johansson, M. J.; Gorin, D. J.; Staben, S. T.; Toste, F. D. *J. Am. Chem. Soc.* **2005,** *127* (51), 18002.

(4) López, S.; Herrero-Gómez, E.; Pérez-Galán, P.; Nieto-Oberhuber, C.; Echavarren, A. M. *Angew. Chem., Int. Ed.* **2006,** *45* (36), 6029.

(5) Fedorov, A.; Chen, P. Electronic Effects in the Reactions of Olefin-Coordinated Gold Carbene Complexes. *Organometallics* **2009,** *28* (5), 1278.

(6) Fructos, M. R.; Díaz-Requejo, M. M.; Pérez, P. J. *Chem. Commun.* **2009**, (34), 5153.

(7) Horino, Y.; Yamamoto, T.; Ueda, K.; Kuroda, S.; Toste, F. D. *J. Am. Chem. Soc.* **2009,** *131* (8), 2809.

(8) Lemière, G.; Gandon, V.; Cariou, K.; Hours, A.; Fukuyama, T.; Dhimane, A.-L.; Fensterbank, L.; Malacria, M. *J. Am. Chem. Soc.* **2009,** *131* (8), 2993.

(9) Prieto, A.; Fructos, M. R.; Mar Díaz-Requejo, M.; Pérez, P. J.; Pérez-Galán, P.; Delpont, N.; Echavarren, A. M. *Tetrahedron* **2009,** *65* (9), 1790.

(10) Zhang, D.; Xu, G.; Ding, D.; Zhu, C.; Li, J.; Sun, J. *Angew. Chem., Int. Ed.* **2014,** *53* (41), 11070.

(11) Qian, D.; Zhang, J. *Chem. Soc. Rev.* **2015,** *44* (3), 677.

(12) Gorin, D. J.; Sherry, B. D.; Toste, F. D. *Chem. Rev.* **2008,** *108* (8), 3351.

(13) Bandini, M. *Chem. Soc. Rev.* **2011,** *40* (3), 1358.

(14) Corma, A.; Leyva-Pérez, A.; Sabater, M. J. *Chem. Rev.* **2011,** *111* (3), 1657.

(15) Gorin, D. J.; Toste, F. D. *Nature* **2007,** *446*, 395.

(16) Shen, H. C. *Tetrahedron* **2008,** *64* (18), 3885.

(17) Li, Z.; Brouwer, C.; He, C. *Chem. Rev.* **2008,** *108* (8), 3239.

(18) Krause, N.; Winter, C. *Chem. Rev.* **2011,** *111* (3), 1994.

(19) Gandon, V.; Lemière, G.; Hours, A.; Fensterbank, L.; Malacria, M. *Angew. Chem., Int. Ed.* **2008,** *47* (39), 7534.

(20) Alonso, I.; Trillo, B.; López, F.; Montserrat, S.; Ujaque, G.; Castedo, L.; Lledós, A.; Mascareñas, J. L. *J. Am. Chem. Soc.* **2009,** *131* (36), 13020.

(21) Benitez, D.; Shapiro, N. D.; Tkatchouk, E.; Wang, Y.; Goddard Iii, W. A.; Toste, F. D.. *Nat. Chem.* **2009,** *1*, 482.

(22) Benitez, D.; Tkatchouk, E.; Gonzalez, A. Z.; Goddard, W. A.; Toste, F. D. *Org. Lett.* **2009,** *11* (21), 4798.

(23) Cuenca, A. B.; Montserrat, S.; Hossain, K. M.; Mancha, G.; Lledós, A.; Medio-Simón, M.; Ujaque, G.; Asensio, G. *Org. Lett.* **2009,** *11* (21), 4906.

(24) Paton, R. S.; Maseras, F. *Org. Lett.* **2009,** *11* (11), 2237.

(25) Trillo, B.; López, F.; Montserrat, S.; Ujaque, G.; Castedo, L.; Lledós, A.; Mascareñas, J. L. *Chem. Eur. J.* **2009,** *15* (14), 3336.

(26) Kovács, G.; Lledós, A.; Ujaque, G. *Organometallics* **2010,** *29* (22), 5919.

(27) Wang, Z. J.; Benitez, D.; Tkatchouk, E.; Goddard Iii, W. A.; Toste, F. D. *J. Am. Chem. Soc.* **2010,** *132* (37), 13064.

(28) Kovács, G.; Lledós, A.; Ujaque, G. *Angew. Chem. Int. Ed.* **2011,** *50* (47), 11147.

(29) Malacria, M.; Fensterbank, L.; Gandon, V. In *Computational Mechanisms of Au and Pt Catalyzed Reactions*; Soriano, E.;Marco-Contelles, J., Eds.; Springer Berlin Heidelberg: Berlin, Heidelberg, 2011.

(30) Fürstner, A.; Davies, P. W. *Angew. Chem. Int. Ed.* **2007,** *46* (19), 3410.

(31) Correa, A.; Marion, N.; Fensterbank, L.; Malacria, M.; Nolan, S. P.; Cavallo, L. *Angew. Chem. Int. Ed.* **2008,** *47* (4), 718.

(32) Jiménez-Núñez, E.; Echavarren, A. M. *Chem. Rev.* **2008,** *108* (8), 3326.

(33) Fürstner, A.. *Chem. Soc. Rev.* **2009,** *38* (11), 3208.

(34) Toullec, P. Y.; Michelet, V. In *Computational Mechanisms of Au and Pt Catalyzed Reactions*; Soriano, E.;Marco-Contelles, J., Eds.; Springer Berlin Heidelberg: Berlin, Heidelberg, 2011.

(35) Obradors, C.; Echavarren, A. M. *Chem. Commun.* **2014,** *50* (1), 16.

(36) Wang, Y.; Muratore, M. E.; Echavarren, A. M. *Chem. Eur. J.* **2015,** *21* (20), 7332.

(37) Pérez-Galán, P.; Herrero-Gómez, E.; Hog, D. T.; Martin, N. J. A.; Maseras, F.; Echavarren, A. M. *Chem. Sci.* **2011,** *2* (1), 141.

(38) Kawabata, N.; Kamemura, I.; Naka, M. *J. Am. Chem. Soc.* **1979,** *101* (8), 2139.

(39) Nishimura, J.; Furukawa, J.; Kawabata, N.; Kitayama, M. *Tetrahedron* **1971,** *27* (9), 1799.

(40) Díaz-Requejo, M. M.; Pérez, P. J.; Brookhart, M.; Templeton, J. L. *Organometallics* **1997,** *16* (20), 4399.

(41) Díaz-Requejo, M. M.; Nicasio, M. C.; Pérez, P. J. *Organometallics* **1998,** *17* (14), 3051.

(42) Fedorov, A.; Moret, M.-E.; Chen, P. *J. Am. Chem. Soc.* **2008,** *130* (28), 8880.

(43) Fedorov, A.; Batiste, L.; Bach, A.; Birney, D. M.; Chen, P. *J. Am. Chem. Soc.* **2011,** *133* (31), 12162.

(44) Swift, C. A.; Gronert, S. *Organometallics* **2014,** *33* (24), 7135.

(45) Seidel, G.; Fürstner, *Angew. Chem. Int. Ed.* **2014,** *53* (19), 4807.

(46) García-Morales, C.; Pei, X.-L.; Sarria Toro, J. M.; Echavarren, A. M. *Angew. Chem. Int. Ed.* **2019,** *58* (12), 3957.

(47) Kim, N.; Widenhoefer, R. A. Ionization of gold (γ-methoxy)vinyl complexes generates reactive gold vinyl carbene complexes. *Chem.l Sci.* **2019**, DOI:10.1039/C9SC01574D 10.1039/C9SC01574D.

(48) Ringger, D. H.; Kobylianskii, I. J.; Serra, D.; Chen, P. *Chem. Eur. J.* **2014,** *20* (44), 14270.

(49) Miege, F.; Meyer, C.; Cossy, J. *Beilstein J. Org. Chem.* **2011,** *7*, 717.

(50) Kazem Shiroodi, R.; Gevorgyan, V.. *Chem. Soc. Rev.* **2013,** *42* (12), 4991.

(51) Fürstner, A. *Acc. Chem. Res.* **2014,** *47* (3), 925.

(52) Obradors, C.; Echavarren, A. M. *Acc. Chem. Res.* **2014,** *47* (3), 902.

(53) Zheng, Z.; Wang, Z.; Wang, Y.; Zhang, L. *Chem. Soc. Rev.* **2016,** *45* (16), 4448.

(54) Doyle, M. P.; Griffin, J. H.; Bagheri, V.; Dorow, R. L. *Organometallics* **1984,** *3* (1), 53.

(55) Doyle, M. P. *Chem. Rev.* **1986,** *86* (5), 919.

(56) Brookhart, M.; Studabaker, W. B. *Chem. Rev.* **1987,** *87* (2), 411.

(57) Bernardi, F.; Bottoni, A.; Miscione, G. P. *Organometallics* **2001,** *20* (13), 2751.

(58) Fraile, J. M.; García, J. I.; Martínez-Merino, V.; Mayoral, J. A.; Salvatella, L. *J. Am. Chem. Soc.* **2001,** *123* (31), 7616.

(59) Rodríguez-García, C.; Oliva, A.; Ortuño, R. M.; Branchadell, V. *J. Am. Chem. Soc.* **2001,** *123* (25), 6157.

(60) Straub, B. F. *J. Am. Chem. Soc.* **2002,** *124* (47), 14195.

(61) Iwakura, I.; Ikeno, T.; Yamada, T. *Org. Lett.* **2004,** *6* (6), 949.

(62) Harris, R. J.; Widenhoefer, R. A. *Chem. Soc. Rev.* **2016,** *45* (16), 4533.

(63) Salomon, R. G.; Kochi, J. K. *J. Am. Chem. Soc.* **1973,** *95* (10), 3300.

(64) Wulfman, D. S.; McDaniel, R. S.; Peace, B. W. *Tetrahedron* **1976,** *32* (11), 1241.

(65) Nakamura, A.; Konishi, A.; Tsujitani, R.; Kudo, M.; Otsuka, S. *J. Am. Chem. Soc.* **1978,** *100* (11), 3449.

(66) Nakamura, A.; Koyama, T.; Otsuka, S. *Bull. Chem. Soc. Jpn.* **1978,** *51* (2), 593.

(67) Usón, R.; Laguna, A.; Laguna, M.; Usón, A.; Gimeno, M. C. *Inorg. Chim. Acta* **1986,** *114* (1), 91.

(68) Maxwell, J. L.; Brown, K. C.; Bartley, D. W.; Kodadek, T.. *Science* **1992,** *256* (5063), 1544.

(69) Bratsch, S. G. Revised Mulliken electronegativities: *J. Chem. Educ.* **1988,** *65* (1), 34.

(70) Huheey, J. E.; Keiter, E. A.; Keiter, R. L. *Inorganic chemistry : principles of structure and reactivity*; HarperCollins College Publishers: New York, NY, 1993.

(71) Schmidbaur, H.; Schier, A. *Organometallics* **2010,** *29* (1), 2.

(72) Brooner, R. E. M.; Widenhoefer, R. A. *Angew. Chem. Int. Ed.* **2013,** *52* (45), 11714.

(73) Jones, A. C. In *Homogeneous Gold Catalysis*; Slaughter, L. M., Ed.; Springer International Publishing: Cham, 2015.

(74) Nieto-Oberhuber, C.; López, S.; Muñoz, M. P.; Jiménez-Núñez, E.; Buñuel, E.; Cárdenas, D. J.; Echavarren, A. M. *Chem. Eur. J.* **2006,** *12* (6), 1694.

(75) Batiste, L.; Fedorov, A.; Chen, P.. *Chem. Commun.* **2010,** *46* (22), 3899.

(76) Ringger, D. H.; Chen, P. *Angew. Chem. Int. Ed.* **2013,** *52* (17), 4686.

(77) Werlé, C.; Goddard, R.; Fürstner, A. *Angew. Chem. Int. Ed.* **2015,** *54* (51), 15452.

(78) Kim, N.; Widenhoefer, R. A. *Angew. Chem. Int. Ed.* **2018,** *57* (17), 4722.

(79) Sarria Toro, J. M.; García-Morales, C.; Raducan, M.; Smirnova, E. S.; Echavarren, A. M. *Angew. Chem. Int. Ed.* **2017,** *56* (7), 1859.

(80) Schmidbaur, H.; Franke, R. *Angew. Chem. Int. Ed.* **1973,** *12* (5), 416.

(81) Schmidbaur, H.; Franke, R. *Chem. Ber.* **1975,** *108* (4), 1321.

(82) Schmidbaur, H.; Franke, R. *Inorg. Chim. Acta* **1975,** *13*, 79.

(83) Schmidbaur, H.; Franke, R.. *Inorg. Chim. Acta* **1975,** *13*, 85.

(84) Yamamoto, Y.; Kanda, Z. *Bul. Chem. Soc. Jpn.* **1979,** *52* (9), 2560.

(85) Yamamoto, Y. *Chem. Lett.* **1980,** *9* (3), 311.

(86) Porter, L. C.; Knachel, H.; Fackler, J. P., Jnr. *Acta Crystallographica Section C* **1987,** *43* (9), 1833.

(87) Vicente, J.; Chicote, M. T.; Saura-Llamas, I.; Turpin, J.; Fernandez-Baeza, J. *J. Organometal. Chem.* **1987,** *333* (1), 129.

(88) Briggs, D. A.; Raptis, R. G.; Fackler, J. P., Jnr.. *Acta Crystallographica Section C* **1988,** *44* (7), 1313.

(89) Kneuper, H.-J.; Harms, K.; Boche, G. *J. Organometl. Chem.* **1989,** *364* (1), 275.

(90) Aguirre, C. J.; Gimeno, M. C.; Laguna, A.; Laguna, M.; López de Luzuriaga, J. M.; Puente, F. *Inorg. Chim. Acta* **1993,** *208* (1), 31.

(91) Steinborn, D.; Becke, S.; Herzog, R.; Günther, M.; Kircheisen, R.; Stoeckli-Evans, H.; Bruhn, C. *Zeitschrift für anorganische und allgemeine Chemie* **1998,** *624* (8), 1303.

(92) Fürstner, A.; Alcarazo, M.; Goddard, R.; Lehmann, C. W. *Angew. Chem. Int. Ed.* **2008,** *47* (17), 3210.

(93) Brandt, S.; Helquist, P. *J. Am. Chem. Soc.* **1979,** *101* (21), 6473.

(94) Kremer, K. A. M.; Helquist, P.; Kerber, R. C. *J. Am. Chem. Soc.* **1981,** *103* (7), 1862.

(95) O'Connor, E. J.; Helquist, P. *J. Am. Chem. Soc.* **1982,** *104* (7), 1869.

(96) O'Connor, E. J.; Brandt, S.; Helquist, P. *J. Am. Chem. Soc.* **1987,** *109* (12), 3739.

(97) McCarten, P.; Barefield, E. K. *Organometallics* **1998,** *17* (21), 4645.

(98) Gandelman, M.; Rybtchinski, B.; Ashkenazi, N.; Gauvin, R. M.; Milstein, D. A *J. Am. Chem. Soc.* **2001,** *123* (22), 5372.

(99) Bravo, P.; Fronza, G.; Ticozzi, C.; Gaudiano, G.. *J. Organometal. Chem.* **1974,** *74* (1), 143.

(100) Collins, T. J.; Roper, W. R. *J. Chem. Soc. Chem. Commun. s* **1977**, 901.

(101) Fackler, J. P.; Paparizos, C.. *J. Am. Chem. Soc.* **1977,** *99* (7), 2363.

(102) Weber, L. *Angew. Chem. Int. Ed.* **1983,** *22* (7), 516.

(103) Davidson, J. G.; Barefield, E. K.; Van Derveer, D. G. *Organometallics* **1985,** *4* (7), 1178.

(104) McCormick, F. B.; Gleason, W. B.; Zhao, X.; Heah, P. C.; Gladysz, J. A.]. *Organometallics* **1986,** *5* (9), 1778.

(105) Fischer, H.; Schmid, J.; Zeuner, S. *Chem. Ber.* **1987,** *120* (4), 583.

(106) Leoni, P.; Marchetti, F.; Paoletti, M.. *Organometallics* **1997,** *16* (10), 2146.

(107) Scartazzini, R.; Mislow, K. *Tetrahedron Lett.* **1967,** *8* (28), 2719.

(108) Darwish, D.; Hui, S. H.; Tomilson, R. *J. Am. Chem. Soc.* **1968,** *90* (20), 5631.

(109) Andersen, K. K.; Cinquini, M.; Papanikolaou, N. E. *J. Org. Chem.* **1970,** *35* (3), 706.

(110) Brower, K. R.; Wu, T.-L. *J. Am. Chem. Soc.* **1970,** *92* (18), 5303.

(111) Garbesi, A.; Corsi, N.; Fava, A. *Helve. Chim. Acta* **1970,** *53* (6), 1499.

(112) Darwish, D.; Scott, C. E. *Can. J. Chem.* **1973,** *51* (21), 3647.

(113) Oki, M.; Yamada, Y.; Murata, S. *Bull. Chem. Soc. Jpn.* **1988,** *61* (3), 707.

(114) Green, T. K.; Whetstine, J. R.; Son, E.-J.-R. *Tetrahedron: Asymmetry* **1997,** *8* (19), 3175.

(115) Barefield, E. K.; McCarten, P.; Hillhouse, M. C. *Organometallics* **1985,** *4* (9), 1682.

(116) Brown, H. C.; Okamoto, Y. *J. Am. Chem. Soc.* **1958,** *80* (18), 4979.

(117) DiLabio, G. A.; Ingold, K. U.. *J. Org. Chem.* **2004,** *69* (5), 1620.

(118) Van Geet, A. L. *Anal. Chem.* **1968,** *40* (14), 2227.

(119) Jang, Y.; Kim, K. T.; Jeon, H. B. *J. Org. Chem.* **2013,** *78* (12), 6328.

(120) Yao, M.-L.; Deng, M.-Z. *Synthesis* **2000,** *2000* (08), 1095.

(121) Creary, X. *J. Org. Chem.* **1980,** *45* (23), 4653.

(122) Savino, T. G.; Kanakarajan, K.; Platz, M. S. *J. Org. Chem.* **1986,** *51* (8), 1305.

(123) Seidel, G.; Mynott, R.; Fürstner, A. *Angew. Chem Int. Ed.* **2009,** *48* (14), 2510.

(124) Hussong, M. W.; Rominger, F.; Krämer, P.; Straub, B. F.. *Angew. Chem. Int. Ed.* **2014,** *53* (35), 9372.

(125) Brooner, R. E. M.; Widenhoefer, R. A. *Chem. Commun.* **2014,** *50* (19), 2420.

(126) Nolan, S. P. *N-Heterocyclic Carbenes: Effective Tools for Organometallic Synthesis*; Wiley, 2014.

(127) Amijs, C. H. M.; López-Carrillo, V.; Raducan, M.; Pérez-Galán, P.; Ferrer, C.; Echavarren, A. M. *J. Org. Chem.* **2008,** *73* (19), 7721.

(128) Barabé, F.; Levesque, P.; Korobkov, I.; Barriault, L. *Org. Lett.* **2011,** *13* (20), 5580.

(129) Azzopardi, K. M.; Bistoni, G.; Ciancaleoni, G.; Tarantelli, F.; Zuccaccia, D.; Belpassi, L. *Dalton Trans.* **2015,** *44* (31), 13999.

(130) Nunes dos Santos Comprido, L.; Klein, J. E. M. N.; Knizia, G.; Kästner, J.; Hashmi, A. S. K. *Chem. Eur. J.* **2016,** *22* (9), 2892.

(131) Nunes dos Santos Comprido, L.; Klein, J. E. M. N.; Knizia, G.; Kästner, J.; Hashmi, A. S. K. *Angew. Chem. Int. Ed.* **2015,** *54* (35), 10336.

(132) Ciancaleoni, G.; Biasiolo, L.; Bistoni, G.; Macchioni, A.; Tarantelli, F.; Zuccaccia, D.; Belpassi, L. *Chem. Eur. Jl* **2015,** *21* (6), 2467.

(133) Döpp, R.; Lothschütz, C.; Wurm, T.; Pernpointner, M.; Keller, S.; Rominger, F.; Hashmi, A. S. K. *Organometallics* **2011,** *30* (21), 5894.

(134) Müller, T.; Margraf, D.; Syha, Y. *J. Am. Chem. Soc.* **2005,** *127* (31), 10852.

(135) Müller, T.; Juhasz, M.; Reed, C. A. *Angew. Chem. Int. Ed.* **2004,** *43* (12), 1543.

(136) Klaer, A.; Müller, T.. *J. Phys. Org. Chem.* **2010,** *23* (11), 1043.

(137) Klaer, A.; Syha, Y.; Nasiri, H. R.; Müller, T. *Chem. Eur. Jl* **2009,** *15* (34), 8414.

(138) Klaer, A.; Saak, W.; Haase, D.; Müller, T. *J. Am. Chem. Soc.* **2008,** *130* (45), 14956.

(139) Müller, T.; Meyer, R.; Lennartz, D.; Siehl, H.-U. *Angew. Chem. Int. Ed.* **2000,** *39* (17), 3074.

(140) Harris, R. J.; Widenhoefer, R. A. *Angew. Chem. Int. Ed.* **2015,** *54* (23), 6867.

(141) Mamane, V.; Hannen, P.; Fürstner, A. *Chem. Eur. J.* **2004,** *10* (18), 4556.

(142) Seregin, I. V.; Gevorgyan, V. *J. Am. Chem. Soc.* **2006,** *128* (37), 12050.

(143) Soriano, E.; Marco-Contelles, J. *Organometallics* **2006,** *25* (19), 4542.

(144) Lavallo, V.; Frey, G. D.; Kousar, S.; Donnadieu, B.; Bertrand, G. *Proc. Nat. Acad. Sci.* **2007,** *104* (34), 13569.

(145) Rabaâ, H.; Engels, B.; Hupp, T.; Hashmi, A. S. K. *International Journal of Quantum Chemistry* **2007,** *107* (2), 359.

(146) Xia, Y.; Dudnik, A. S.; Li, Y.; Gevorgyan, V. *Org. Lett.* **2010,** *12* (23), 5538.

(147) Gómez-Suárez, A.; Nolan, S. P. *Angew. Chem. Int. Ed.* **2012,** *51* (33), 8156.

(148) Hashmi, A. S. K.; Wieteck, M.; Braun, I.; Nösel, P.; Jongbloed, L.; Rudolph, M.; Rominger, F. *Adv. Synth. Catal.* **2012,** *354* (4), 555.

(149) Hashmi, A. S. K.; Wieteck, M.; Braun, I.; Rudolph, M.; Rominger, F. *AAngew. Chem. Int. Ed.* **2012,** *51* (42), 10633.

(150) Ye, L.; Wang, Y.; Aue, D. H.; Zhang, L. *J. Am. Chm. Soc.* **2012,** *134* (1), 31.

(151) Braun, I.; Asiri, A. M.; Hashmi, A. S. K. *ACS Catal.* **2013,** *3* (8), 1902.

(152) Hansmann, M. M.; Rominger, F.; Hashmi, A. S. K.. *Chem. Sci.* **2013,** *4* (4), 1552.

(153) Nösel, P.; Lauterbach, T.; Rudolph, M.; Rominger, F.; Hashmi, A. S. K. *Chem. Eur. J.* **2013,** *19* (26), 8634.

(154) Bucher, J.; Wurm, T.; Nalivela, K. S.; Rudolph, M.; Rominger, F.; Hashmi, A. S. K. *Angew. Chem. Int. Ed.* **2014,** *53* (15), 3854.

(155) Hansmann, M. M.; Tšupova, S.; Rudolph, M.; Rominger, F.; Hashmi, A. S. K. *Chem. Eur. J.* **2014,** *20* (8), 2215.

(156) Hashmi, A. S. K. *Acc. Chem. Res.* **2014,** *47* (3), 864.

(157) Pickup, O. J. S.; Khazal, I.; Smith, E. J.; Whitwood, A. C.; Lynam, J. M.; Bolaky, K.; King, T. C.; Rawe, B. W.; Fey, N. *Organometallics* **2014,** *33* (7), 1751.

(158) Vilhelmsen, M. H.; Hashmi, A. S. K. *Chem. Eur. J.* **2014,** *20* (7), 1901.

(159) Xie, J.; Pan, C.; Abdukader, A.; Zhu, C. *Chem. Soc. Rev.* **2014,** *43* (15), 5245.

(160) Bucher, J.; Stößer, T.; Rudolph, M.; Rominger, F.; Hashmi, A. S. K. *Angew. Chem. Int. Ed.* **2015,** *54* (5), 1666.

(161) Morán-Poladura, P.; Rubio, E.; González, J. M. *Angew. Chem. Int. Ed.* **2015,** *54* (10), 3052.

(162) Nösel, P.; Müller, V.; Mader, S.; Moghimi, S.; Rudolph, M.; Braun, I.; Rominger, F.; Hashmi, A. S. K. *Adv. Synth. Catal.* **2015,** *357* (2-3), 500.

(163) Tokimizu, Y.; Wieteck, M.; Rudolph, M.; Oishi, S.; Fujii, N.; Hashmi, A. S. K.; Ohno, H. *Org. Lett.* **2015,** *17* (3), 604.

(164) Hansen, P. E.; Wray, V. *Organic Magnetic Resonance* **1981,** *15* (1), 102.

(165) Frei, K.; Bernstein, H. J. *J. Chem. Phys.* **1963,** *38* (5), 1216.

(166) Lambert, J. B. *Tetrahedron* **1990,** *46* (8), 2677.

(167) Siehl, H. U. In *Pure and Applied Chemistry*, 1995; Vol. 67.

(168) Zhang, W.; Stone, J. A.; Brook, M. A.; McGibbon, G. A. *J. Am. Chem. Soc.* **1996,** *118* (24), 5764.

(169) Li, X.; Stone, J. A. *J. Am. Chem. Soc.* **1989,** *111* (15), 5586.

(170) Lambert, J. B.; Zhao, Y. *J. Am. Chem. Soc.* **1996,** *118* (33), 7867.

(171) Reed, C. A. *Acc. Chem. Res.* **1998,** *31* (6), 325.

(172) Lambert, J. B.; Zhao, Y.; Wu, H. *J. Org. Chem.* **1999,** *64* (8), 2729.

(173) Stock, L. M.; Brown, H. C. In *Advances in Physical Organic Chemistry*; Gold, V., Ed.; Academic Press, 1963; Vol. 1.

(174) Schulte, P.; Behrens, U.. *Chem. Commun.* **1998**, 1633.

(175) Eaborn, C.; Feichtmayr, F.; Horn, M.; Murrell, J. N. *J. Organometal. Chem.* **1974,** *77* (1), 39.

(176) Apeloig, Y.; Schleyer, P. v. R.; Pople, J. A. *J. Am. Chem. Soc.* **1977,** *99* (5), 1291.

(177) Pople, J. A.; Apeloig, Y.; von R. Schleyer, P. *Chem. Phys. Lett.* **1982,** *85* (5), 489.

(178) Wierschke, S. G.; Chandrasekhar, J.; Jorgensen, W. L. *J. Am. Chem. Soc.* **1985,** *107* (6), 1496.

(179) Bernardi, F.; Bottoni, A.; Venturini, A. *J. Am. Chem. Soc.* **1986,** *108* (18), 5395.

(180) van Alem, K.; Lodder, G.; Zuilhof, H.. *J. Phys. Chem. A* **2002,** *106* (44), 10681.

(181) Song, C.; Schwarzkopf, D. S.; Rees, G. *Nat. Commun.* **2013,** *4*, 2201.

(182) Taft, R. W. *J. Am. Chem. Soc.* **1957,** *79* (5), 1045.

(183) Taft, R. W.; Price, E.; Fox, I. R.; Lewis, I. C.; Andersen, K. K.; Davis, G. T. *J. Am. Chem. Soc.* **1963,** *85* (20), 3146.

(184) Rayshys, J. W.; Taft, R. W.; Sheppard, W. A. *J. Am. Chem. Soc.* **1968,** *90* (19), 5236.

(185) Hansch, C.; Leo, A.; Taft, R. W. *Chem. Rev.* **1991,** *91* (2), 165.

(186) Parshall, G. W. Electronic Character of Metal-Anion Bonds.*J. Am. Chem. Soc.* **1966,** *88* (4), 704.

(187) Adcock, W.; Hegarty, B. F.; Kitching, W.; Smith, A. J. *J. Organometal. Chem.* **1968,** *12* (2), P21.

(188) Church, M. J.; Mays, M. J. Spectroscopic studies on some new cationic complexes of platinum(II). *Journal of the Chemical Society A: Inorganic, Physical, Theoretical* **1968**, 3074.

(189) Kitching, W.; Adcock, W.; Hegarty, B. *Austr. J. Chem.* **1968,** *21* (10), 2411.

(190) Bolton, E. S.; Knox, G. R.; Robertson, C. G. Electronic and reactivity effects in XC6H4Fe(CO)(L)C5H5 complexes. *J. Chem. Soc. D: Chem. Commun.* **1969**, 664.

(191) Stewart, R. P.; Treichel, P. M. *J. Am. Chem. Soc.* **1970,** *92* (9), 2710.

(192) Hill, H. A. O.; Morallee, K. G.; Cernivez, F.; Pellizer, G. *J. Am. Chem. Soc.* **1972,** *94* (1), 277.

(193) Nichols, D. I. *Journal of the Chemical Society A: Inorganic, Physical, Theoretical* **1970**, , 1216.

(194) Hashmi, A. S. K.; Ramamurthi, T. D.; Rominger, F. *J. Organometal. Chem.* **2009,** *694* (4), 592.

(195) Schubert, U.; Ackermann, K.; Aumann, R. *Crystal Structure Communications* **1982,** *11* (2), 591.

(196) Liu, L.-P.; Xu, B.; Mashuta, M. S.; Hammond, G. B. *J. Am. Chem. Soc.* **2008,** *130* (52), 17642.

(197) Fañanás-Mastral, M.; Aznar, F. *Organometallics* **2009,** *28* (3), 666.

(198) Olah, G. A.; DeMember, J. R.; Mo, Y. K.; Svoboda, J. J.; Schilling, P.; Olah, J. A. *J. Am. Chem. Soc.* **1974,** *96* (3), 884.

(199) Olah, G. A.; Berrier, A. L.; Prakash, G. K. S. *J. Am. Chem. Soc.* **1982,** *104* (9), 2373.

(200) Kysel, O.; Jany, I. *Chemicke Zvesti* **1974,** *28* (1), 70.

(201) Stewart, R.; Yates, K. *J. Am. Chem. Soc.* **1958,** *80* (23), 6355.

(202) Yates, K.; Stewart, R. *Can. J. Chem.* **1959,** *37* (4), 664.

(203) Olah, G. A.; Watkins, M. I. *Proc. Nat. Acad. Sci.* **1980,** *77* (2), 703.

(204) Marion, N.; Nolan, S. P. *Chem. Soc. Rev.* **2008,** *37* (9), 1776.

(205) Díez-González, S.; Marion, N.; Nolan, S. P. *Chem. Rev.* **2009,** *109* (8), 3612.

(206) Lin, J. C. Y.; Huang, R. T. W.; Lee, C. S.; Bhattacharyya, A.; Hwang, W. S.; Lin, I. J. B. *Chem. Rev.* **2009,** *109* (8), 3561.

(207) Klahn, P.; Kirsch, S. F. *ChemCatChem* **2011,** *3* (4), 649.

(208) Nolan, S. P. *Acc. Chem. Res.* **2011,** *44* (2), 91.

(209) Gatineau, D.; Goddard, J.-P.; Mouriès-Mansuy, V.; Fensterbank, L. *Israel Journal of Chemistry* **2013,** *53* (11-12), 892.

(210) Li, H.; Harris, R. J.; Nakafuku, K.; Widenhoefer, R. A. *Organometallics* **2016,** *35* (13), 2242.

(211) Wang, Z. J.; Benitez, D.; Tkatchouk, E.; Goddard, W. A.; Toste, F. D. *J. Am. Chem. Soc.* **2010,** *132*, 13064.

(212) Patil, N. T. Chirality Transfer and Memory of Chirality in Gold-Catalyzed Reactions. *Chem. - Asian J.* **2012,** *7*, 2186.

(213) Teller, H.; Corbet, M.; Mantilli, L.; Gopakumar, G.; Goddard, R.; Thiel, W.; Fürstner, A.. *J. Am. Chem. Soc.* **2012,** *134*, 15331.

(214) Campolo, D.; Gastaldi, S.; Roussel, C.; Bertrand, M. P.; Nechab, M.. *Chem. Soc. Rev.* **2013,** *42*, 8434.

(215) Cox, N.; Uehling, M. R.; Haelsig, K. T.; Lalic, G. *Angew. Chem., Int. Ed.* **2013,** *52*, 4878.

(216) Miles, D. H.; Veguillas, M.; Toste, F. D. *Chem. Sci.* **2013,** *4*, 3427.

(217) Handa, S.; Lippincott, D. J.; Aue, D. H.; Lipshutz, B. H. *Angew. Chem., Int. Ed.* **2014,** *53*, 10658.

(218) Shu, X. Z.; Nguyen, S. C.; He, Y.; Oba, F.; Zhang, Q.; Canlas, C.; Somorjai, G. A.; Alivisatos, A. P.; Toste, F. D. *J. Am. Chem. Soc.* **2015,** *137*, 7083.

(219) Zi, W.; Toste, F. D. *Angew. Chem., Int. Ed.* **2015,** *54*, 14447.

(220) Widenhoefer, R. A. *Chem. - Eur. J.* **2008,** *14*, 5382.

(221) Sengupta, S.; Shi, X. *ChemCatChem* **2010,** *2*, 609.

(222) Pradal, A.; Toullec, P. Y.; Michelet, V. *Synthesis* **2011,** *2011*, 1501.

(223) Shen, H. C. *Tetrahedron* **2008,** *64*, 3885.

(224) Krause, N.; Winter, C. *Chem. Rev.* **2011,** *111*, 1994.

(225) Liu, Z.; Wasmuth, A. S.; Nelson, S. G. *J. Am. Chem. Soc.* **2006,** *128*, 10352.

(226) Zeldin, R. M.; Toste, F. D.. *Chem. Sci.* **2011,** *2*, 1706.

(227) Bates, R. W.; Dewey, M. R. A *Org. Lett.* **2009,** *11,* 3706.

(228) Sawama, Y.; Sawama, Y.; Krause, N.. *Org. Biomol. Chem.* **2008,** *6,* 3573.

(229) Schmiedel, V. M.; Stefani, S.; Reissig, H. U. *Beilstein J. Org. Chem.* **2013,** *9,* 2564.

(230) Jeker, O. F.; Carreira, E. M. *Angew. Chem., Int. Ed.* **2012,** *51,* 3474.

(231) Okada, T.; Sakaguchi, K.; Shinada, T.; Ohfune, Y. *Tetrahedron Lett.* **2011,** *52,* 5744.

(232) Gandon, V.; Lemiére, G.; Hours, A.; Fensterbank, L.; Malacria, M. *Angew. Chem., Int. Ed.* **2008,** *47,* 7534.

(233) Benitez, D.; Tkatchouk, E.; Gonzalez, A. Z.; Goddard, W. A.; Toste, F. D. *Org. Lett.* **2009,** *11,* 4798.

(234) Paton, R. S.; Maseras, F.. *Org. Lett.* **2009,** *11,* 2237.

(235) Zhu, R. X.; Zhang, D. J.; Guo, J. X.; Mu, J. L.; Duan, C. G.; Liu, C. B. *J. Phys. Chem. A* **2010,** *114,* 4689.

(236) Alcaide, B.; Almendros, P.; Campo, T. M.; Soriano, E.; Marco-Contelles, J. *Top. Curr. Chem.* **2011,** *302,* 183.

(237) Malacria, M.; Fensterbank, L.; Gandon, V. *Top. Curr. Chem.* **2011,** *302,* 157.

(238) Montserrat, S.; Ujaque, G.; López, F.; Mascarenãs, J. L.; Lledós, A.. *Top. Curr. Chem.* **2011,** *302,* 225.

(239) Montserrat, S.; Faustino, H.; Lledós, A.; Mascareñas, J. L.; López, F.; Ujaque, G. *Chem. - Eur. J.* **2013,** *19,* 15248.

(240) Faza, O. N.; López, C. S. *Top. Curr. Chem.* **2014,** *357*, 213.

(241) Soriano, E.; Fernández, I. *Chem. Soc. Rev.* **2014,** *43*, 3041.

(242) Brown, T. J.; Sugie, A.; Dickens, M. G.; Widenhoefer, R. A. *Organometallics* **2010,** *29*, 4207.

(243) Brown, T. J.; Sugie, A.; Dickens, M. G.; Widenhoefer, R. A. *Chem. - Eur. J.* **2012,** *18*, 6959.

(244) Brooner, R. E. M.; Brown, T. J.; Widenhoefer, R. A. *Chem. - Eur. J.* **2013,** *19*, 8276.

(245) Akana, J. A.; Bhattacharyya, K. X.; Müller, P.; Sadighi, J. P. *J. Am. Chem. Soc.* **2007,** *129*, 7736.

(246) Liu, L. P.; Xu, B.; Mashuta, M. S.; Hammond, G. B. *J. Am. Chem. Soc.* **2008,** *130*, 17642.

(247) Hashmi, A. S. K.; Schuster, A. M.; Rominger, F. *Angew. Chem., Int. Ed.* **2009,** *48*, 8247.

(248) Liu, L. P.; Hammond, G. B.. *Chem. - Asian J.* **2009,** *4*, 1230.

(249) Shi, Y.; Roth, K. E.; Ramgren, S. D.; Blum, S. A.. *J. Am. Chem. Soc.* **2009,** *131*, 18022.

(250) Weber, D.; Gagné, M. R. *Org. Lett.* **2009,** *11*, 4962.

(251) Weber, D.; Tarselli, M. A.; Gagné, M. R. *Angew. Chem., Int. Ed.* **2009,** *48*, 5733.

(252) Chen, Y.; Wang, D.; Petersen, J. L.; Akhmedov, N. G.; Shi, X. *Chem. Commun.* **2010,** *46*, 6147.

(253) Hashmi, A. S. K.; Ramamurthi, T. D.; Rominger, F.*Adv. Synth. Catal.* **2010,** *352*, 971.

(254) Schmidbaur, H.; Schier, A. *Organometallics* **2010,** *29*, 2.

(255) Seidel, G.; Lehmann, C. W.; Fürstner, *Angew. Chem., Int. Ed.* **2010,** *49*, 8466.

(256) Zeng, X.; Kinjo, R.; Donnadieu, B.; Bertrand, G.. *Angew. Chem., Int. Ed.* **2010,** *49*, 942.

(257) Hashmi, A. S. K.; Schuster, A. M.; Gaillard, S.; Cavallo, L.; Poater, A.; Nolan, S. P.. *Organometallics* **2011,** *30*, 6328.

(258) Brown, T. J.; Weber, D.; Gagné, M. R.; Widenhoefer, R. A. *J. Am. Chem. Soc.* **2012,** *134*, 9134.

(259) Hashmi, A. S. K.; Braun, I.; Nösel, P.; Schädlich, J.; Wieteck, M.; Rudolph, M.; Rominger, F. *Angew. Chem., Int. Ed.* **2012,** *51*, 4456.

(260) Hashmi, A. S. K.; Braun, I.; Rudolph, M.; Rominger, F. *Organometallics* **2012,** *31*, 644.

(261) Hashmi, A. S. K.; Wieteck, M.; Braun, I.; Nösel, P.; Jongbloed, L.; Rudolph, M.; Rominger, F. *Adv. Synth. Catal.* **2012,** *354*, 555.

(262) Liu, L. P.; Hammond, G. B. *Chem. Soc. Rev.* **2012,** *41*, 3129.

(263) Brooner, R. E. M.; Widenhoefer, R. A. *Angew. Chem., Int. Ed.* **2013,** *52*, 11714.

(264) Weber, D.; Gagné, M. R.. *Chem. Sci.* **2013,** *4*, 335.

(265) Jones, A. C. *Top. Curr. Chem.* **2014,** *357*, 133.

(266) Lauterbach, T.; Asiri, A. M.; Hashmi, A. S. K. *Adv. Organomet. Chem.* **2014,** *62*, 261.

(267) Obradors, C.; Echavarren, A. M. *Chem. Commun.* **2014,** *50*, 16.

(268) Weber, D.; Gagne, M. R. *Top. Curr. Chem.* **2014,** *357*, 167.

(269) Ranieri, B.; Escofet, I.; Echavarren, A. M. A. *Org. Biomol. Chem.* **2015,** *13*, 7103.

(270) Gockel, B.; Krause, N. *Org. Lett.* **2006,** *8*, 4485.

(271) Morita, N.; Krause, N. *Angew. Chem., Int. Ed.* **2006,** *45*, 1897.

(272) Zhang, Z.; Liu, C.; Kinder, R. E.; Han, X.; Qian, H.; Widenhoefer, R. A. *J. Am. Chem. Soc.* **2006,** *128*, 9066.

(273) Zhang, Z.; Bender, C. F.; Widenhoefer, R. A. *J. Am. Chem. Soc.* **2007,** *129*, 14148.

(274) Zhang, Z.; Widenhoefer, R. A. *Angew. Chem., Int. Ed.* **2007,** *46*, 283.

(275) Zhang, Z.; Widenhoefer, R. A. *Org. Lett.* **2008,** *10*, 2079.

(276) Winter, C.; Krause, N. *Angew. Chem., Int. Ed.* **2009,** *48*, 6339.

(277) Zhdanko, A.; Maier, M. E. *Chem. - Eur. J.* **2013,** *19*, 3932.

(278) Zhdanko, A.; Maier, M. E. *Organometallics* **2013,** *32*, 2000.

(279) Zhdanko, A.; Maier, M. E. *Chem. - Eur. J.* **2014,** *20*, 1918.

(280) Zhdanko, A.; Maier, M. E. *ACS Catal.* **2015,** *5*, 5994.

(281) Brown, T. J.; Dickens, M. G.; Widenhoefer, R. A. *J. Am. Chem. Soc.* **2009,** *131*, 6350.

(282) Cornell, T. P.; Shi, Y.; Blum, S. A. *Organometallics* **2012,** *31*, 5990.

(283) Hashmi, A. S. K. *Acc. Chem. Res.* **2014,** *47*, 864.

(284) Zhdanko, A.; Ströbele, M.; Maier, M. E. *Chem. - Eur. J.* **2012,** *18*, 14732.

(285) Briggs, G. E.; Haldane, J. B. S.. *Biochem. J.* **1925,** *19*, 338.

(286) Kochi, J. K.; Bockman, T. M. *Adv. Organomet. Chem.* **1991,** *33*, 51.

(287) Macchioni, A. *Chem. Rev.* **2005,** *105*, 2039.

(288) Zuccaccia, D.; Belpassi, L.; Tarantelli, F.; Macchioni, A. *J. Am. Chem. Soc.* **2009,** *131*, 3170.

(289) Zuccaccia, D.; Belpassi, L.; Rocchigiani, L.; Tarantelli, F.; Macchioni, A. *Inorg. Chem.* **2010,** *49*, 3080.

(290) Zuccaccia, D.; Belpassi, L.; Macchioni, A.; Tarantelli, F. *Eur. J. Inorg. Chem.* **2013,** *2013*, 4121.

(291) Alibrandi, C.; Romeo, R.; Scolaro, L. M.; Tobe, M. L.. *Inorg. Chem.* **1992,** *31*, 5061.

(292) Song, L.; Trogler, W. C. *J. Am. Chem. Soc.* **1992,** *114*, 3355.

(293) Marcus, Y.; Hefter, G. *Chem. Rev.* **2006,** *106*, 4585.

(294) Maryott, A. A.; Smith, E. R. *Table of dielectric constants of pure liquids,* 1951.

(295) Jouyban, A.; Soltanpour, S. *J. Chem. Eng. Data* **2010,** *55,* 2951.

(296) Romeo, R.; Arena, G.; Scolaro, L. M.; Plutino, M. R. *Inorg. Chim. Acta* **1995,** *240,* 81.

(297) Romeo, R.; Nastasi, N.; Scolaro, L. M.; Plutino, M. R.; Albinati, A.; Macchioni, *Inorg. Chem.* **1998,** *37,* 5460.

(298) Aizawa, S. i.; Sone, Y.; Kawamoto, T.; Yamada, S.; Nakamura, M. *Inorg. Chim. Acta* **2002,** *338*, 235.

(299) Mo, H.; Wang, A.; Wilkinson, P. S.; Pochapsky, T. C. Solvent. *J. Am. Chem. Soc.* **1997,** *119,* 11666.

(300) Rocchigiani, L.; Bellachioma, G.; Ciancaleoni, G.; Crocchianti, S.; Laganà, A.; Zuccaccia, C.; Zuccaccia, D.; Macchioni, A. *ChemPhysChem* **2010,** *11,* 3243.

(301) Biasiolo, L.; Trinchillo, M.; Belanzoni, P.; Belpassi, L.; Busico, V.; Ciancaleoni, G.; D'Amora, A.; Macchioni, A.; Tarantelli, F.; Zuccaccia, D. *Chem. - Eur. J.* **2014,** *20,* 14594.

(302) Zhdanko, A.; Maier, M. E. *ACS Catal.* **2014,** *4*, 2770.

(303) Ciancaleoni, G.; Belpassi, L.; Zuccaccia, D.; Tarantelli, F.; Belanzoni, P. *ACS Catal.* **2015,** *5,* 803.

(304) Brooner, R. E. M.; Brown, T. J.; Chee, M. A.; Widenhoefer, R. A. *Organometallics* **2016,** *35,* 2014.

(305) Larive, W. F. P. a. C. K. *J. Chem. Ed.* **2008,** *85* (4), 484.

(306) McCoy, A. B.; Darbeau, R. W.. *J. Chem. Ed.* **2013,** *90* (4), 398.

(307) Moore, J. W.; Stanitski, C. L. *J. Chem. Ed.* **2017,** *94* (11), 1603.

(308) Kosbar, L. L.; Wenzel, T. J. *J. Chem. Ed.* **2017,** *94* (11), 1599.

(309) Chemistry, A. P.

(310) Clark, R. W. *J. Chem. Ed.* **1999,** *76* (12), 1612.

(311) Goedhart, M. J. *J. Chem. Ed.* **2007,** *84* (6), 971.

(312) Bhowon, M. G., Laulloo, S. J., Wah, H. L. K. , Ramasami, P. *Chemistry Education in the ICT Age*; Springer: Dordrecht, Netherlands, 2009.

(313) Devetak, I., Glazer, S. A. *Learning with Understanding in the Chemistry Classroom*; Springer: New York, 2014.

(314) Minkin, V. I. *Chemical Reviews* **2004,** *104* (5), 2751.

(315) Davis, D. A.; Hamilton, A.; Yang, J.; Cremar, L. D.; Van Gough, D.; Potisek, S. L.; Ong, M. T.; Braun, P. V.; Martinez, T. J.; White, S. R.. *Nature* **2009,** *459* (7243), 68.

(316) Gossweiler, G. R.; Hewage, G. B.; Soriano, G.; Wang, Q.; Welshofer, G. W.; Zhao, X.; Craig, S. L. *ACS Macro Lett.* **2014,** *3* (3), 216.

(317) Garkov, V. *Chemistry: Bulgarian Journal of Science Education* **2006,** *15* (2), 86.

(318) Gilbert, J. K. B., C. *Developing Models in Science Education*; Springer: Dordrecht, Netherlands, 2000.

(319) Jones, L. L. *J. Chem. Ed.* **2013,** *90* (12), 1571.

(320) Caruso, M. M.; Davis, D. A.; Shen, Q.; Odom, S. A.; Sottos, N. R.; White, S. R.; Moore, J. S. *Chem. Rev.* **2009,** *109* (11), 5755.

(321) Brown, C. L.; Craig, S. L.. *Chem. Sci.* **2015,** *6* (4), 2158.

(322) Gossweiler, G. R.; Brown, C. L.; Hewage, G. B.; Sapiro-Gheiler, E.; Trautman, W. J.; Welshofer, G. W.; Craig, S. L. *ACS Appl. Mater. Inter.* **2015,** *7* (40), 22431.

(323) Bopegedera, A. M. R. P. P. *J. Chem. Ed.* **2011,** *88* (4), 443.

(324) Canelas, D. A. Teaching College Chemistry to the Edges Rather Than to the Average. **2015,** *1193*, 11.

(325) Hall, D. M.; Curtin-Soydan, A. J.; Canelas, D. A. *J. Chem. Ed.* **2013,** *91* (1), 37.

(326) Michaelsen, L. K.; Sweet, M. *New Directions for Teaching and Learning* **2008,** *2008* (116), 7.

(327) Brown, C. L.; Barbee, M. H.; Ko, J. H.; Maynard, H. D.; Craig, S. L. *J. Chem. Ed.* **2017,** *94* (11), 1752.

(328) Loudon, G. M. *Organic Chemistry*; 4th ed.; Oxford University Press: New York, 2002.

(329) Wade, L. G. *Organic Chemistry*; 6th ed.; Pearson Prentice Hall: Upper Saddle River, New Jersey, 2006.

(330) Swansburg, S.; Buncel, E.; Lemieux, R. P. *Journal of the American Chemical Society* **2000,** *122* (28), 6594.

(331) Spencer, H. E. *J. Chem. Ed.* **1996,** *73* (12), 1150.

(332) Tai, R. H.; Sadler, P. M.; Loehr, J. F. *J. Res. Sci. Teach.* **2005,** *42* (9), 987.

Biography

Robert Gerard Carden, Jr. graduated *magna cum laude* from Saint Joseph's University in May 2014 with a Bachelor of Science degree in Chemistry with a minor in music. While a Saint Joseph's he conducted research with Prof. Peter M. Graham on the

synthesis and reactivity of tungsten and molybdenum carbon dioxide complexes. In 2013, he received an ACS Undergraduate Award in Inorganic Chemistry and was inducted as a member of Sigma Xi. In 2014, he was awarded an American Institute of Chemists Award for Academic Achievement and was inducted as a member of Phi Beta Kappa.

In August 2014, he began graduate studies at Duke University and formally affiliated with Prof. Ross Widenhoefer's research group in January of 2015. While at Duke, his research interests focused on the kinetic and mechanistic analysis of gold(I)-catalyzed reactions as well as the synthesis of cationic gold(I) carbene complexes. In 2015, he received the Pelham Wilder Award for excellence in undergraduate teaching. His graduate studies were supported by both a Department of Education GAANN fellowship and a Burroughs Wellcome fellowship. He has presented his research both locally and nationally. In July 2019, he will begin a postdoctoral fellowship at Villanova University, working with Prof. Kevin Minbiole on the synthesis of novel antiseptics and chemical ecology projects.

Publications

1) **Carden, Robert G**.; Widenhoefer, Ross. A. "Gold(I) Benzylide Complex Undergo Efficient Transfer to Alkenes" Submitted to *Angew. Chem.*

2) Canelas, Dorian A; Hill, Jennifer A.; **Carden, Robert G.** "Cooperative Learning in Large Sections of Organic Chemistry: Transitioning to POGIL" *Submitted to ACS Books.*

3) Harris, Robert J.; Nakafuku, Kohki; Duncan, Alethea H.; **Carden, Robert G.**; Timmerman, Jacob C. Widenhoefer, Ross A. "Kinetics and Mechanism of the Gold-Catalyzed Intermolecular Hydroamination of Allenes with Aryl Amines" *Chem. Eur. J.* in revision.

4) Harris, Robert J.; **Carden, Robert G.**; Duncan, Alethea H.; Widenhoefer, Ross A. "Kinetics and Mechanism of the Gold-Catalyzed Intermolecular Hydroalkoxylation of Allenes with Alcohols" *ACS Catal.*, **2018**, *8*, 8941–8952.

5) Barbee, Meredith H.†; **Carden, Robert G.**†; Johnson, Julia H. R.; Brown, Cameron L.; Canelas, Dorian A.; Craig, Stephen L. "A single reaction thread to tie multiple core concepts in an introductory chemistry course" *J. Chem. Educ*., **2018**, *95* (6), 936–946. († equal contribution)

6) **Carden, Robert G.**; Lam, Nathan*; Widenhoefer, Ross A. "Experimental Evaluation of L(Au) Electron Donor Ability in Cationic Gold Carbene Complexes" *Chem. Eur. J.* **2017**, *23*, 17992–18001.

7) **Carden, Robert G.**; Ohane, James J.; Pike, Robert D.; Graham, Peter M. "Synthesis of tungsten and molybdenum carbon dioxide complexes" *Organometallics* **2013,** *32*, 2505–2508.

Recent Research Presentations

1) **Carden, Robert G.**; Barbee, Meredith H.; Johnson, Julia H. R.; Brown, Cameron L.; Canelas, Dorian A.; Craig, Stephen L. "A single reaction thread to tie multiple core

concepts in an introductory chemistry course" Graduate Research Symposium, Duke University, Durham, NC, 8 October 2018. ***Poster***

2) **Carden, Robert G.**; Lam, Nathan; Widenhoefer, Ross A. "Synthesis and Experimental Evaluation of Gold (I) Carbene Complexes Relevant to Gold (I) Catalysis" Abstracts of Papers, 255th ACS National Meeting & Exposition, New Orleans, LA United States, 20 March 2018, ORGN-394. ***Talk***

3) **Carden, Robert G.**; Lam, Nathan; Widenhoefer, Ross A. "Experimental Evaluation of L(Au) Electron Donor Ability in Cationic Gold Carbene Complexes" Graduate Research Symposium, Duke University, Durham, NC, 9 October 2017. ***Talk*** "Best Oral Presentation"

4) **Carden, Robert G.**; Lam, Nathan; Widenhoefer, Ross A. "Quantification of α-Gold Positive Charge Stabilization in Gold Carbene Complexes" 45th National Organic Symposium, University of California-Davis, Davis, CA, 25 June 2017. ***Poster***

5) **Carden, Robert G.**; Lam, Nathan; Stevenson, Nicholas P.; Widenhoefer, Ross A. "Quantification of α-Gold Positive Charge Stabilization in Gold Carbene Complexes" Graduate Research Symposium, Duke University, Durham, NC, 10 October 2016. ***Poster***